MEMBRANE ORGANIZATION AND DYNAMICS IN MAMMALIAN SPERM

A Dissertation

Presented to the Faculty of the Graduate School

of Cornell University

In Partial Fulfillment of the Requirements for the Degree of

Doctor of Philosophy

by

Vimal Selvaraj

January 2008

MEMBRANE ORGANIZATION AND DYNAMICS IN MAMMALIAN SPERM

Vimal Selvaraj, Ph. D.

Cornell University 2008

In somatic cells, membrane rafts are dynamic, existing in various time and space scales. The transient nature of these membrane microdomains and the use of detergents or multivalent probes/cross-linkers to isolate or visualize them have incited controversy in this field. In the following studies, I demonstrate for the first time in live spermatozoa, the presence of a micrometer-scale, stable domain in the plasma membrane enriched in sterols and the glycosphingolipid G_{M1} at physiological temperature. This sterol-enriched membrane platform is positioned to regulate the acquisition of sperm fertilization competence. I examine the properties of this domain and the mechanism behind its segregation and maintenance. I also conduct in-depth functional studies on FABP9, which was a strong candidate for tethering membrane lipids to underlying cytoskeletal elements in this region.

My studies showed that the maintenance of this stable segregation in the sperm head was at least in part due to a specialized diffusion barrier at a region called the sub-acrosomal ring. I found that FABP9 did not play a role in this membrane segregation. Interesting dynamics of G_{M1} bound to cholera toxin subunit B (CTB) revealed that complex membrane interactions occur in this region. This led to the finding that the acrosomal vesicle that immediately underlies this domain is a G_{M1}-enriched organelle. The dynamics of CTB-bound G_{M1} also resulted in our ability to distinguish different functional changes in sperm membrane properties occurring in response to capacitating stimuli.

Based on these stimulus specific changes seen with CTB-bound G_{M1} distribution, we found that sperm could respond to bicarbonate ions or mediators of sterol efflux independently, thereby refining existing models of capacitation. The applicability of CTB-bound G_{M1} dynamics as a diagnostic tool to assay sperm response to stimuli for capacitation is potentially of significant clinical importance.

These studies set the stage for exploring both capacitation-related changes in the microheterogeneities within this domain and ensuing signaling events in response to stimuli for capacitation. Furthermore, my data have led to a complex model that involves several complementary mechanisms of lipid segregation acting at different spatial scales. Testing this model will be the subject of continuing investigations.

BIOGRAPHICAL SKETCH

Vimal Selvaraj was born in Nagercoil, India in June 10, 1976. His parents Selvaraj and Jessie moved with Vimal and his sister Vinoo to Calabar, Nigeria in 1981. Here Vimal started at Kadana International School. Outside school, Vimal often accompanied his father on field trips into the swamps and jungles of Nigeria and it was here that he developed a passion for nature and biology. His family brought him back to India in 1986 and Vimal entered Scott Christian Higher Secondary School, a small hometown school. Here Vimal was appointed as captain of the table-tennis team and won district level competitions for 3 years in a row. He was also the secretary of the school's Interact Club and participated in several community development activities. He graduated with merit in 1993 and was accepted into the prestigious American College in Madurai, India. Here he majored in physics for 8 months, and later that year he made a hard decision to quit and pursue his interests elsewhere. In 1994, he accepted a competitive merit scholarship to study at the Madras Veterinary College in Chennai, India. Here he headed the Wildlife Club and was actively involved in several local conservation initiatives and during his tenure, he launched a student monthly wildlife journal called the "Wild Wind." At Madras Veterinary College, Vimal also had a keen interest in research; under the mentorship of Dr. Mathew C. John, he worked on field projects involving water bird nesting preferences and spotted deer behavior. At the time of his graduation in December 2000, he had published seven peer-reviewed articles on wildlife and veterinary medicine.

In July 2001, Vimal joined the Reproductive Biology group at the University of Illinois at Urbana-Champaign. He pursued a M.S. degree in the

laboratory of Dr. Paul S. Cooke working on the estrogenicity and immuno-modulatory effects of phytoestrogens. He published two peer-reviewed articles from this work and was a co-author in two critical reviews in this field. He was also honored with the Constance Campbell Memorial Research Award for poster presentation at the 24th Annual Mini-symposium in Reproductive Biology at Northwestern University, Chicago. He graduated with a M.S. in December 2003.

In January 2004, Vimal joined the laboratory of Dr. Alexander J. Travis at Cornell University as a post-doctoral associate and started work on the male gamete. In June 2004, he accepted a competitive post-DVM graduate research assistantship from the College of Veterinary Medicine, Cornell University and joined the program in Physiology to pursue his Ph.D. He continued graduate work in the laboratory of Dr. Travis but never passed opportunities to collaborate in wildlife conservation projects. This interest led him to train in the laboratory of Dr. Budhan Pukazhenthi at the National Zoo and Conservation Research Center of the Smithsonian Institution, Washington DC and concurrently perform collaborative work during his graduate program. Upon completion of his Ph.D., Vimal will be joining his wife in Davis, California as they both pursue post-doctoral training.

To my late grandfather Karuthudaiyan James

ACKNOWLEDGMENTS

This has been a really long journey of scientific pursuit. I thank the numerous people that have shaped the way I think about science and the lifestyle that goes with it. If you are reading this dissertation because something in this area of research piqued your curiosity, I am truly honored and I hope you find a fitting theory embedded in this body of work.

First of all, I express my deepest gratitude to Dr. Alexander Travis, mentor extraordinaire. I thank him for his constant encouragement and interest shown in my overall development as a scientist and a veterinarian. He really shared his expertise in gamete biology through countless discussions and made me think critically. I will be eternally grateful for his dedicated tutelage.

I also express my gratitude to Dr. Robert Weiss for his excellent guidance during manipulation of the mouse genome. In addition to a wealth of information, he really taught me to be patient and to persevere. Working in his lab provided me with an enriching experience of scientific diversity.

I also thank the other members of my graduate committee, Dr. Susan Suarez, Dr. David Holowka, Dr. Mark Roberson and Dr. Budhan Pukazhenthi for truly being involved in my work and providing expert opinions and constructive criticisms for my experiments. It was a privilege to work with each of them; I consider them my role models.

I would also like to thank Dr. Paul Cooke, my former mentor, for introducing me to the world of molecular biology and constantly encouraging me to pursue my interests. I also thank my father Dr. A. M. Selvaraj and Dr. Mathew John who nurtured my interests in zoology and wildlife very early in my career.

All lessons I learned from the professional attitude and approaches to scientific problem solving and management from the above scientists have instilled in me hope for a fighting future in science.

However, my journey through graduate school would not have been possible without strong bonds of camaraderie. I warmly thank all my friends and colleagues; I had a truly great time working with them all. I especially thank Atsushi Asano, Jacque Nelson, Yeun-Hee Kim, Chinatsu Mukai, Jenn Page, Xia Xu, Stephanie Yazinski, Min Zhu, Steve Rodriguez and Weipeng Mu. Thanks for all the laughs and special late-night parties that made my life feel worthwhile!

Above all, I thank my wife and parents for their love and constant support throughout the years. I sincerely thank my wife for allowing me to pursue my interests that took me away from her for the past 4 years.

I cannot end without thanking everyone at the Baker Institute for a wonderful family-like supportive work environment and the Cornell University College of Veterinary Medicine GRA program for my funding.

TABLE OF CONTENTS

LIST OF FIGURES

LIST OF TABLES

LIST OF ABBREVIATIONS

2-OHCD: 2-hydroxypropyl-β-cyclodextrin

AA: Apical acrosome

APM: Plasma membrane overlying the acrosome

CTB: Cholera Toxin Subunit B

DRM: Detergent Resistant Membrane

EGFP: Enhanced Green Flurorescent Protein

ES: Equatorial segment

FABP9: Fatty Acid Binding Protein 9

FLIP: Fluorescence loss in photobleaching

FRAP: Fluorescence recovery after photobleaching

GPI: Glycophosphatidyl inositol

IAM: Inner acrosomal membrane

IP3: Inositol 1,4,5-triphosphate

LPC: Lysophosphatidyl choline

OAM: Outer acrosomal membrane

PAPM: Region of plasma membrane lying between the sub-acrosomal ring and posterior ring

PFO: Perfringolysin O (θ-Toxin)

PFO-D4: Domain 4 of Perfringolysin O

PFO-D4-T: Non-functional Truncated Domain 4 of Perfringolysin O

PI: Phosphatidyl inositol

PNA: Peanut agglutinin

SAR: Sub-acrosomal ring

SEM: Scanning electron microscopy

PREFACE

An essential feature of the “fluid mosaic model” (Singer SJ and Nicolson, GL, 1972, Science 175:720-731) of the cell plasma membrane is the ability of membrane lipids and proteins to diffuse laterally in the plane of the membrane. In the 1980s, discovery of preferential sorting of membrane lipids in polarized cells suggested that there is some kind of lateral heterogeneity of lipid composition in the membrane. Biochemical studies bolstered these findings and initiated the “raft hypothesis,” led by the discovery of glycosphingolipid clusters in the membrane insoluble in anionic detergents at low temperatures were enriched in cholesterol and glycosylphosphatidyl inositol-anchored proteins. This incited studies focusing on the function of glycosphingolipid-cholesterol rich domains in biological membranes and also exploring biophysical properties of different synthetic membranes. However, the complexity of biological membranes and modulations in live cells including maintenance of membrane asymmetry, membrane dynamics, intracellular trafficking and tethered protein obstacles have led to the conclusion that biological membranes behave in an “unusual fluid-like” manner. Attempts to visualize lateral heterogeneities have proven immensely difficult and artifacts induced by fixation and cross-linking agents have instigated controversy in this field. In the studies presented, I use the polarized sperm known for its distinct regional membrane properties as means of functional compartmentalization facilitating union with the oocyte.

Fertilization is a membrane-driven event. In mammals, there is first fusion required for exocytosis of the acrosomal vesicular contents to aid penetration of the oocyte zona pellucida; then the sperm plasma membrane needs to fuse with the oocyte plasma membrane; a membrane fusion event is also required for the exocytosis of cortical granules of the oocyte critical for preventing polyspermy; finally, the fusion of the male and female pronuclei is required for forming the diploid zygote. Therefore understanding gamete membranes are of great importance from a functional standpoint. This understanding can advance fields of assisted reproduction and cryopreservation both relevant for animal and human reproduction. In this dissertation, I use the murine sperm as a mammalian model for studying membrane organization, rafts and dynamics of function. My results speak to a broad audience on questions related to membrane biology in general and sperm-specific membrane functionalities.

CHAPTER 1

Introduction and Literature Review

In order to understand the plasma membrane characteristics of mammalian sperm, one has to follow the course of evolutionary pressures shaping development and function. In this first chapter, I intend to introduce the spermatozoon highlighting current knowledge of its development, organization, structure and function.

History and Evolutionary Perspectives

In 1677, Antony Von Leeuwenhoek observed some flagellate microorganisms in the ejaculate of a person with syphilis. He first associated these cells with the disease, but later discovered that they were a normal component of ejaculates in several species. This led him to suggest their involvement in procreation. However, this idea remained controversial for more than a century until the experiments of Lazzaro Spallanzani and others with artificial fertilization in the 1700s led to the conclusion that the sperm is a cell produced by the male that enters the egg to create a new organism (Baccetti, 1986). Additional details and evolutionary theory were worked out in the next century, which led to a deeper understanding of the structure and function of sperm from different organisms.

Evolutionary pressure on sexual reproduction has shaped structural and functional features of spermatozoa and oocytes. Sperm competition, when several males compete to fertilize a female's oocytes, was proposed to be the fundamental force shaping the male gamete (Parker, 1970, 1982). In marine invertebrates that practice external fertilization, sperm competition is believed to have led to the development of anisogamy with small and numerous male gametes produced with little investment compared to female gametes. Anisogamy, which provides a selective advantage to the male producing

relatively numerous sperm, is also conserved in species that perform internal fertilization in the female reproductive tract (Gage and Morrow, 2003). However, other recent evidence also points that there is some degree of complexity in internally fertilizing organisms, in which co-evolution of female tract dimensions and sperm length was also deemed important (Miller and Pitnick, 2002). In mammals, there is a clear relationship between sperm competition and sperm size (Gomendio and Roldan, 1991); longer sperm are capable of swimming faster in polyandrous competitions. Directed evolution for better swimming with efficient energy production and minimal energy expenditure has also led to a conserved design of sperm morphology. The classic construction of spermatozoa from marine invertebrates to humans comprises of a cellular body containing the nucleus and a flagellum capable of propelling it forward (Baccetti, 1986). Structural components within these cells are also well conserved, e.g. the exocytotic acrosome, mitochondria and axoneme are features seen in most sperm (Baccetti, 1986).

Designing a hydrodynamic structure by stripping off unessential components and simultaneously maintaining specialized functions required for fertilization requires an intricate interplay of efforts from numerous factors that together generate the male germ cell. The investment made by the male in these regulations is also highly significant. It has been calculated that in the mammalian genome, 4 % of the genes are exclusively dedicated for spermatogenesis (Schultz et al., 2003). In this present post-genomics era, we are only beginning to understand the genes regulating spermatogenesis and those playing a role in sperm function.

Spermatogenesis

Spermatogonia undergo a series of mitotic divisions, the last of which form spermatocytes. These enter meiosis, the first division producing secondary spermatocytes and the second division producing haploid round spermatids that undergo spermiogenesis. The organization of the different stages of germ cell development in relation to the somatic cells of the testis are shown in Figure 1.1.

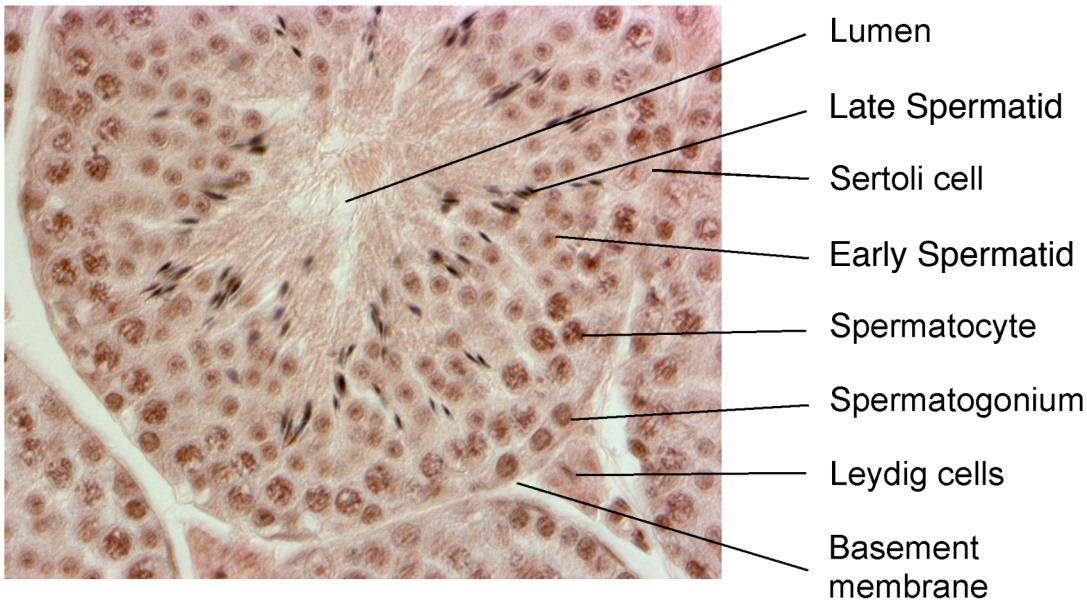

Figure 1.1. Testis section showing somatic and germ cell components. A hematoxylin and eosin stained cross-section through a seminiferous tubule (Stage IV) shows developing germ cells highly organized around the somatic Sertoli cells. The adluminal compartment of the tubule contains advanced stages of germ cells (round and elongating spermatids) and the basal compartment is occupied by spermatocytes and spermatogonial stages. Testosterone producing Leydig cells are seen in the interstitial space between the tubules.

Spermiogenesis

Round spermatids undergo a dramatic differentiation process progressing from a non-polar cell to a highly specialized motile spermatozoon. In the mouse, different stages of spermiogenic differentiation are observed as 16 distinct steps based on changes observed in the nucleus and the acrosome (Oud and de Rooij, 1977; Moreno and Alvarado, 2006) (Figure 1.2). The major morphogenic changes during spermiogenesis are: [1] Acrosomal biogenesis: the development of a Golgi-derived specialized exocytotic vesicle critical for oocyte penetration (described in greater detail below), [2] Nuclear condensation and shaping: the complete replacement of somatic histones by unwinding of spermatid DNA and rewinding onto more compact sperm-specific protamines (Marushige and Dixon, 1969; Mezquita, 1985). The acquisition of the characteristic shape of the sperm nucleus is a species-specific trait and in addition to nuclear condensation is mediated by unknown mechanisms (Fawcett et al., 1971). [3] Development of the flagellum: the centrioles migrate to the posterior pole of the spermatid and the distal centriole forms the microtubular axoneme. The manchette is an ephemeral structure composed of microtubules which forms a peri-nuclear ring and a skirt-like structure from the point of tight adhesions between the spermatid and the Sertoli cell (the upper third of the spermatid head). The manchette mediates organization, storage and sorting of both structural and signaling proteins in the acrosome and flagellum (Kierszenbaum, 2001; Kierszenbaum and Tres, 2004). The acroplaxome, an F-actin and keratin-5 containing marginal ring is organized alongside the peri-nuclear ring of the manchette (Kierszenbaum et al., 2003). Together with Sertoli cell F-actin containing hoops, constrictive forces

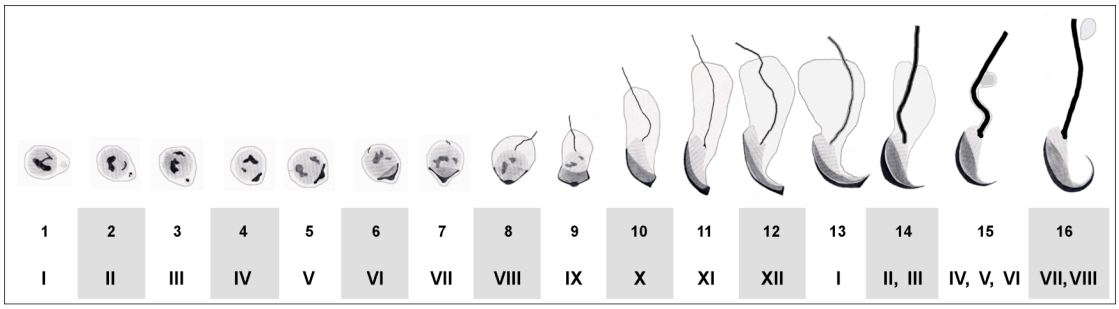

Figure 1.2. Schematic showing the steps in murine spermiogenesis. Steps 1 – 3 is the Golgi phase, 4 – 7 the cap phase, 8 – 12 the acrosome phase, and 13 – 16 the maturation phase. Note: these steps may overlap in the different cycles of the seminiferous tubule (indicated below the steps in roman numerals). Schematic drawn based on (Oakberg, 1956a).

generated from the gradual reduction in the diameter of the marginal ring of the acroplaxome and the perinuclear ring of the manchette has been suggested to ensure determine apical-to-caudal elongation of the sperm head (Kierszenbaum and Tres, 2004). Mitochondria in the elongating spermatid are sequestered and organized along the mid-piece of the flagellum. Close to terminal differentiation (step 15-16), elongating spermatids gain the appearance of a mature sperm; however, a cytoplasmic droplet containing residual organelles/material is still seen as a bleb in the flagellar membrane. This is cast off either in the testis or during epididymal maturation.

Acrosomal biogenesis

Although acrosomal biogenesis commences soon after secondary spermatocytes divide to produce spermatids, the process continues until late spermiogenesis (Leblond and Clermont, 1952; Lalli and Clermont, 1981). However, synthesis of several acrosome-specific proteins begins as early as

pachytene spermatocytes (e.g. proacrosin and acrogranin) (Bermudez et al., 1994; Moreno et al., 2000a). Based on the morphology of the developing acrosome, spermiogenesis in the mouse is divided into Golgi (step 1-3), cap (step 4-7), acrosome (8-12) and maturation (step 13-16) phases (Oakberg 1956a; Oakberg, 1956b). In round spermatids, progressively from steps 1-3, the Golgi apparatus produces small condensing vacuoles called pro-acrosomal vacuoles containing dense material called pro-acrosomal granules (Figure 1.3). These vacuoles migrate towards the nucleus and cluster together (Moreno et al., 2000a). They then fuse to form one large membrane-bound vesicle called the acrosome containing a single granule (Moreno et al., 2000b). Initially this vesicle is round in step 4 spermatids until it makes contact with the nucleus, when it gets flattened and spreads out over the surface. The acrosomal granule remains dense compared to the remainder of the material in the vesicle. The Golgi apparatus continues to contribute material to the developing acrosome via vesicular transport (Sutovsky et al., 1999; Moreno et al., 2000b), a process mediated by microtubules (Huang and Ho, 2006). Membrane fusion events occurring during the endocytotic and exocytotic pathways from the Golgi to the acrosome follow tenets of the SNARE hypothesis (Ungermann and Langosch, 2005). It has been speculated that proteins involved in these membrane fusion events are retained in the acrosomal membrane to later facilitate exocytosis in mature capacitated sperm (Moreno and Alvarado, 2006). Caveolin-1, a sterol binding protein has been shown to partially co-localize to the acrosomal vesicle (Travis et al., 2001b). Progressively from step 8 spermatids, the acrosomal membrane becomes closely apposed to the plasma membrane by an anterior movement of the

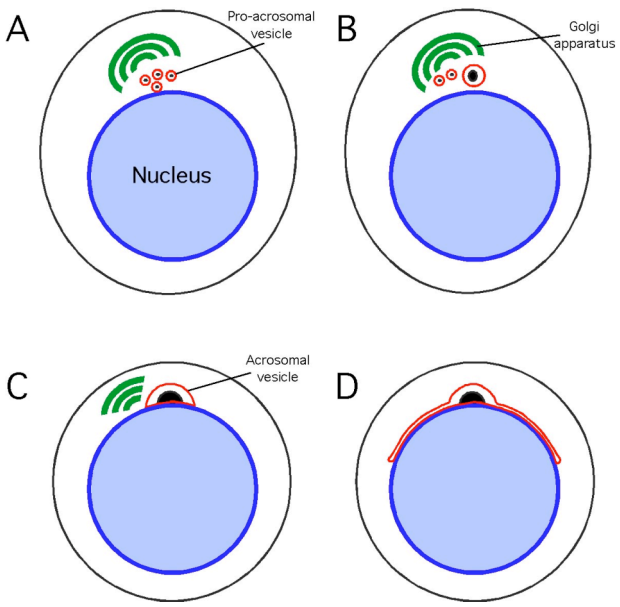

Figure 1.3. Schematic showing initial events during acrosomal biogenesis. (A) The pro-acrosomal vesicles emerge from the Golgi apparatus. These vesicles carry a dense substance called the pro-acrosomal granule. (B) The pro-acrosomal vesicles progressively coalesce to form the acrosomal vesicle carrying a core of the dense material. (C) The single acrosomal vesicle attaches to the nucleus and the Golgi apparatus begins to disorganize at this stage. (D) The pro-acrosomal vesicle then flattens out over the surface of the nucleus. Further remodeling of the acrosome occurs during the subsequent elongation stages. Schematic drawn based on (Moreno et al., 2000a; Moreno et al., 2000b)

spermatid nucleus through an unknown mechanism (Russell et al., 1983). From this point the cell begins to elongate and the acrosome undergoes a condensation process showing an increase in density of the material contained in the vesicle. The acrosomal contents that have been well characterized in sperm from different species include: hyaluronidase/PH20 (Swyer, 1947; Hunnicutt et al., 1996), proacrosin/acrosin (Polakoski et al., 1971, 1972), sperm protein 56 (Cheng et al., 1994; Foster et al., 1997), angiotensin-converting enzyme (ACE) (Kohn et al., 1995; Kohn et al., 1998),

acid phosphatase (Pietrobon et al., 2001), beta-D-galactosidase (Skudlarek et al., 1993; Skudlarek et al., 2000), catalase (Figueroa et al., 2000), beta-N-acetyl-glucosaminidase (Brandon et al., 1997), cathepsin D (Igdoura et al., 1995), cathepsin H (Haraguchi et al., 2003), glucosamine-6-phosphate deaminase (Montag et al., 1999), and N-acetyl-beta-hexosaminidase (Tulsiani et al., 1998; Abou-Haila and Tulsiani, 2000).

Structural Features of the Mature Sperm

Testicular spermatozoa released from the seminiferous tubules by a process called spermiation undergo a process of post-testicular maturation in the epididymis. In most mammalian species, the epididymis acts as a post-testicular processing and storage organ for sperm. This post-testicular maturation process is essential for sperm to acquire motility and functional competence. Based on external morphology, the epididymis is divided into 3 major parts: [1] the caput, where sperm are exposed to an active environment of secretion and reabsorption, [2] the corpus, where sperm maturation is often completed and [3] the cauda, involved in sperm storage (Glover and Nicander, 1971; Nicander and Glover, 1973). In mice experimental sperm samples are routinely collected from the cauda epididymis. The salient features of a mature spermatozoon are shown in Figure 1.4.

Head

The major structural components of the sperm head are the nucleus and the perinuclear theca (Figure 1.5). The condensed nuclear shape provides a hydrodynamically streamlined sperm head (Lalli and Clermont, 1981) and this varies between species. The perinuclear theca is the dense cytoskeletal

Figure 1.4. Schematic diagram of a mammalian spermatozoon. Note that the shape of the sperm head varies dramatically with species, but general structural features are conserved. The sperm head contains the acrosomal vesicle capping the nucleus in the anterior region. In the flagellum, the axonemal microtubules are surrounded by unique cytoskeletal structures called outer dense fibers. The mitochondria are arranged in a helical fashion in the mid-piece. In the principal piece, the fibrous sheath surrounds the outer dense fibers, which surrounds the axoneme. At the tip of the flagellum, there exists a region without the fibrous sheath or the outer dense fibers called the end piece. [Modified from (Fawcett, 1975); note that in this schematic the plasma membrane is not depicted to show the organization of internal structures]

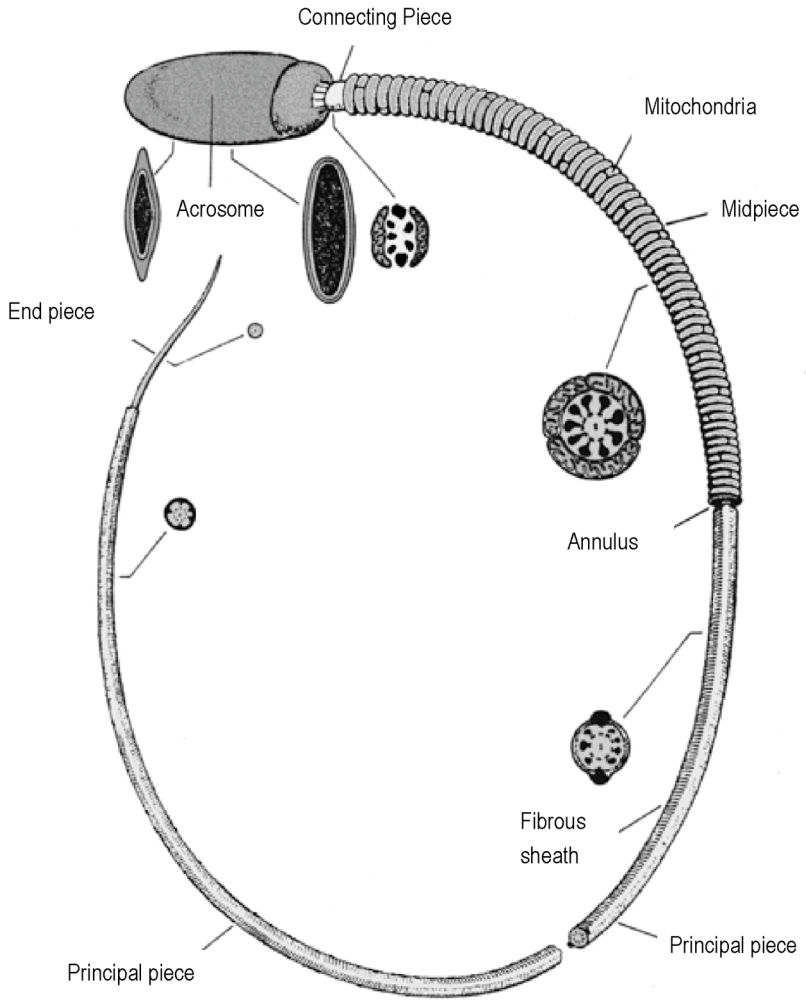
Connecting Piece
Mitochondria
Acrosome
Midpiece
End piece
Annulus
Fibrous
sheath
Principal piece
Principal piece

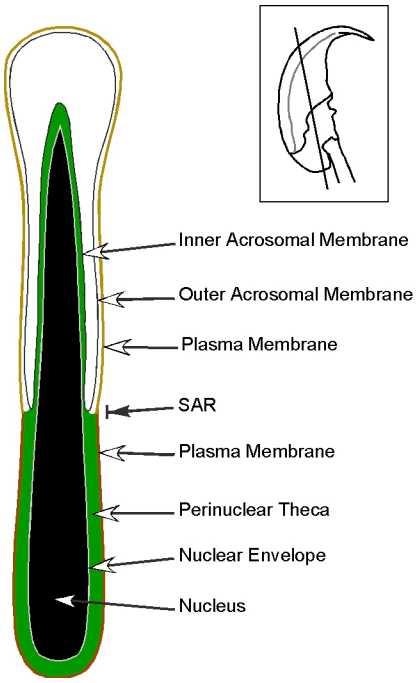

Figure 1.5. Schematic showing a longitudinal section through the murine sperm head. Inset: lateral view schematic of the sperm head shows the orientation of this longitudinal section. The nucleus (black) and nuclear membrane (grey) are surrounded by a cytoskeletal meshwork called the peri-nuclear theca (green). The acrosome (white) is seated over the apical region of the nucleus. The section of acrosomal membrane closest to the nucleus is the inner acrosomal membrane (IAM) and the acrosomal membrane apposing the plasma membrane is the outer acrosomal membrane (OAM). The plasma membrane is tightly wrapped around the structures of the sperm head.

network that surrounds the nucleus; it forms two distinct structural components in the sperm head: the perforatorium also referred to as the sub-acrosomal lamina and the post-acrosomal dense lamina or the post-acrosomal sheath (Fawcett, 1970). The post-acrosomal dense lamina covers the entire nucleus except for a region around the implantation fossa where the flagellum is docked; this theca-free region is referred to as the peri-fossal zone (Lalli and

Clermont, 1981). In murine sperm with a falciform-shaped head, the perforatorium is composed of three rods extending over the tip of the sickle-shaped nucleus, one on the apical boundary and two on either side of the post-acrosomal dense lamina that extends to the ventral tip of the perforatorium. In most parts, the perforatorium appears to be continuous with the cytoskeletal structures forming the perinuclear theca but biochemical and compositional differences between these two have been demonstrated (Oko et al., 1990; Oko and Maravei, 1994). The organization of the perinuclear theca appears to be more specialized with two distinct layers sandwiched between the plasma membrane and the nuclear envelope (Lalli and Clermont, 1981). The layer apposed to the plasma membrane appears denser than the region associated with the nuclear envelope. Interestingly, the inner layer of the perinuclear theca presents a thickening along the ventral part of the nucleus called the ventral spur (Figure 1.6). Functional significance of this structure is not known (Lalli and Clermont, 1981).

The perinuclear theca appears to bind the membranes of the sperm head. The membrane of the acrosomal vesicle is tightly attached to the nucleus by this cytoskeletal structure in the sperm head (Oko and Maravei, 1995). Several studies on infertile acrosome-less sperm from humans show that the proteins of the perinuclear theca are important for attachment of the acrosomal vesicle to the nucleus (Courtot et al., 1987; Escalier, 1990). Components of the perinuclear theca cytoskeleton also anchor the plasma membrane in the sperm head. The protein compositions of the perinuclear theca were studied for rat (Oko and Clermont, 1988), bull (Oko and Maravei, 1994), and mouse (Korley et al., 1997) sperm and were found to be relatively similar. Biochemically well-characterized proteins in the perinuclear theca

include calcins (Longo et al., 1987; Lecuyer et al., 2000), cyclin I and II (Hess et al., 1993; Rousseaux-Prevost et al., 2003), testis-specific actin capping proteins CPα3 (Hurst et al., 1998) and CPβ3 (von Bulow et al., 1997), PERF15 (Oko and Morales, 1994; Korley et al., 1997), somatic histones (Tovich and Oko, 2003), a histone H2B variant (Aul and Oko, 2002), STAT4 (Herrada and Wolgemuth, 1997) and actin-related protein Arp-T1 and Arp-T2 (Heid et al., 2002). In all the species examined, the 15 KDa protein representing PERF15 or Fatty Acid Binding Protein 9 (FABP9) formed the major component of these cytoskeletal networks (Oko and Morales, 1994).

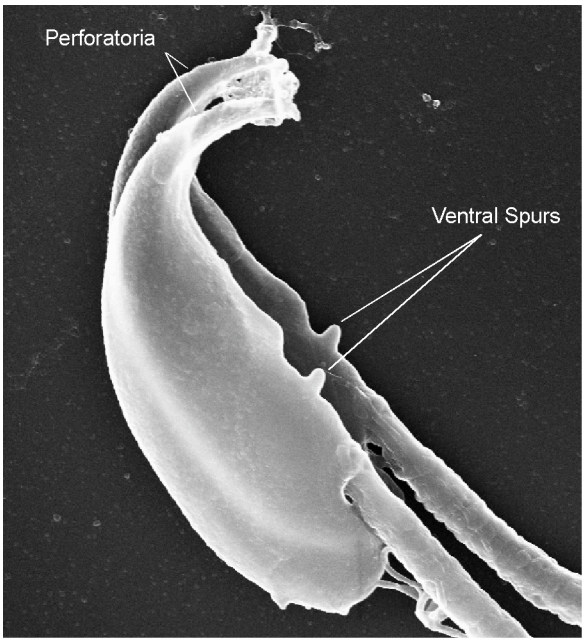

Figure 1.6. Scanning electron micrograph showing the sickle shape and structural features of two murine sperm heads. The perforatorium is composed of three rods extending over the tip of the sickle-shaped nucleus, one on the apical boundary and two on either side of the perinuclear theca cytoskeleton that extends to its ventral tip. The ventral spur arises from a thickening in the inner layer of the perinuclear theca that surrounds the nucleus.

Homology of FABP9 to the other 9 identified tissue-specific FABPs is highly conserved (Pouresmaeili et al., 1997). FABP9 has highest homology to myelin P2 protein of the peripheral nervous system, which is bound to the cytoplasmic aspect of the plasma membrane bilayer in the compact myelin sheath (Trapp et al., 1984). Although myelin P2 is known for its antigenic properties inducing allergic peripheral neuritis in rats (Rostami et al., 1984) similar to Guillan-Barre syndrome in humans (Viegas, 1997), its specific functions have not been elucidated. Based on similarities in amino acid sequences between FABP9 and myelin P2, it has been speculated that FABP9 could play a role in tethering membrane lipids to the perinuclear theca cytoskeleton in sperm (Pouresmaeili et al., 1997).

The acrosomal vesicle has two distinct regions, a thickened portion over the apical aspect of the nucleus forming the apical acrosome and a thinner region extending over the lateral surfaces of the nucleus called the equatorial region. Ultrastructural studies have shown that in murine sperm, only the apical acrosome undergoes exocytosis and releases its contents (Yanagimachi, 1994). One structure noted adjacent to the perifossal zone is the redundant nuclear envelope. This is a coiled sheath of nuclear membrane containing nuclear pores as a close hexagonal array formed as a result of nuclear condensation during spermiogenesis (Friend and Fawcett, 1974). The redundant nuclear envelope has been shown to contain an internal store for calcium (Ho and Suarez, 2003). The centrioles are contained in this perifossal zone and the distal centriole gives rise to the flagellar axoneme (Turner, 2003).

Flagellum

The flagellum of mammalian spermatozoa varies considerably in length depending on the species (e.g. ~190 μm long in the rat and only ~60 μm long in humans). It is commonly organized into four major parts: the connecting piece, the mid-piece, the principal piece and the end piece (Figure 1.4) (Fawcett, 1975). The connecting piece is the portion that is attached to the implantation fossa of the sperm head. From the modified distal centriole at this point, the microtubular axoneme extends the entire length of the sperm flagellum. A ring of 9 microtubule doublets surrounds a central pair to form the axoneme. Each of the outer doublets anchors inner and outer dynein arms

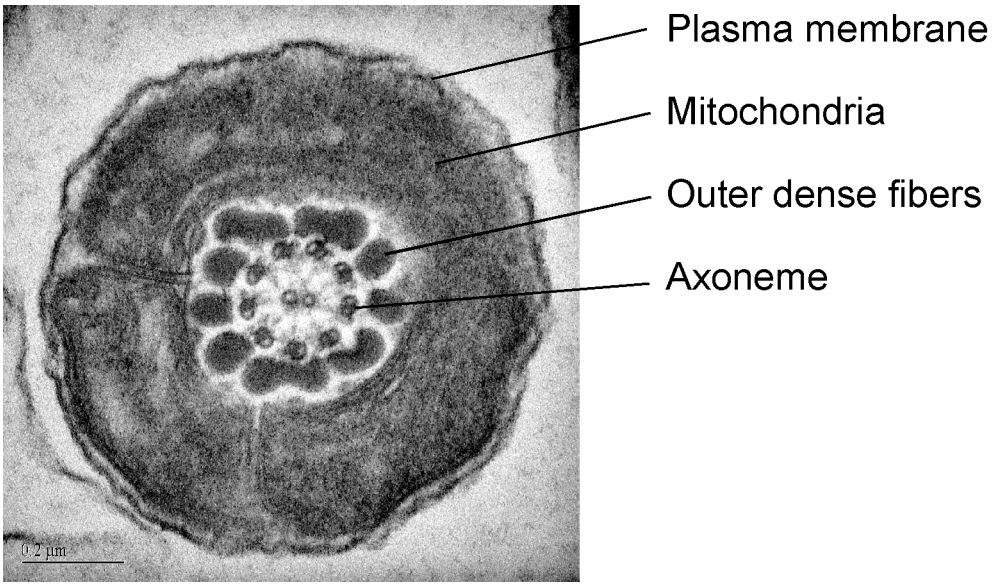

Figure 1.7. Transmission electron micrograph showing a cross-section through the mid-piece of the flagellum. A ring of 9 microtubule doublets surrounds a central pair to form the axoneme. 9 outer dense fibers run down in a radial fashion, one outside each outer microtubule doublet. These outer dense fibers are surrounded by a sheath formed by a characteristic helical arrangement of mitochondria enclosing the flagellum in this region.

responsible for generating flagellar motility (Baccetti et al., 1981). Radial spokes extend inwardly from the 9 microtubule doublets towards the central pair. The mid-piece extends from the connecting piece to about one-fourth of the sperm flagellum in murine sperm. The mid-piece marks the origin of sperm-specific cytoskeletal structures called the outer dense fibers (Yasuzumi, 1956; Fawcett and Ito, 1965); 9 outer dense fibers run down in a radial fashion, one outside each outer microtubule doublet. The outer dense fibers are composed of 6 major peptides (Vera et al., 1984) that are heavily disulfide bonded of which only 3 components have been identified: ODF1 (Morales et al., 1994), ODF2 (Shao et al., 1997) and Spag4 (Shao et al., 1999). These outer dense fibers are surrounded by a sheath formed by a characteristic helical arrangement of mitochondria enclosing the flagellum in this region (Hrudka, 1968b, a). A reticular network of cytoskeletal elements called the sub-mitochondrial lattice organizes this arrangement of mitochondria (Olson and Winfrey, 1986). The mitochondrial sheath and the sub-mitochondrial lattice terminate at a region called the annulus, marking the end of the mid-piece. The annulus is a specialized ring-like structure separating the mid-piece and the principal piece. The plasma membrane architecture and cytoskeletal framework of the annulus is distinct from other regions. Cortical organization by septin 4 has been shown to be required for formation of the annulus (Ihara et al., 2005; Kissel et al., 2005). From the annulus, the principal piece forms the major part of the flagellum. In the principal piece, the outer dense fibers associated with outer microtubular doublets 3 and 8 are replaced by longitudinal columns of the fibrous sheath. Lateral ribs of cytoskeletal elements of the fibrous sheath extend circumferentially and stabilize the principal piece (Turner, 2003). The plasma membrane lies directly apposed to

the fibrous sheath (Figure 1.7). Close to the distal end of the principal piece, the outer dense fibers and fibrous sheath terminate. The short remaining region of axonemal microtubules surrounded by plasma membrane forms the end piece.

Functional Compartmentalization in Sperm

Sperm have been efficiently designed to deliver the male genetic material to the egg. In order to facilitate the steps required while maintaining their streamlined form, they are constructed with compartmentalized metabolic and signaling pathways that allow them to carry out specific functions in specific regions. They do not carry any machinery for protein transcription or translation [reviewed in (Travis and Kopf, 2002)]. Therefore, functional pathways are pre-packaged into specific regions where responses can be modulated only at the post-translational level.

There are two aspects of compartmentalization in sperm: [1] concomitant with its polarized nature, regional compartments of signaling pathways exist (e.g., molecules required for sperm-egg interactions and mediating acrosomal exocytosis are localized to the sperm head) and [2] based on energy requirements, metabolic pathways are confined to specific regions in sperm (e.g., enzymes required for glycolysis are localized in the principal piece of the flagellum). Selected points regarding the compartmentalized functional design are shown in Figure 1.8.

Figure 1.8. Compartmentalization of selected signaling molecules, metabolic proteins and pathways in sperm. ***Signaling:*** The sperm head contains receptors for the zona pellucida glycoprotein ZP3, oocyte plama membrane fusion molecule like Izumo-1, heterotrimeric G proteins, adenylyl cyclases, protein kinase A (PKA), A-kinase anchoring protein 110 (AKAP 110), various voltage dependent cation channels (VDCC), protein kinase C (PKC), and various tyrosine kinases and phosphatases. The mid-piece has been shown to contain olfactory receptors, G-protein related kinases (GRK), cNMP-gated channels, PKA, and sperm AKAP 84. The principal piece also contains many of the signaling molecules found in other regions in addition to fibrous sheath-specific AKAPs, calcineurin and CATSPER channels. ***Metabolism:*** Glucose transporter 3 (Glut3) is present throughout the sperm, as is hexokinase-1-SC (HK1-SC). Glycolytic enzymes such as germ cell-specific isoform of glyceraldehyde 3-phosphate dehydrogenase (GAPDHs) are restricted to the principal piece. The voltage dependent anion channel porin 1 occurs in the mid-piece, whereas porin 2 occurs in the principal piece. Monocarboxylate transporters (MCT) 1 and 2 are found in the head and flagellum respectively coupled with lactate dehydrogenase (LDH-C4). [Modified from (Travis and Kopf, 2002)]

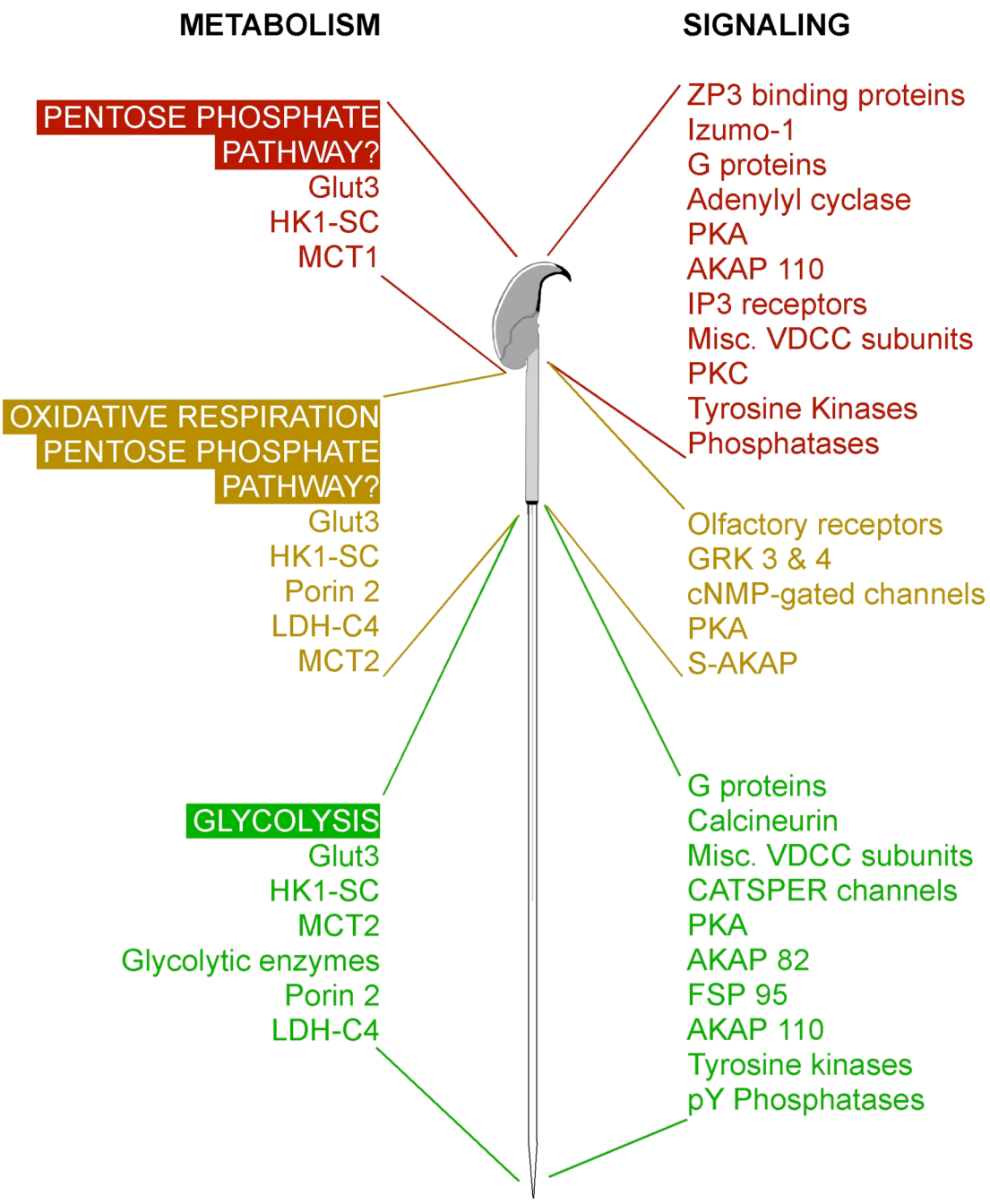
METABOLISM
SIGNALING
PENTOSE PHOSPHATE PATHWAY?
Glut3
HK1-SC
MCT1
OXIDATIVE RESPIRATION
PENTOSE PHOSPHATE PATHWAY?
Glut3
HK1-SC
Porin 2
LDH-C4
MCT2
GLYCOLYSIS
Glut3
HK1-SC
MCT2
Glycolytic enzymes
Porin 2
LDH-C4
ZP3 binding proteins
Izumo-1
G proteins
Adenylyl cyclase
PKA
AKAP 110
IP3 receptors
Misc. VDCC subunits
PKC
Tyrosine Kinases
Phosphatases
Olfactory receptors
GRK 3 & 4
cNMP-gated channels
PKA
S-AKAP
G proteins
Calcineurin
Misc. VDCC subunits
CATSPER channels
PKA
AKAP 82
FSP 95
AKAP 110
Tyrosine kinases
pY Phosphatases

Plasma membrane

The plasma membrane of the sperm forms distinct domains within the sperm head and tail (Friend, 1989). Topographical differences in these structures have been studied using electron microscopy (Friend, 1982). The existence of this domain architecture has been directly associated with specific functional compartmentalization of signaling and metabolic pathways (Travis et al., 2001a). Such organization in sperm membranes is also of interest because of the conserved and key role of sterol efflux in functional maturation of sperm by a process called capacitation (Chang, 1951; Austin, 1952; Davis, 1976) described below. The sterol content in the different sperm membrane domains has been visually evaluated using freeze-fracture techniques localizing filipin-sterol complexes under a scanning electron microscope (Friend and Fawcett, 1974; Friend, 1982; Pelletier and Friend, 1983; Suzuki, 1988; Lin and Kan, 1996). These results in sperm from several species show that sterols in the plasma membrane are unevenly distributed. Consistently, in all species studied, the plasma membrane overlying the acrosome (APM) is highly enriched in sterols whereas the post-acrosomal plasma membrane (PAPM) is deficient in sterols (Figure 1.9) (Suzuki, 1988; Visconti et al., 1999b). There are again structurally distinct regions within the APM termed the equatorial segment (ES), and the apical acrosome (AA) (Lin and Kan, 1996).

Two roles have been hypothesized for the sterol enrichment seen in the APM: (a) Targeting proteins involved in sperm-egg interactions and the regulation of acrosomal exocytosis to this region; (b) Making the APM rigid thereby preventing premature fusion with the acrosomal membrane and release of lytic contents. For (b), it is suggested that the induction of sterol efflux during capacitation could make the APM more responsive to signal

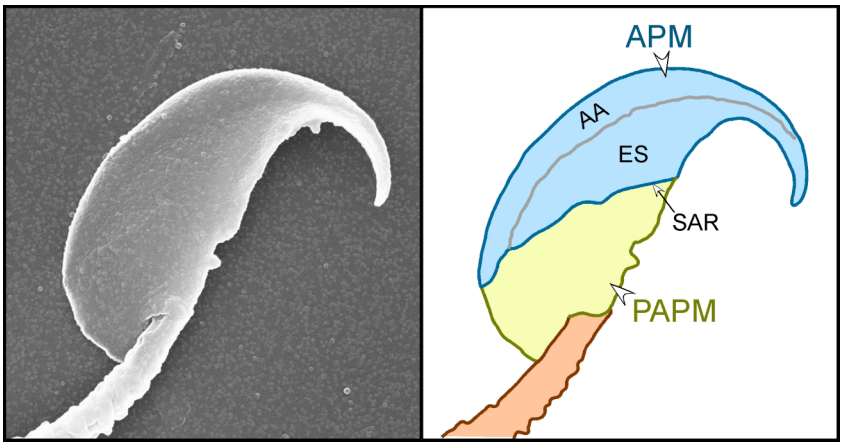

Figure 1.9. Scanning electron micrograph and a matched schematic trace showing the lateral view of a murine sperm head. The plasma membrane of the sperm head is divided into two major regions, the APM and the PAPM, based on morphology and differences in membrane protein and lipid compositions. The APM and PAPM are delimited by a topographical feature known as the sub-acrosomal ring (SAR). On the basis of structure and function the APM is itself divided into the apical acrosome (AA), the region where membrane fusion will take place between the plasma membrane and the acrosomal vesicle, and the equatorial segment (ES). The hook-like structure is called the perforatorium.

transduction and fusogenic (Visconti et al., 1999a). Sterol distribution also contributes to structural heterogeneities within the sperm tail plasma membrane (Friend and Fawcett, 1974; Koehler, 1983). Membrane specializations seen in the tail are distinct by surface topology over regions of the posterior ring, annulus and the flagellar zipper (Friend and Fawcett, 1974; Koehler, 1983; Friend, 1989; Lin and Kan, 1996). TEM studies show that the posterior ring demarcating the boundary between the PAPM and the connecting piece, and the annulus separating the mid-piece from the principal piece, overlie dense plaque-like fibrillar material potentially segregating the cytoplasmic components between these regions (Friend and Fawcett, 1974;

Koehler, 1983). The flagellar zipper extends from the annulus down to variable lengths in the principal piece (Koehler, 1983). In fixed cells, both the annulus and zipper have been shown to be deficient in sterols compared to the remainder of the flagellar membranes (Pelletier and Friend, 1983; Lin and Kan, 1996). The flagellar zipper has been suggested to be a sense organ transmitting selected substances or information to navigate the flagellar propulsion apparatus (Koehler, 1983). The plasma membrane specializations seen in the sperm flagellum could play a role in regulating signaling events required for modulating sperm motility patterns and hyperactivation.

Capacitation

In the 1950s, it was discovered that sperm are not immediately ready to fertilize the oocyte after ejaculation; they first need to undergo a process of functional maturation called “capacitation” (Chang, 1951; Austin, 1952). Capacitation results in two specific changes in sperm function. First, the sperm head acquires the ability to respond to stimuli triggering exocytosis of the acrosomal vesicle. Second, the flagellum of the sperm acquires a “hyperactivated” pattern of motility. By mimicking *in vivo* conditions encountered by sperm in the oviductal fluid, several studies have dissected the requirements for sperm capacitation *in vitro* using defined media. Although these studies made it is possible to capacitate sperm from several species *in vitro*, the complex cascade of molecular events that occur during capacitation is not completely understood [reviewed in (Visconti et al., 2002)].

Stimuli required for capacitation

Sterol efflux from the plasma membrane mediated by albumin and HDLs in the female tract is a conserved and key stimulus for capacitation (Davis et al., 1979; Davis, 1980, 1981; Go and Wolf, 1985; Langlais et al., 1988; Ehrenwald et al., 1990). This can be mimicked *in vitro* using high-density lipoproteins (HDLs), bovine serum albumin (BSA) or 2-hydroxy propyl cyclodextrin (2-OHCD) in the medium (Therien et al., 1997; Choi and Toyoda, 1998; Visconti et al., 1999a). Functional reversal of the capacitation process or decapacitation can be achieved by adding exogenous cholesterol back to sperm (Davis, 1974, 1976) showing the importance of sterol efflux in sperm function. The removal of sterols (cholesterol and desmosterol) from the plasma membrane is highly conserved in mammals and is upstream of other signaling events driving the capacitation process (Visconti et al., 2002). Besides sterol efflux, many species including rodents also require the presence of calcium and bicarbonate ions (Neill and Olds-Clarke, 1987; DasGupta et al., 1993; Visconti et al., 1995a) and glucose (Urner et al., 2001; Travis et al., 2004). Capacitation of sperm using these stimuli effects changes in membrane properties and initiates signaling leading to several events (Figure 1.10).

From a functional standpoint, removal of sterols results in a decrease in sterol:phospholipid ratio in sperm membranes during capacitation (Davis, 1981). In particular, this accounts for a decrease in sterol content of the sterol-rich APM (Tesarik and Flechon, 1986; Suzuki-Toyota et al., 2000) and an increase in overall membrane fluidity (Wolf et al., 1986; Companyo et al., 2007). Both loss of sterols in the APM and increase in membrane fluidity have been hypothesized as events rendering the APM fusogenic and primed for

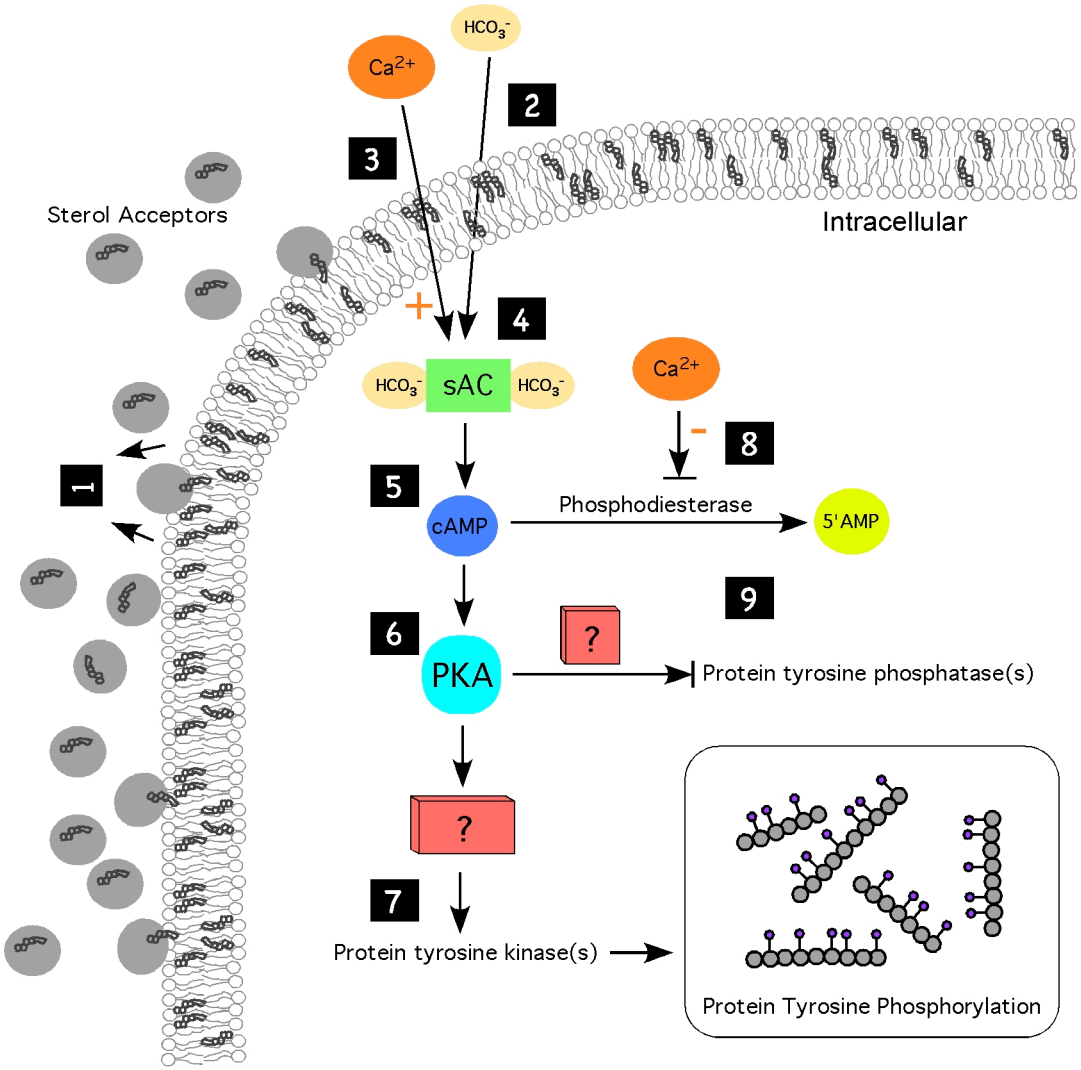

Figure 1.10. Schematic showing signaling events during sperm capacitation. (1) Efflux of sterols from the plasma membrane by sterol acceptors, e.g. oviductal albumin and HDLs; (2) Bicarbonate influx; the order of events for (1) and (2) is still unclear; (3) Calcium influx; (4) Bicarbonate stimulates soluble adenylyl cyclase activity; (5) This leads to the production of cyclic AMP; (6) cAMP activates PKA; (7) PKA acts either directly or indirectly to activate protein tyrosine kinase(s); (8) Calcium facilitates elevated cAMP levels by negatively regulating its breakdown; (9) PKA could simultaneously prevent dephosphorylation events by negatively regulating phosphatases. [Modified from (Visconti et al., 2002)]

responding to triggers regulating acrosomal exocytosis. These changes have been linked to redistribution of membrane components within the APM, for example, unidentified glycoconjugates (Cross and Overstreet, 1987; Rochwerger and Cuasnicu, 1992), proteins associated with putative membrane rafts e.g. caveolin-1 and flotillin-1 (van Gestel et al., 2005), and more recently proteins involved in membrane fusion events e.g. syntaxin and VAMP (Tsai et al., 2007) have been reported to redistribute during capacitation.

Another plasma membrane change during capacitation is the loss of bilayer phospholipid asymmetry and lipid order (Harrison et al., 1996; Flesch et al., 2001). This was reported to occur through a cAMP dependent pathway driven by bicarbonate ions (HCO_3^-) in the medium (Gadella and Harrison, 2000). In the extracellular environment, sperm are exposed to different ion concentrations and osmolarities. Sperm are maintained under high K^+, low Na^+ and HCO_3^- concentrations (Brooks, 1983) encountered in the cauda epididymis. They then encounter the seminal plasma and the uterine/oviductal secretions that contain low K^+ and high Na^+ and HCO_3^- concentrations (Brooks, 1983; Yanagimachi, 1994). Changes in ion flux across the sperm plasma membrane mediated by both membrane changes and extracellular ion concentrations leads to shift in the resting membrane potential of sperm during capacitation to a hyperpolarized state (Zeng et al., 1995; Arnoult et al., 1999). This has been suggested to be partially due to an enhanced K^+ permeability due to the loss of inhibitory modulation of K^+ channels during capacitation (Zeng et al., 1995). Hyperpolarization during capacitation is considered to prime the ability to generate transient Ca^{2+} elevations required for acrosomal exocytosis (Visconti et al., 2002).

Encountering HCO_3^- in the seminal plasma by sperm during ejaculation results in transmembrane movement of this anion and could explain the observed increase in intracellular pH (Zeng et al., 1996). An additional target for HCO_3^- is cAMP metabolism (Visconti et al., 1990; Chen et al., 2000). The sperm soluble adenylyl cyclase (sAC) activity is highly responsive to HCO_3^- anion (Okamura et al., 1985; Chen et al., 2000). Triggering the cAMP pathway results in protein kinase A (PKA) activation; there is subsequent tyrosine phosphorylation of multiple proteins in sperm mediated through a still unclear mechanism (Visconti et al., 1995a; Visconti et al., 1995b; Visconti et al., 2002). However, the functional significance of these phosphorylation events remains unclear. Another pathway activated during capacitation is phosphatidyl inositol (PI) signaling. PI signaling has been reported to mediate cytoskeletal remodeling events during capacitation (Brener et al., 2003; Breitbart et al., 2005) and elevate intracellular calcium by release from internal stores via the inositol 1,4,5-triphosphate (IP3)-gated calcium channels (Ho and Suarez, 2001a; Herrick et al., 2005). All these signaling events that occur during capacitation are ultimately transduced into hyperactivated motility in the flagellum and priming of the membranes of the sperm head for exocytosis, both events essential for fertility.

Hyperactivation

Capacitated sperm attain a vigorous motility pattern called hyperactivation (Yanagimachi, 1969). Several studies have shown that hyperactivation would facilitate sperm movement in thick oviductal mucus (Suarez and Dai, 1992; Suarez et al., 1992), and increases the rate of successful zona penetration (Stauss et al., 1995). Hyperactivation is driven by

increases in intracellular Ca^{2+} (Suarez et al., 1992; Suarez et al., 1993; Yanagimachi, 1994). Signaling via the PI pathway and IP3-mediated release of Ca^{2+} from internal stores play an important role in hyperactivated motility (Ho and Suarez, 2001a, b). Recent findings show that Ca^{2+} entry via the plasma membrane CatSper1 and CatSper2 channels supplement Ca^{2+} released from internal stores and are required for sustained hyperactivated motility (Marquez et al., 2007). However, factors behind the initiation of hyperactivation of capacitated sperm are not completely clear.

Acrosomal Exocytosis

Acrosomal exocytosis is a unique type of regulated exocytosis where the apical acrosomal vesicle fuses at multiple points with the overlying plasma membrane releasing its contents over time (Figure 1.11). One characteristic of this exocytotic reaction is the vesiculation and release of the plasma membrane and the outer acrosomal membrane (OAM) as hybrid vesicles resulting in the exposure of the inner acrosomal membrane (IAM) after the release of acrosomal contents (Barros et al., 1967).

Signaling events driving acrosomal exocytosis

This exocytotic reaction is initiated *in vivo* by sperm binding to the zona pellucida of the oocyte, which induces a transient increase in cytosolic calcium triggering the exocytotic machinery (Yanagimachi and Usui, 1974). A glycoprotein component of the zona pellucida, ZP3 has been implicated as the major trigger for acrosomal exocytosis (Roldan et al., 1994). Several receptors for ZP3 on/in sperm have been identified [for a review see (Tanphaichitr et al., 2007)], suggesting a functional redundancy for this important interaction. One

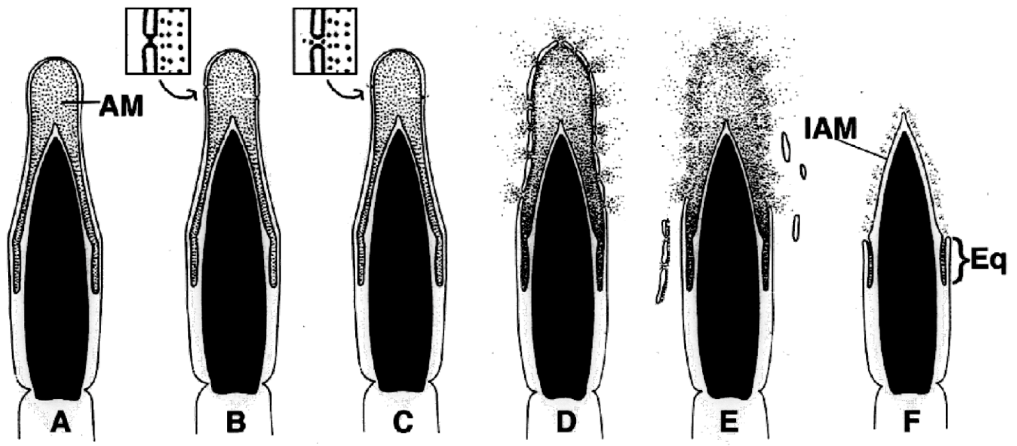

Figure 1.11. Schematic showing stages of acrosomal exocytosis. Longitudinal section through the sperm head shows the acrosomal vesicle seated over the apical region of the nucleus (AM: acrosomal matrix; Part A). In capacitated cells exposed to specific stimuli, point fusions begin to occur between the outer acrosomal membrane (OAM) and the overlying plasma membrane (APM; Part B). This progressively increases (Parts C and D) resulting in the regulated release of acrosomal matrix contents. This leads to more advanced stages of the exocytotic process (Part E) when multiple points of fusion between the OAM and APM results in the formation of hybrid vesicles that are released. After dispersal of the acrosomal contents, the inner acrosomal membrane (IAM) becomes exposed (Eq: Equatorial region). [Modified from (Yanagimachi, 1994)]

component of ZP3-mediated signal transduction required for this exocytotic reaction is membrane PI-signaling (Fukami et al., 2001; Fukami et al., 2003). Phosphorylation of membrane PI results in the production of phosphatidylinositol-4,5-bisphosphate (PIP2) resulting in the elevation of intracellular Ca^{2+} due to sustained influx via TRPC channels (O'Toole et al., 2000; Jungnickel et al., 2001). ZP3 simultaneously triggers the accumulation of membrane phosphatidylinositol-3,4,5-triphosphate (PIP3) via a phosphatidylinositol-3-kinase (PI3K) activation (Jungnickel et al., 2007). The

first calcium increase driven by PIP2 activates PLC isoforms, generating inositol-3,4,5-triphosphate (IP3) from PIP2 which opens IP3-receptor gated Ca^{2+} channels in the acrosomal membrane; this increase triggers store-operated Ca^{2+} channels in the plasma membrane causing a second sustained Ca^{2+} increase that triggers acrosomal exocytosis (Darszon et al., 2001; Jungnickel et al., 2001). The free intracellular calcium increase during acrosomal exocytosis has been measured to be approximately 10 μM compared to 0.1 μM or less in non-capacitated cells (Bailey and Storey, 1994; Arnoult et al., 1999). Diacyl glycerol (DAG), another membrane product of PIP2 hydrolysis can modulate membrane curvature and has been suggested to play a role in membrane fusion (Corda et al., 2002). PIP3 has also been shown to directly modulate signaling events associated with acrosomal exocytosis via downstream kinases Akt and PKCζ (Jungnickel et al., 2007). PKC inhibitors have been demonstrated to inhibit acrosomal exocytosis (De Jonge et al., 1991). In addition to downstream effectors of PI-signaling, several studies have indicated that other membrane lipid signaling pathways including hydrolysis of lysophospholipids and arachidonic acid by PLA_2 play a role in acrosomal exocytosis (Yuan et al., 2003; Pietrobon et al., 2005). Using inhibitors, it was shown that preventing hydrolysis of lysophospholipids and arachidonic acid by PLA2 could inhibit the exocytotic reaction (Meizel and Turner, 1984). However, mechanistic insight into this pathway in sperm is still unclear.

Exocytotic regulation and machinery

Based on current knowledge, the SNARE hypothesis still forms the core of the acrosomal exocytosis model. According to this model (Mayorga et al.,

2007), soluble NSF attachment receptors (SNAREs) are locked in inactive cis complexes (De Blas et al., 2005). Signaling events resulting in cAMP and cytosolic Ca^{2+} increase activate Rab3A (Belmonte et al., 2005; Lopez et al., 2007). Subsequently, N-ethylmaleimide sensitive factor (NSF) and synaptosome-associated protein (SNAP) disassemble SNARE complexes that are then able to form trans complexes (De Blas et al., 2005). It has been suggested that the exocytotic event is paused at this stage until the final calcium surge triggers fusion events (De Blas et al., 2002). In contrast to the above model, it has been suggested that transitional intermediates of membrane fusion events takes place between the plasma membrane and the outer acrosomal membrane (Kim and Gerton, 2003). This would be analogous to “kiss and run” vesicular exocytotic events demonstrated in neuronal synapses (He et al., 2006). However, it could be that despite completion of membrane fusion events, acrosomal contents in these cases are gradually dispersed as a result of their inherent solubilities (Hardy et al., 1991; Kim et al., 2001) or require proteolytic processing prior to release (DiCarlantonio and Talbot, 1988). Furthermore, pH increase in the exposed peripheral acrosomal matrix compared to the acidic core could lead to localized activation of acrosomal proteases that can act to process the regulated release of matrix contents (Nakanishi et al., 2001).

Biomembranes

According to the Singer and Nicholson model (Singer and Nicolson, 1972), the fluid mosaic structure of biological membranes is formally analogous to a two-dimensional oriented solution of integral proteins (or lipoproteins) in a viscous phospholipid bilayer solvent. This model has

survived for more than three decades and its basic features predict both interspersion of proteins and lipids and their ability to undergo dynamic rearrangements. However, some recent functional findings on mobility of membrane lipids and proteins suggest a considerable lateral heterogeneity in the biological membrane structure, at least on a nanometer scale [reviewed in (Vereb et al., 2003)].

The raft hypothesis

One postulate of the Singer-Nicholson model, that molecular components in the membrane have lateral and rotational freedom and random distribution has been challenged by several observations. Initial evidence for the existence of membrane lipid organization into structurally distinct domains came from a study examining emission polarization using 1,6-diphenul-1,3,5-hexatriene (DPH) and 8-anilino-1-napthalene sulfomate (ANS) in mammalian cells (Klausner et al., 1980). Recent studies provided additional compelling evidence lateral heterogeneity in cell membranes, for example the sorting of membrane glycosphingolipids in a non-random manner to the apical membrane of polarized epithelial cells (Simons and van Meer, 1988; van Meer and Simons, 1988). This was followed by observations that glycosphingolipid clusters are relatively insoluble in Triton X-100 at 4˚C, forming what were termed “detergent-resistant membranes” (DRMs) (Schroeder et al., 1994; Brown and London, 1997). DRMs were shown to have a light buoyant density in sucrose density gradients and were rich in both cholesterol and glycophosphatidyl inositol (GPI)-anchored proteins (Brown, 1994). Although the existence of lateral heterogeneity in biological and synthetic membranes showing fluid-fluid phase separations at low temperatures had been long

demonstrated (Hui and Parsons, 1975, 1976), debate on the existence of lateral heterogeneity in live cell membranes persisted. In addition to phase separations, synthetic membranes constructed with glycosphingolipids, GPI-anchored proteins and cholesterol recapitulated detergent-resistant characteristics of glycosphingolipid clusters (Dietrich et al., 2001a; Dietrich et al., 2001b) as seen in biological membranes. This finding related the concept of lateral heterogeneity to detergent resistance and suggested that these are properties purely driven by the membrane lipid composition.

Characterizing these membrane heterogeneities in a definitive way has proven difficult and artifacts induced by the use of fixation and/or crosslinking reagents used to visualize these domains in live cells incited controversy in this field [reviewed in (Munro, 2003)]. The unusual spatial and temporal properties of lateral heterogeneities in live biological membranes are due to: (a) an abundance of transmembrane/membrane-associated/lipid -binding proteins, (b) interactions with underlying cytoskeletal structures, (c) maintenance of bilayer asymmetry and (d) vesicular traffic and membrane recycling systems These properties of live biological membranes have made visualization and mechanistic understanding of these heterogeneities in live cells a challenge (Jacobson et al., 2007).

Summing the present state of knowledge, several models have been put forth to explain how membrane domains might be segregated. One property easily demonstrated in synthetic model membranes is lipid-lipid interactions, which show a range of domain sizes at different transition temperatures based on the membrane lipid mixture used (Dietrich et al., 2001a; de Almeida et al., 2005). This existence of multiple thermodynamic phases has also been recently demonstrated in plasma membrane-derived

vesicles (Baumgart et al., 2007). However, in complex biological systems, the nature of membrane phases is complicated by interactions with a vast diversity of proteins and the maintenance of bilayer asymmetry. Some of these proteins associate with different membrane lipids and exist as multiple lipid-protein composites (Jacobson et al., 2007). The lipid “shell” model suggests that specific membrane-associated proteins might induce membrane micro-domains to form due to their preferential binding to certain lipid species or pre-assembled lipid complexes (Anderson and Jacobson, 2002). Although this model allows for dynamic lipid exchange with other bilayer lipids, protein concentrations of the specific lipid-associating proteins could govern the scale and stability of this lateral organization.

Alternatively, the membrane-associated cytoskeleton has been implicated in organizing membrane domains by providing certain lipid and protein tethers within the membrane. Some of the membrane-associated proteins are cytoskeletal elements themselves (e.g. spectrin) (Maksymiw et al., 1987), or are proteins anchored to cytoskeletal structures (e.g. cadherins) (Causeret et al., 2005). By observing single molecule trajectories moving within the membrane, stable regions (200 to 300 nm) called transient confinement zones were identified in which a traveling molecule can be trapped for several seconds (Simson et al., 1995; Dietrich et al., 2002). These regions are temperature independent and their integrity depends on the level of cholesterol. Transient confinement zones have been suggested to be either contiguous cholesterol-dependent liquid ordered regions in the membrane or involve the membrane cytoskeleton. A variation of this model involves the existence of transmembrane proteins as a “picket fence” thereby restricting lateral diffusion (Sheets et al., 1997; Dietrich et al., 2002). Also relating to

membrane-cytoskeletal interactions, studies have shown that the plasma membrane is fabricated as distinct compartments. According to this membrane compartmentation model, lipid and protein molecules can diffuse freely within the defined compartments; however, the diffusion rate of lipids in a compartmentalized area is determined by size of the compartments and the frequency of jumps (termed “hop diffusion”) between compartments (Sako and Kusumi, 1994, 1995). For all the above models, it is understood that cell type specific factors (e.g. membrane and protein composition) could also govern the mechanism(s) involved in the formation of lateral heterogeneities.

After careful consideration of all the variables, a recent consensus on the definition for membrane rafts was reached at the 2006 Keystone Symposium: “Membrane rafts are small (10-200 nm), heterogenous, highly dynamic, sterol- and sphingolipid-enriched domains that compartmentalize cellular processes. Small rafts can sometimes be stabilized to form larger platforms through protein-protein and protein-lipid interactions” (Pike, 2006). This definition encompasses the complexities and current understanding of membrane rafts in live cells.

Characteristics of sperm membranes

In addition to the distinct regional organization as described above, there are fundamental differences between the plasma membrane compositions of mammalian sperm compared to that of most somatic cells. This is characterized by an abundance of ether-linked lipids (Evans et al., 1980) and very long chain fatty acids (Poulos et al., 1986), the presence of desmosterol as a mature sterol in the membrane (Bleau and VandenHeuvel, 1974) and the presence of a large fraction of poly-unsaturated lipid chains

(e.g. 22:6 and 22:5) (Selivonchick et al., 1980; Wolf et al., 1990) and sulfogalactosylglycerolipids (Bou Khalil et al., 2006). In addition to these basic differences, there is dramatic remodeling of the membrane during epididymal maturation, exposure to seminal plasma and transit in the female reproductive tract.

When sperm exit the testes, membrane remodeling is mainly due to local external influences. First, they are exposed to a diversity of epididymosomes (membrane vesicles secreted by the epididymal epithelium) during transit through the epididymis (Evans and Setchell, 1979; Sullivan et al., 2005; Rejraji et al., 2006). These epididymosomes have been shown to modulate both protein and lipid composition of sperm plasma membrane during epididymal transit [reviewed in (Sullivan et al., 2007)]. Second, they are exposed to seminal plasma components at ejaculation. Most studies of seminal plasma have been conducted on bulls due to economic value and ready availability. From these studies, it was discovered that several seminal plasma proteins could bind to the sperm surface (Manjunath and Therien, 2002). These bind specifically to choline phospholipids (phosphatidyl choline, phosphatidyl choline plasmalogen and sphingomyelin) (Desnoyers and Manjunath, 1992). Also, seminal plasma proteins are capable of inducing sterol efflux in a time and dose dependent manner (Therien et al., 1998) and a functional role for seminal plasma in facilitating capacitation in ejaculated sperm has been suggested (Lusignan et al., 2007). The binding of seminal plasma proteins to sperm membranes can dramatically alter their properties (Greube et al., 2001; Buttke et al., 2006; Kawano and Yoshida, 2007; Tannert et al., 2007). This has been a source of variation in studies addressing sperm membrane properties even within the same species. Most of these can be

addressed by how the sperm was collected, either from the epididymis or after ejaculation. However, the functional relevance of membrane lipid modifications in sperm on exposure to seminal plasma is yet to be definitively demonstrated.

Very little is known about the properties of endogenous lipids in non-capacitated sperm membranes. However, several studies have been performed using exogenous lipid probes to reflect membrane properties of sperm. Exogenous probes [DiIC16 and 5-(N-octa-decanoyl) aminofluorescein (ODAF)] have been used to measure lipid diffusion in the different morphologically distinct membrane regions of sperm (APM, PAPM, mid-piece and principal piece)(Wolf and Voglmayr, 1984; Wolf, 1995; Ladha et al., 1997; Wolfe et al., 1998). Taken together, the major conclusions from these studies were: (a) There were regional differences in lipid diffusion in sperm; (b) There was lateral diffusion between the major morphological regions of the plasma membrane; (c) Epididymal maturation changes diffusibility in the different regions of the plasma membrane. None of these studies reported a substantial decrease in diffusion rates in the sterol-rich APM compared to the PAPM. However, an early report on ram sperm has suggested that non-diffusing membrane regions exist in the anterior region of the sperm head; in their experiments vesicles derived from sperm membranes also retained these non-diffusing fractions (Wolf et al., 1988). Another interesting finding is that lateral diffusion of ODAF in membranes of bull sperm was abolished after cell death (Ladha et al., 1997). However, mouse, boar, ram and guinea pig sperm did not have this property (Wolfe et al., 1998). Several of these studies were performed using ejaculated sperm, which as mentioned are exposed to an abundance of lipids and lipid-binding proteins in the seminal plasma. A more recent report on murine epididymal sperm has claimed that the APM in live

cells is liquid ordered based on DiIC16 segregation to this domain (Sleight et al., 2005). However, this property was not observed in earlier studies described on several different species with the same reagent (Ladha et al., 1997; James et al., 2004).

Objectives

As highlighted in the above review, sperm are highly structured cells embarking on a single mission: procreation. The functional importance of sperm membrane organization is highlighted by the fact that efflux of sterols from the plasma membrane in the female reproductive tract is a required stimulus for capacitation. However, there is no information connecting the efflux of sterols to downstream signaling effectors mainly because little is known about the organization and properties of endogenous membrane lipids in live sperm.

Therefore, the objectives of the present study are: [1] to examine the organization of sterols and an endogenous glycosphingolipid G_{M1} in the sperm plasma membrane, [2] to investigate membrane changes that occur after exposure to stimuli mediating the process of capacitation, [3] to understand the nature and dynamics of the sperm membrane and, [4] to understand the mechanisms behind membrane lipid segregation in sperm.

REFERENCES

Abou-Haila, A., and Tulsiani, D.R. (2000). Mammalian Sperm Acrosome: Formation, Contents, and Function. Arch Biochem Biophys 379, 173-182.

Anderson, R.G., and Jacobson, K. (2002). A Role for Lipid Shells in Targeting Proteins to Caveolae, Rafts, and Other Lipid Domains. Science 296, 1821-1825.

Arnoult, C., Kazam, I.G., Visconti, P.E., Kopf, G.S., Villaz, M., and Florman, H.M. (1999). Control of the Low Voltage-Activated Calcium Channel of Mouse Sperm by Egg Zp3 and by Membrane Hyperpolarization During Capacitation. Proc Natl Acad Sci U S A 96, 6757-6762.

Aul, R.B., and Oko, R.J. (2002). The Major Subacrosomal Occupant of Bull Spermatozoa Is a Novel Histone H2b. Dev Biol 242, 376-387.

Austin, C.R. (1952). The Capacitation of the Mammalian Sperm. Nature 170, 326.

Baccetti, B. (1986). Evolutionary Trends in Sperm Structure. Comp Biochem Physiol A 85, 29-36.

Baccetti, B., Burrini, A.G., Pallini, V., and Renieri, T. (1981). Human Dynein and Sperm Pathology. J Cell Biol 88, 102-107.

Bailey, J.L., and Storey, B.T. (1994). Calcium Influx into Mouse Spermatozoa Activated by Solubilized Mouse Zona Pellucida, Monitored with the Calcium Fluorescent Indicator, Fluo-3. Inhibition of the Influx by Three Inhibitors of the Zona Pellucida Induced Acrosome Reaction: Tyrphostin A48, Pertussis Toxin, and 3-Quinuclidinyl Benzilate. Mol Reprod Dev 39, 297-308.

Barros, C., Bedford, J.M., Franklin, L.E., and Austin, C.R. (1967). Membrane Vesiculation as a Feature of the Mammalian Acrosome Reaction. J Cell Biol 34, C1-5.

Baumgart, T., Hammond, A.T., Sengupta, P., Hess, S.T., Holowka, D.A., Baird, B.A., and Webb, W.W. (2007). Large-Scale Fluid/Fluid Phase Separation of Proteins and Lipids in Giant Plasma Membrane Vesicles. Proc Natl Acad Sci U S A 104, 3165-3170.

Belmonte, S.A., Lopez, C.I., Roggero, C.M., De Blas, G.A., Tomes, C.N., and Mayorga, L.S. (2005). Cholesterol Content Regulates Acrosomal Exocytosis by Enhancing Rab3a Plasma Membrane Association. Dev Biol 285, 393-408.

Bermudez, D., Escalier, D., Gallo, J.M., Viellefond, A., Rius, F., Perez de Vargas, I., and Schrevel, J. (1994). Proacrosin as a Marker of Meiotic and Post-Meiotic Germ Cell Differentiation: Quantitative Assessment of Human Spermatogenesis with a Monoclonal Antibody. J Reprod Fertil 100, 567-575.

Bleau, G., and VandenHeuvel, W.J. (1974). Desmosteryl Sulfate and Desmosterol in Hamster Epididymal Spermatozoa. Steroids 24, 549-556.

Bou Khalil, M., Chakrabandhu, K., Xu, H., Weerachatyanukul, W., Buhr, M., Berger, T., Carmona, E., Vuong, N., Kumarathasan, P., Wong, P.T., Carrier, D., and Tanphaichitr, N. (2006). Sperm Capacitation Induces an Increase in Lipid Rafts Having Zona Pellucida Binding Ability and Containing Sulfogalactosylglycerolipid. Dev Biol 290, 220-235.

Brandon, C.I., Jr., Srivastava, P.N., Heusner, G.L., and Fayrer-Hosken, R.A. (1997). Extraction and Quantification of Acrosin, Beta-N-Acetylglucosaminidase, and Arylsulfatase-a from Equine Ejaculated Spermatozoa. J Exp Zool 279, 301-308.

Breitbart, H., Cohen, G., and Rubinstein, S. (2005). Role of Actin Cytoskeleton in Mammalian Sperm Capacitation and the Acrosome Reaction. Reproduction 129, 263-268.

Brener, E., Rubinstein, S., Cohen, G., Shternall, K., Rivlin, J., and Breitbart, H. (2003). Remodeling of the Actin Cytoskeleton During Mammalian Sperm Capacitation and Acrosome Reaction. Biol Reprod 68, 837-845.

Brooks, D.E. (1983). Epididymal Functions and Their Hormonal Regulation. Aust J Biol Sci 36, 205-221.

Brown, D. (1994). Gpi-Anchored Proteins and Detergent-Resistant Membrane Domains. Braz J Med Biol Res 27, 309-315.

Brown, D.A., and London, E. (1997). Structure of Detergent-Resistant Membrane Domains: Does Phase Separation Occur in Biological Membranes? Biochem Biophys Res Commun 240, 1-7.

Buttke, D.E., Nelson, J.L., Schlegel, P.N., Hunnicutt, G.R., and Travis, A.J. (2006). Visualization of Gm1 with Cholera Toxin B in Live Epididymal Versus Ejaculated Bull, Mouse, and Human Spermatozoa. Biol Reprod 74, 889-895.

Causeret, M., Taulet, N., Comunale, F., Favard, C., and Gauthier-Rouviere, C. (2005). N-Cadherin Association with Lipid Rafts Regulates Its Dynamic Assembly at Cell-Cell Junctions in C2c12 Myoblasts. Mol Biol Cell 16, 2168-2180.

Chang, M.C. (1951). Fertilizing Capacity of Spermatozoa Deposited into the Fallopian Tubes. Nature 168, 697-698.

Chen, Y., Cann, M.J., Litvin, T.N., Iourgenko, V., Sinclair, M.L., Levin, L.R., and Buck, J. (2000). Soluble Adenylyl Cyclase as an Evolutionarily Conserved Bicarbonate Sensor. Science 289, 625-628.

Cheng, A., Le, T., Palacios, M., Bookbinder, L.H., Wassarman, P.M., Suzuki, F., and Bleil, J.D. (1994). Sperm-Egg Recognition in the Mouse: Characterization of Sp56, a Sperm Protein Having Specific Affinity for Zp3. J Cell Biol 125, 867-878.

Choi, Y.H., and Toyoda, Y. (1998). Cyclodextrin Removes Cholesterol from Mouse Sperm and Induces Capacitation in a Protein-Free Medium. Biol Reprod 59, 1328-1333.

Companyo, M., Iborra, A., Villaverde, J., Martinez, P., and Morros, A. (2007). Membrane Fluidity Changes in Goat Sperm Induced by Cholesterol Depletion Using Beta-Cyclodextrin. Biochim Biophys Acta 1768, 2246-2255.

Corda, D., Hidalgo Carcedo, C., Bonazzi, M., Luini, A., and Spano, S. (2002). Molecular Aspects of Membrane Fission in the Secretory Pathway. Cell Mol Life Sci 59, 1819-1832.

Courtot, A.M., Escalier, D., Jouannet, P., and David, G. (1987). Impaired Ability of Human Spermatozoa to Penetrate Zona-Free Hamster Oocytes: Is a Postacrosomal Sheath Anomaly Involved? Gamete Res 17, 145-156.

Cross, N.L., and Overstreet, J.W. (1987). Glycoconjugates of the Human Sperm Surface: Distribution and Alterations That Accompany Capacitation in Vitro. Gamete Res 16, 23-35.

Darszon, A., Beltran, C., Felix, R., Nishigaki, T., and Trevino, C.L. (2001). Ion Transport in Sperm Signaling. Dev Biol 240, 1-14.

DasGupta, S., Mills, C.L., and Fraser, L.R. (1993). Ca(2+)-Related Changes in the Capacitation State of Human Spermatozoa Assessed by a Chlortetracycline Fluorescence Assay. J Reprod Fertil 99, 135-143.

Davis, B.K. (1974). Decapacitation and Recapacitation of Rabbit Spermatozoa Treated with Membrane Vesicles from Seminal Plasma. J Reprod Fertil 41, 241-244.

Davis, B.K. (1976). Inhibitory Effect of Synthetic Phospholipid Vesicles Containing Cholesterol on the Fertilizing Ability of Rabbit Spermatozoa. Proc Soc Exp Biol Med 152, 257-261.

Davis, B.K. (1980). Interaction of Lipids with the Plasma Membrane of Sperm Cells. I. The Antifertilization Action of Cholesterol. Arch Androl 5, 249-254.

Davis, B.K. (1981). Timing of Fertilization in Mammals: Sperm Cholesterol/Phospholipid Ratio as a Determinant of the Capacitation Interval. Proc Natl Acad Sci U S A 78, 7560-7564.

Davis, B.K., Byrne, R., and Hungund, B. (1979). Studies on the Mechanism of Capacitation. Ii. Evidence for Lipid Transfer between Plasma Membrane of Rat Sperm and Serum Albumin During Capacitation in Vitro. Biochim Biophys Acta 558, 257-266.

de Almeida, R.F., Loura, L.M., Fedorov, A., and Prieto, M. (2005). Lipid Rafts Have Different Sizes Depending on Membrane Composition: A Time-Resolved Fluorescence Resonance Energy Transfer Study. J Mol Biol 346, 1109-1120.

De Blas, G., Michaut, M., Trevino, C.L., Tomes, C.N., Yunes, R., Darszon, A., and Mayorga, L.S. (2002). The Intraacrosomal Calcium Pool Plays a Direct Role in Acrosomal Exocytosis. J Biol Chem 277, 49326-49331.

De Blas, G.A., Roggero, C.M., Tomes, C.N., and Mayorga, L.S. (2005). Dynamics of Snare Assembly and Disassembly During Sperm Acrosomal Exocytosis. PLoS Biol 3, e323.

De Jonge, C.J., Han, H.L., Mack, S.R., and Zaneveld, L.J. (1991). Effect of Phorbol Diesters, Synthetic Diacylglycerols, and a Protein Kinase C Inhibitor on the Human Sperm Acrosome Reaction. J Androl 12, 62-70.

Desnoyers, L., and Manjunath, P. (1992). Major Proteins of Bovine Seminal Plasma Exhibit Novel Interactions with Phospholipid. J Biol Chem 267, 10149-10155.

DiCarlantonio, G., and Talbot, P. (1988). Evidence for Sequential Deployment of Secretory Enzymes During the Normal Acrosome Reaction of Guinea Pig Sperm in Vitro. Gamete Res 21, 425-438.

Dietrich, C., Bagatolli, L.A., Volovyk, Z.N., Thompson, N.L., Levi, M., Jacobson, K., and Gratton, E. (2001a). Lipid Rafts Reconstituted in Model Membranes. Biophys J 80, 1417-1428.

Dietrich, C., Volovyk, Z.N., Levi, M., Thompson, N.L., and Jacobson, K. (2001b). Partitioning of Thy-1, Gm1, and Cross-Linked Phospholipid Analogs into Lipid Rafts Reconstituted in Supported Model Membrane Monolayers. Proc Natl Acad Sci U S A 98, 10642-10647.

Dietrich, C., Yang, B., Fujiwara, T., Kusumi, A., and Jacobson, K. (2002). Relationship of Lipid Rafts to Transient Confinement Zones Detected by Single Particle Tracking. Biophys J 82, 274-284.

Ehrenwald, E., Foote, R.H., and Parks, J.E. (1990). Bovine Oviductal Fluid Components and Their Potential Role in Sperm Cholesterol Efflux. Mol Reprod Dev 25, 195-204.

Escalier, D. (1990). Failure of Differentiation of the Nuclear-Perinuclear Skeletal Complex in the Round-Headed Human Spermatozoa. Int J Dev Biol 34, 287-297.

Evans, R.W., and Setchell, B.P. (1979). Lipid Changes in Boar Spermatozoa During Epididymal Maturation with Some Observations on the Flow and Composition of Boar Rete Testis Fluid. J Reprod Fertil 57, 189-196.

Evans, R.W., Weaver, D.E., and Clegg, E.D. (1980). Diacyl, Alkenyl, and Alkyl Ether Phospholipids in Ejaculated, in Utero-, and in Vitro-Incubated Porcine Spermatozoa. J Lipid Res 21, 223-228.

Fawcett, D.W. (1970). A Comparative View of Sperm Ultrastructure. Biol Reprod 2, Suppl 2:90-127.

Fawcett, D.W. (1975). The Mammalian Spermatozoon. Dev Biol 44, 394-436.

Fawcett, D.W., Anderson, W.A., and Phillips, D.M. (1971). Morphogenetic Factors Influencing the Shape of the Sperm Head. Dev Biol 26, 220-251.

Fawcett, D.W., and Ito, S. (1965). The Fine Structure of Bat Spermatozoa. Am J Anat 116, 567-609.

Figueroa, C., Kawada, M.E., Veliz, L.P., Hidalgo, U., Barros, C., Gonzalez, S., and Santos, M.J. (2000). Peroxisomal Proteins in Rat Gametes. Cell Biochem Biophys 32 Spring, 259-268.

Flesch, F.M., Brouwers, J.F., Nievelstein, P.F., Verkleij, A.J., van Golde, L.M., Colenbrander, B., and Gadella, B.M. (2001). Bicarbonate Stimulated Phospholipid Scrambling Induces Cholesterol Redistribution and Enables Cholesterol Depletion in the Sperm Plasma Membrane. J Cell Sci 114, 3543-3555.

Foster, J.A., Friday, B.B., Maulit, M.T., Blobel, C., Winfrey, V.P., Olson, G.E., Kim, K.S., and Gerton, G.L. (1997). Am67, a Secretory Component of the Guinea Pig Sperm Acrosomal Matrix, Is Related to Mouse Sperm Protein Sp56 and the Complement Component 4-Binding Proteins. J Biol Chem 272, 12714-12722.

Friend, D.S. (1982). Plasma-Membrane Diversity in a Highly Polarized Cell. J Cell Biol 93, 243-249.

Friend, D.S. (1989). Sperm Maturation: Membrane Domain Boundaries. Ann N Y Acad Sci 567, 208-221.

Friend, D.S., and Fawcett, D.W. (1974). Membrane Differentiations in Freeze-Fractured Mammalian Sperm. J Cell Biol 63, 641-664.

Fukami, K., Nakao, K., Inoue, T., Kataoka, Y., Kurokawa, M., Fissore, R.A., Nakamura, K., Katsuki, M., Mikoshiba, K., Yoshida, N., and Takenawa, T. (2001). Requirement of Phospholipase Cdelta4 for the Zona Pellucida-Induced Acrosome Reaction. Science 292, 920-923.

Fukami, K., Yoshida, M., Inoue, T., Kurokawa, M., Fissore, R.A., Yoshida, N., Mikoshiba, K., and Takenawa, T. (2003). Phospholipase Cdelta4 Is Required for Ca2+ Mobilization Essential for Acrosome Reaction in Sperm. J Cell Biol 161, 79-88.

Gadella, B.M., and Harrison, R.A. (2000). The Capacitating Agent Bicarbonate Induces Protein Kinase a-Dependent Changes in Phospholipid Transbilayer Behavior in the Sperm Plasma Membrane. Development 127, 2407-2420.

Gage, M.J., and Morrow, E.H. (2003). Experimental Evidence for the Evolution of Numerous, Tiny Sperm Via Sperm Competition. Curr Biol 13, 754-757.

Glover, T.D., and Nicander, L. (1971). Some Aspects of Structure and Function in the Mammalian Epididymis. J Reprod Fertil Suppl 13, Suppl 13:39-50.

Go, K.J., and Wolf, D.P. (1985). Albumin-Mediated Changes in Sperm Sterol Content During Capacitation. Biol Reprod 32, 145-153.

Gomendio, M., and Roldan, E.R. (1991). Sperm Competition Influences Sperm Size in Mammals. Proc Biol Sci 243, 181-185.

Greube, A., Muller, K., Topfer-Petersen, E., Herrmann, A., and Muller, P. (2001). Influence of the Bovine Seminal Plasma Protein Pdc-109 on the Physical State of Membranes. Biochemistry 40, 8326-8334.

Haraguchi, C.M., Ishido, K., Kominami, E., and Yokota, S. (2003). Expression of Cathepsin H in Differentiating Rat Spermatids: Immunoelectron Microscopic Study. Histochem Cell Biol 120, 63-71.

Hardy, D.M., Oda, M.N., Friend, D.S., and Huang, T.T., Jr. (1991). A Mechanism for Differential Release of Acrosomal Enzymes During the Acrosome Reaction. Biochem J 275 (Pt 3), 759-766.

Harrison, R.A., Ashworth, P.J., and Miller, N.G. (1996). Bicarbonate/Co2, an Effector of Capacitation, Induces a Rapid and Reversible Change in the Lipid Architecture of Boar Sperm Plasma Membranes. Mol Reprod Dev 45, 378-391.

He, L., Wu, X.S., Mohan, R., and Wu, L.G. (2006). Two Modes of Fusion Pore Opening Revealed by Cell-Attached Recordings at a Synapse. Nature 444, 102-105.

Heid, H., Figge, U., Winter, S., Kuhn, C., Zimbelmann, R., and Franke, W. (2002). Novel Actin-Related Proteins Arp-T1 and Arp-T2 as Components of the Cytoskeletal Calyx of the Mammalian Sperm Head. Exp Cell Res 279, 177-187.

Herrada, G., and Wolgemuth, D.J. (1997). The Mouse Transcription Factor Stat4 Is Expressed in Haploid Male Germ Cells and Is Present in the Perinuclear Theca of Spermatozoa. J Cell Sci 110 (Pt 14), 1543-1553.

Herrick, S.B., Schweissinger, D.L., Kim, S.W., Bayan, K.R., Mann, S., and Cardullo, R.A. (2005). The Acrosomal Vesicle of Mouse Sperm Is a Calcium Store. J Cell Physiol 202, 663-671.

Hess, H., Heid, H., and Franke, W.W. (1993). Molecular Characterization of Mammalian Cylicin, a Basic Protein of the Sperm Head Cytoskeleton. J Cell Biol 122, 1043-1052.

Ho, H.C., and Suarez, S.S. (2001a). An Inositol 1,4,5-Trisphosphate Receptor-Gated Intracellular Ca(2+) Store Is Involved in Regulating Sperm Hyperactivated Motility. Biol Reprod 65, 1606-1615.

Ho, H.C., and Suarez, S.S. (2001b). Hyperactivation of Mammalian Spermatozoa: Function and Regulation. Reproduction 122, 519-526.

Ho, H.C., and Suarez, S.S. (2003). Characterization of the Intracellular Calcium Store at the Base of the Sperm Flagellum That Regulates Hyperactivated Motility. Biol Reprod 68, 1590-1596.

Hrudka, F. (1968a). The Mitochondrial Sheath of the Bovine Spermatozoid. I. The Organization of Mitochondria. Folia Morphol (Praha) 16, 48-59.

Hrudka, F. (1968b). The Mitochondrial Sheath of the Bovine Spermatozoid. Ii. Ultrastructure of the Mitochondria. Folia Morphol (Praha) 16, 60-66.

Huang, W.P., and Ho, H.C. (2006). Role of Microtubule-Dependent Membrane Trafficking in Acrosomal Biogenesis. Cell Tissue Res 323, 495-503.

Hui, S.W., and Parsons, D.F. (1975). Direct Observation of Domains in Wet Lipid Bilayers. Science 190, 383-384.

Hui, S.W., and Parsons, D.F. (1976). Phase Transition of Plasma Membranes of Rat Hepatocyte and Hepatoma Cells by Electron Diffraction. Cancer Res 36, 1918-1923.

Hunnicutt, G.R., Mahan, K., Lathrop, W.F., Ramarao, C.S., Myles, D.G., and Primakoff, P. (1996). Structural Relationship of Sperm Soluble Hyaluronidase to the Sperm Membrane Protein Ph-20. Biol Reprod 54, 1343-1349.

Hurst, S., Howes, E.A., Coadwell, J., and Jones, R. (1998). Expression of a Testis-Specific Putative Actin-Capping Protein Associated with the Developing Acrosome During Rat Spermiogenesis. Mol Reprod Dev 49, 81-91.

Igdoura, S.A., Morales, C.R., and Hermo, L. (1995). Differential Expression of Cathepsins B and D in Testis and Epididymis of Adult Rats. J Histochem Cytochem 43, 545-557.

Ihara, M., Kinoshita, A., Yamada, S., Tanaka, H., Tanigaki, A., Kitano, A., Goto, M., Okubo, K., Nishiyama, H., Ogawa, O., Takahashi, C., Itohara, S., Nishimune, Y., Noda, M., and Kinoshita, M. (2005). Cortical Organization by the Septin Cytoskeleton Is Essential for Structural and Mechanical Integrity of Mammalian Spermatozoa. Dev Cell 8, 343-352.

Jacobson, K., Mouritsen, O.G., and Anderson, R.G. (2007). Lipid Rafts: At a Crossroad between Cell Biology and Physics. Nat Cell Biol 9, 7-14.

James, P.S., Hennessy, C., Berge, T., and Jones, R. (2004). Compartmentalisation of the Sperm Plasma Membrane: A Frap, Flip and Spfi Analysis of Putative Diffusion Barriers on the Sperm Head. J Cell Sci 117, 6485-6495.

Jungnickel, M.K., Marrero, H., Birnbaumer, L., Lemos, J.R., and Florman, H.M. (2001). Trp2 Regulates Entry of Ca2+ into Mouse Sperm Triggered by Egg Zp3. Nat Cell Biol 3, 499-502.

Jungnickel, M.K., Sutton, K.A., Wang, Y., and Florman, H.M. (2007). Phosphoinositide-Dependent Pathways in Mouse Sperm Are Regulated by Egg Zp3 and Drive the Acrosome Reaction. Dev Biol 304, 116-126.

Kawano, N., and Yoshida, M. (2007). Semen-Coagulating Protein, Svs2, in Mouse Seminal Plasma Controls Sperm Fertility. Biol Reprod 76, 353-361.

Kierszenbaum, A.L. (2001). Spermatid Manchette: Plugging Proteins to Zero into the Sperm Tail. Mol Reprod Dev 59, 347-349.

Kierszenbaum, A.L., Rivkin, E., and Tres, L.L. (2003). Acroplaxome, an F-Actin-Keratin-Containing Plate, Anchors the Acrosome to the Nucleus During Shaping of the Spermatid Head. Mol Biol Cell 14, 4628-4640.

Kierszenbaum, A.L., and Tres, L.L. (2004). The Acrosome-Acroplaxome-Manchette Complex and the Shaping of the Spermatid Head. Arch Histol Cytol 67, 271-284.

Kim, K.S., Foster, J.A., and Gerton, G.L. (2001). Differential Release of Guinea Pig Sperm Acrosomal Components During Exocytosis. Biol Reprod 64, 148-156.

Kim, K.S., and Gerton, G.L. (2003). Differential Release of Soluble and Matrix Components: Evidence for Intermediate States of Secretion During Spontaneous Acrosomal Exocytosis in Mouse Sperm. Dev Biol 264, 141-152.

Kissel, H., Georgescu, M.M., Larisch, S., Manova, K., Hunnicutt, G.R., and Steller, H. (2005). The Sept4 Septin Locus Is Required for Sperm Terminal Differentiation in Mice. Dev Cell 8, 353-364.

Klausner, R.D., Kleinfeld, A.M., Hoover, R.L., and Karnovsky, M.J. (1980). Lipid Domains in Membranes. Evidence Derived from Structural Perturbations Induced by Free Fatty Acids and Lifetime Heterogeneity Analysis. J Biol Chem 255, 1286-1295.

Koehler, J.K. (1983). Structural Heterogeneity of the Mammalian Sperm Flagellar Membrane. J Submicrosc Cytol 15, 247-253.

Kohn, F.M., Dammshauser, I., Neukamm, C., Renneberg, H., Siems, W.E., Schill, W.B., and Aumuller, G. (1998). Ultrastructural Localization of Angiotensin-Converting Enzyme in Ejaculated Human Spermatozoa. Hum Reprod 13, 604-610.

Kohn, F.M., Miska, W., and Schill, W.B. (1995). Release of Angiotensin-Converting Enzyme (Ace) from Human Spermatozoa During Capacitation and Acrosome Reaction. J Androl 16, 259-265.

Korley, R., Pouresmaeili, F., and Oko, R. (1997). Analysis of the Protein Composition of the Mouse Sperm Perinuclear Theca and Characterization of Its Major Protein Constituent. Biol Reprod 57, 1426-1432.

Ladha, S., James, P.S., Clark, D.C., Howes, E.A., and Jones, R. (1997). Lateral Mobility of Plasma Membrane Lipids in Bull Spermatozoa: Heterogeneity between Surface Domains and Rigidification Following Cell Death. J Cell Sci 110 (Pt 9), 1041-1050.

Lalli, M., and Clermont, Y. (1981). Structural Changes of the Head Components of the Rat Spermatid During Late Spermiogenesis. Am J Anat 160, 419-434.

Langlais, J., Kan, F.W., Granger, L., Raymond, L., Bleau, G., and Roberts, K.D. (1988). Identification of Sterol Acceptors That Stimulate Cholesterol Efflux from Human Spermatozoa During in Vitro Capacitation. Gamete Res 20, 185-201.

Leblond, C.P., and Clermont, Y. (1952). Spermiogenesis of Rat, Mouse, Hamster and Guinea Pig as Revealed by the Periodic Acid-Fuchsin Sulfurous Acid Technique. Am J Anat 90, 167-215.

Lecuyer, C., Dacheux, J.L., Hermand, E., Mazeman, E., Rousseaux, J., and Rousseaux-Prevost, R. (2000). Actin-Binding Properties and Colocalization with Actin During Spermiogenesis of Mammalian Sperm Calicin. Biol Reprod 63, 1801-1810.

Lin, Y., and Kan, F.W. (1996). Regionalization and Redistribution of Membrane Phospholipids and Cholesterol in Mouse Spermatozoa During in Vitro Capacitation. Biol Reprod 55, 1133-1146.

Longo, F.J., Krohne, G., and Franke, W.W. (1987). Basic Proteins of the Perinuclear Theca of Mammalian Spermatozoa and Spermatids: A Novel Class of Cytoskeletal Elements. J Cell Biol 105, 1105-1120.

Lopez, C.I., Belmonte, S.A., De Blas, G.A., and Mayorga, L.S. (2007). Membrane-Permeant Rab3a Triggers Acrosomal Exocytosis in Living Human Sperm. Faseb J.

Lusignan, M.F., Bergeron, A., Crete, M.H., Lazure, C., and Manjunath, P. (2007). Induction of Epididymal Boar Sperm Capacitation by Pb1 and Bsp-A1/-A2 Proteins, Members of the Bsp Protein Family. Biol Reprod 76, 424-432.

Maksymiw, R., Sui, S.F., Gaub, H., and Sackmann, E. (1987). Electrostatic Coupling of Spectrin Dimers to Phosphatidylserine Containing Lipid Lamellae. Biochemistry 26, 2983-2990.

Manjunath, P., and Therien, I. (2002). Role of Seminal Plasma Phospholipid-Binding Proteins in Sperm Membrane Lipid Modification That Occurs During Capacitation. J Reprod Immunol 53, 109-119.

Marquez, B., Ignotz, G., and Suarez, S.S. (2007). Contributions of Extracellular and Intracellular Ca2+ to Regulation of Sperm Motility: Release of Intracellular Stores Can Hyperactivate Catsper1 and Catsper2 Null Sperm. Dev Biol 303, 214-221.

Marushige, K., and Dixon, G.H. (1969). Developmental Changes in Chromosomal Composition and Template Activity During Spermatogenesis in Trout Testis. Dev Biol 19, 397-414.

Mayorga, L.S., Tomes, C.N., and Belmonte, S.A. (2007). Acrosomal Exocytosis, a Special Type of Regulated Secretion. IUBMB Life 59, 286-292.

Meizel, S., and Turner, K.O. (1984). The Effects of Products and Inhibitors of Arachidonic Acid Metabolism on the Hamster Sperm Acrosome Reaction. J Exp Zool 231, 283-288.

Mezquita, C. (1985). Chromatin Composition, Structure and Function in Spermatogenesis. Revis Biol Celular 5, V-XIV, 1-124.

Miller, G.T., and Pitnick, S. (2002). Sperm-Female Coevolution in Drosophila. Science 298, 1230-1233.

Montag, M., van der Ven, K., Dorbecker, C., and van der Ven, H. (1999). Characterization of Testicular Mouse Glucosamine 6-Phosphate Deaminase (Gnpda). FEBS Lett 458, 141-144.

Morales, C.R., Oko, R., and Clermont, Y. (1994). Molecular Cloning and Developmental Expression of an Mrna Encoding the 27 Kda Outer Dense Fiber Protein of Rat Spermatozoa. Mol Reprod Dev 37, 229-240.

Moreno, R.D., and Alvarado, C.P. (2006). The Mammalian Acrosome as a Secretory Lysosome: New and Old Evidence. Mol Reprod Dev 73, 1430-1434.

Moreno, R.D., Ramalho-Santos, J., Chan, E.K., Wessel, G.M., and Schatten, G. (2000a). The Golgi Apparatus Segregates from the Lysosomal/Acrosomal Vesicle During Rhesus Spermiogenesis: Structural Alterations. Dev Biol 219, 334-349.

Moreno, R.D., Ramalho-Santos, J., Sutovsky, P., Chan, E.K., and Schatten, G. (2000b). Vesicular Traffic and Golgi Apparatus Dynamics During Mammalian Spermatogenesis: Implications for Acrosome Architecture. Biol Reprod 63, 89-98.

Munro, S. (2003). Lipid Rafts: Elusive or Illusive? Cell 115, 377-388.

Nakanishi, T., Ikawa, M., Yamada, S., Toshimori, K., and Okabe, M. (2001). Alkalinization of Acrosome Measured by Gfp as a Ph Indicator and Its Relation to Sperm Capacitation. Dev Biol 237, 222-231.

Neill, J.M., and Olds-Clarke, P. (1987). A Computer-Assisted Assay for Mouse Sperm Hyperactivation Demonstrates That Bicarbonate but Not Bovine Serum Albumin Is Required. Gamete Res 18, 121-140.

Nicander, L., and Glover, T.D. (1973). Regional Histology and Fine Structue of the Epididymal Duct in the Golden Hamster (Mesocricetus Auratus). J Anat 114, 347-364.

Oakberg, E.F. (1956a). A description of spermiogenesis in the mouse and its use in analysis of the cycle of the seminiferous epithelium and germ cell renewal. Am J Anat 99, 391-413.

Oakberg, E.F. (1956b). Duration of spermatogenesis in the mouse and timing of stages of the cycle of the seminiferous epithelium. Am J Anat 99, 507-516.

O'Toole, C.M., Arnoult, C., Darszon, A., Steinhardt, R.A., and Florman, H.M. (2000). Ca(2+) Entry through Store-Operated Channels in Mouse Sperm Is Initiated by Egg Zp3 and Drives the Acrosome Reaction. Mol Biol Cell 11, 1571-1584.

Okamura, N., Tajima, Y., Soejima, A., Masuda, H., and Sugita, Y. (1985). Sodium Bicarbonate in Seminal Plasma Stimulates the Motility of Mammalian Spermatozoa through Direct Activation of Adenylate Cyclase. J Biol Chem 260, 9699-9705.

Oko, R., and Clermont, Y. (1988). Isolation, Structure and Protein Composition of the Perforatorium of Rat Spermatozoa. Biol Reprod 39, 673-687.

Oko, R., and Maravei, D. (1994). Protein Composition of the Perinuclear Theca of Bull Spermatozoa. Biol Reprod 50, 1000-1014.

Oko, R., and Maravei, D. (1995). Distribution and Possible Role of Perinuclear Theca Proteins During Bovine Spermiogenesis. Microsc Res Tech 32, 520-532.

Oko, R., and Morales, C.R. (1994). A Novel Testicular Protein, with Sequence Similarities to a Family of Lipid Binding Proteins, Is a Major Component of the Rat Sperm Perinuclear Theca. Dev Biol 166, 235-245.

Oko, R., Moussakova, L., and Clermont, Y. (1990). Regional Differences in Composition of the Perforatorium and Outer Periacrosomal Layer of the Rat Spermatozoon as Revealed by Immunocytochemistry. Am J Anat 188, 64-73.

Olson, G.E., and Winfrey, V.P. (1986). Identification of a Cytoskeletal Network Adherent to the Mitochondria of Mammalian Spermatozoa. J Ultrastruct Mol Struct Res 94, 131-139.

Oud, J.L., and de Rooij, D.G. (1977). Spermatogenesis in the Chinese Hamster. Anat Rec 187, 113-124.

Parker, G.A. (1970). Sperm Competition and Its Evolutionary Consequences in the Insects. Biological Reviews 45, 525-567.

Parker, G.A. (1982). Why Are There So Many Tiny Sperm? Sperm Competition and the Maintenance of Two Sexes. J Theor Biol 96, 281-294.

Pelletier, R.M., and Friend, D.S. (1983). Development of Membrane Differentiations in the Guinea Pig Spermatid During Spermiogenesis. Am J Anat 167, 119-141.

Pietrobon, E.O., Dominguez, L.A., Vincenti, A.E., Burgos, M.H., and Fornes, M.W. (2001). Detection of the Mouse Acrosome Reaction by Acid Phosphatase. Comparison with Chlortetracycline and Electron Microscopy. J Androl 22, 96-103.

Pietrobon, E.O., Soria, M., Dominguez, L.A., Monclus Mde, L., and Fornes, M.W. (2005). Simultaneous Activation of Pla2 and Plc Are Required to Promote Acrosomal Reaction Stimulated by Progesterone Via G-Proteins. Mol Reprod Dev 70, 58-63.

Pike, L.J. (2006). Rafts Defined: A Report on the Keystone Symposium on Lipid Rafts and Cell Function. J Lipid Res 47, 1597-1598.

Polakoski, K.L., Zaneveld, L.J., and Williams, W.L. (1971). An Acrosin-Acrosin Inhibitor Complex in Ejaculated Boar Sperm. Biochem Biophys Res Commun 45, 381-386.

Polakoski, K.L., Zaneveld, L.J., and Williams, W.L. (1972). Purification of a Proteolytic Enzyme from Rabbit Acrosomes. Biol Reprod 6, 23-29.

Poulos, A., Sharp, P., Johnson, D., White, I., and Fellenberg, A. (1986). The Occurrence of Polyenoic Fatty Acids with Greater Than 22 Carbon Atoms in Mammalian Spermatozoa. Biochem J 240, 891-895.

Pouresmaeili, F., Morales, C.R., and Oko, R. (1997). Molecular Cloning and Structural Analysis of the Gene Encoding Perf 15 Protein Present in the Perinuclear Theca of the Rat Spermatozoa. Biol Reprod 57, 655-659.

Rejraji, H., Sion, B., Prensier, G., Carreras, M., Motta, C., Frenoux, J.M., Vericel, E., Grizard, G., Vernet, P., and Drevet, J.R. (2006). Lipid Remodeling of Murine Epididymosomes and Spermatozoa During Epididymal Maturation. Biol Reprod 74, 1104-1113.

Rochwerger, L., and Cuasnicu, P.S. (1992). Redistribution of a Rat Sperm Epididymal Glycoprotein after in Vitro and in Vivo Capacitation. Mol Reprod Dev 31, 34-41.

Roldan, E.R., Murase, T., and Shi, Q.X. (1994). Exocytosis in Spermatozoa in Response to Progesterone and Zona Pellucida. Science 266, 1578-1581.

Rostami, A., Brown, M.J., Lisak, R.P., Sumner, A.J., Zweiman, B., and Pleasure, D.E. (1984). The Role of Myelin P2 Protein in the Production of Experimental Allergic Neuritis. Ann Neurol 16, 680-685.

Rousseaux-Prevost, R., Lecuyer, C., Drobecq, H., Sergheraert, C., Dacheux, J.L., and Rousseaux, J. (2003). Characterization of Boar Sperm Cytoskeletal Cylicin Ii as an Actin-Binding Protein. Biochem Biophys Res Commun 303, 182-189.

Russell, L.D., Lee, I.P., Ettlin, R., and Peterson, R.N. (1983). Development of the Acrosome and Alignment, Elongation and Entrenchment of Spermatids in Procarbazine-Treated Rats. Tissue Cell 15, 615-626.

Sako, Y., and Kusumi, A. (1994). Compartmentalized Structure of the Plasma Membrane for Receptor Movements as Revealed by a Nanometer-Level Motion Analysis. J Cell Biol 125, 1251-1264.

Sako, Y., and Kusumi, A. (1995). Barriers for Lateral Diffusion of Transferrin Receptor in the Plasma Membrane as Characterized by Receptor Dragging by Laser Tweezers: Fence Versus Tether. J Cell Biol 129, 1559-1574.

Schroeder, R., London, E., and Brown, D. (1994). Interactions between Saturated Acyl Chains Confer Detergent Resistance on Lipids and Glycosylphosphatidylinositol (Gpi)-Anchored Proteins: Gpi-Anchored Proteins in Liposomes and Cells Show Similar Behavior. Proc Natl Acad Sci U S A 91, 12130-12134.

Schultz, N., Hamra, F.K., and Garbers, D.L. (2003). A Multitude of Genes Expressed Solely in Meiotic or Postmeiotic Spermatogenic Cells Offers a Myriad of Contraceptive Targets. Proc Natl Acad Sci U S A 100, 12201-12206.

Selivonchick, D.P., Schmid, P.C., Natarajan, V., and Schmid, H.H. (1980). Structure and Metabolism of Phospholipids in Bovine Epididymal Spermatozoa. Biochim Biophys Acta 618, 242-254.

Shao, X., Tarnasky, H.A., Lee, J.P., Oko, R., and van der Hoorn, F.A. (1999). Spag4, a Novel Sperm Protein, Binds Outer Dense-Fiber Protein Odf1 and Localizes to Microtubules of Manchette and Axoneme. Dev Biol 211, 109-123.

Shao, X., Tarnasky, H.A., Schalles, U., Oko, R., and van der Hoorn, F.A. (1997). Interactional Cloning of the 84-Kda Major Outer Dense Fiber Protein Odf84. Leucine Zippers Mediate Associations of Odf84 and Odf27. J Biol Chem 272, 6105-6113.

Sheets, E.D., Lee, G.M., Simson, R., and Jacobson, K. (1997). Transient Confinement of a Glycosylphosphatidylinositol-Anchored Protein in the Plasma Membrane. Biochemistry 36, 12449-12458.

Simons, K., and van Meer, G. (1988). Lipid Sorting in Epithelial Cells. Biochemistry 27, 6197-6202.

Simson, R., Sheets, E.D., and Jacobson, K. (1995). Detection of Temporary Lateral Confinement of Membrane Proteins Using Single-Particle Tracking Analysis. Biophys J 69, 989-993.

Singer, S.J., and Nicolson, G.L. (1972). The Fluid Mosaic Model of the Structure of Cell Membranes. Science 175, 720-731.

Skudlarek, M.D., Abou-Haila, A., and Tulsiani, D.R. (2000). Rat Spermatogenic Cell Beta-D-Galactosidase: Characterization, Biosynthesis, and Immunolocalization. Exp Cell Res 261, 139-149.

Skudlarek, M.D., Tulsiani, D.R., Nagdas, S.K., and Orgebin-Crist, M.C. (1993). Beta-D-Galactosidase of Rat Spermatozoa: Subcellular Distribution, Substrate Specificity, and Molecular Changes During Epididymal Maturation. Biol Reprod 49, 204-213.

Sleight, S.B., Miranda, P.V., Plaskett, N.W., Maier, B., Lysiak, J., Scrable, H., Herr, J.C., and Visconti, P.E. (2005). Isolation and Proteomic Analysis of Mouse Sperm Detergent-Resistant Membrane Fractions. Evidence for Dissociation of Lipid Rafts During Capacitation. Biol Reprod 73, 721-729.

Stauss, C.R., Votta, T.J., and Suarez, S.S. (1995). Sperm Motility Hyperactivation Facilitates Penetration of the Hamster Zona Pellucida. Biol Reprod 53, 1280-1285.

Suarez, S.S., and Dai, X. (1992). Hyperactivation Enhances Mouse Sperm Capacity for Penetrating Viscoelastic Media. Biol Reprod 46, 686-691.

Suarez, S.S., Dai, X.B., DeMott, R.P., Redfern, K., and Mirando, M.A. (1992). Movement Characteristics of Boar Sperm Obtained from the Oviduct or Hyperactivated in Vitro. J Androl 13, 75-80.

Suarez, S.S., Varosi, S.M., and Dai, X. (1993). Intracellular Calcium Increases with Hyperactivation in Intact, Moving Hamster Sperm and Oscillates with the Flagellar Beat Cycle. Proc Natl Acad Sci U S A 90, 4660-4664.

Sullivan, R., Frenette, G., and Girouard, J. (2007). Epididymosomes Are Involved in the Acquisition of New Sperm Proteins During Epididymal Transit. Asian J Androl 9, 483-491.

Sullivan, R., Saez, F., Girouard, J., and Frenette, G. (2005). Role of Exosomes in Sperm Maturation During the Transit Along the Male Reproductive Tract. Blood Cells Mol Dis 35, 1-10.

Sutovsky, P., Ramalho-Santos, J., Moreno, R.D., Oko, R., Hewitson, L., and Schatten, G. (1999). On-Stage Selection of Single Round Spermatids Using a Vital, Mitochondrion-Specific Fluorescent Probe Mitotracker(Tm) and

High Resolution Differential Interference Contrast Microscopy. Hum Reprod 14, 2301-2312.

Suzuki, F. (1988). Changes in the Distribution of Intramembranous Particles and Filipin-Sterol Complexes During Epididymal Maturation of Golden Hamster Spermatozoa. J Ultrastruct Mol Struct Res 100, 39-54.

Suzuki-Toyota, F., Itoh, Y., and Naito, K. (2000). Reduction of Intramembranous Particles in the Periacrosomal Plasma Membrane of Boar Spermatozoa During in Vitro Capacitation: A Statistical Study. Dev Growth Differ 42, 265-273.

Swyer, G.I. (1947). The Release of Hyaluronidase from Spermatozoa. Biochem J 41, 413-417.

Tannert, A., Kurz, A., Erlemann, K.R., Muller, K., Herrmann, A., Schiller, J., Topfer-Petersen, E., Manjunath, P., and Muller, P. (2007). The Bovine Seminal Plasma Protein Pdc-109 Extracts Phosphorylcholine-Containing Lipids from the Outer Membrane Leaflet. Eur Biophys J 36, 461-475.

Tanphaichitr, N., Carmona, E., Bou Khalil, M., Xu, H., Berger, T., and Gerton, G.L. (2007). New Insights into Sperm-Zona Pellucida Interaction: Involvement of Sperm Lipid Rafts. Front Biosci 12, 1748-1766.

Tesarik, J., and Flechon, J.E. (1986). Distribution of Sterols and Anionic Lipids in Human Sperm Plasma Membrane: Effects of in Vitro Capacitation. J Ultrastruct Mol Struct Res 97, 227-237.

Therien, I., Moreau, R., and Manjunath, P. (1998). Major Proteins of Bovine Seminal Plasma and High-Density Lipoprotein Induce Cholesterol Efflux from Epididymal Sperm. Biol Reprod 59, 768-776.

Therien, I., Soubeyrand, S., and Manjunath, P. (1997). Major Proteins of Bovine Seminal Plasma Modulate Sperm Capacitation by High-Density Lipoprotein. Biol Reprod 57, 1080-1088.

Tovich, P.R., and Oko, R.J. (2003). Somatic Histones Are Components of the Perinuclear Theca in Bovine Spermatozoa. J Biol Chem 278, 32431-32438.

Trapp, B.D., Dubois-Dalcq, M., and Quarles, R.H. (1984). Ultrastructural Localization of P2 Protein in Actively Myelinating Rat Schwann Cells. J Neurochem 43, 944-948.

Travis, A.J., Jorgez, C.J., Merdiushev, T., Jones, B.H., Dess, D.M., Diaz-Cueto, L., Storey, B.T., Kopf, G.S., and Moss, S.B. (2001a). Functional Relationships between Capacitation-Dependent Cell Signaling and Compartmentalized Metabolic Pathways in Murine Spermatozoa. J Biol Chem 276, 7630-7636.

Travis, A.J., and Kopf, G.S. (2002). The Spermatozoon as a Machine: Compartmentalized Pathways Bridge Cellular Structure and Function. In: Assisted reproductive technology: Accomplishments and new horizons. DeJonge CJ, Barratt CL, editors. Cambridge University Press, 26-39.

Travis, A.J., Merdiushev, T., Vargas, L.A., Jones, B.H., Purdon, M.A., Nipper, R.W., Galatioto, J., Moss, S.B., Hunnicutt, G.R., and Kopf, G.S. (2001b). Expression and Localization of Caveolin-1, and the Presence of Membrane Rafts, in Mouse and Guinea Pig Spermatozoa. Dev Biol 240, 599-610.

Travis, A.J., Tutuncu, L., Jorgez, C.J., Ord, T.S., Jones, B.H., Kopf, G.S., and Williams, C.J. (2004). Requirements for Glucose Beyond Sperm Capacitation During in Vitro Fertilization in the Mouse. Biol Reprod 71, 139-145.

Tsai, P.S., De Vries, K.J., De Boer-Brouwer, M., Garcia-Gil, N., Van Gestel, R.A., Colenbrander, B., Gadella, B.M., and Van Haeften, T. (2007). Syntaxin and Vamp Association with Lipid Rafts Depends on Cholesterol Depletion in Capacitating Sperm Cells. Mol Membr Biol 24, 313-324.

Tulsiani, D.R., Abou-Haila, A., Loeser, C.R., and Pereira, B.M. (1998). The Biological and Functional Significance of the Sperm Acrosome and Acrosomal Enzymes in Mammalian Fertilization. Exp Cell Res 240, 151-164.

Turner, R.M. (2003). Tales from the Tail: What Do We Really Know About Sperm Motility? J Androl 24, 790-803.

Ungermann, C., and Langosch, D. (2005). Functions of Snares in Intracellular Membrane Fusion and Lipid Bilayer Mixing. J Cell Sci 118, 3819-3828.

Urner, F., Leppens-Luisier, G., and Sakkas, D. (2001). Protein Tyrosine Phosphorylation in Sperm During Gamete Interaction in the Mouse: The Influence of Glucose. Biol Reprod 64, 1350-1357.

van Gestel, R.A., Brewis, I.A., Ashton, P.R., Helms, J.B., Brouwers, J.F., and Gadella, B.M. (2005). Capacitation-Dependent Concentration of Lipid Rafts in the Apical Ridge Head Area of Porcine Sperm Cells. Mol Hum Reprod 11, 583-590.

van Meer, G., and Simons, K. (1988). Lipid Polarity and Sorting in Epithelial Cells. J Cell Biochem 36, 51-58.

Vera, J.C., Brito, M., Zuvic, T., and Burzio, L.O. (1984). Polypeptide Composition of Rat Sperm Outer Dense Fibers. A Simple Procedure to Isolate the Fibrillar Complex. J Biol Chem 259, 5970-5977.

Vereb, G., Szollosi, J., Matko, J., Nagy, P., Farkas, T., Vigh, L., Matyus, L., Waldmann, T.A., and Damjanovich, S. (2003). Dynamic, yet Structured: The Cell Membrane Three Decades after the Singer-Nicolson Model. Proc Natl Acad Sci U S A 100, 8053-8058.

Viegas, G.V. (1997). Guillain-Barre Syndrome. Review and Presentation of a Case with Pedal Manifestations. J Am Podiatr Med Assoc 87, 209-218.

Visconti, P.E., Bailey, J.L., Moore, G.D., Pan, D., Olds-Clarke, P., and Kopf, G.S. (1995a). Capacitation of Mouse Spermatozoa. I. Correlation between the Capacitation State and Protein Tyrosine Phosphorylation. Development 121, 1129-1137.

Visconti, P.E., Galantino-Homer, H., Ning, X., Moore, G.D., Valenzuela, J.P., Jorgez, C.J., Alvarez, J.G., and Kopf, G.S. (1999a). Cholesterol Efflux-Mediated Signal Transduction in Mammalian Sperm. Beta-Cyclodextrins Initiate Transmembrane Signaling Leading to an Increase in Protein Tyrosine Phosphorylation and Capacitation. J Biol Chem 274, 3235-3242.

Visconti, P.E., Moore, G.D., Bailey, J.L., Leclerc, P., Connors, S.A., Pan, D., Olds-Clarke, P., and Kopf, G.S. (1995b). Capacitation of Mouse Spermatozoa. Ii. Protein Tyrosine Phosphorylation and Capacitation Are Regulated by a Camp-Dependent Pathway. Development 121, 1139-1150.

Visconti, P.E., Muschietti, J.P., Flawia, M.M., and Tezon, J.G. (1990). Bicarbonate Dependence of Camp Accumulation Induced by Phorbol Esters in Hamster Spermatozoa. Biochim Biophys Acta 1054, 231-236.

Visconti, P.E., Ning, X., Fornes, M.W., Alvarez, J.G., Stein, P., Connors, S.A., and Kopf, G.S. (1999b). Cholesterol Efflux-Mediated Signal Transduction in Mammalian Sperm: Cholesterol Release Signals an Increase in Protein Tyrosine Phosphorylation During Mouse Sperm Capacitation. Dev Biol 214, 429-443.

Visconti, P.E., Westbrook, V.A., Chertihin, O., Demarco, I., Sleight, S., and Diekman, A.B. (2002). Novel Signaling Pathways Involved in Sperm Acquisition of Fertilizing Capacity. J Reprod Immunol 53, 133-150.

von Bulow, M., Rackwitz, H.R., Zimbelmann, R., and Franke, W.W. (1997). Cp Beta3, a Novel Isoform of an Actin-Binding Protein, Is a Component of the Cytoskeletal Calyx of the Mammalian Sperm Head. Exp Cell Res 233, 216-224.

Wolf, D.E. (1995). Lipid Domains in Sperm Plasma Membranes. Mol Membr Biol 12, 101-104.

Wolf, D.E., Hagopian, S.S., and Ishijima, S. (1986). Changes in Sperm Plasma Membrane Lipid Diffusibility after Hyperactivation During in Vitro Capacitation in the Mouse. J Cell Biol 102, 1372-1377.

Wolf, D.E., Lipscomb, A.C., and Maynard, V.M. (1988). Causes of Nondiffusing Lipid in the Plasma Membrane of Mammalian Spermatozoa. Biochemistry 27, 860-865.

Wolf, D.E., Maynard, V.M., McKinnon, C.A., and Melchior, D.L. (1990). Lipid Domains in the Ram Sperm Plasma Membrane Demonstrated by Differential Scanning Calorimetry. Proc Natl Acad Sci U S A 87, 6893-6896.

Wolf, D.E., and Voglmayr, J.K. (1984). Diffusion and Regionalization in Membranes of Maturing Ram Spermatozoa. J Cell Biol 98, 1678-1684.

Wolfe, C.A., James, P.S., Mackie, A.R., Ladha, S., and Jones, R. (1998). Regionalized Lipid Diffusion in the Plasma Membrane of Mammalian Spermatozoa. Biol Reprod 59, 1506-1514.

Yanagimachi, R. (1969). In Vitro Capacitation of Hamster Spermatozoa by Follicular Fluid. J Reprod Fertil 18, 275-286.

Yanagimachi, R. (1994). Mammalian Fertilization (New York: Raven Press, Ltd.).

Yanagimachi, R., and Usui, N. (1974). Calcium Dependence of the Acrosome Reaction and Activation of Guinea Pig Spermatozoa. Exp Cell Res 89, 161-174.

Yasuzumi, G. (1956). Spermatogenesis in Animals Revealed by Electron Microscopy. I. Formation and Submicroscopic Structure of the Middle-Piece of the Albino Rat. J Biophys Biochem Cytol 2, 445-450.

Yuan, Y.Y., Chen, W.Y., Shi, Q.X., Mao, L.Z., Yu, S.Q., Fang, X., and Roldan, E.R. (2003). Zona Pellucida Induces Activation of Phospholipase A2 During Acrosomal Exocytosis in Guinea Pig Spermatozoa. Biol Reprod 68, 904-913.

Zeng, Y., Clark, E.N., and Florman, H.M. (1995). Sperm Membrane Potential: Hyperpolarization During Capacitation Regulates Zona Pellucida-Dependent Acrosomal Secretion. Dev Biol 171, 554-563.

Zeng, Y., Oberdorf, J.A., and Florman, H.M. (1996). Ph Regulation in Mouse Sperm: Identification of Na(+)-, Cl(-)-, and Hco3(-)-Dependent and Arylaminobenzoate-Dependent Regulatory Mechanisms and Characterization of Their Roles in Sperm Capacitation. Dev Biol 173, 510-520.

CHAPTER 2

Segregation of membrane domains in live sperm

Vimal Selvaraj[†], Atsushi Asano[†], Danielle E. Buttke, John L. McElwee, Jacquelyn L. Nelson, Collin A. Wolff, Tanya Merdiushev, Miguel W. Fornés, Alex W. Cohen, Michael P. Lisanti, George H. Rothblat, Gregory S. Kopf, and Alexander J. Travis. (2006). Segregation of Micron-scale Membrane Sub-domains in Live Murine Sperm. *J Cell Physiol* 206: 636-646.

Abstract

Lipid rafts, membrane sub-domains enriched in sterols and sphingolipids, are controversial because demonstrations of rafts have often utilized fixed cells. We showed in living sperm that the ganglioside G_{M1} localizes to a micron-scale membrane sub-domain in the plasma membrane overlying the acrosome. We investigated four models proposed for membrane raft formation and maintenance based on studies in somatic cells. G_{M1} segregation was maintained in live sperm incubated under non-capacitating condition, and after sterol efflux, a membrane alteration necessary for capacitation. The complete lack of G_{M1} diffusion to the post-acrosomal plasma membrane in live cells argued against the transient confinement zone model. However, within seconds after cessation of sperm motility, G_{M1} dramatically redistributed several microns from the acrosomal sub-domain to the post-acrosomal, non-raft sub-domain. This redistribution was not accompanied by movement of sterols, and was induced by the pentameric cholera toxin subunit B. These data argued against a lipid-lipid interaction model for sub-domain maintenance. Although impossible to rule out a lipid shell model definitively, mice lacking caveolin-1 maintained segregation of both sterols and G_{M1}, arguing against a role for lipid shells surrounding caveolin-1 in the maintenance of this G_{M1}-enriched sub-domain. Scanning electron microscopy of sperm freeze-dried without fixation identified cytoskeletal structures at the sub-domain boundary. Although drugs used to disrupt actin and intermediate filaments had no effect on the segregation of G_{M1}, we found that disulfide-bonded proteins played a role in sub-domain segregation[†]. Together, these data provide an example of membrane sub-domains extreme in terms of size

and stability of lipid segregation, and implicate a protein-based membrane compartmentation mechanism.

[†] The work in this manuscript on disulfide-bonded proteins performed by Atsushi Asano is included in this dissertation for continuity of this work.

Introduction

Lipid rafts are regions of membrane enriched in sterols and sphingolipids as opposed to phospholipids, and have been suggested to act as foci for a wide variety of cellular functions (Simons and Toomre, 2000). Two forms of raft have been proposed: the first are small (nm scale) and highly dynamic, and the second, induced by physiological cross-linking of molecules, can be larger and more stable (Kusumi et al., 2004). Several models have been put forth to explain the formation and maintenance of such sub-domains, including lipid-lipid interactions (such as tendencies for some lipids to self-aggregate, or for the aggregation of different lipids such as sterols and gangliosides), the preferential interaction of lipids with specific membrane proteins ("lipid shells"), the slowing of molecules in "transient confinement zones," and restricted lateral diffusion of molecules between membrane compartments due to borders of transmembrane proteins/underlying cytoskeletal elements [reviewed in (Kusumi et al., 2004)].

However, there is great controversy regarding the nature and dynamics of lipid rafts in cells; specifically, that artifacts might result from exposure of cells or membranes to detergents or cross-linking reagents/fixatives [reviewed in (Munro, 2003)]. For example, the pentameric "B" subunit of cholera toxin (CTB) is used for specific localization of the ganglioside, G_{M1} (Lauer et al., 2002), but can cause patching artifacts. It has been suggested that definitive proof of lipid rafts will require visualization in living cells (Munro, 2003).

Recent studies have attempted to address such concerns. Acyl chains on modified fluorescent proteins were shown to promote the clustering or close proximity of these constructs (Zacharias et al., 2002). Shifts in fluorescence wavelength of laurdan have suggested that living macrophages have 10-15%

of their cell surface covered by liquid-ordered domains (i.e. rafts), especially cell extensions and contact points (Gaus et al., 2003). These domains are larger than the nm-scale rafts believed to exist in most cells, and suggest that lipid rafts of varying size might be organized to particular regions of cells where their biophysical properties can impart specific functionality.

Mammalian sperm are highly polarized, with distinct functions restricted to specific regions. There are three major domains in the plasma membrane (the head, the mid-piece and the principal piece of the flagellum), with sub-domains within each of these regions, making sperm an intriguing model for the study of membrane compartmentalization [reviewed in (Travis and Kopf, 2002)]. Based on work in fixed cells, the plasma membrane of the sperm head is suggested to have two major sub-domains, distinct with regard to their functions as well as their lipid and protein compositions.

The physiological relevance of studies on sperm lipid sub-domains is great, in that for sperm to fertilize an egg, they must undergo sterol efflux from their plasma membrane during the process of capacitation, which renders them competent to fertilize an egg (Davis, 1976; Visconti et al., 1999b). The acrosomal plasma membrane (APM) of a capacitated sperm interacts with the extracellular matrix of the egg, and in response, fuses with the underlying outer acrosomal membrane which triggers the regulated exocytotic release of the acrosomal contents (Kim and Gerton, 2003). The APM itself has at least two distinct areas within the sub-domain, one over the apical acrosome (AA) and a larger one over the equatorial segment (ES). The post-acrosomal plasma membrane (PAPM) is not involved in the initial interaction with the egg's extracellular matrix, but later fuses with the egg's plasma membrane (Clark and Koehler, 1990). In fixed sperm of a number of species the APM is

enriched in sterols, whereas the PAPM is largely devoid of sterols (Friend, 1982; Pelletier and Friend, 1983; Suzuki, 1988; Lin and Kan, 1996; Visconti et al., 1999b).

Despite the potential connections between lipid sub-domains on the sperm head and the functional requirement for sterol efflux during sperm capacitation, little mechanistic information linking these observations is available. To improve understanding of lipid dynamics in live sperm, we investigated the localization of an endogenous ganglioside, G_{M1}, on the plasma membrane of the sperm head. Our findings address the current controversy surrounding whether lipid rafts can exist in live cells, demonstrating the stable segregation of endogenous G_{M1} to the plasma membrane overlying the acrosome in live murine sperm. We also investigated the mechanism underlying this segregation and provide evidence supporting a protein-based membrane compartmentation model of lipid segregation.

Experimental Methods

Reagents and animals

All reagents were purchased from Sigma (St. Louis, MO), unless otherwise noted. CTB (Molecular Probes, Eugene, OR) was purchased conjugated with Alexa Fluor 488 or Alexa Fluor 647 as indicated. Male CD-1 mice were from Charles River Laboratories (Kingston, NY).

Preparation of media and incubations of sperm

A modified Whitten's medium (MW; 22 mM HEPES, 1.2 mM $MgCl_2$, 100 mM NaCl, 4.7 mM KCl, 1 mM pyruvic acid, 4.8 mM lactic acid hemi-calcium salt, pH 7.35) (Travis et al., 2001a) containing 5.5 mM glucose was used for all

incubations unless otherwise indicated. Media were supplemented with 2-hydroxypropyl-β-cyclodextrin (2-OHCD; 3 mM) as needed. The sterol acceptor 2-OHCD supports sperm capacitation and in vitro fertilization and is preferred over the more potent methyl-β-cyclodextrin (Visconti et al., 1999a). Mature sperm were collected from the cauda epididymides by a swim-out procedure as described previously (Travis et al., 2001a). All steps of washing of sperm, centrifugation and all incubations for experiments were performed at 37˚C.

Fluorescence localization of lipids

All incubations during localization experiments were carried out under dim lighting at 37˚C in a humidity chamber. Sperm ($2x10^6$) were incubated in 300 μl MW. The localization of G_{M1} was visualized with CTB in live sperm or after fixation under different conditions. In both cases, cells were viewed with a Nikon Eclipse TE 2000-U microscope (Nikon, Melville, NY) equipped with a Photometrics Coolsnap HQ CCD camera (Roper Scientific, Ottobrunn, Germany), and Openlab 3.1 (Improvision, Lexington, MA) automation and imaging software. Assignments of sperm to G_{M1} localization patterns were performed in a blind fashion regarding incubation condition. To compare shifts in population tendencies, the numbers were converted to percentages prior to statistical evaluation. In all cases, ≥ 100 cells were counted for each test condition, and every sperm in a given field was counted to avoid potential bias.

For localization in live sperm, a stage-mounted incubation chamber (LiveCell, Neue Product Group, Westminister, MD) was used along with an objective heater (Bioptechs, Butler, PA). Samples were observed using glass bottom culture dishes (MatTek Corporation, Ashland, MA) overlaid with mineral oil, or using small aliquots on slides under coverslips. Samples were

incubated for 10 min with CTB (10 μg/ml). To avoid any membrane damage, some samples were not washed, but viewed with CTB in the final medium as indicated. To study the effect of sterol efflux in live sperm, MW medium supplemented with 3 mM 2-OHCD was used and the sperm were incubated for 45 minutes before addition of CTB. Images of motile sperm were captured using programmed exposure intervals, and serial images were layered into QuickTime (Apple Computers, Cupertino, CA) movies.

Alternatively, for experiments designed to quantify the relative fluorescence intensities over the APM versus the PAPM, live sperm were allowed to attach to coverslips, incubated in CTB (5 μg/ml) for 10 minutes, and then washed five times with MW medium. Images of motile sperm were taken before and after changes in pattern of G_{M1} localization. Using image analysis tools in Openlab 3.1, minimum, maximum, mean, and mode fluorescence intensity per pixel (arbitrary units) were recorded for the whole sperm head and for equal-sized circles drawn within the APM and PAPM, before and after change in G_{M1} localization. Background fluorescence intensity was measured in identically sized circles immediately adjacent to the sperm head, and these values were subtracted from each measurement within the sperm head to adjust for local differences in background and for any signal quenching that might have occurred between images taken of the same cell. Means for the signal intensity over the whole sperm head, the APM, and the PAPM were compared within cells that exhibited a change in localization pattern, using the Wilcoxon-signed rank test for non-parametric data.

For localization of G_{M1} in fixed sperm, the cells were incubated in MW medium, allowed to attach to coverslips for 30 min, and then fixed for 15 min with either: (I) 0.004% paraformaldehyde (PF) in PBS [hereafter referred to as

"fixative A"], (II) 2% PF in PBS, (III) 2% PF and 1% glutaraldehyde in PBS (IV) 1.25% PF and 2.5 % glutaraldehyde in 100 mM sodium cacodylate and 0.5 mM $CaCl_2$ or (V) 4% PF and 0.1% glutaraldehyde with 5 mM $CaCl_2$ in PBS [hereafter referred to as "fixative B"]. The sperm were washed with PBS and incubated for 10 min with CTB (10 μg/ml). The sperm were washed again and mounted. Alternatively, sperm were fixed while in suspension, washed by centrifugation and resuspension, incubated with CTB as above, and then washed again by centrifugation and resuspension. This method was less preferred because of membrane damage. Further, to confirm that cross-linking by CTB, and not the weak fixation itself, was inducing an observed redistribution of G_{M1}, serial fixation experiments were carried out. These sperm were first fixed with fixative A for 15 minutes followed by incubation with fixative B for 15 minutes prior to labeling with CTB, washing and mounting.

Filipin localization of membrane sterols

For localization of filipin-sterol complexes in sperm membranes in conjunction with G_{M1}, sperm were incubated in MW medium with glucose, allowed to attach to coverslips for 30 min, and then fixed for 15 min with either fixative A or fixative B. The sperm were washed with PBS and incubated for 10 min with Alexa Fluor 647 CTB (10 μg/ml), washed and then incubated with filipin complex [50 μg/ml in methanol, final concentration 0.3% (v/v)] for 10 minutes. Sperm were then washed and coverslips were mounted on slides with ProLong Gold Antifade (Molecular Probes, Eugene, OR). Filipin-sterol complexes were visualized at 340-380 nm excitation.

Indirect immunofluorescence

Sperm were incubated, allowed to attach to coverslips, and fixed as described above. Sperm were washed, blocked for 30 min in PBS with 1% bovine serum albumin, and then incubated with anti-G_{M1} (1:500; Matreya, Pleasant Gap, PA) for 1 hr. They were then washed, incubated with secondary antibody (1:500) for 30 min, washed again, and mounted as above. A control for non-specific binding was performed with sperm incubated with secondary antibody alone.

Caveolin-1 null mice

Caveolin-1 null mice (Cav-$1^{-/-}$) in the C57BL/6 genetic background, were generated as previously described (Razani et al., 2001). For these experiments, sperm were collected from 20-week-old homozygous Cav-$1^{-/-}$ and corresponding wild-type cohorts (n=2 for each) as described above. Fluorescence localization of G_{M1} using CTB on both live and fixed sperm and localization of membrane sterols using filipin complex on fixed sperm were also carried out as described above.

ATP depletion and assay

Sperm ($2x10^6$/30 μl) were pre-incubated with 10 mM sodium azide and 0.2 mM pentachlorophenol (PCP) or DMSO (0.1% v/v; solvent control) for 10 minutes in MW with no glucose, pyruvate or lactate. Samples were then diluted to $2x10^6$ sperm/300 μl and incubated for an additional 20 minutes. Sperm motility was monitored under the microscope after each incubation step. Samples were then fixed with fixative B for 15 minutes. Fixed sperm were processed for G_{M1} labeling using CTB as described earlier.

For quantification of ATP, sperm treated with 10 mM sodium azide and 0.2 mM PCP were incubated as above, monitored for the cessation of motility, and then used for determining sperm ATP concentration post-ATP depletion with the ENLITEN® ATP Assay System Bioluminescence Detection Kit according to the manufacturer's instructions (Promega, Madison, WI). 100 μl of 2% TCA and 0.2% Triton were added to 50 μl of a dilution of sperm. Tubes were incubated on ice for 15 minutes and vortexed every 5 minutes. After centrifugation to remove the pellet, the supernatant was diluted again, prior to mixing with the assay reagents and quantifying luminescence. Controls included untreated cells and medium alone.

Disruption of actin and intermediate filaments

Sperm in MW medium were treated for 20 minutes with either 50 μM cytochalasin D, 5 μM latrunculin A, 1 μM swinholide A, or DMSO (0.1% v/v; solvent control) to disrupt the actin cytoskeleton. Similarly, sperm were incubated in MW medium containing either 10 or 100 mM acrylamide (Bio-Rad, Hercules, CA) for 20 minutes to disrupt intermediate filament organization. After treatment, sperm were either incubated with CTB and viewed as live cells as above, or were fixed with fixative B for 15 minutes. Fixed sperm were processed for G_{M1} labeling using CTB as described earlier. Statistical analyses for the different treatments were carried out first comparing patterns across all the groups using Kruskal-Wallis rank sum test for non-parametric data. Pairwise comparisons between treatment groups were done on arcsine-transformed data using Tukey's HSD.

Treatment with disulfide-reducing agents

Sperm were incubated in the presence of different concentrations of L-dithiothreitol (DTT) or β-mercaptoethanol (βME) for 20 minutes, and were either incubated with CTB and viewed as live cells as above, or were fixed with fixative B for 15 minutes. The cells were then washed 2 times by centrifugation and resuspension to remove DTT. Sperm were then processed for G_{M1} labeling using CTB as described. Prior to fixation, sperm motility was estimated in all samples using light microscopy. To investigate the effect of DTT on sperm post-fixation, sperm fixed for 15 minutes with either fixative A or fixative B were washed by centrifugation and resuspension using PBS and then incubated with 1 mM DTT for 20 minutes. After treatment, sperm fixed with fixative A were again fixed with fixative B for 15 minutes. All samples were washed to remove DTT and fixatives and processed for G_{M1} labeling using CTB as described. Statistical analyses for the different treatments were carried out first comparing patterns across all the groups using Kruskal-Wallis rank sum test for non-parametric data. Pairwise comparisons between treatment groups were done on arcsine-transformed data using Tukey's HSD.

Scanning Electron Microscopy

SEM was performed on both unfixed, freeze-dried sperm, and on fixed sperm subjected to critical point drying. In the first method, sperm in PBS were frozen in nitrogen slush and then freeze-dried for 3 days at -42˚C at 95 mTorr in a VirTis Freeze-mobile (VirTis, Gardiner, NY). The chip was coated with 30 nm of gold palladium in a Bal-tec SCD 050 sputter coater (Balzers Union, Liechtenstein), and viewed with a Hitachi S4500 scanning electron microscope (Mountain View, CA). In the second method, sperm were fixed for 2 h with

2.5% glutaraldehyde in 100 mM sodium cacodylate and 1% tannic acid at pH 7.4 in a culture tube. After washing by centrifugation and resuspension, they were fixed with 2% osmium tetroxide and 2% sodium cacodylate at 4˚C overnight. The cells were washed and dehydrated in ethanol with a 20 min incubation in 2% uranyl acetate at 70% ethanol. Once in absolute ethanol, they were critical point dried, coated, and viewed. Digital micrographs were collected using a Princeton Gamma Tech digital beam acquisition program (Imix, Princeton, NJ).

Results

G_{M1} localization and redistribution in the sperm head

In live motile sperm, G_{M1} localized to the APM (Figure 2.1A and B). The distribution of G_{M1} to the APM was uniform with a clear separation of signal from the PAPM at the level of the sub-acrosomal ring (SAR). All motile sperm in the medium had the same localization pattern. This pattern of localization was very stable and did not alter the entire time a sperm was viable and motile. CTB fluorescence was always confined to the APM and was never seen to diffuse across the SAR in live sperm. This finding argues against a transient confinement zone model of sub-domain maintenance, which would instead describe a state in which G_{M1} would diffuse more slowly over the APM, but not be excluded from the PAPM. Importantly, this segregation of G_{M1} to the APM was maintained even after sterol efflux with 2-OHCD (3 mM) for 60 minutes (data not shown), a concentration and duration of incubation sufficient to induce the level of sterol efflux necessary for sperm capacitation (Visconti et al., 1999a).

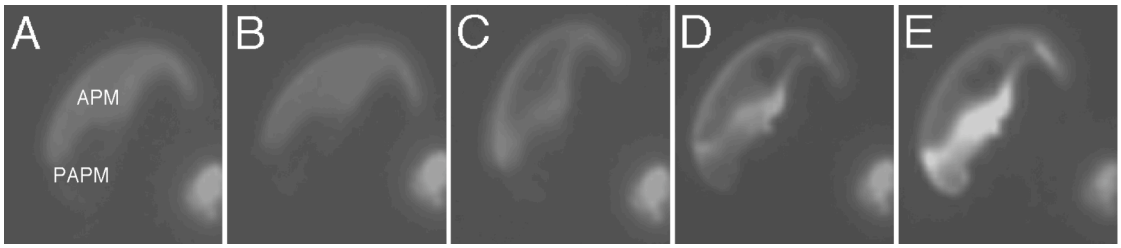

Figure 2.1. Localization of G_{M1} in live sperm with CTB. Panels A-E are single exposures taken from a series of images of an attached live, non-capacitated sperm, showing redistribution of G_{M1} upon the cessation of motility. Panels A and B represent the pattern seen in the motile sperm, whereas panels C-E show stages in the redistribution of G_{M1} in the same cell when immotile.

However, within seconds after the cessation of motility, the pattern of CTB fluorescence changed dramatically, appearing to lessen over the APM and brightening strongly over the PAPM (Figure 2.1 C-E). First, the signal decreased from within the ES and increased at the borders of the APM (the AA, the SAR and the perforatorium), prior to extending into the PAPM. The redistribution occurred within 10 to 100 seconds after the cessation of motility. This change was consistent with the pattern seen in dead sperm and was not associated with acrosomal exocytosis (data not shown). Similar localization of G_{M1} to the PAPM was also seen in most sperm that were not motile at the beginning of these same experiments, suggesting that the loss of segregation coincided with the sperm becoming non-viable.

Two possibilities exist for the change in pattern seen upon the cessation of motility/death. The first would be a redistribution of G_{M1} from the APM to the PAPM, whereas the second would involve the unmasking or appearance of new G_{M1} on the outer leaflet of the PAPM in conjunction with some degree of redistribution. To distinguish between these possibilities, we

repeated these experiments with repetitive washing out of unbound CTB from the medium. This would minimize free CTB available to bind to new molecules of G_{M1} that might become exposed in the PAPM. Quantification of fluorescence intensity in the APM versus the PAPM revealed a statistically significant decrease in the APM coincident with a significant increase in signal in the PAPM (Figure 2.2 A, B and D). These changes, and the pattern of movement seen in Figure 2.1 indicate that redistribution did indeed occur.

However, the decrease in signal over the APM could not account for the disproportionate increase in fluorescence intensity over the PAPM, even taking into consideration the fact that the PAPM is approximately one-half the size of the APM (Figure 2.2 B and D). The increase in fluorescence associated with the PAPM also caused an increase in whole head intensity after redistribution (Figure 2.2C). To determine if redistribution induced some change in the fluorescence properties of the fluorophore (Maxfield, 1982), we used both a fluorimeter and ELISA plate reader to quantify total fluorescence intensity of AlexaFluor 488-conjugated CTB in entire incubation tubes before and after the CTB-induced redistribution of G_{M1} (In separate experiments with $n \geq 3$, these readings were taken both with excess CTB in the medium, and after washing out unbound CTB. In addition, in separate experiments, sperm were allowed to lose motility on their own, or by the addition of fixative A.).

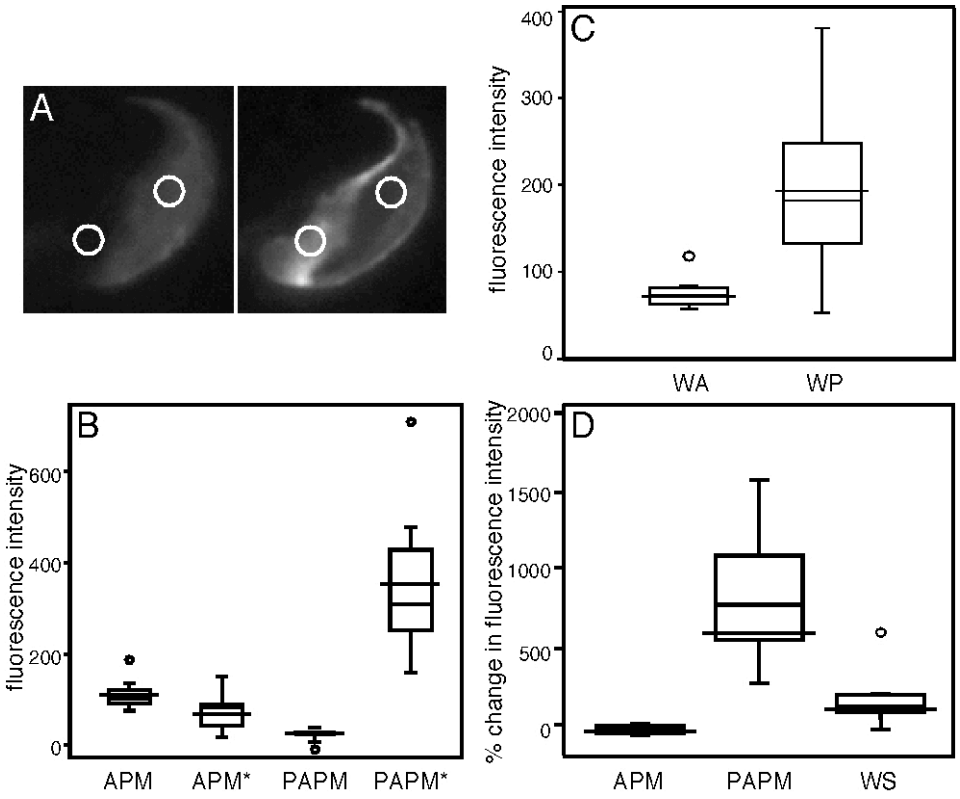

Figure 2.2. Fluorescence intensity of CTB in different regions of the sperm head. Images were taken of live sperm having an APM pattern of fluorescence and then again at the same exposure settings after cessation of motility when they displayed a PAPM pattern (n=9). Mean fluorescence intensities within the APM and PAPM were recorded before and after (*) the shift in pattern of localization (Panel B), using an equal-sized circle within each region (Panel A). Fluorescence intensity was also recorded for the whole sperm head before (WA) and after (WP) the shift in localization pattern (Panel C). Results are shown as box-whisker plots in Panels B, C and D, with the boundaries of the boxes representing the 25th and 75th quantiles, the 50th quantile displayed as a line within the box, and the mean as a line extending through the box. Whiskers extend to the 10th and 90th quantiles, and circles represent outliers. Statistically significant differences were found between groups (Panel B, $P<0.004$), and between the whole sperm heads upon shift in pattern (Panel C, $P<0.03$), using Wilcoxon's signed rank test. The percent change in intensity was also determined for the APM, PAPM, and whole sperm head (Panel D). In this panel, a negative value denotes a decrease in fluorescence intensity, and a positive value an increase in fluorescence intensity.

We did not detect a significant change in total fluorescence of the system under any of these conditions (data not shown). Interestingly, experiments involving the quenching of fluorophores conjugated to CTB have suggested that internalization and reappearance of G_{M1} in the APM is also occurring prior to redistribution, suggesting that a combination of mechanisms is responsible for the change in pattern (manuscript in preparation, Buttke, Selvaraj, Asano, and Travis). We are therefore continuing to investigate this phenomenon.

Immunolocalization with anti-G_{M1} antibody

To corroborate that CTB was in fact binding to G_{M1} in the APM, we performed indirect immunofluorescence experiments with a bivalent primary antibody against G_{M1} on sperm fixed with fixative A (Figure 2.3) or with a strong fixative (fixative B; results were identical between the two fixation conditions, data not shown). This low concentration of PF (fixative A) was tested because it has been reported to immobilize sperm without permeabilization (Harrison and Vickers, 1990). We observed fluorescence over the APM of most sperm incubated under both non-capacitating conditions or in the presence of 2-OHCD (Figure 2.3). These findings verified the segregation of G_{M1} seen in live cells with CTB.

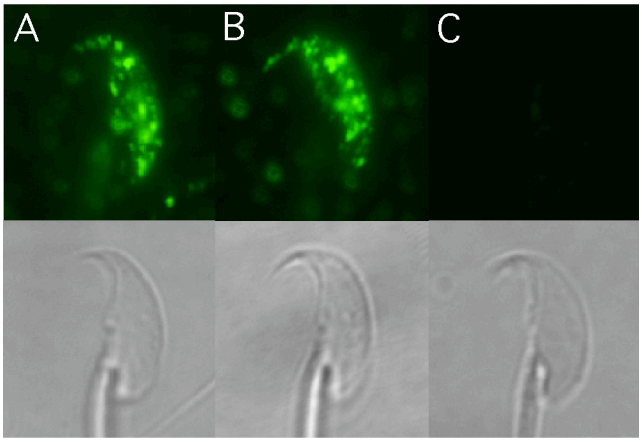

Figure 2.3. Indirect immunofluorescence localization of G_{M1} in sperm fixed lightly with fixative A. G_{M1} localization and corresponding bright field images are shown in the panels. G_{M1} localized to the APM in the heads of sperm incubated prior to fixation under both non-capacitating conditions (Panel A) and after incubation with 2-OHCD (Panel B) (n = 5). A negative control performed with no primary antibody demonstrated the specificity of the secondary antibody (Panel C). In addition to the antibody not inducing redistribution to the PAPM in these lightly fixed cells, another subtle difference was also observed versus the use of CTB. With the antiserum, the fluorescence signal was patchier over the ES and AA, suggesting that cross-linking was occurring, but was different in some way versus the pentameric binding of the CTB.

Specific fixation conditions prevented G_{M1} redistribution

Different fixation conditions were tested to see whether the G_{M1} could be immobilized and redistribution prevented, three of which are shown in Table 1. The patterns of G_{M1} localization seen in sperm under different fixation conditions are described as “APM” for fluorescence over the APM, “D” for a diffuse fluorescence all over the sperm head, “AA/PAPM” where the apical acrosome and PAPM show fluorescence, and “PAPM” for fluorescence over the PAPM.

The weak fixative (fixative A) caused almost all sperm to show G_{M1} redistribution with CTB, with signal over the PAPM (Table 2.1). Fixation with 2% PF in PBS and fixation with 2% PF and 1% glutaraldehyde could prevent CTB-induced G_{M1} redistribution in a small proportion of sperm, and results for these conditions between samples were variable (data not shown). The next fixation condition tested, 1.25% PF and 2.5% glutaraldehyde in 100 mM sodium cacodylate and 0.5 mM $CaCl_2$, immobilized G_{M1} to the APM in about 75% of sperm incubated under non-capacitating conditions (Table 2.1). However, this fixative was not adequate to immobilize G_{M1} in cells incubated with 2-OHCD (data not shown). Ultimately, the use of fixative B was adequate to immobilize the lipids in 80% of the sperm regardless of the incubation condition. These data underscore that fixation conditions can have dramatic effects on the apparent localization of lipids, and should be determined for specific cell types by work in live cells.

G_{M1} redistribution was induced by CTB

Although the data from experiments with both live and fixed sperm suggested that G_{M1} redistribution was induced by CTB in non-viable cells, a direct test was needed to show that G_{M1} redistribution was not also induced by the weak fixation conditions apart from the cross-linking by CTB. Serial fixations, first using fixative A and then fixing the same sample with fixative B prior to incubation with CTB, were employed to rule out this possibility. If the light fixative itself induced redistribution, then this would have resulted in the majority of the cells having a PAPM signal. However, these results showed that G_{M1} was immobilized to the APM in ~90% of the sperm (Figure 2.4). This demonstrated that the redistribution of G_{M1} was due to the specific

Table 2.1. Patterns of G_{M1} Distribution in Non-Capacitated Sperm with Different Fixation Conditions

Fixative	Pattern			
	APM	D	AA/PAPM	PAPM
0.004% paraformaldehyde* *(Fixative A)*	ns†	8.3±2.4	16.5±3.0	73.1±2.4
1.25% paraformaldehyde, 2.5% glutaraldehyde, 100mM sodium cacodylate, 0.5 mM calcium chloride*	75.2±1.4	24.8±1.4	0	0
4% paraformaldehyde, 0.1% glutaraldehyde, 5 mM calcium chloride* *(Fixative B)*	83.7±1.7	16.2±1.7	0.2±0.1	0

*Kruskal-Wallis analysis showed significant differences between patterns ($p<0.05$)
†ns: not scored because this pattern had consistently less fluorescence intensity than the other patterns, and occurred in <5% of cells
Patterns: APM, acrosomal; D, diffuse; AA/PAPM, apical acrosome and post-acrosomal; PAPM, post-acrosomal. (n = 6-15 samples for each fixation condition)

cross-linking with CTB and not induced by weak fixation. Indirect immunofluorescence on sperm fixed with fixative A (shown previously in Figure 2.3), also suggested that the specific nature of cross-linking by the pentameric CTB was critical for G_{M1} redistribution, because there can be significant cross-linking when using an indirect method with secondary antibodies, yet this did not induce redistribution. However, this variation in the nature of the cross-linking might have contributed to the subtle difference in the degree of "patchiness" over the APM when using indirect immunofluorescence localization. To demonstrate further the critical role of CTB in induction of redistribution, sperm were left overnight at 37˚C then assessed the next morning to verify that all were immotile. They were then

fixed with fixative B, and incubated with CTB. The vast majority of these cells displayed an APM pattern (n=3; data not shown). This finding showed that the cessation of motility itself was not the driving force behind redistribution, but that incubation with CTB without prior heavy fixation was required for redistribution. If left at 37˚C for even longer periods, the segregation of the sub-domains eventually did break down, and CTB fluorescence labeling in the sperm head took on a more diffuse pattern. By this point in time, the sperm structure and membranes showed signs of damage (data not shown).

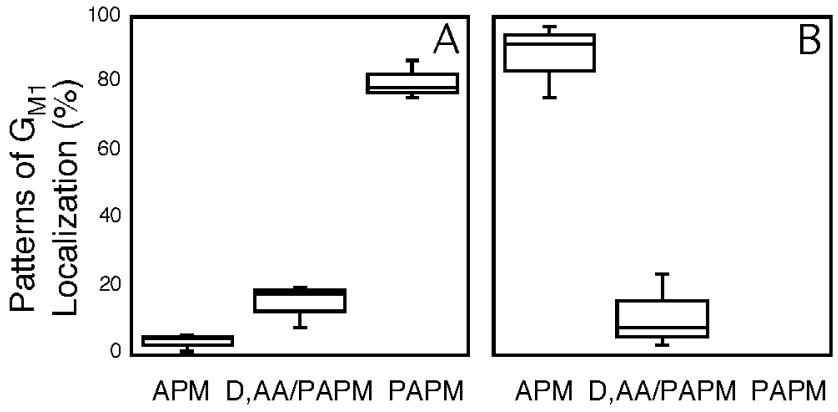

Figure 2.4. Patterns of G_{M1} localization seen in sperm using weak, then strong, fixation conditions. Box plots showing percent of sperm with specific G_{M1} patterns (APM, Acrosomal; D, AA/PAPM, Diffuse or Apical Acrosomal and Post-acrosomal; PAPM, Post-acrosomal) seen with (A) incubation in fixative A prior to incubation with CTB, and (B) serial fixation: first fixative A, then incubating the same sample with fixative B prior to incubation with CTB. G_{M1} distribution was predominantly seen over the PAPM with weak fixation (A); subsequent fixation of fixative A-treated samples with fixative B showed sperm with G_{M1} distribution predominantly over the APM (B). These data showed that the redistribution of G_{M1} to the PAPM was not induced by the weak fixation but was due to specific cross-linking by CTB.

G_{M1} redistribution was not associated with the movement of sterols

G_{M1} and sterol dual localization using CTB conjugated with Alexa Fluor 647, and filipin, respectively, was performed on sperm fixed with fixative B (Figure 2.5 A and B) and fixative A (Figure 2.5 C and D). With the heavy fixative, both G_{M1} (Figure 2.5A) and the filipin sterol complex (Figure 2.5B) localized to the APM, mirroring the localization of G_{M1} in live sperm (Figure 2.1A and B), and previous reports of filipin-sterol complex localization in fixed cells. As noted above with weak fixation, G_{M1} redistributed from the APM and localized to the PAPM (Figure 2.5C); however, sterols did not redistribute in these same cells (Figure 2.5D). These data suggest that despite the segregation of both these "raft associated" lipids to the APM in live sperm,

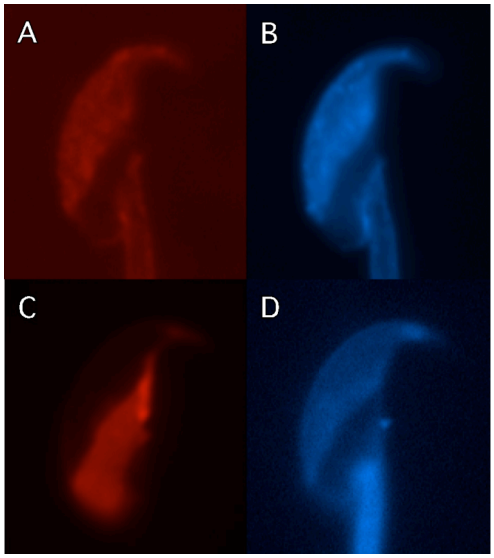

Figure 2.5. Localization of G_{M1} and filipin-sterol complexes in fixed sperm. G_{M1} was localized using CTB Alexa Fluor 647 (red) and sterols were localized using filipin complex (blue) in sperm fixed with fixative B (panels A and B) and fixative A (panels C and D). With the stronger fixative, both G_{M1} (A) and the filipin sterol complex (B) localized to the APM. With weak fixation, G_{M1} redistributed from the APM (as seen in live cells; Fig. 2A) and localized to the PAPM (C), although sterols did not redistribute in these same cells (D).

CTB could induce separation of G_{M1} from sterols, which maintained their original localization. When coupled with the lack of redistribution after sterol efflux, these data suggest that interactions between sterols and G_{M1} did not exclusively maintain APM sub-domain segregation.

Membrane sub-domain segregation in caveolin-1 null mice

The preferential interaction of lipids with specific proteins has been suggested to be a mechanism for the generation and maintenance of membrane sub-domains. A definitive demonstration that this model is not operative in the sperm head would require individual deletions of each membrane protein and is not practical. However, specific proteins found in sperm have been shown to interact with lipids. Of these, caveolin-1 was an attractive candidate for investigation because we have demonstrated its

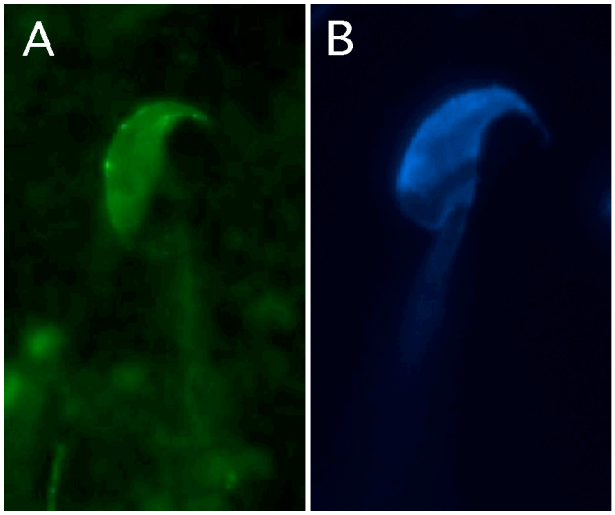

Figure 2.6. Localization of G_{M1} and filipin-sterol complexes in sperm from caveolin-1$^{-/-}$ mice. G_{M1} was localized in live sperm using CTB Alexa Fluor 488 (green, A) and sterols were localized using filipin complex (blue, B) in sperm fixed with fixative B. Both G_{M1} and sterols localized to the APM as they did in wild-type mice of this same strain (data not shown).

presence in the region of the APM (Travis et al., 2001b), and it interacts with sterols. We therefore investigated the distribution of G_{M1} and sterols in caveolin-1 null mice. We found both G_{M1} and sterols to be segregated to the APM (Figure 2.6A and B). These data suggest that a preferential interaction between specific lipids and caveolin-1 was not needed for the maintenance of these sub-domains, and that they could be generated in the absence of caveolin-1. Upon cessation of motility in unfixed cells or in the presence of fixative A, G_{M1} in these caveolin-1 knock-out mice also redistributed to the PAPM (data not shown). These findings indicated that caveolin-1 was not required for the redistribution phenomenon.

Sub-domain segregation was not dependent upon ATP generation

The fact that redistribution of G_{M1} occurred at the time of cessation of motility suggested that the maintenance of sub-domain segregation might be dependent upon ATP generation. To test this possibility, we incubated sperm in the absence of metabolic substrates and in the presence of PCP and azide. After motility ceased, we treated the sperm with the strong fixative (Fixative B) to immobilize the G_{M1} as it had been prior to incubation with CTB. We found the pattern of fluorescence to be once again predominantly in the APM (data not shown). The concentration of ATP in sperm treated in this fashion was found to be at basal levels, equivalent to that seen in dead sperm left to incubate overnight in the absence of metabolic substrates, and approximately $\leq$5% of that seen in live sperm (data not shown).

The membrane compartmentation model

In fixed cells, the SAR appears as a distinct ridge at the boundary between the APM and PAPM sub-domains of the sperm head when visualized by freeze fracture, atomic force microscopy, or surface replica (Friend and Fawcett, 1974; Lin and Kan, 1996; Ellis et al., 2002). A cytoskeletal barrier at this point would be consistent with the membrane compartmentation model of sub-domain segregation. In Figure 2.7A, SEM of unfixed, freeze-dried sperm showed that the SAR was not an artifact of fixation, but was a bona fide topographical feature. The SAR was also visible in demembranated, fixed sperm (Figure 2.7B), confirming that it was an extension of the dense perinuclear theca (Olson et al., 2003), as are two of the three rods of the perforatorium (Oko and Clermont, 1988; Korley et al., 1997). Within the APM, the ES is demarcated from the AA by a groove running from the SAR to the perforatorium (Figure 2.7A and B). The posterior ring delimits the lower boundary of the PAPM (Figure 2.7B). These data suggested that the SAR was not an artifact of fixation or detergent, and that cytoskeletal elements delimit the APM, shown here and elsewhere to be enriched in sterols, caveolin-1 and G_{M1} (Friend, 1982; Lin and Kan, 1996; Visconti et al., 1999b; Travis et al., 2001b).

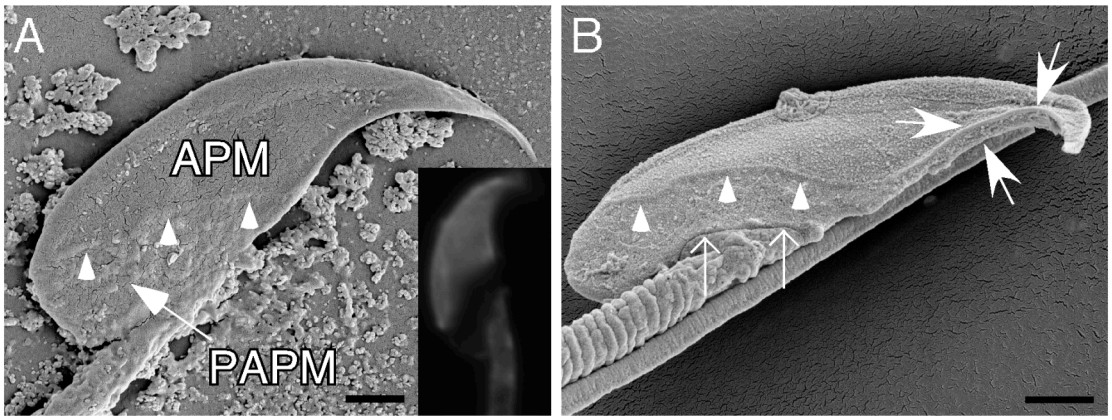

Figure 2.7. Evidence of structures delineating membrane sub-domains in the sperm head. In panel A, SEM of unfixed, freeze-dried sperm reveals the SAR (arrowheads) at the boundary of the APM and PAPM. The cells were neither fixed nor washed out of medium, but were freeze-dried while live in PBS, accounting for the deposits. The inset shows the localization pattern of filipin-sterol complex in a sperm fixed with fixative A. Panel B shows SEM of a sperm, which became demembranated during the process of fixing/critical point drying. The SAR (arrowheads) and posterior ring (thin arrows) are noted, as are the two linear rods of the perforatorium (filled arrows).

A cytoskeletal border around a membrane sub-domain is consistent with a membrane compartmentation model of segregation. To investigate potential roles for actin in this regard, we incubated sperm with cytochalasin D and latrunculin A (which sequester monomeric actin and shift the equilibrium of dynamic actin filaments to depolymerization), and swinholide A (which severs actin filaments). These agents had no effect on sub-domain segregation (Figure 2.8). We next incubated sperm with acrylamide, a disruptor of intermediate filaments. Again, we saw no effect on sub-domain maintenance (Figure 2.8). These agents also did not prevent the redistribution of G_{M1} to the PAPM in unfixed sperm upon the cessation of motility, or in sperm treated with the disruptors and then fixed with fixative A (n=3; data not shown).

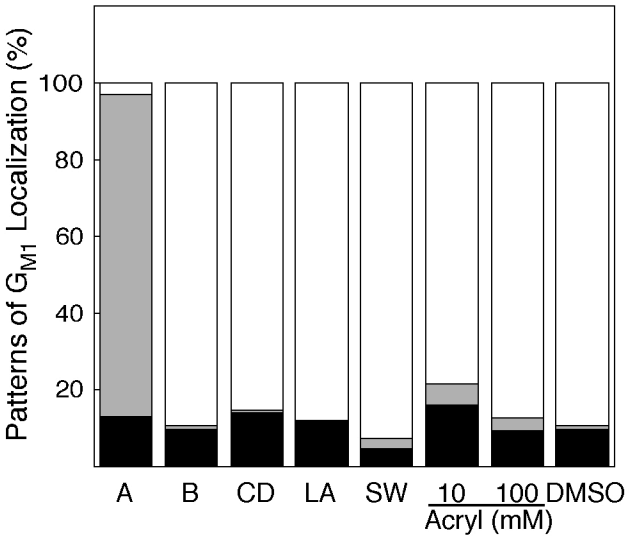

Figure 2.8. Localization of G_{M1} after treatment of sperm with compounds known to disrupt the cytoskeleton. Sperm were fixed with fixative A (A) or with fixative B (B) as controls to induce or prevent redistribution of G_{M1} to the PAPM. Live sperm were treated with 50 μM cytochalasin D (CD), 5 μM latrunculin A (LA), 1 μM swinholide (SW), two concentrations of acrylamide (Acryl) as indicated, or an equivalent volume of DMSO as a solvent control for the agents affecting actin, prior to fixation with fixative B. In all bars, the black fill indicates the mean percentage of sperm demonstrating a diffuse pattern of G_{M1} localization, the gray fill indicates a post-acrosomal pattern, and the white fill indicates an acrosomal pattern (n=3 for all conditions). Statistically significant differences between conditions were noted with a Kruskal-Wallis analysis for the acrosomal pattern ($P<0.0001$) and post-acrosomal pattern ($P<0.0001$), whereas there was no significant difference within the diffuse pattern. No differences were apparent in pairwise comparisons between treatments with individual disruptors of the cytoskeleton and the heavy fixative (bar B).

However, when we incubated sperm with DTT, we observed an interesting effect. We saw that exposure to reducing agents prior to incubation with fixative B resulted in the majority of sperm having a post-acrosomal pattern of fluorescence (Figure 2.9). A similar effect was seen with bME, although to a lesser extent (data not shown). These data implicated that

disulfide bonds play an important role in the maintenance of these sub-domains. It should be noted that these effects were observed at concentrations low enough that they did not affect viability as determined by both motility and propidium iodide fluorescence (0.05 mM through 1 mM DTT; data not shown). In live cells, a small percentage of DTT-treated motile sperm also displayed a PAPM pattern of G_{M1} localization (data not shown), suggesting both that disulfide bonds were important for the maintenance of these sub-domains, and that those proteins were either not the entire mechanism of segregation, or that the cell had some mechanism to counteract the effects of the reducing agent. Heavy fixation (Fixative B) prior to exposure to a reducing agent resulted in the maintenance of the sub-domain segregation. This finding reinforced a role for the cross-linking of specific proteins in sub-domain maintenance, as opposed to a specific role for the disulfide bonds themselves.

Figure 2.9. Localization of G_{M1} after treatment of sperm with disulfide-reducing agents. *Panel A*: Sperm were fixed with fixative A (bar A) or with fixative B (bar B) as controls to induce or prevent redistribution of G_{M1} to the PAPM. Live sperm were treated with varying concentrations of DTT as indicated. After treatment with DTT, the sperm were incubated with fixative B, and G_{M1} was localized using CTB. In all bars, the black fill indicates the mean percentage of sperm demonstrating a diffuse pattern of G_{M1} localization, the gray fill indicates a post-acrosomal pattern, and the white fill indicates an acrosomal pattern (n=3 for all conditions). Statistically significant differences between conditions were noted with a Kruskal-Wallis analysis for the acrosomal pattern ($P<0.002$) and post-acrosomal pattern ($P<0.004$), whereas there was no significant difference within the diffuse pattern. Concentrations of DTT $\geq$ 0.1 mM were significantly different regarding the acrosomal and post-acrosomal patterns in pairwise comparisons with the heavy fixative (bar B) ($P<0.025$ for all comparisons). *Panel B*: Bars A and B were fixed as in Panel A. In bar C, sperm were fixed first in fixative A and then with fixative B. In bar D, sperm were treated while live with 1 mM DTT, then fixed in fixative B. In bar E, sperm were fixed first in fixative A, then treated with 1 mM DTT, then fixed with fixative B, whereas in bar F, the sperm were fixed first with fixative B then treated with DTT. The shades of fill represent the same patterns of localization as in Panel A (n=5 trials for each condition with at least 2 animals/trial). Statistically significant differences between conditions were noted with a Kruskal-Wallis analysis for the acrosomal pattern ($P<0.0001$) and post-acrosomal pattern ($P<0.0001$), whereas there was no significant difference within the diffuse pattern. Pairwise comparisons between treatment conditions showed no significant differences between bars B, C, and F for the acrosomal and post-acrosomal patterns. These results show that fixation alone did not induce a change in pattern of G_{M1} localization, and that heavy fixation (fixative B) prior to treatment with DTT prevented redistribution (bar F), whereas light fixation (fixative A) only moderately weakened the effect of DTT.

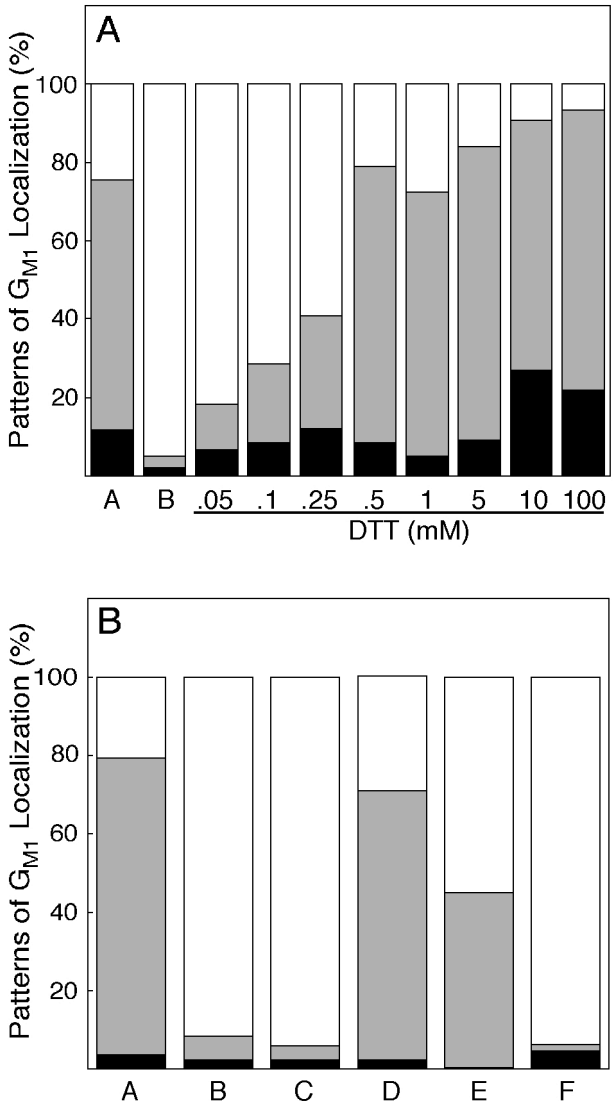
A
Patterns of G_{M1} Localization (%)
100
80
60
40
20
A
B
.05
.1
.25
.5
1
5
10
100
DTT (mM)
B
Patterns of G_{M1} Localization (%)
100
80
60
40
20
A
B
C
D
E
F

Discussion

There have been several studies of G_{M1} localization in sperm, with results varying widely between and within species. For example, in the mouse it has been shown that G_{M1} localizes to the PAPM and that this localization does not change with capacitation (Trevino et al., 2001). Another study has localized G_{M1} to the midpiece and then moving to the head during capacitation (Shadan et al., 2004). These were both performed at 16˚C, and phase transitions between this and physiologic temperatures (Wolf et al., 1990) might account for some disparity with our results. In rat sperm, it was suggested that G_{M1} localizes to the PAPM and then moves to the APM during capacitation (Roberts et al., 2003), whereas in human sperm it was recently reported that G_{M1} has a diffuse localization pattern (Cross, 2004). In all of these reports, temperatures, timing of CTB treatment, the use of live, viable sperm versus different fixation conditions, and the use of epididymal versus ejaculated sperm have varied.

In this study, we observed the endogenous ganglioside G_{M1} in the plasma membrane of live murine sperm. Underscoring the difficulties inherent when studying membrane sub-domains, our data reinforce that patching artifacts dramatic in terms of size and speed of redistribution can be induced and have the potential to overcome otherwise immutable diffusion barriers, and that a given fixation condition can vary widely in its ability to immobilize membrane lipids in a given cell depending upon modulation of membrane lipids. These difficulties are likely to be found in other cell systems as well.

In living cells, we found that G_{M1} localized to the APM and segregated at the level of the SAR, matching the localization of sterols and caveolin-1 (Travis et al., 2001b) in fixed cells. Lack of movement of G_{M1} from the APM to the

PAPM, even over periods of hours, argued against a “transient confinement zone” model of sub-domain segregation. Within 10 to 100 seconds of the cessation of motility, the CTB fluorescence redistributed dramatically, decreasing in the APM and intensifying in the PAPM. The timing of this change suggested that in a live cell, the mechanism of segregation functioned to resist the perturbation energy imparted by the cross-linking CTB. At the time of cessation of motility/cell death, that mechanism was compromised in some way such that the cross-linked G_{M1} was induced to move across the SAR. Interestingly, ATP was not required for maintenance of segregation. This was not unexpected given the lack of ATP-generating pathways in the sperm head [Please see (Travis and Kopf, 2002) for a review.].

Sterols visualized with filipin in the APM were stably segregated even after the redistribution of G_{M1} to the PAPM. This finding suggests that even though sterols and G_{M1} co-localized in the APM and were segregated at the same boundary of the SAR, the mechanisms that maintain segregation of these two lipids could be different or that the lipids are separable. In either case, both this finding and the fact that sterol efflux did not facilitate movement of G_{M1} across the SAR, suggest that interactions between sterols and G_{M1} do not maintain sub-domain segregation. Whether the co-localized G_{M1}, sterols, and caveolin-1 are all members of an integrated, single APM raft, or are components of numerous small-scale heterogeneities within the APM, awaits further investigation.

Although segregation of sterol-rich and sterol-poor membrane sub-domains has been noted in fixed sperm at the SAR boundary, results from protein and lipid localization experiments, including fluorescence recovery after photobleaching in live sperm, often disagree regarding the ability of the SAR or

other potential “fences” (e.g. posterior ring and annulus) to act as barriers to lateral diffusion. For example, some proteins and lipid probes have been shown to be restricted to specific membrane domains (Myles et al., 1984; Phelps et al., 1988; Friend, 1989; Nehme et al., 1993), but others have been demonstrated to diffuse freely across the cytoskeletal structures underlying these putative barriers (Wolfe et al., 1998; Mackie et al., 2001; Christova et al., 2004). Apart from methodology, one explanation for these differences might be that the barriers are effective primarily against endogenous membrane constituents. This would imply either defined interactions between membrane molecules and the “fence”, or interactions between membrane constituents with underlying structures (i.e. “anchors”). Exogenous probes might behave anomalously, moving between the anchored native molecules or penetrating the fence to varying degrees.

Either a lipid shell or membrane compartmentation model would be consistent with these kinds of variations in data observed with exogenous probes, and could be consistent with the structures underlying a proposed barrier to lateral diffusion at the SAR. As noted, it is impossible to rule out the lipid shell model definitively, but we did observe that the absence of the sterol-binding protein, caveolin-1, did not affect the segregation of G_{M1} or sterols. We hypothesized that the “fence” of the SAR would likely be composed of cytoskeletal proteins such as actin and/or vimentin, both of which help comprise larger structures such as the perinuclear theca and perforatorium (Virtanen et al., 1984; Oko et al., 1990; Breed et al., 2000), and associate with lipid-binding proteins such as PERF-15 (Oko and Morales, 1994; Schmitt et al., 1994). However, it is not surprising that dynamic actin filaments are not involved in the segregation (as indicated by the data from cytochalasin D and

latrunculin A treatments), due to the facts that sperm must be kept in a quiescent state while stored in the epididymis, and do not have ATP-generating pathways in the sperm head. The finding that disulfide bonds between proteins are essential for sub-domain segregation is intriguing. Given that sperm have minimal cytoplasm underlying the plasma membrane, this membrane could interact intimately with structures such as the SAR and perforatorium. These structures arise from the perinuclear theca, and have components attached to them via disulfide bonds (Perry et al., 1999); however, the perinuclear theca is itself not solubilized by treatment with disulfide-reducing agents (Sutovsky et al., 1997). We are now investigating the proteome of these structures to identify the critical proteins and interactions involved.

The question arises as to why sperm possess such large, stable membrane sub-domains when compared with other cells. Several possible functions are consistent with the data: 1) a rigid/highly-ordered APM might prevent premature fusion with the outer acrosomal membrane, perhaps by decreasing permeability to Ca^{++}, a trigger of acrosomal exocytosis, 2) sterol efflux from an ordered APM to oviductal HDL and albumin (Langlais et al., 1988; Ehrenwald et al., 1990) could provide a “sensing mechanism” so that capacitation occurs in the oviduct, 3) a single, large membrane sub-domain might help target protein machinery needed to interact with the egg, and 4), differences in APM raft composition might define sub-populations of sperm capable of capacitating at different times, expanding the window of opportunity to fertilize eggs (Flesch et al., 2001).

The localization and movement of G_{M1} in murine sperm is remarkable for several reasons. First, it provides evidence in living cells for the existence

of membrane sub-domains, still a matter of some controversy (Munro, 2003). Second, it shows that these sub-domains can exist on a micron scale and over a long time period in viable cells. The large size of these sub-domains makes sperm an ideal model system for the study of sub-domain segregation, in particular when compared with the types of sub-domains more typical of somatic cells. Finally, understanding of these sub-domains sheds important light on understanding the nature of sperm capacitation, such as how stimuli such as sterol efflux can be transduced into the functional changes that allow a sperm to fertilize an egg.

Acknowledgements

We thank Dr. Hollis Erb (Cornell University) for her help with statistical analysis and Carole Daugherty at the Cornell Integrated Microscopy for performing the SEM.

REFERENCES

Breed, W.G., Idriss, D., and Oko, R.J. (2000). Protein Composition of the Ventral Processes on the Sperm Head of Australian Hydromyine Rodents. Biol Reprod 63, 629-634.

Christova, Y., James, P., Mackie, A., Cooper, T.G., and Jones, R. (2004). Molecular Diffusion in Sperm Plasma Membranes During Epididymal Maturation. Mol Cell Endocrinol 216, 41-46.

Clark, J.M., and Koehler, J.K. (1990). Observations of Hamster Sperm-Egg Fusion in Freeze-Fracture Replicas Including the Use of Filipin as a Sterol Marker. Mol Reprod Dev 27, 351-365.

Cross, N.L. (2004). Reorganization of Lipid Rafts During Capacitation of Human Sperm. Biol Reprod 71, 1367-1373.

Davis, B.K. (1976). Influence of Serum Albumin on the Fertilizing Ability in Vitro of Rat Spermatozoa. Proc Soc Exp Biol Med 151, 240-243.

Ehrenwald, E., Foote, R.H., and Parks, J.E. (1990). Bovine Oviductal Fluid Components and Their Potential Role in Sperm Cholesterol Efflux. Molecular Reproduction and Development 25, 195-204.

Ellis, D.J., Shadan, S., James, P.S., Henderson, R.M., Edwardson, J.M., Hutchings, A., and Jones, R. (2002). Post-Testicular Development of a Novel Membrane Substructure within the Equatorial Segment of Ram, Bull, Boar, and Goat Spermatozoa as Viewed by Atomic Force Microscopy. J Struct Biol 138, 187-198.

Flesch, F.M., Brouwers, J.F., Nievelstein, P.F., Verkleij, A.J., van Golde, L.M., Colenbrander, B., and Gadella, B.M. (2001). Bicarbonate Stimulated Phospholipid Scrambling Induces Cholesterol Redistribution and Enables Cholesterol Depletion in the Sperm Plasma Membrane. J Cell Sci 114, 3543-3555.

Friend, D.S. (1982). Plasma-Membrane Diversity in a Highly Polarized Cell. J Cell Biol 93, 243-249.

Friend, D.S. (1989). Sperm Maturation: Membrane Domain Boundaries. Ann N Y Acad Sci 567, 208-221.

Friend, D.S., and Fawcett, D.W. (1974). Membrane Differentiations in Freeze-Fractured Mammalian Sperm. J Cell Biol 63, 641-664.

Gaus, K., Gratton, E., Kable, E.P., Jones, A.S., Gelissen, I., Kritharides, L., and Jessup, W. (2003). Visualizing Lipid Structure and Raft Domains in

Living Cells with Two-Photon Microscopy. Proc Natl Acad Sci U S A 100, 15554-15559.

Harrison, R.A., and Vickers, S.E. (1990). Use of Fluorescent Probes to Assess Membrane Integrity in Mammalian Spermatozoa. J Reprod Fertil 88, 343-352.

Kim, K.S., and Gerton, G.L. (2003). Differential Release of Soluble and Matrix Components: Evidence for Intermediate States of Secretion During Spontaneous Acrosomal Exocytosis in Mouse Sperm. Dev Biol 264, 141-152.

Korley, R., Pouresmaeili, F., and Oko, R. (1997). Analysis of the Protein Composition of the Mouse Sperm Perinuclear Theca and Characterization of Its Major Protein Constituent. Biol Reprod 57, 1426-1432.

Kusumi, A., Koyama-Honda, I., and Suzuki, K. (2004). Molecular Dynamics and Interactions for Creation of Stimulation-Induced Stabilized Rafts from Small Unstable Steady-State Rafts. Traffic 5, 213-230.

Langlais, J., Kan, F.W.K., Granger, L., Raymond, L., Bleau, G., and Roberts, K.D. (1988). Identification of Sterol Acceptors That Stimulate Cholesterol Efflux from Human Spermatozoa During in Vitro Capacitation. Gamete Research 20, 185-201.

Lauer, S., Goldstein, B., Nolan, R.L., and Nolan, J.P. (2002). Analysis of Cholera Toxin-Ganglioside Interactions by Flow Cytometry. Biochemistry 41, 1742-1751.

Lin, Y., and Kan, F.W. (1996). Regionalization and Redistribution of Membrane Phospholipids and Cholesterol in Mouse Spermatozoa During in Vitro Capacitation. Biol Reprod 55, 1133-1146.

Mackie, A.R., James, P.S., Ladha, S., and Jones, R. (2001). Diffusion Barriers in Ram and Boar Sperm Plasma Membranes: Directionality of Lipid Diffusion across the Posterior Ring. Biol Reprod 64, 113-119.

Maxfield, F.R. (1982). Weak Bases and Ionophores Rapidly and Reversibly Raise the Ph of Endocytic Vesicles in Cultured Mouse Fibroblasts. J Cell Biol 95, 676-681.

Munro, S. (2003). Lipid Rafts: Elusive or Illusive? Cell 115, 377-388.

Myles, D.G., Primakoff, P., and Koppel, D.E. (1984). A Localized Surface Protein of Guinea Pig Sperm Exhibits Free Diffusion in Its Domain. J Cell Biol 98, 1905-1909.

Nehme, C.L., Cesario, M.M., Myles, D.G., Koppel, D.E., and Bartles, J.R. (1993). Breaching the Diffusion Barrier That Compartmentalizes the

Transmembrane Glycoprotein Ce9 to the Posterior-Tail Plasma Membrane Domain of the Rat Spermatozoon. J.Cell Biol. 120, 687-694.

Oko, R., and Clermont, Y. (1988). Isolation, Structure and Protein Composition of the Perforatorium of Rat Spermatozoa. Biol Reprod 39, 673-687.

Oko, R., and Morales, C., R. (1994). A Novel Testicular Protein, with Sequence Similarities to a Family of Lipid Binding Proteins, Is a Major Component of the Rat Sperm Perinuclear Theca. Development biology 166, 235-245.

Oko, R., Moussakova, L., and Clermont, Y. (1990). Regional Differences in Composition of the Perforatorium and Outer Periacrosomal Layer of the Rat Spermatozoon as Revealed by Immunocytochemistry. Am J Anat 188, 64-73.

Olson, G.E., Winfrey, V.P., and Nagdas, S.K. (2003). Structural Modification of the Hamster Sperm Acrosome During Posttesticular Development in the Epididymis. Microsc Res Tech 61, 46-55.

Pelletier, R.M., and Friend, D.S. (1983). Development of Membrane Differentiations in the Guinea Pig Spermatid During Spermiogenesis. Am J Anat 167, 119-141.

Perry, A.C., Wakayama, T., and Yanagimachi, R. (1999). A Novel Trans-Complementation Assay Suggests Full Mammalian Oocyte Activation Is Coordinately Initiated by Multiple, Submembrane Sperm Components. Biol Reprod 60, 747-755.

Phelps, B.M., Primakoff, P., Koppel, D.E., Low, M.G., and Myles, D.G. (1988). Restricted Lateral Diffusion of Ph-20, a Pi-Anchored Sperm Membrane Protein. Science 240, 1780-1782.

Razani, B., Engelman, J.A., Wang, X.B., Schubert, W., Zhang, X.L., Marks, C.B., Macaluso, F., Russell, R.G., Li, M., Pestell, R.G., Di Vizio, D., Hou, H., Jr., Knietz, B., Lagaud, G., Christ, G.J., Edelmann, W., and Lisanti, M.P. (2001). Caveolin-1 Null Mice Are Viable, but Show Evidence of Hyper-Proliferative and Vascular Abnormalities. J Biol Chem 16, 16.

Roberts, K.P., Wamstad, J.A., Ensrud, K.M., and Hamilton, D.W. (2003). Inhibition of Capacitation-Associated Tyrosine Phosphorylation Signaling in Rat Sperm by Epididymal Protein Crisp-1. Biol Reprod 69, 572-581.

Schmitt, M.C., Jamison, R.S., Orgebin-Crist, M.C., and Ong, D.E. (1994). A Novel, Testis-Specific Member of the Cellular Lipophilic Transport Protein Superfamily, Deduced from a Complimentary Deoxyribonucleic Acid Clone. Biol Reprod 51, 239-245.

Shadan, S., James, P.S., Howes, E.A., and Jones, R. (2004). Cholesterol Efflux Alters Lipid Raft Stability and Distribution During Capacitation of Boar Spermatozoa. Biol Reprod 71, 253-265.

Simons, K., and Toomre, D. (2000). Lipid Rafts and Signal Transduction. Nature Reviews: Molecular Cell Biology 1, 31-39.

Sutovsky, P., Oko, R., Hewitson, L., and Schatten, G. (1997). The Removal of the Sperm Perinuclear Theca and Its Association with the Bovine Oocyte Surface During Fertilization. Dev Biol 188, 75-84.

Suzuki, F. (1988). Changes in the Distribution of Intramembranous Particles and Filipin- Sterol Complexes During Epididymal Maturation of Golden Hamster Spermatozoa. J Ultrastruct Mol Struct Res 100, 39-54.

Travis, A.J., Jorgez, C.J., Merdiushev, T., Jones, B.H., Dess, D.M., Diaz-Cueto, L., Storey, B.T., Kopf, G.S., and Moss, S.B. (2001a). Functional Relationships between Capacitation-Dependent Cell Signaling and Compartmentalized Metabolic Pathways in Murine Spermatozoa. J. Biol. Chem. 276, 7630-7636.

Travis, A.J., and Kopf, G.S. (2002). The Spermatozoon as a Machine: Compartmentalized Pathways Bridge Cellular Structure and Function. In Assisted Reproductive Technology: Accomplishments and New Horizons, C.J. De Jonge, and C.L. Barratt, eds. (Cambridge: Cambridge University Press), pp. 26-39.

Travis, A.J., Merdiushev, T., Vargas, L.A., Jones, B.H., Purdon, M.A., Nipper, R.W., Galatioto, J., Moss, S.B., Hunnicutt, G.R., and Kopf, G.S. (2001b). Expression and Localization of Caveolin-1, and the Presence of Membrane Rafts, in Mouse and Guinea Pig Spermatozoa. Dev Biol 240, 599-610.

Trevino, C.L., Serrano, C.J., Beltran, C., Felix, R., and Darszon, A. (2001). Identification of Mouse Trp Homologs and Lipid Rafts from Spermatogenic Cells and Sperm. FEBS Lett 509, 119-125.

Virtanen, I., Badley, R.A., Paasivuo, R., and Lehto, V.P. (1984). Distinct Cytoskeletal Domains Revealed in Sperm Cells. J Cell Biol 99, 1083-1091.

Visconti, P.E., Galantino-Homer, H., Ning, X., Moore, G.D., Valenzuela, J.P., Jorgez, C.J., Alvarez, J.G., and Kopf, G.S. (1999a). Cholesterol Efflux-Mediated Signal Transduction in Mammalian Sperm. B-Cyclodextrins Initiate Transmembrane Signaling Leading to an Increase in Protein Tyrosine Phosphorylation and Capacitation. J. Biol. Chem. 274, 3235-3242.

Visconti, P.E., Ning, X., Fornes, M.W., Alvarez, J.G., Stein, P., Connors, S.A., and Kopf, G.S. (1999b). Cholesterol Efflux-Mediated Signal

Transduction in Mammalian Sperm: Cholesterol Release Signals an Increase in Protein Tyrosine Phosphorylation During Mouse Sperm Capacitation. Dev. Biol. 214, 429-443.

Wolf, D.E., Maynard, V.M., McKinnon, C.A., and Melchior, D.L. (1990). Lipid Domains in the Ram Sperm Plasma Membrane Demonstrated by Differential Scanning Calorimetry. Proc Natl Acad Sci U S A 87, 6893-6896.

Wolfe, C.A., James, P.S., Mackie, A.R., Ladha, S., and Jones, R. (1998). Regionalized Lipid Diffusion in the Plasma Membrane of Mammalian Spermatozoa. Biol Reprod 59, 1506-1514.

Zacharias, D.A., Violin, J.D., Newton, A.C., and Tsien, R.Y. (2002). Partitioning of Lipid-Modified Monomeric Gfps into Membrane Microdomains of Live Cells. Science 296, 913-916.

CHAPTER 3

Membrane changes associated with capacitation

Vimal Selvaraj[†], Danielle E. Buttke[†], Atsushi Asano, John L. McElwee, Collin A. Wolff, Jacquelyn L. Nelson, Angela V. Klaus, Gary R. Hunnicutt, and Alexander J. Travis. (2007). G_{M1} dynamics as a marker for membrane changes associated with the process of capacitation in murine and bovine spermatozoa. *J Androl* 28 (4): 588-599.

Abstract

We previously showed that in live murine and bovine† sperm heads, the ganglioside G_{M1} localizes to the sterol-rich plasma membrane overlying the acrosome (APM). Labeling G_{M1} using the pentameric cholera toxin subunit B (CTB) induced a dramatic redistribution of signal from the APM to the sterol-poor post-acrosomal plasma membrane (PAPM) upon sperm death. We now show a similar phenomenon in the flagellum where CTB induces G_{M1} redistribution to sterol-poor membrane sub-domains of the annulus and flagellar zipper. Because sterol efflux from the plasma membrane is required for capacitation, we now examined whether G_{M1} localization might be useful to detect membrane changes associated with capacitation and/or acrosomal exocytosis. First, incubation of murine sperm with stimuli required for capacitation did not change G_{M1} distribution in live cells. However, incubation with the different stimuli, followed by the use of specific fixation conditions, induced reproducible, stimulus-specific patterns of G_{M1} distribution. By assessing changes in G_{M1} distribution in response to progesterone-induced acrosomal exocytosis, we show that these patterns reflect the response of sperm populations to capacitating stimuli. These data suggest that G_{M1} localization can be used as a diagnostic tool for evaluating sperm response to stimuli for capacitation and/or acrosomal exocytosis. The different patterns seen with the exposure to different stimuli required for capacitation showed the heterogeneity in the sperm population in which only a sub-population of sperm responds. Such information could be useful when deciding between technologies of assisted reproduction, or when screening for male fertility. Furthermore, stimulus-specific changes in G_{M1} distribution showed that sperm

could respond to $NaHCO_3$ or mediators of sterol efflux independently, thereby refining existing models of capacitation.

[†] Bovine sperm showed similar responses to capacitating stimuli based on the work by Danielle Buttke reported in the original manuscript published in the *Journal of Andrology*.

Introduction

"Capacitation" describes the maturational changes a sperm must undergo in the female reproductive tract to gain competence to fertilize an egg (Chang, 1951; Austin, 1952). The external stimuli required for capacitation can differ among species based on conditions encountered in the respective female tracts. For many species, these stimuli include efflux of sterols from the sperm plasma membrane (Davis, 1974; Davis et al., 1979), and the presence of bicarbonate and calcium ions (Neill and Olds-Clarke, 1987; DasGupta et al., 1993; Visconti et al., 1995a) and glucose (Travis et al., 2001a; Urner et al., 2001).

In vitro capacitation of sperm using such stimuli effects changes in membrane properties that have been reported to lead either directly or indirectly to several downstream events. These include plasma membrane hyperpolarization (Zeng et al., 1995; Arnoult et al., 1999), cAMP-dependent PKA activation and protein tyrosine phosphorylation (Visconti et al., 1995a; Visconti et al., 1995b), loss of plasma membrane bilayer phospholipid asymmetry and lipid order (Harrison et al., 1996; Gadella and Harrison, 2000; Flesch et al., 2001; Gadella and Harrison, 2002; Cross, 2003), phosphatidyl inositol signaling-mediated cytoskeletal remodeling (Brener et al., 2003; Breitbart et al., 2005), and calcium influx/release from internal stores (Ho and Suarez, 2001b, a; Carlson et al., 2003; Herrick et al., 2005). However, it remains unclear how the changes at the level of the membrane and the downstream signaling events are transduced into hyperactivated motility in the tail and priming of the membranes of the sperm head for acrosomal exocytosis. Although it has been shown that only a sub-population of live sperm respond to the stimuli for capacitation through protein tyrosine

phosphorylation (Urner et al., 2001), there is lack of reliable and easy means to evaluate the capacitation status of sperm in response to a given stimulus/stimuli, be it within a population or a comparison between populations.

Currently, the most widely used assay for capacitation status involves patterns of fluorescence intensity in the sperm head using the fluorescent antibiotic chlortetracycline (Saling and Storey, 1979). More recently, studies on sperm membrane lipid organization have led to assays utilizing merocyanine 540 to detect changes in packing order of lipids on the outer leaflet of the plasma membrane (Williamson et al., 1983) that are believed to change with capacitation (Rathi et al., 2001), and annexin V, used to bind and detect phosphatidyl serine on the outer leaflet of the plasma membrane indicating activation of phospholipid scramblase activity (Flesch et al., 2001). However, concerns about the effectiveness of merocyanine 540 in detecting capacitated versus abnormal/damaged sperm have been raised (Muratori et al., 2004), and phospholipid scramblase-mediated phosphatidyl serine exposure in capacitated sperm does not appear to be conserved in all species (Baumber and Meyers, 2006). Further complicating the study of changes to the state of the plasma membrane of the sperm head is the organization of this membrane into discrete micron-scale sub-domains based on sterol and sphingolipid composition (Friend and Fawcett, 1974; Selvaraj et al., 2006). In the heads of fixed sperm from several species, the plasma membrane overlying the acrosome (APM) was found to be enriched in sterols and distinctly segregated from the post-acrosomal plasma membrane (PAPM) that was found to be relatively sterol-poor (Friend, 1982; Pelletier and Friend, 1983; Friend, 1989; Lin and Kan, 1996). In addition, within the APM are at least two distinct areas,

one over the apical acrosome (AA) and a larger one over the equatorial segment (ES) (Friend, 1989; Lin and Kan, 1996; Selvaraj et al., 2006).

"Membrane rafts" are defined as small (10-200 nm), heterogeneous, highly dynamic, sterol- and sphingolipid-enriched domains that compartmentalize cellular processes. Groups of small rafts can sometimes be stabilized to form larger platforms through protein-protein and protein-lipid interactions (Pike, 2006). However, studies on membrane rafts have generated significant controversy regarding the existence and dynamics of these sub-domains in cells; specifically, that artifacts appearing as rafts might be induced by the use of detergents or crosslinking reagents/fixatives used in attempts to visualize these sub-domains (Munro, 2003).

To visualize potential membrane sub-domains in live sperm in the absence of any fixative, we utilized the B subunit of cholera toxin (CTB) to bind the ganglioside G_{M1}. We found that this sphingolipid does indeed segregate to the APM, as do sterols and the sterol-binding protein caveolin-1 in fixed sperm (Travis et al., 2001b). Other investigators have reported the use of fluorescent lipid probes to suggest that the APM sub-domain behaves in a liquid-ordered fashion consistent with a raft (Sleight et al., 2005). The size and stability of the APM and PAPM sub-domains in mammalian sperm are quite extreme in comparison to their counterparts in somatic cells, making it possible that the APM of live sperm represents a "super-raft" of stably segregated smaller sub-sub domains. Fitting the proposed theory behind larger raft platforms, we found that the lipid segregation in sperm is maintained at least in part by disulfide-bonded proteins (Selvaraj et al., 2006). This is consistent, albeit at a larger scale, with a membrane compartmentation model of segregation (Kusumi et al., 2004). We found that this segregation to the APM was highly

conserved across mammals, being present in murine, bovine, and human sperm, and that discrepancies in the literature between species were at least in part due to confounding effects of seminal plasma (Buttke et al., 2006). The organization of these membrane sub-domains in sperm continues to be of great interest because of the pathways that potentially might be targeted to the APM "super raft," which could function in capacitation, binding to the zona pellucida, and/or acrosomal exocytosis (AE).

Although able to demonstrate distinct segregation of endogenous lipids in live sperm, the pitfalls inherent to localizing lipids in a biological system did reveal themselves in our studies. For example, we observed the interesting phenomenon that within *seconds* of a sperm's death (inferred by cessation of motility), CTB bound to G_{M1} helped induce a dramatic redistribution to the PAPM (Selvaraj et al., 2006). In this study, we show a similar redistribution phenomenon seen in the sperm tail while exploring variations in sperm G_{M1} dynamics in response to stimuli for capacitation and AE. Our results not only demonstrate changes in individual cells, but also shed light on the nature of functional sub-populations of sperm, and the temporal dynamics of capacitation pathways.

Experimental Methods

Reagents and Animals

All reagents were purchased from Sigma (St. Louis, MO), unless otherwise noted. CTB conjugated with Alexa Fluor 488 (Invitrogen, Carlsbad, CA) was used. Male CD-1 mice were purchased from Charles River Laboratories (Kingston, NY). All animal procedures were performed under the guidelines of the Institutional Animal Care and Use Committee at Cornell University.

Preparation of Media

A modified Whitten's medium [MW; 22 mM HEPES, 1.2 mM $MgCl_2$, 100 mM NaCl, 4.7 mM KCl, 1 mM pyruvic acid, 4.8 mM lactic acid hemi-calcium salt, pH 7.35; (Travis et al., 2001a)] was used for all incubations. Glucose (5.5 mM), $NaHCO_3$ (10 mM), and 2-hydroxypropyl-β-cyclodextrin (2-OHCD; 3 mM) were supplemented as needed. 2-OHCD supports sperm capacitation and *in vitro* fertilization by functioning as a sterol acceptor, and is preferred over the more potent methyl-β-cyclodextrin (Visconti et al., 1999).

Sperm Collection and Handling

Murine sperm were collected from the cauda epididymides of male CD-1 mice by a swim-out procedure as described previously (Travis et al., 2001b). All steps of collection and washing were performed at 37˚C using MW medium, and large orifice transfer pipettes or large orifice pipette tips were used for handling sperm to minimize membrane damage. After the initial washes but prior to experimental incubations, motility assessment was carried out and samples showing <60% motility were not used.

Sperm capacitation and induction of AE

Incubation with different stimuli for capacitation was carried out with $2x10^6$ sperm in 300 μl of medium with glucose under one of four conditions: (a) MW base medium, (b) MW supplemented with 10 mM $NaHCO_3$, (c) MW supplemented with 3 mM 2-OHCD and (d) MW with both 10 mM $NaHCO_3$ and 3 mM 2-OHCD, for 45 minutes (or 60 minutes for all conditions when inducing AE). The pH of medium for all incubation conditions was adjusted to 7.35. The medium in incubation condition "(d)," has been shown to be sufficient to support IVF (Travis et al., 2004) and capacitation-induced tyrosine phosphorylation (Travis et al., 2001a) in murine sperm. Progesterone was added to a final concentration of 20 μM to induce AE in capacitated murine sperm (Roldan et al., 1994; Murase and Roldan, 1996; Kobori et al., 2000) [A 2 mM working stock was prepared in MW immediately before use from a 20 mM stock of progesterone in DMSO; 0.2% v/v final DMSO concentration.]. The dead spaces of tubes used for all incubations were filled with nitrogen to avoid the generation of bicarbonate anions in the aqueous media in conditions "a" and "c." This had no effect on protein tyrosine phosphorylation events associated with capacitation (data not shown).

For live sperm, the localization pattern of G_{M1} was visualized using CTB, after incubation under one of the conditions described and/or after the induction of AE.

Fluorescence Localization of G_{M1} in Mature Sperm

All steps of localization experiments using either live or fixed sperm were carried out under dim lighting at 37˚C in a humidity chamber. In all cases, the localization of G_{M1} was visualized with CTB. For localization of G_{M1} in fixed

samples, sperm were allowed to adhere to coverslips for 20 min (at the end of incubations for capacitation experiments) and then fixed for 10 min with 0.004% paraformaldehyde (PF) in PBS. The sperm were then washed with PBS and incubated for 10 min with CTB (5 μg/ml). The sperm were washed again and mounted using a GVA mountant (Invitrogen). For all conditions in experiments evaluating pattern change associated with AE, sperm were fixed while in suspension by adding an equal volume of 0.008% PF, were incubated with CTB as above, and aliquots were then placed directly on slides for microscopy.

Microscopy and image collection

Cells were viewed with a Nikon Eclipse TE 2000-U microscope (Nikon, Melville, NY**)** equipped with a Photometrics Coolsnap HQ CCD camera (Roper Scientific, Ottobrunn, Germany), and Openlab 3.1 (Improvision, Lexington, MA) automation and imaging software. Assignments of sperm to G_{M1} localization patterns were performed in a blind fashion regarding incubation condition. To compare shifts in population tendencies, the numbers of sperm having a given pattern were converted to percentages prior to statistical evaluation. In all cases, $\geq$ 100 cells were counted for each test condition, and every sperm in a given field was counted to avoid potential bias. Sperm with morphological abnormalities showing aberrant G_{M1} localization patterns [as described in (Buttke et al., 2006)] were not included in the count.

Scanning electron microscopy

SEM was performed using two techniques to visualize surface topography. In the first method, sperm were fixed for 2 h with 2.5%

glutaraldehyde in 100 mM sodium cacodylate and 1% tannic acid at pH 7.4 in a culture tube. After washing by centrifugation and resuspension, they were again fixed with 2% osmium tetroxide and 2% sodium cacodylate at 4˚C overnight. The cells were washed and dehydrated in ethanol with a 20 min incubation in 2% uranyl acetate at 70% ethanol. Once in absolute ethanol, they were critical point dried, coated, and viewed using a Hitachi S4500 scanning electron microscope (Hitachi, Pleasanton, CA). Digital micrographs were collected using a Princeton Gamma Tech digital beam acquisition program (Imix, Princeton, NJ).

In the second method, sperm were fixed in 2.5% glutaraldehyde in 100 mM sodium cacodylate (pH 7.4) overnight at 4˚C. A 20 μl aliquot of sperm suspension was then washed in 100 mM sodium cacodylate buffer by centrifugation and resuspension. Aliquots were placed on poly-L-lysine coated 12 mm, round coverslips and allowed to incubate for 45 minutes at 4˚C. The coverslips were rinsed by gently dipping 3 times in cacodylate buffer, then dehydrated in ethanol followed by 2 changes in 100% ethanol for 20 minutes each. Coverslips were critical point dried, sputter-coated with Au/Pd, and imaged on a Hitachi S4700 cold field-emission scanning electron microscope operating at 10 kV accelerating voltage and 7 μA emission current. Digital images were captured at 2500 x 1900 pixel resolution.

Results

Effect of stimuli for capacitation on CTB-induced G_{M1} patterns

We previously showed in live murine sperm that CTB bound to G_{M1} exclusively in the APM. However, almost immediately upon sperm death, the cross-linking produced by the pentameric CTB induced a redistribution of G_{M1} to the PAPM. We also showed that weak fixatives (e.g. 0.004 - 1% PF) did not prevent this redistribution, but that strong fixation (e.g. 4% PF with 0.1% glutaraldehyde) could immobilize G_{M1} as it was in live murine sperm (Selvaraj et al., 2006). In this study, we investigated whether membrane changes brought about by different stimuli for capacitation (alone or in combination) could affect the distribution of G_{M1} in murine sperm. In live sperm, as we demonstrated for sterol efflux (Selvaraj et al., 2006), bicarbonate had no effect on the localization of G_{M1} (data not shown). However, we found interesting variations in patterns of G_{M1} localization in response to different stimuli for capacitation followed by incubation under species-specific fixation conditions.

For fixation, we used 0.004% PF in PBS which has been reported to be sufficient to immobilize sperm but not permeabilize their membranes (Harrison and Vickers, 1990). After fixation, non-capacitated murine sperm showed G_{M1} over the PAPM as previously observed (Selvaraj et al., 2006); but, in the presence of capacitating stimuli, new patterns of G_{M1} distribution were seen (Figure 3.1A). These patterns were highly reproducible in terms of specific patterns occurring in response to specific stimuli. Under all conditions, labeling over the APM similar to that seen in live sperm was only seen in rare cells after weak fixation. In the presence of $NaHCO_3$, a significant percentage of

Figure 3.1. Patterns of G_{M1} localization seen in epididymal murine sperm after incubation under different conditions, either live or followed by fixation. A. Fluorescence images and schematic diagrams (drawn as negative images) showing the range of patterns seen in live sperm and sperm fixed with 0.004% PF in PBS. Pattern "APM" denotes signal over the APM and was seen almost exclusively in live sperm. Pattern "D" denotes diffuse localization. Pattern "AA/PA" denotes signal over the apical acrosome and in the PAPM. Pattern "PAPM" denotes post-acrosomal signal. It should be noted that two thin lines of fluorescence labeling, bordering a central unlabeled area of membrane, were sometimes seen over the AA in the D pattern and less frequently, in the PAPM pattern, suggestive of a smaller "sub-sub domain" in the AA area. The images also represent G_{M1} labeling patterns seen in the mid-piece, annulus, and principal piece, which did not depend on specific treatment conditions, and are described further below. B. Box-whisker plots showing percentages of the different G_{M1} patterns in sperm incubated under a non-capacitating condition (NC) or in the presence of bicarbonate (NaHCO3), cyclodextrin (CD) or both bicarbonate and cyclodextrin (CAP) for 45 minutes. The lower and upper ends of the box mark the 25th and 75th quantiles; the median is represented as a horizontal line within the box, and the mean as a horizontal line through the box. Vertical whiskers extend from the ends of the box to the 10th and 90th quantiles. A Kruskal-Wallis rank sum analysis showed significant differences between the different conditions ($P<0.05$). Pair-wise comparisons made with individual Wilcoxon tests for each pattern between the different conditions are indicated by the letters above the whiskers ($P<0.025$). These results show that the AA/PA pattern increased significantly in the presence of NaHCO3, that the D pattern increased significantly in the presence of 2-OHCD and CAP conditions, and that the increases in those patterns were accompanied by significant decreases in sperm showing the PAPM pattern.

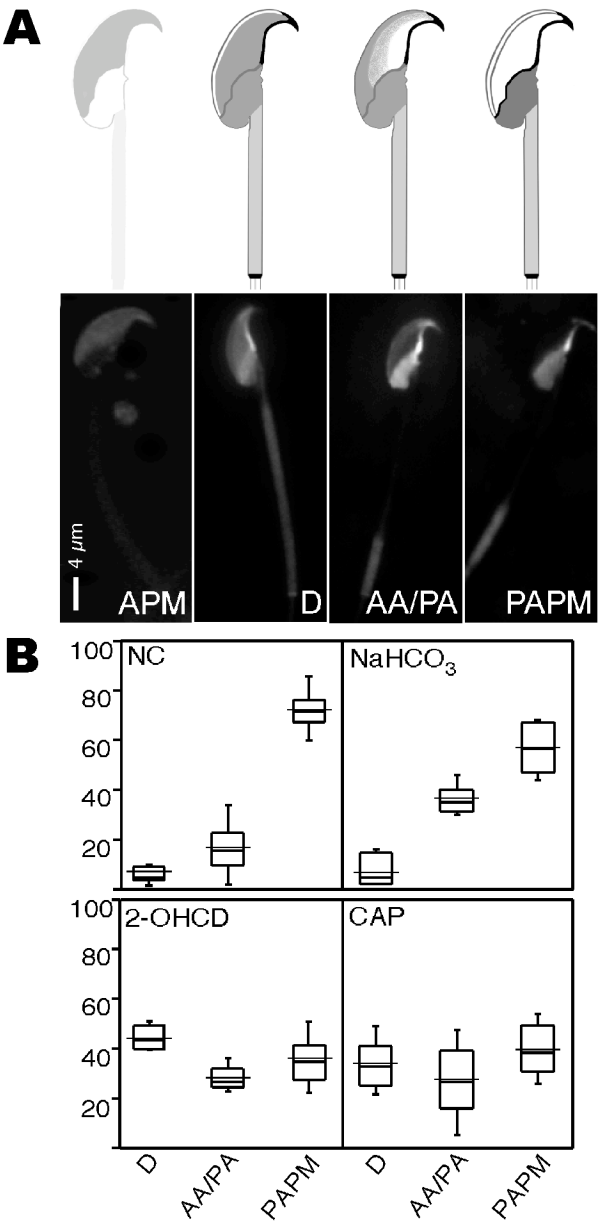
A
4 μm
APM
D
AA/PA
PAPM
B
NC
NaHCO3
2-OHCD
CAP
100
80
60
40
20
D
AA/PA
PAPM

cells (36.1 ± 2.5%) showed an incomplete redistribution to the PAPM with residual G_{M1} labeling over the AA (the "AA/PA" pattern; Figure 3.1B), when compared to non-capacitated sperm. In the presence of 2-OHCD, a significant percentage of cells (42.0 ± 3.4%) had G_{M1} diffusely distributed over the entire APM in addition to the PAPM (the "D" pattern; Figure 3.1B), when compared to non-capacitated sperm. The presence of both $NaHCO_3$ and 2-OHCD caused no additional increase in the percentages of sperm showing either of the AA/PA or the D patterns (Figure 3.1B).

G_{M1} localization in acrosome-reacted sperm

Distribution of G_{M1} in live epididymal murine sperm remained unchanged even after incubation with stimuli for capacitation. However, induction of acrosomal exocytosis using progesterone in capacitated sperm showed increase in a pattern distinct from those seen after exposure to stimuli for capacitation followed by fixation as described above. After capacitation, a subset of murine sperm induced to undergo acrosomal exocytosis demonstrated a pattern characterized by a hollow AA, suggestive of loss of both acrosomal contents and membranes from the AA (the "AR" pattern; Figure 3.2A). This pattern was characterized by the apical acrosome showing somewhat ragged borders consistent with the nature of vesiculations associated with this exocytotic process. There was a significant increase in the AR pattern after the induction of acrosomal exocytosis (21.8 ± 1.3%; Figure 3.2B), when compared with sperm incubated under non-capacitating and capacitating conditions. This increase in AR pattern was associated with a significant decrease in the D pattern after the induction of acrosomal exocytosis when compared to sperm

Figure 3.2. Localization pattern of G_{M1} in acrosome reacted murine sperm. A. Mouse sperm were capacitated in MW medium with NaHCO3 (10 mM) and 2-OHCD (3 mM) for 45 mintues and acrosomal exocytosis was induced by treatment with progesterone (10 μM) for 5 minutes. Sperm were then fixed with 0.004% PF in PBS and G_{M1} labeling using CTB was carried out as described. B. Box-whisker plots showing percentages of the different G_{M1} localization patterns in murine sperm incubated for 60 minutes under a non-capacitating condition (NC), or both bicarbonate and cyclodextrin (CAP), or after the induction of acrosomal exocytosis at the end of incubation. The lower and upper ends of the box mark the 25th and 75th quantiles; the median is represented as a horizontal line within the box, and the mean as a horizontal line through the box. Vertical whiskers extend from the ends of the box to the 10th and 90th quantiles. Abbreviations for patterns are same as in Fig 1A. "AR" refers to the acrosome reacted pattern shown in panel A. A Kruskal-Wallis rank sum analysis showed significant differences between the different conditions ($P<0.05$). Pair-wise comparisons made with individual Wilcoxon tests for each pattern between the different conditions are indicated by the letters above the whiskers ($P<0.025$). These results show that both the D and AA/PA patterns increased significantly under CAP conditions, and that there was a corresponding decrease in the PAPM pattern. Moreover, there was a statistically significant increase in the AR pattern upon incubation of capacitated sperm with progesterone. This increase was accompanied by a corresponding decrease in the D pattern under these incubation conditions, and no significant decline in the AA/PA pattern, showing that the sperm having the AR pattern came from the "D" sub-population.

A

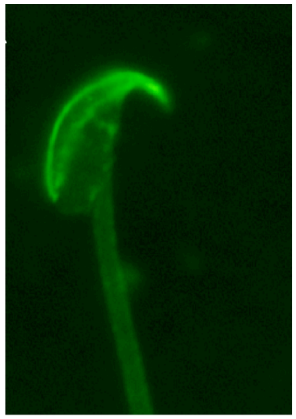

B

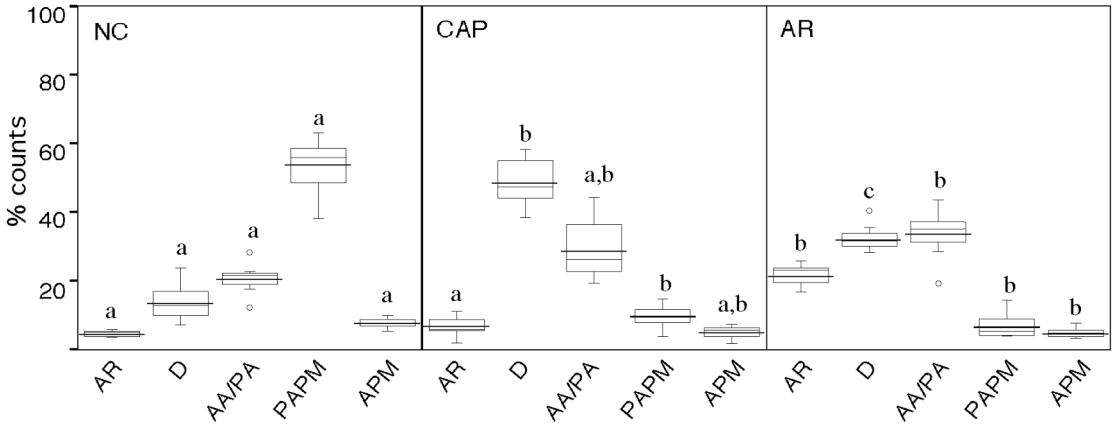
NC
CAP
AR
% counts
100
80
60
40
20
a
a
a
a
a
a
b
a,b
b
a,b
b
c
b
b
b
AR
D
AA/PA
PAPM
APM

incubated under capacitating conditions [D pattern: (48.9 ± 2.8%) in capacitated sperm and (32.5 ± 1.6%) after acrosomal exocytosis].

G_{M1} localization in the mid-piece and principal piece

G_{M1} was also seen in the flagellum of murine sperm. In live sperm, the CTB signal was faint and appeared diffuse (data not shown). After fixation with 0.004% PF, the localization of G_{M1} in the mid-piece did not conform to a specific pattern. It appeared either distributed evenly across the entire mid-piece or was somewhat more prominent in the distal half/third of the mid-piece (Figure 3.1A). G_{M1} became greatly enriched in the plasma membrane at the region of the annulus, where the mitochondrial sheath of the mid-piece abuts the fibrous sheath of the principal piece (Friend and Fawcett, 1974) (Figure 3.3 and Figure 3.1A). In the principal piece, G_{M1} fluorescence was seen as a fine line coursing caudally from the annulus (Figure 3.3). To our knowledge, there is only one linear feature that runs the length of the plasma membrane in the principal piece. This is a distinct membrane sub-domain known as the "flagellar zipper" that has been identified primarily through the use of freeze-fracture techniques in several species (Friend and Fawcett, 1974; Lin and Kan, 1996). We now show by SEM that the flagellar zipper is a morphologically distinct membrane sub-domain within the flagellar plasma membrane (Figure 3.4A). In an SEM micrograph of a demembranated sperm (Figure 3.4B), structures underlying or comprising internal components of the annulus and the flagellar zipper can be seen.

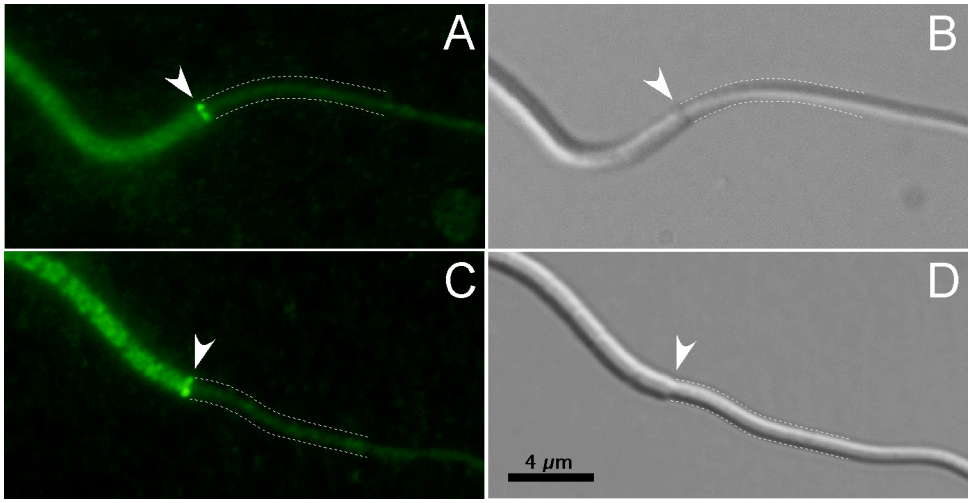

Figure 3.3. Localization of G_{M1} at the annulus and principal piece in murine sperm fixed with 0.004% PF. Non-capacitated sperm were fixed and labeling for G_{M1} was carried out as described. The region of the annulus (arrowheads) showed intense G_{M1} labeling. A linear track of CTB fluorescence in the principal piece suggested G_{M1} localization over the flagellar zipper starting at the annulus and running down the length of the principal piece (panels A and C). It should be noted that panels A and C have had their brightness and contrast adjusted to highlight the fluorescence over the extremely thin sub-domain of the flagellar zipper, although this does result in an effective "over-exposure" of the mid-piece and annulus. Corresponding Nomarski DIC images are shown in panels B and D. Dotted lines in both figures outline the proximal part of the principal piece showing that G_{M1} labeling was confined to a linear track, more narrow than the width of the principal piece.

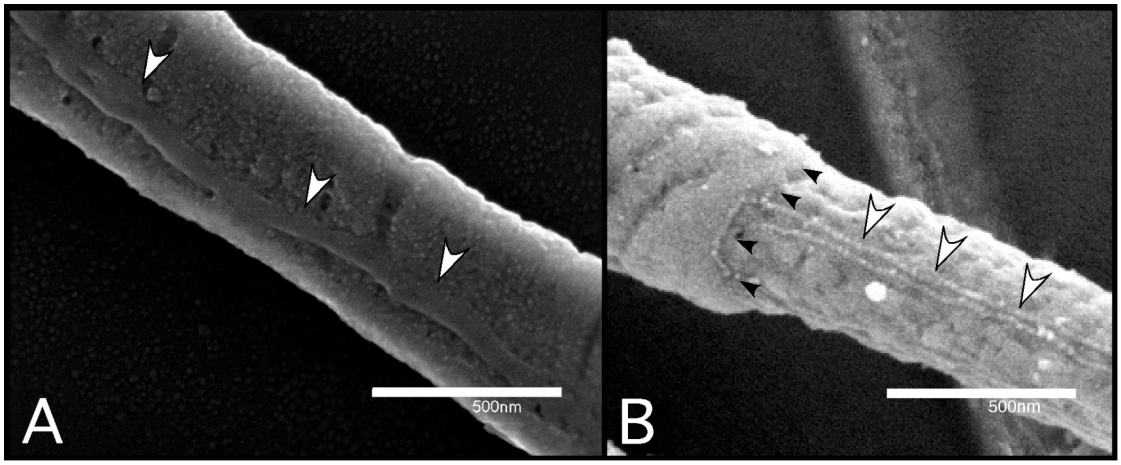

Figure 3.4. Scanning electron micrographs of murine sperm showing the annulus and flagellar zipper. A. SEM of a sperm fixed with glutaraldehyde showing a region of the proximal principal piece. Although membranous structures were not specifically stabilized with osmium tetroxide post-fixation, it appears that the membrane overlying the surface of the flagellar zipper (white arrowheads) is distinct as a narrow sub-domain running longitudinally down the principal piece. B. In comparison is SEM of a fixed sperm that was completely demembranated during handling. This panel shows the annulus (small black arrowheads), and characteristic sub-structure, which lends the flagellar zipper its name (white arrowheads).

Discussion

G_{M1} patterns reflect capacitation-associated membrane changes

Efflux of sterols from the sperm plasma membrane (Davis, 1974; Davis et al., 1979), and the presence of bicarbonate and calcium ions (Neill and Olds-Clarke, 1987; DasGupta et al., 1993; Visconti et al., 1995a) have long been known to play a critical role in capacitation. Two models have arisen describing the order of membrane events during capacitation, perhaps reflecting species differences. The first, based on work in the mouse, suggests that sterol efflux is an initial event, stimulating bicarbonate and calcium uptake (Travis and Kopf, 2002; Demarco et al., 2003). Alternatively, based primarily on work in the boar, bicarbonate and calcium uptake have been suggested to trigger an increase in intracellular cAMP and PKA activity, stimulating the activity of phospholipid scramblases (Harrison et al., 1996; Gadella and Harrison, 2000). The resultant increase in lipid disorder was suggested to facilitate raft formation and sterol efflux (Flesch et al., 2001).

Although G_{M1} redistribution upon cell death appears to be induced by CTB, variations in the pattern of G_{M1} revealed several important points of information about the nature of membrane changes during capacitation, both within single cells and at the level of sperm populations. Supporting the hypothesis that different populations of sperm exist within a single ejaculate or collection, only a subset of sperm (approximately 40%) responded fully to stimuli for capacitation. This figure corresponded to the approximate percentage of sperm showing protein tyrosine phosphorylation in response to incubation under capacitating conditions (Urner et al., 2001).

Interestingly, we observed that both 2-OHCD and $NaHCO_3$ could independently alter membrane properties, showing that unlike either existing

model for the chronology of response to stimuli for capacitation, both stimuli could induce membrane changes as an initial event. Here the “D” pattern was indicative of sperm that responded to sterol efflux (2-OHCD) and the “AA/PA” pattern indicated sperm that responded to $NaHCO_3$. If the two patterns were induced together in the same sperm, they would overlap to provide a “D” pattern. Because there was no net increase in the percentage of sperm showing the “D” pattern when both stimuli were included in the medium, this result indicates that the sperm that responded to the presence of $NaHCO_3$ were the same population as those that responded to sterol efflux.

These results suggested that the “D” pattern represented capacitated sperm. Capacitation can be assessed by means of different end points, and is most rigorously defined by the ability to fertilize an egg. However, use of that endpoint would not allow visualization of the membrane G_{M1} pattern. Therefore, we utilized the acquisition of the ability to undergo acrosomal exocytosis as a marker for capacitation. We saw an increase in the AR pattern after acrosomal exocytosis, and an almost identically-sized decrease in the D pattern in this treatment. These results showed that it was indeed the population of sperm having the D pattern that responded to progesterone, which would be consistent with the D pattern being a marker for capacitated sperm. This finding confirmed our hypothesis that CTB-labeling of G_{M1} could function as an indicator of membrane changes associated with capacitation, able to identify populations of sperm responding to specific capacitating stimuli.

There have been several studies demonstrating changes in membrane distribution or mobility of membrane raft-associated proteins and/or lipids in the sperm head with capacitation (Cowan et al., 2001; Roberts et al., 2003;

Cross, 2004; Shadan et al., 2004; Belmonte et al., 2005; van Gestel et al., 2005). Some of these studies have also examined G_{M1} localization in sperm from different species, with varying results. In the mouse, it was suggested that G_{M1} localizes to the PAPM and that this localization does not change with capacitation (Trevino et al., 2001); another study localized G_{M1} to the midpiece and moving to the head during capacitation (Shadan et al., 2004). Both these studies were done at 16˚C, and phase transitions between this and physiologic temperatures (Wolf et al., 1990) might account for some disparity with our results. In rat sperm, it was suggested that G_{M1} localizes to the PAPM and then moves to the APM during capacitation (Roberts et al., 2003). In both this and the study in murine sperm showing no movement, it is clear that the initial localization to the PAPM was an effect of fixation condition (Selvaraj et al., 2006). In human sperm, it was reported that G_{M1} has a diffuse localization pattern and then assembles in the APM (Cross, 2004). Also as discussed, this was likely due to exposure of sperm to seminal plasma (Buttke et al., 2006).

Possible explanation for the redistribution phenomenon

Based on our observations and current models of sperm membrane properties, we have arrived at one possibility that could explain why CTB induced G_{M1} redistribution from the APM to the PAPM. We suggest that once cross-linked by CTB, G_{M1} moves from sterol-rich, liquid-ordered membrane regions to sterol-poor, less-ordered areas on the sperm. In both live and fixed sperm, it has been suggested that in non-capacitated sperm, the sterol-rich APM is a liquid-ordered sub-domain whereas the sterol-poor PAPM is liquid-disordered (Sleight et al., 2005).

Therefore, in sperm incubated under non-capacitating conditions, G_{M1} redistributed to the PAPM, being excluded from or forced out of the sterol-rich, more-ordered APM. Upon incubation of murine sperm with $NaHCO_3$ in the presence of calcium [stimulators of sperm phospholipid scramblases (Gadella and Harrison, 2000)], some G_{M1} redistributed to the PAPM, but some also remained in the AA. The aminophospholipid transporter (SAPLT) with homology to a flippase localizes to this region (Wang et al., 2004). Studies comparing sperm from wild type versus SAPLT-null mice suggest that phospholipid scramblase activity in this region depends on the activity of the flippase as well as the presence of $NaHCO_3$ (Wang et al., 2004). Therefore, the presence of $NaHCO_3$ could be inducing liquid-disorder at the region of the AA giving rise to the "AA/PA" pattern. Sterol efflux from murine sperm has been shown to occur throughout the APM (Visconti et al., 1999), increasing lipid disorder throughout this sub-domain (Cross, 2003; Sleight et al., 2005). Accordingly, there was a diffuse pattern of G_{M1} localization throughout the head (APM and PAPM) of sperm incubated with 2-OHCD. The presence of both $NaHCO_3$ and 2-OHCD induced no additional increase in the percentage of sperm showing a diffuse pattern, suggesting again that these populations of sperm were the same.

Also supporting the notion that cross-linked G_{M1} redistributed to membrane sub-domains of reduced order/lower sterol abundance, was the redistribution seen in the flagellum of murine sperm upon death or fixation with 0.004% PF. Originally diffuse throughout the flagellum, G_{M1} became concentrated at the annulus and the flagellar zipper of the principal piece, structures shown by freeze fracture to be devoid of sterols (Pelletier and Friend, 1983; Lin and Kan, 1996).

Our data on the stimulus-specific patterns of changes in G_{M1} localization suggest strongly that temporally, sperm can respond to $NaHCO_3$ or mediators of sterol efflux independently of one another. This finding provides a refinement to existing models of capacitation. Yet, in addition to these points of basic science, our findings also suggest a clinical application for G_{M1} as a marker for detecting capacitation-associated membrane changes in murine sperm. Changes in localization patterns of G_{M1} in response to specific stimuli for capacitation could provide a diagnostic tool for predicting a male's reproductive fitness based on the proportion of sperm that are capable of responding to such stimuli. This information could be used in agricultural industries to make broad classifications regarding a male's fertility, or could be used to help guide clinicians when choosing between techniques such as in vitro fertilization or intra-cytoplasmic sperm injection. Furthermore, because this potential assay is based upon functional membrane responses, it might also be useful when evaluating or comparing media or conditions used to handle sperm *in vitro* or cryopreserve them.

Acknowledgements

We thank Tanya Merdiushev, Gregory S. Kopf, Miguel W. Fornes, and Stuart B. Moss for helpful discussions and assistance with early studies.

REFERENCES

Arnoult, C., Kazam, I.G., Visconti, P.E., Kopf, G.S., Villaz, M., and Florman, H.M. (1999). Control of the Low Voltage-Activated Calcium Channel of Mouse Sperm by Egg Zp3 and by Membrane Hyperpolarization During Capacitation. Proc Natl Acad Sci U S A 96, 6757-6762.

Austin, C.R. (1952). The Capacitation of the Mammalian Sperm. Nature 170, 326.

Baumber, J.A., and Meyers, S.A. (2006). Changes in Membrane Lipid Order with Capacitation in Rhesus Macaque (Macaca Mulatta) Spermatozoa. J Androl 27, 578-587.

Belmonte, S.A., Lopez, C.I., Roggero, C.M., De Blas, G.A., Tomes, C.N., and Mayorga, L.S. (2005). Cholesterol Content Regulates Acrosomal Exocytosis by Enhancing Rab3a Plasma Membrane Association. Dev Biol 285, 393-408.

Breitbart, H., Cohen, G., and Rubinstein, S. (2005). Role of Actin Cytoskeleton in Mammalian Sperm Capacitation and the Acrosome Reaction. Reproduction 129, 263-268.

Brener, E., Rubinstein, S., Cohen, G., Shternall, K., Rivlin, J., and Breitbart, H. (2003). Remodeling of the Actin Cytoskeleton During Mammalian Sperm Capacitation and Acrosome Reaction. Biol Reprod 68, 837-845.

Buttke, D.E., Nelson, J.L., Schlegel, P.N., Hunnicutt, G.R., and Travis, A.J. (2006). Visualization of Gm1 with Cholera Toxin B in Live Epididymal Versus Ejaculated Bull, Mouse, and Human Spermatozoa. Biol Reprod 74, 889-895.

Carlson, A.E., Westenbroek, R.E., Quill, T., Ren, D., Clapham, D.E., Hille, B., Garbers, D.L., and Babcock, D.F. (2003). Catsper1 Required for Evoked Ca2+ Entry and Control of Flagellar Function in Sperm. Proc Natl Acad Sci U S A 100, 14864-14868.

Chang, M.C. (1951). Fertilizing Capacity of Spermatozoa Deposited into the Fallopian Tubes. Nature 168, 697-698.

Cowan, A.E., Koppel, D.E., Vargas, L.A., and Hunnicutt, G.R. (2001). Guinea Pig Fertilin Exhibits Restricted Lateral Mobility in Epididymal Sperm and Becomes Freely Diffusing During Capacitation. Dev Biol 236, 502-509.

Cross, N.L. (2003). Decrease in Order of Human Sperm Lipids During Capacitation. Biol Reprod 69, 529-534.

Cross, N.L. (2004). Reorganization of Lipid Rafts During Capacitation of Human Sperm. Biol Reprod 71, 1367-1373.

DasGupta, S., Mills, C.L., and Fraser, L.R. (1993). Ca(2+)-Related Changes in the Capacitation State of Human Spermatozoa Assessed by a Chlortetracycline Fluorescence Assay. J Reprod Fertil 99, 135-143.

Davis, B.K. (1974). Decapacitation and Recapacitation of Rabbit Spermatozoa Treated with Membrane Vesicles from Seminal Plasma. J Reprod Fertil 41, 241-244.

Davis, B.K., Byrne, R., and Hungund, B. (1979). Studies on the Mechanism of Capacitation. Ii. Evidence for Lipid Transfer between Plasma Membrane of Rat Sperm and Serum Albumin During Capacitation in Vitro. Biochim Biophys Acta 558, 257-266.

Demarco, I.A., Espinosa, F., Edwards, J., Sosnik, J., De La Vega-Beltran, J.L., Hockensmith, J.W., Kopf, G.S., Darszon, A., and Visconti, P.E. (2003). Involvement of a Na+/Hco-3 Cotransporter in Mouse Sperm Capacitation. J Biol Chem 278, 7001-7009.

Flesch, F.M., Brouwers, J.F., Nievelstein, P.F., Verkleij, A.J., van Golde, L.M., Colenbrander, B., and Gadella, B.M. (2001). Bicarbonate Stimulated Phospholipid Scrambling Induces Cholesterol Redistribution and Enables Cholesterol Depletion in the Sperm Plasma Membrane. J Cell Sci 114, 3543-3555.

Friend, D.S. (1982). Plasma-Membrane Diversity in a Highly Polarized Cell. J Cell Biol 93, 243-249.

Friend, D.S. (1989). Sperm Maturation: Membrane Domain Boundaries. Ann N Y Acad Sci 567, 208-221.

Friend, D.S., and Fawcett, D.W. (1974). Membrane Differentiations in Freeze-Fractured Mammalian Sperm. J Cell Biol 63, 641-664.

Gadella, B.M., and Harrison, R.A. (2000). The Capacitating Agent Bicarbonate Induces Protein Kinase a-Dependent Changes in Phospholipid Transbilayer Behavior in the Sperm Plasma Membrane. Development 127, 2407-2420.

Gadella, B.M., and Harrison, R.A. (2002). Capacitation Induces Cyclic Adenosine 3',5'-Monophosphate-Dependent, but Apoptosis-Unrelated, Exposure of Aminophospholipids at the Apical Head Plasma Membrane of Boar Sperm Cells. Biol Reprod 67, 340-350.

Harrison, R.A., Ashworth, P.J., and Miller, N.G. (1996). Bicarbonate/Co2, an Effector of Capacitation, Induces a Rapid and Reversible Change in the

Lipid Architecture of Boar Sperm Plasma Membranes. Mol Reprod Dev 45, 378-391.

Harrison, R.A., and Vickers, S.E. (1990). Use of Fluorescent Probes to Assess Membrane Integrity in Mammalian Spermatozoa. J Reprod Fertil 88, 343-352.

Herrick, S.B., Schweissinger, D.L., Kim, S.W., Bayan, K.R., Mann, S., and Cardullo, R.A. (2005). The Acrosomal Vesicle of Mouse Sperm Is a Calcium Store. J Cell Physiol 202, 663-671.

Ho, H.C., and Suarez, S.S. (2001a). An Inositol 1,4,5-Trisphosphate Receptor-Gated Intracellular Ca(2+) Store Is Involved in Regulating Sperm Hyperactivated Motility. Biol Reprod 65, 1606-1615.

Ho, H.C., and Suarez, S.S. (2001b). Hyperactivation of Mammalian Spermatozoa: Function and Regulation. Reproduction 122, 519-526.

Kobori, H., Miyazaki, S., and Kuwabara, Y. (2000). Characterization of Intracellular Ca(2+) Increase in Response to Progesterone and Cyclic Nucleotides in Mouse Spermatozoa. Biol Reprod 63, 113-120.

Kusumi, A., Koyama-Honda, I., and Suzuki, K. (2004). Molecular Dynamics and Interactions for Creation of Stimulation-Induced Stabilized Rafts from Small Unstable Steady-State Rafts. Traffic 5, 213-230.

Lin, Y., and Kan, F.W. (1996). Regionalization and Redistribution of Membrane Phospholipids and Cholesterol in Mouse Spermatozoa During in Vitro Capacitation. Biol Reprod 55, 1133-1146.

Munro, S. (2003). Lipid Rafts: Elusive or Illusive? Cell 115, 377-388.

Murase, T., and Roldan, E.R. (1996). Progesterone and the Zona Pellucida Activate Different Transducing Pathways in the Sequence of Events Leading to Diacylglycerol Generation During Mouse Sperm Acrosomal Exocytosis. Biochem J 320 (Pt 3), 1017-1023.

Muratori, M., Porazzi, I., Luconi, M., Marchiani, S., Forti, G., and Baldi, E. (2004). Annexinv Binding and Merocyanine Staining Fail to Detect Human Sperm Capacitation. J Androl 25, 797-810.

Neill, J.M., and Olds-Clarke, P. (1987). A Computer-Assisted Assay for Mouse Sperm Hyperactivation Demonstrates That Bicarbonate but Not Bovine Serum Albumin Is Required. Gamete Res 18, 121-140.

Pelletier, R.M., and Friend, D.S. (1983). Development of Membrane Differentiations in the Guinea Pig Spermatid During Spermiogenesis. Am J Anat 167, 119-141.

Pike, L.J. (2006). Rafts Defined: A Report on the Keystone Symposium on Lipid Rafts and Cell Function. J Lipid Res 47, 1597-1598.

Rathi, R., Colenbrander, B., Bevers, M.M., and Gadella, B.M. (2001). Evaluation of in Vitro Capacitation of Stallion Spermatozoa. Biol Reprod 65, 462-470.

Roberts, K.P., Wamstad, J.A., Ensrud, K.M., and Hamilton, D.W. (2003). Inhibition of Capacitation-Associated Tyrosine Phosphorylation Signaling in Rat Sperm by Epididymal Protein Crisp-1. Biol Reprod 69, 572-581.

Roldan, E.R., Murase, T., and Shi, Q.X. (1994). Exocytosis in Spermatozoa in Response to Progesterone and Zona Pellucida. Science 266, 1578-1581.

Saling, P.M., and Storey, B.T. (1979). Mouse Gamete Interactions During Fertilization in Vitro. Chlortetracycline as a Fluorescent Probe for the Mouse Sperm Acrosome Reaction. J Cell Biol 83, 544-555.

Selvaraj, V., Asano, A., Buttke, D.E., McElwee, J.L., Nelson, J.L., Wolff, C.A., Merdiushev, T., Fornes, M.W., Cohen, A.W., Lisanti, M.P., Rothblat, G.H., Kopf, G.S., and Travis, A.J. (2006). Segregation of Micron-Scale Membrane Sub-Domains in Live Murine Sperm. J Cell Physiol 206, 636-646.

Shadan, S., James, P.S., Howes, E.A., and Jones, R. (2004). Cholesterol Efflux Alters Lipid Raft Stability and Distribution During Capacitation of Boar Spermatozoa. Biol Reprod 71, 253-265.

Sleight, S.B., Miranda, P.V., Plaskett, N.W., Maier, B., Lysiak, J., Scrable, H., Herr, J.C., and Visconti, P.E. (2005). Isolation and Proteomic Analysis of Mouse Sperm Detergent-Resistant Membrane Fractions. Evidence for Dissociation of Lipid Rafts During Capacitation. Biol Reprod 73, 721-729.

Travis, A.J., Jorgez, C.J., Merdiushev, T., Jones, B.H., Dess, D.M., Diaz-Cueto, L., Storey, B.T., Kopf, G.S., and Moss, S.B. (2001a). Functional Relationships between Capacitation-Dependent Cell Signaling and Compartmentalized Metabolic Pathways in Murine Spermatozoa. J Biol Chem 276, 7630-7636.

Travis, A.J., and Kopf, G.S. (2002). The Role of Cholesterol Efflux in Regulating the Fertilization Potential of Mammalian Spermatozoa. J Clin Invest 110, 731-736.

Travis, A.J., Merdiushev, T., Vargas, L.A., Jones, B.H., Purdon, M.A., Nipper, R.W., Galatioto, J., Moss, S.B., Hunnicutt, G.R., and Kopf, G.S. (2001b). Expression and Localization of Caveolin-1, and the Presence of Membrane Rafts, in Mouse and Guinea Pig Spermatozoa. Dev Biol 240, 599-610.

Travis, A.J., Tutuncu, L., Jorgez, C.J., Ord, T.S., Jones, B.H., Kopf, G.S., and Williams, C.J. (2004). Requirements for Glucose Beyond Sperm Capacitation During in Vitro Fertilization in the Mouse. Biol Reprod 71, 139-145.

Trevino, C.L., Serrano, C.J., Beltran, C., Felix, R., and Darszon, A. (2001). Identification of Mouse Trp Homologs and Lipid Rafts from Spermatogenic Cells and Sperm. FEBS Lett 509, 119-125.

Urner, F., Leppens-Luisier, G., and Sakkas, D. (2001). Protein Tyrosine Phosphorylation in Sperm During Gamete Interaction in the Mouse: The Influence of Glucose. Biol Reprod 64, 1350-1357.

van Gestel, R.A., Brewis, I.A., Ashton, P.R., Helms, J.B., Brouwers, J.F., and Gadella, B.M. (2005). Capacitation-Dependent Concentration of Lipid Rafts in the Apical Ridge Head Area of Porcine Sperm Cells. Mol Hum Reprod 11, 583-590.

Visconti, P.E., Bailey, J.L., Moore, G.D., Pan, D., Olds-Clarke, P., and Kopf, G.S. (1995a). Capacitation of Mouse Spermatozoa. I. Correlation between the Capacitation State and Protein Tyrosine Phosphorylation. Development 121, 1129-1137.

Visconti, P.E., Galantino-Homer, H., Ning, X., Moore, G.D., Valenzuela, J.P., Jorgez, C.J., Alvarez, J.G., and Kopf, G.S. (1999). Cholesterol Efflux-Mediated Signal Transduction in Mammalian Sperm. Beta-Cyclodextrins Initiate Transmembrane Signaling Leading to an Increase in Protein Tyrosine Phosphorylation and Capacitation. J Biol Chem 274, 3235-3242.

Visconti, P.E., Moore, G.D., Bailey, J.L., Leclerc, P., Connors, S.A., Pan, D., Olds-Clarke, P., and Kopf, G.S. (1995b). Capacitation of Mouse Spermatozoa. Ii. Protein Tyrosine Phosphorylation and Capacitation Are Regulated by a Camp-Dependent Pathway. Development 121, 1139-1150.

Wang, L., Beserra, C., and Garbers, D.L. (2004). A Novel Aminophospholipid Transporter Exclusively Expressed in Spermatozoa Is Required for Membrane Lipid Asymmetry and Normal Fertilization. Dev Biol 267, 203-215.

Williamson, P., Mattocks, K., and Schlegel, R.A. (1983). Merocyanine 540, a Fluorescent Probe Sensitive to Lipid Packing. Biochim Biophys Acta 732, 387-393.

Wolf, D.E., Maynard, V.M., McKinnon, C.A., and Melchior, D.L. (1990). Lipid Domains in the Ram Sperm Plasma Membrane Demonstrated by Differential Scanning Calorimetry. Proc Natl Acad Sci U S A 87, 6893-6896.

Zeng, Y., Clark, E.N., and Florman, H.M. (1995). Sperm Membrane Potential: Hyperpolarization During Capacitation Regulates Zona Pellucida-Dependent Acrosomal Secretion. Dev Biol 171, 554-563.

CHAPTER 4

Membrane properties and dynamics in sperm

Vimal Selvaraj, Atsushi Asano, Danielle E. Buttke, Prabuddha Sengupta, Robert S. Weiss, and Alexander J. Travis. (Under review). Visualizing membrane domains in live cells: micron-scale sterol segregation in live sperm membranes.

Abstract

In somatic cells, plasma membrane domains are dynamic, existing in various time and space scales. The transient nature of these domains and use of detergents or multivalent probes/cross-linkers to isolate or visualize them have incited controversy in this field. Here, we demonstrate the existence of a micrometer-scale, stable domain enriched in sterols in the plasma membrane overlying the acrosome of live murine and human sperm at physiological temperature without crosslinking agents. We also demonstrate that a diffusion barrier exists at the region segregating this domain. Previously, we showed that CTB-bound G_{M1} also localizes to this domain in live sperm, but undergoes redistribution upon cell death. We now demonstrate that G_{M1} is enriched in the acrosome, the exocytotic vesicle immediately underlying this domain, and that communication between these membranes occurs at cell death, increasing G_{M1} in the plasma membrane. We also show that exogenous lipid probes do not segregate in the same manner as endogenous lipids, and that these probes also redistributed after cell death. This is the first report showing stable, micron-scale segregation of membrane sterols in live sperm. This stabilized, sterol-enriched membrane platform is positioned to regulate the acquisition of sperm fertilization competence.

Introduction

Vigorous debate regarding the existence of “membrane rafts” has led membrane biophysicists and cell biologists to a working definition that is consistent with current observations. Membrane rafts are now recognized as small, heterogeneous, highly dynamic, sterol- and sphingolipid-enriched domains. Debate was largely focused on artifacts that could result from use of detergents to isolate these domains, or fixatives or cross-linking agents (polyvalent probes and antibodies) used to visualize them. Several review articles have explored the “raft hypothesis” by examining what is known from biological systems and by extending observations from model membranes (Simons and Ikonen, 1997; Anderson and Jacobson, 2002; Mayor and Rao, 2004; Kusumi and Suzuki, 2005; London, 2005; Pike, 2006). However, evidence for the existence of membrane rafts in live cell membranes is still considered inconclusive by some. One problem recognized by all is the difficulty of direct visualization of these membrane domains in live cells. Lack of visualization with standard light microscopy has led to an appreciation of the small size of these domains in cells, although larger-scale domains can be observed in artificial membrane systems. A recent study utilizing giant plasma membrane vesicles showed that micrometer-scale fluid/fluid phase separations could be resolved in complex biological membranes, although this occurred at lower than physiological temperatures (Baumgart et al., 2007). Membrane rafts likely vary in internal composition and the extent to which they comprise the membranes of different types of cells. For example, an examination of GPI-anchored proteins in live CHO cells showed that they mostly existed as monomers with only 20-40% in small clusters of at most 4 proteins (Sharma et al., 2004), whereas 10-15% of macrophage membranes

was shown to exist as liquid-ordered regions through the use of the exogenous probe, laurdan (Gaus et al., 2003). An explanation for the absence of large-scale phase separations in live cells has been suggested to be due to the maintenance of membrane asymmetry, complex membrane dynamics including intracellular trafficking, and tethered protein obstacles (Kusumi and Suzuki, 2005; Jacobson et al., 2007). Therefore, complex biological membranes have been classified as unusual liquid-like structures (Jacobson et al., 2007). The nanometer-scale size of membrane rafts combined with limitations in the temporal and spatial resolution of physical tools used to study them have made detecting rafts elusive in live cells (Munro, 2003).

Biological membranes contain an extensive diversity of lipids and proteins, and mammalian sperm are no exception. Sperm are terminally differentiated, highly polarized cells. They have a distinct flagellum and head, the latter of which contains the sperm's one intracellular secretory vesicle, the acrosome (Figure 4.1). The existence of membrane trafficking in sperm is thought not to occur, although recent reports suggest that there might be communications between the plasma membrane and acrosomal membranes that do not result in full exocytosis of the acrosomal contents (Kim and Gerton, 2003).

Several studies have suggested that the plasma membrane overlying the acrosome (APM) is unusual in composition. We previously showed that in live sperm cholera toxin subunit B (CTB), which binds to the ganglioside G_{M1}, localizes to the APM (Selvaraj et al., 2006). Freeze-fracture studies utilizing filipin to complex with membrane sterols in fixed cells have shown that this domain is also enriched in sterols (Friend, 1982; Pelletier and Friend, 1983; CTB localization occur between live and dead or weakly fixed cells, with CTB

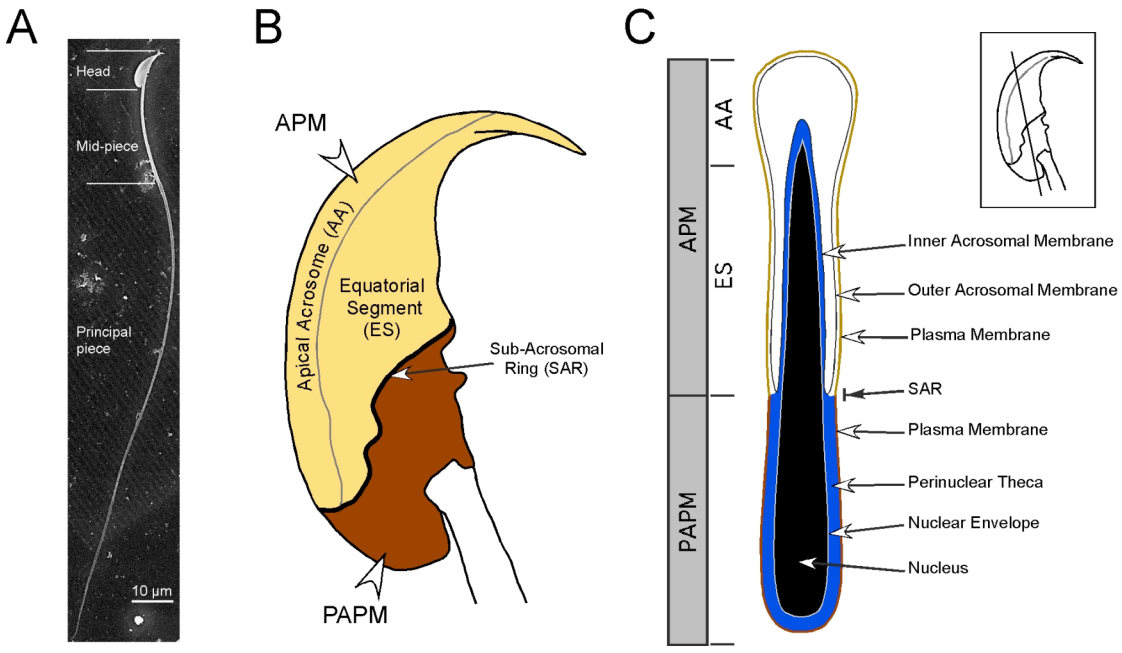

Figure 4.1. Organization of the membranes and structures of the murine sperm head. (A) Scanning electron micrograph showing the entire length of a murine sperm, including the falciform head and the flagellum. The flagellum is again divided into the midpiece and the principal piece, and a small terminal endpiece. (B) Schematic showing a lateral view of a murine sperm head. The plasma membrane of the sperm head is divided into two major regions, the APM and the PAPM, based on morphology and differences in membrane protein and lipid compositions. The APM and PAPM are delimited by a topographical feature known as the sub-acrosomal ring (SAR). On the basis of structure and function the APM is itself divided into the apical acrosome (AA), the region where membrane fusion will take place between the plasma membrane and the acrosomal vesicle, and the equatorial segment (ES). The hook-like structure is called the perforatorium. (C) Schematic showing a longitudinal section through the murine sperm head. Inset lateral view schematic of the sperm head shows the orientation of this longitudinal section. Areas corresponding to the APM (AA and ES) and PAPM are indicated. The nucleus (black) and nuclear membrane (grey) are surrounded by a cytoskeletal meshwork called the peri-nuclear theca (blue). The acrosome (white) is seated over the apical region of the nucleus. The section of acrosomal membrane closest to the nucleus is the inner acrosomal membrane (IAM) and the acrosomal membrane apposing the plasma membrane is the outer acrosomal membrane (OAM). The plasma membrane is tightly wrapped around the structures of the sperm head and is closely associated with the OAM in the region forming the APM, and with the peri-nuclear theca in the PAPM.

Suzuki, 1988; Lin and Kan, 1996). We have shown that several differences in redistributing to the post acrosomal plasma membrane (PAPM) in dead or weakly fixed cells. We also showed that this redistribution is associated with a disproportionate increase in CTB fluorescence which was not due to a change in fluorescence properties or quenching (Selvaraj et al., 2006). The dramatic changes in CTB labeling, the potential for binding of CTB to multiple G_{M1} molecules, and the fact that all studies localizing sterols to the APM domain have been performed in fixed cells combine to limit the conclusions one can draw regarding sperm membrane properties. Yet, the tremendous importance of this membrane region in fertilization makes it essential that we understand the native properties of this domain in live sperm. Should sterol segregation to the APM exist in live sperm, then this could explain the functional requirement for sperm sterol efflux to occur within the female tract. The removal of sterols helps render sperm fertilization competent through a process called "capacitation" (Chang, 1951; Austin, 1952; Davis, 1976; Visconti et al., 1999). Upon appropriate stimulation, the plasma membrane of capacitated sperm can fuse at the region of the apical acrosome (AA, Figure 4.1B) with the underlying outer acrosomal membrane (OAM, Figure 4.1C), resulting in exocytosis.

In this study, we observe sterol localization in live sperm for the first time in the absence of cross-linking reagents, and examine sperm membrane properties by tracking endogenous lipids as well as by using exogenous lipid probes. We also report several findings regarding the localization and behavior of CTB-bound G_{M1} in sperm membranes, together clarifying our understanding of membrane organization and dynamics in these cells.

Experimental Methods

Reagents and biological materials

All reagents were purchased from Sigma (St. Louis, MO), unless otherwise noted. CTB conjugated with biotin or AlexaFluor 488 and 555 (Invitrogen, Carlsbad, CA) or conjugated with FITC was used as indicated. For testing acrosomal integrity, AlexaFluor 488 conjugated peanut agglutinin (PNA; Invitrogen) was used to label sperm. For indirect immunofluorescence, a monoclonal antibody against mouse acrosomal protein sp56 (clone 7C5; QED Bioscience Inc., San Diego, CA) was used. Secondary antibody used was AlexaFluor 488- or 555-conjugated goat anti-mouse serum (Invitrogen). An anti-biotin 10 nm gold-conjugated antibody (British BioCell Intl., Redding, CA) was used for electron microscopy. Lipid probes for membrane labeling used were DiIC12, DiIC16, DiIC18Δ9, DiIC18Δ9,12, NBD-sphingomyelin, BODIPY-G_{M1} and NBD-cholesterol (all from Invitrogen). DiIC22 used was a gift from G. W. Feigenson, Cornell University. Male CD-1 mice were purchased from Charles River Laboratories (Kingston, NY). Human semen samples were obtained with consent from patients visiting the department of urology at Weill Cornell Medical College, New York City, NY. All collections and experiments were performed with approval and oversight by the appropriate Institutional Animal Care and Use Committee or Institutional Review Board.

Media

For murine sperm, a modified Whitten's medium (MW; 22 mM HEPES, 1.2 mM $MgCl_2$, 100 mM NaCl, 4.7 mM KCl, 1 mM pyruvic acid, 4.8 mM lactic acid hemi-calcium salt; pH 7.35) supplemented with glucose (5.5 mM) was used (Travis et al., 2001a). For germ cell preparation from murine testes,

Kreb's ringer bicarbonate medium (KRB; 120.1 mM NaCl, 4.8 mM KCl, 25.2 mM $NaHCO_3$, 1.2 mM KH_2PO_4, 1.2 mM $MgSO_4$, 1.3 mM $CaCl_2$ and 11.1 mM glucose, pH 7.35) was used (Bellve et al., 1977a; Bellve et al., 1977b). For human sperm, a modified Human Tubal Fluid medium (mHTF; 97.8 mM NaCl, 4.69 mM KCl, 0.2 mM $MgSO_4$, 0.37 mM KH_2PO_4, 2.04 mM $CaCl_2$, 4 mM $NaHCO_3$, 21 mM HEPES, 2.78 mM glucose, 0.33 mM sodium pyruvate, 21.4 mM sodium lactate and 10 μg/ml gentamicin sulfate) was used (Quinn et al., 1985).

Sperm Collection and Handling

Murine sperm were collected from the cauda epididymides of male CD-1 mice by a swim-out procedure as described previously (Travis et al., 2001b). Human ejaculates were collected and allowed to liquefy at 37˚C for 30 minutes and then washed three times with mHTF to remove seminal plasma. All steps of collection and washing were performed at 37˚C using large orifice pipette tips to handle sperm minimizing membrane damage. Prior to experimental treatments, motility was assessed for both mouse and human sperm.

Mixed germ cell preparation

Murine testes were decapsulated and incubated in KRB medium supplemented with 0.75 mg/ml collagenase in a shaking water bath at 33˚C for 30 minutes. The resultant preparation of seminiferous tubules was then washed to remove collagenase and interstitial cells. The separated tubules were teased apart and minced using needles under a dissection microscope to yield a cell suspension. The suspension was then triturated and filtered

through a 70 μm nylon mesh (BD Biosciences, Franklin Lakes, NJ), and the flow-through containing individualized cells was collected.

Localization of sterols using filipin III in fixed cells

For localization of filipin-sterol complexes in sperm membranes, sperm were fixed on coverslips for 15 minutes using 4% paraformaldehyde (PF) in PBS. Coverslips were then washed with PBS and incubated with filipin III (10 μg/ml) for 10 minutes. After labeling, the sperm were washed with PBS and mounted on slides using ProLong Gold Antifade (Invitrogen). Filipin-sterol complexes in sperm were visualized at 340-380 nm excitation.

Recombinant perfringolysin O

Plasmid DNA coding PFO was provided by Markus Grebe, Swedish University of Agricultural Sciences, Umeå, Sweden. The sterol-binding domain 4 of PFO (PFO-D4), cloned together with an N-terminal EGFP (pEGFP-N1, Clontech, Mountain View, CA), was amplified using PCR and cloned into a GST-containing vector (pET41a, Novagen, Madison, WI) with an engineered HRV 3C protease cleavage site. [Primers: 5'- ATGGTGAGCAAGGGCGA GGA-3'; 5'-TTAATTGTAAGTAATACTAG-3']. A control peptide with a truncated domain 4 (Δ429) lacking the sterol-binding region (PFO-D4-T) was generated by introducing a stop codon using a site directed mutagenesis in the GST-EGFP-D4 construct. [Primers: 5'-ATAAGAATAAAAGCAAGATAGTG TACAGGCCTTGCTTGGGAATGG-3'; 5'-CCATTCCCAAGCAAGGCCTGTAC ACTATCTTGCTTTTATTCTTAT-5']. Protein expression was induced using 4 mM IPTG in BL21(DE3)pLysS bacteria (Novagen). Cells were pelleted and treated with lysis buffer (50 mM Tris, 120 mM NaCl, 50 mM EDTA, 1% v/v

Triton X-100, 3 mg/ml lysozyme) with Complete protease inhibitors (Roche, Switzerland) and soluble proteins were collected by centrifugation. Recombinant PFO-D4 or PFO-D4-T was purified from the soluble lysate using GSTrap FF columns (GE Healthcare, Piscataway, NJ) followed by in-column digestion using a 3C protease (PreScission™, GE Healthcare). Column binding, washing and elution steps were carried out using a fully automated liquid chromatography system (ÄKTA design, GE Healthcare).

Localization of sterols and G_{M1} in live cells

For visualizing membrane sterols in live sperm, cells were incubated with PFO-D4 (4 μg/ml) in MW medium for 20 minutes at 37˚C; a control using PFO-D4-T (4 μg/ml) was performed concurrently. Similarly, for visualizing G_{M1}, cells were incubated with CTB (AlexaFluor 488; 5 μg/ml) for 10 minutes. For experiments assessing acrosomal status, PNA (5 μg/ml) was used after incubating with CTB as above. For induction of sterol efflux, sperm were incubated in MW medium supplemented with 3 mM 2-OHCD for 30 minutes. For all the above conditions, samples were not washed, but viewed with the respective reagents in the final medium to avoid damage to membranes.

Localization of G_{M1} and sp56 in developing male germ cells

For labeling G_{M1} in developing male germ cells, the cells were spread on coverslips and incubated in KRB in a humidity chamber at 37˚C for 10 minutes to allow attachment. The cells were then fixed using 4% PF for 10 minutes, permeabilized using 0.1% Triton X-100 for 1 minute, washed and air-dried. They were then rehydrated with phosphate buffered saline (PBS) and incubated with CTB (5 μg/ml) for 10 minutes, and washed again using PBS.

For dual labeling experiments, these cells were first blocked for 30 min in PBS with 1% bovine serum albumin, and then incubated with anti-sp56 (1:50) for 1 hr. The cells were then washed using PBS, incubated with the secondary antibody (1:500) for 30 min, and washed again. In dual labeling experiments, the cells were incubated with CTB (AlexaFluor 488 or 555) as a final step. Coverslips were mounted using a GVA mountant (Invitrogen). A control for non-specific binding of the secondary antibody was performed.

Saturation experiment using labeled CTB

To test whether there was exposure of additional G_{M1} during or after redistribution from the APM to the PAPM, we performed experiments in which G_{M1} was saturated in murine sperm before and after weak fixation. As a control to demonstrate our ability to saturate all surface-accessible G_{M1}, live sperm were incubated with CTB conjugated with FITC (250 μg/ml) for 1 minute, while simultaneously allowing attachment to coverslips. This was followed by fixation using 0.004% PF and then a final addition of AlexaFluor 555-conjugated CTB (5 μg/ml). If successful, saturation with a 50-fold excess of FITC-conjugated CTB should prevent AlexaFluor 555-conjugated CTB from binding. To investigate if there was exposure of additional G_{M1} upon redistribution, live sperm were incubated with CTB conjugated with FITC (250 μg/ml) for 1 minute while simultaneously allowing attachment to coverslips, followed by concurrent addition of AlexaFluor 555-conjugated CTB (5 μg/ml) and 0.004% PF. In this experiment, if new G_{M1} became exposed on the surface, then AlexaFluor 555-conjugated CTB would compete for any new binding sites as they appeared during redistribution. The concentration of

FITC-conjugated CTB was selected empirically so that all surface-accessible G_{M1} was saturated in both live and fixed sperm.

Sequential labeling after Saponin permeabilization

To test whether there was exposure of additional G_{M1} in the region of the APM after permeabilization of sperm, we used two different approaches. In the first approach, sperm were allowed to attach on two cover slips and fixed using 4% PF and 0.1% glutaraldehyde in 2.5 mM $CaCl_2$ in PBS for 10 minutes; one of the coverslips was then subjected to permeabilization using 0.1% saponin in PBS. Sperm on both coverslips were then labeled using AlexaFluor 488-CTB (5 μg/ml final concentration) for 10 minutes, washed using PBS and mounted. Images were captured from both permeabilized and unpermeabilized cells using a constant exposure time. Absolute mean pixel intensity values in the APM were computed from the images by mapping the APM domain and subtracting the mean background intensity using Openlab 3.1 software (Improvision, Lexington, MA). Mean intensity values were plotted and statistically compared using the students t test in Kaleidagraph (Synergy Software, Reading, PA). In the second approach, a similar experiment was performed using CTB conjugated to different fluorophores before and after saponin permeabilization. Sperm were allowed to attach on cover slips and fixed using 4% PF and 0.1% glutaraldehyde in 2.5 mM $CaCl_2$ in PBS for 10 minutes. Labeling was carried out using AlexaFluor 488-CTB for 10 minutes. Coverslips were then washed using PBS and one coverslip was subjected to permeabilization using 0.1% saponin in PBS for 5 minutes. Coverslips were again washed with PBS and labeling was carried out using AlexaFluor 647-CTB. In the second approach, AlexaFluor 647-CTB would detect any G_{M1} in

intracellular compartments that became accessible after saponin permeabilization.

Scanning electron microscopy

Samples were prepared by first allowing sperm to attach to silicon-chips for 20 minutes. The attached cells were fixed either weakly using 0.004% PF or strongly using 4% PF and 0.1% glutaraldehyde in 2.5 mM $CaCl_2$ in PBS (Selvaraj et al., 2006). These conditions had previously been found to induce or prevent CTB-G_{M1} redistribution, respectively. Cells were then incubated with 25 mM glycine for 15 minutes to quench free aldehyde groups. G_{M1} was then labeled using biotinylated-CTB (5 μg/ml final concentration in PBS) for 10 minutes. After washing with PBS, cells were incubated in blocking solution (0.2% BSA and 0.2% fish gelatin in PBS) for 15 minutes. The chips were then inverted over drops of 10 nm gold-conjugated anti-biotin antibody (1:8 in blocking solution) and incubated for 1 hour. Chips were then washed 4 times in PBS and once with phosphate buffer and fixed with freshly diluted 2.5% glutaraldehyde in phosphate buffer for 15 minutes. Cells were subsequently washed 5 times with distilled water and snap frozen in liquid nitrogen and freeze dried. Finally, samples were sputter coated with carbon and correlated secondary electron and backscatter images were collected using a Zeiss LEO 1550 field emission SEM with a Gemini column (Carl Zeiss Inc., Oberkochen, Germany).

Exogenous lipid probes

The following exogenous lipid probes and analogs: DiIC12, DiIC16, DiIC22, DiIC18Δ9, DiIC18Δ9,12, NBD-sphingomyelin (NBD-SM), BODIPY-G_{M1}

and NBD-Cholesterol (NBD-Chol) were used. Labeling was carried out by adding the respective probe (all at 3 μM final concentration in methanol 0.1% v/v) to live cells in suspension in MW medium at 37˚C. After probe dispersion in the medium and incubation for 5 minutes, sperm were visualized by exciting at wavelengths 549 nm for the DiI probes and 488 nm for the NBD and BODIPY conjugated probes.

Fluorescence microscopy and image collection

For localization experiments in live sperm, a stage-mounted incubation chamber (LiveCell, Neue Product Group, Westminister, MD) was used along with an objective heater (Bioptechs, Butler, PA) both maintained at 37˚C and viewed with a Nikon Eclipse TE 2000-U microscope (Nikon, Melville, NY) equipped with a Photometrics Coolsnap HQ CCD camera (Roper Scientific, Ottobrunn, Germany), and Openlab 3.1 (Improvision) automation and imaging software. For testing co-localization in dual-labeled germ cells, images were acquired using an Olympus IX70 laser-scanning confocal microscope (Olympus, Melville, NY) and merged. Image deconvolution and 3D rendering were performed using Vector 3 (Improvision). Serial z image stacks from spermatids labeled with CTB and anti-sp56 were acquired using the Nikon Eclipse TE 2000-U epifluorescence microscope with a programmed automation in Openlab at z=0.2 μm for 3 channels, AlexaFluor 488, AlexaFluor 555 and Hoechst 33258 respectively. Images were calibrated and transferred as a series to Vector 3 and deconvoluted using an iterative algorithm with a 98% confidence limit. Reconstructed image compilations were made into QuickTime™ animations showing rotations on several axes as noted.

Lateral diffusion of CTB-bound G_{M1} in live and dead cells

Photo-bleaching experiments measuring the mobility of CTB-bound G_{M1} on the sperm plasma membrane were performed using a programmed module of the Zeiss software on a LSM 510 Meta confocal microscope (Zeiss, Germany). An optical slice thickness of 8 μm was used for the imaging and bleaches (thickness of the sperm head ~1 μm). Fluorescence loss in photo-bleaching (FLIP) (van Drogen and Peter, 2004) experiments were carried out selecting a region (~1 μm diameter) at different points within the APM. The selected regions were subjected to a series of 5-iteration bleach scans with a 5-second recovery period after each iteration. Frames were captured after each series of bleach iterations to examine the fluorescence over the entire sperm head. A control was performed to test: (a) whether bleaching a region over the PAPM would affect fluorescence over the APM and (b) whether capturing frames after each bleach series would produce a bleach effect of the entire sperm head at the imaging fluorescence intensity. Line intensity profiles were generated utilizing the Zeiss software and graphed. Fluorescence recovery after photo-bleaching (FRAP) experiments were carried out in immotile dead cells after the redistribution of G_{M1} to the PAPM region. Regions (~1 μm diameter) were selected within the PAPM and subjected to a single series of a continuous 5-iteration bleach scan. Data for fluorescence recovery after bleaching were obtained from intensity estimates for the region of bleach every 90 milli-seconds for 4 – 20 seconds for each cell and graphed. Fluorescence intensity was also monitored for a control region within the PAPM not subjected to bleaching. Frames of the entire sperm head showing the bleached and control regions were captured in separate runs as representative images for presentation and not for analysis.

Annexin V labeling in live and dead cells

Labeling was carried out by adding AlexaFluor 488-conjugated annexin V (1:5 according to manufacturers instructions; Invitrogen) to live cells in suspension in MW medium at 37˚C. After incubation for 20 minutes at 37˚C, live and dead sperm were visualized from the same preparation and images recorded as described above.

Results

Sterol enrichment in a micron-scale plasma membrane domain in live cells

Using a recombinant EGFP-conjugated domain 4 of perfringolysin O (PFO-D4; Figure 4.2A) that has been demonstrated to bind membrane sterols specifically (but which requires a high local mole percent of sterols) (Waheed et al., 2001; Ohno-Iwashita et al., 2004), we localized sterols in the plasma membrane of live sperm. PFO-D4 localized exclusively to the APM in live swimming cells indicating the segregation of focally enriched sterols to this region (Figure 4.2B). Although PFO-D4 labeled the entire APM, fluorescence appeared as closely apposed punctate spots rather than a diffuse localization. We found that the time taken for PFO-D4 labeling differed between individual cells, but that the pattern of onset of labeling was consistent within cells, with the AA usually being labeled first followed by the membrane in the vicinity of the sub-acrosomal ring (SAR), and then the equatorial segment (ES). The PAPM and flagellum were not labeled with PFO-D4.

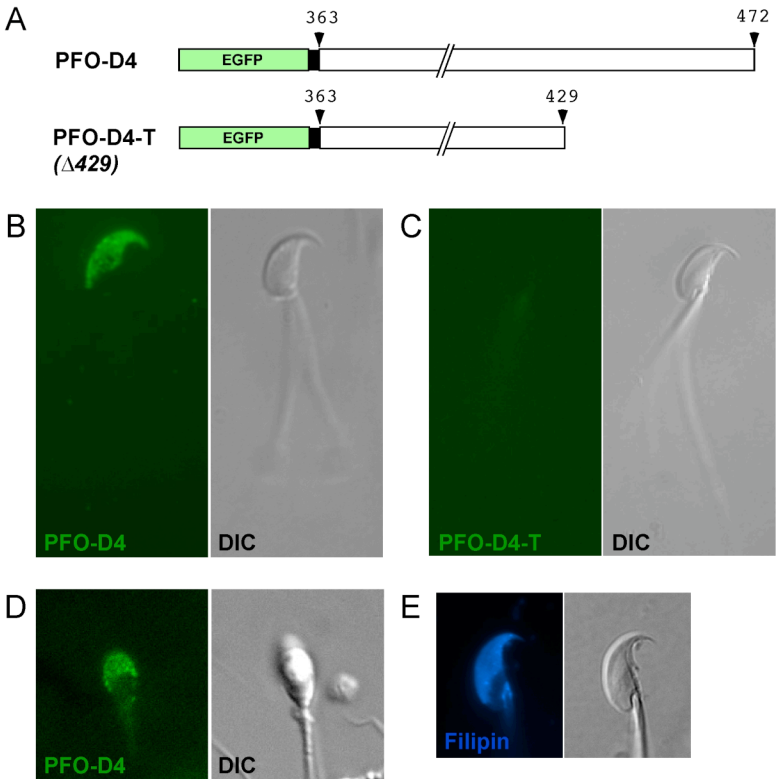

Figure 4.2. Localization of sterols in murine and human sperm. (A) Schematic showing the recombinant PFO peptides used for localization studies. Constructs were made producing the sterol-binding D4 domain of PFO fused with EGFP (PFO-D4; amino acids 363-472). A non-functional control construct was also made in which the sterol-binding region of the D4 domain was truncated (PFO-D4-T; Δ429). (B) Live murine epididymal sperm labeled with PFO-D4. Panels show an epifluorescence and corresponding DIC image of a live swimming sperm (note the movement of the tail) labeled using PFO-D4. There was clear segregation of the PFO-D4 fluorescence to the APM . There was no change in localization in dead cells. (C) Live murine sperm labeled with PFO-D4-T. Panels show an epifluorescence and corresponding DIC image of a live swimming sperm (again, note the movement of the tail) labeled using PFO-D4-T. There was no binding of this EGFP-conjugated non-functional truncated mutant protein confirming the binding specificity of PFO-D4. (D) Live human ejaculated sperm labeled with PFO-D4. Panels show an epifluorescence and corresponding DIC image of a live swimming sperm. Segregation of the PFO-D4 fluorescence to the APM was conserved in human sperm. (E) Fluorescence localization of filipin-sterol complexes in a fixed murine sperm. Panels show an epifluorescence and corresponding DIC image; there is sterol-enrichment in the APM domain of sperm in agreement with the observation in live cells.

A control protein was generated that was predicted to be non-functional by means of removal of the sterol-binding sequence of amino acids. EGFP-conjugated domain 4 of perfringolysin O with a truncation (PFO-D4-T; Figure 4.2A), failed to bind the APM showing the specificity of binding in these cells (Figure 4.2C). Similarly, in live human sperm, PFO-D4 localized to the APM (Figure 4.2D). This localization in the APM is in agreement with the fluorescence localization of filipin-sterol complexes in fixed murine sperm (Figure 4.2E). The localization of PFO-D4 seen in live cells did not change with cell death or fixation (data not shown).

Differences in G_{M1} labeling using CTB

Using fluorescence localization, we previously showed that CTB labels the APM in live cells; however, at the time of cell death as assessed by the cessation of motility, the CTB fluorescence in the APM dramatically redistributed to the PAPM within 10 to 100 seconds (Selvaraj et al., 2006). One reproducible observation during this redistribution was the enhancement of total CTB fluorescence in the sperm head; this relative difference in fluorescence intensity between a live and a dead cell is shown (Figure 4.3A), and has previously been quantified (Selvaraj et al., 2006). Cells that underwent sterol efflux induced by 2-hydroxypropyl-β-cyclodextrin (2-OHCD), which is a stimulus for capacitation, showed a diffuse pattern of CTB fluorescence in both the APM and PAPM after cell death (Figure 4.3B). The effects of sterol efflux on CTB-bound G_{M1} have been previously described, and vary between sperm (Selvaraj et al., 2007). This observation is of physiological relevance because it indicates which sperm among a heterogeneous

Figure 4.3. Differences seen in G_{M1} localization using CTB in live, dead, strongly fixed and unfixed cells. (A) Panels show an epifluorescence and corresponding DIC image of a live (left) and dead (right) unfixed murine sperm labeled with CTB. Fluorescence is in the APM in live cells and in the PAPM in dead cells. Note the higher intensity of fluorescence in the dead cell compared to the live cell. (B) Panels show an epifluorescence and corresponding DIC image of a dead, unfixed murine sperm labeled with CTB after efflux of sterols using 2-OHCD. CTB labeled the entire sperm head with a diffuse localization pattern. (C) Panels show backscatter SEM images of a murine sperm head labeled using CTB after strong fixation. For C, D, and E, the boxed regions in the miniatures orient the region shown in the high magnification, secondary electron and backscatter images. In these panels, white arrowheads indicate the SAR. CTB-gold particles were segregated to the APM in this cell similar to that seen in live cells. (D) Panels show SEM images of an unfixed murine sperm head labeled using CTB. CTB-gold particles were enriched in the PAPM and the AA. Note the apparent increased intensity of labeling in this cell after redistribution. (E) Panels show SEM images of an unfixed murine sperm head labeled using CTB. This particular cell shows a partial redistribution. Note the enrichment of CTB-gold at the SAR and along the edge of the AA.

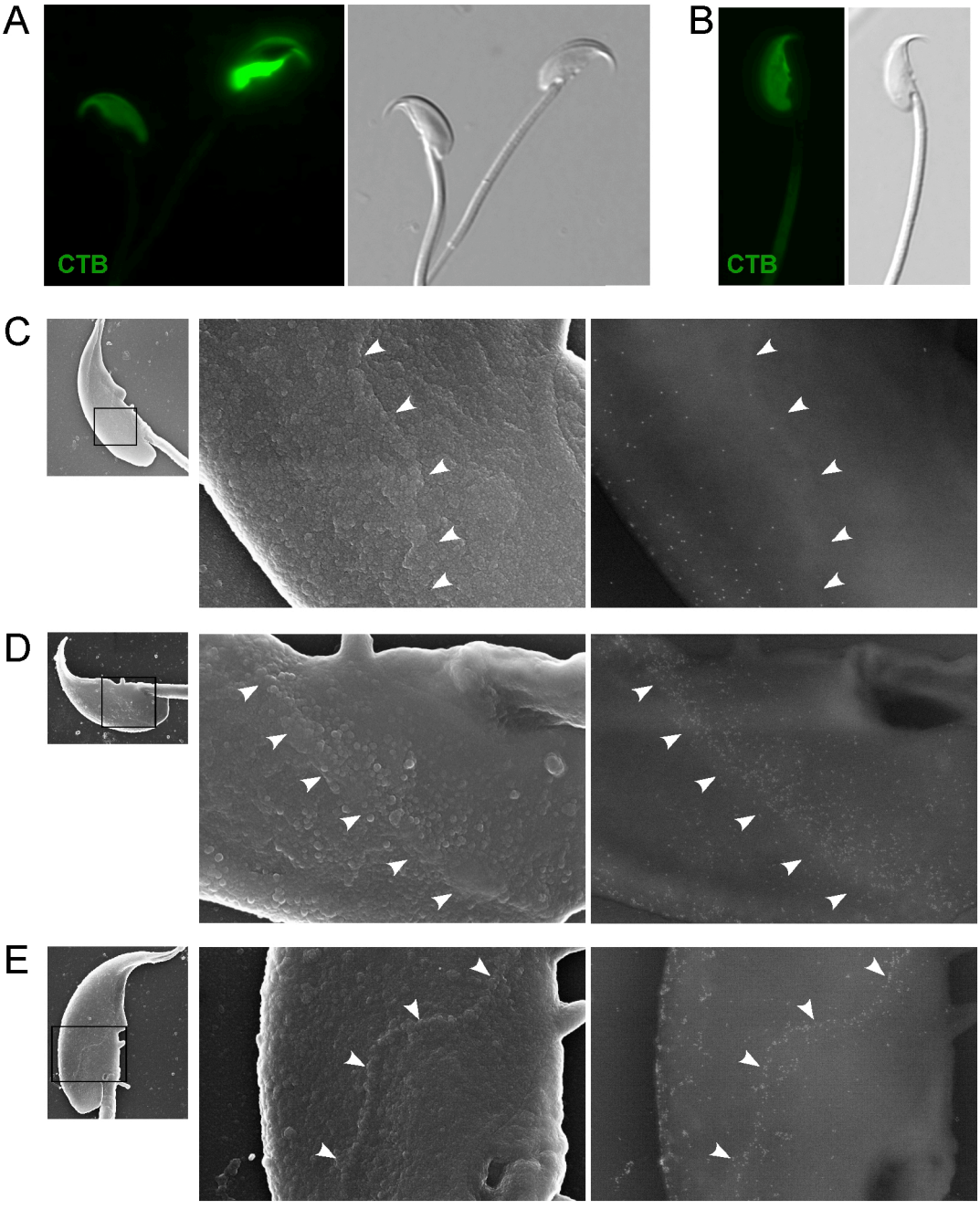
A
CTB
B
CTB
C
D
E

population have responded to sterol efflux up to that time (Selvaraj et al., 2007). We also reported that the use of a strong fixative (4% PF with 0.1%glutaraldehyde in PBS with 2.5 mM $CaCl_2$) could prevent the redistribution of CTB. We examined CTB distribution using backscatter SEM with 10 nm gold particles to verify the localization seen with fluorescence images and observe in much greater detail the localization of CTB-bound G_{M1}. Backscatter SEM imaging after the strong fixation showed CTB-gold particles segregated in the APM (Figure 4.3C). Labeling in the absence of fixatives resulted primarily in a PAPM distribution in dead cells (Figure 4.3D). Consistent with the observation using fluorophore-conjugated CTB, we saw an enrichment of CTB-gold particles at the level of the SAR and the PAPM. Although not quantitative, there was an apparent increase in the number of CTB-gold particles when labeling was performed after redistribution (compare Figures 4.3C and 4.3D). This also held true for unfixed cells that showed incomplete redistribution. CTB-gold particles were seen in both the APM and PAPM, but a clear enrichment of particles was noted at the SAR (Figure 4.3E).

Redistribution caused an increase in G_{M1} on the plasma membrane

To address the increase in total CTB fluorescence as a result of redistribution upon cell death, we investigated whether intra-cellular compartments were contributing to an increase in surface G_{M1}. For these experiments, we employed a general strategy of saturating all surface-accessible G_{M1} with FITC-conjugated CTB (250 mg/ml), and then probing with AlexaFluor 555-conjugated CTB (5 mg/ml) to look for any newly exposed binding sites. First, to verify that saturation could be attained, we incubated live sperm with the FITC-CTB, and then probed with AlexaFluor 555-CTB; no

binding by the latter conjugate was seen (data not shown). To confirm that saturation could be attained after redistribution to the PAPM, we incubated live sperm with the FITC-CTB, and then induced redistribution with 0.004% PF, still in the presence of the FITC conjugate. We have shown previously that this concentration of PF does not interfere with CTB binding and that it induces redistribution (Selvaraj et al., 2006). In this way, all surface-accessible G_{M1} should be bound by FITC-CTB before, during and after redistribution. We then added AlexaFluor 555-conjugated CTB to see if any unbound G_{M1} remained. No new binding was detected, confirming saturation (Figure 4.4A). Next, we repeated the first incubation of live sperm with FITC-CTB. Then we added the AlexaFluor 555-conjugated CTB simultaneously with the 0.004% PF. If new G_{M1} were exposed on the surface during redistribution, there should be a competition between the FITC-CTB and AlexaFluor 555-CTB for these new sites. Assuming they have equal binding efficiencies and based on relative concentrations, only approximately 2% of newly exposed G_{M1} should be bound by the AlexaFluor 555-CTB. For technical reasons related to risk of membrane damage and sperm death during washing, we chose this approach over first washing out the unbound FITC-CTB. Nonetheless, when we performed this experiment, a percentage of the sperm corresponding roughly with the initial percentage of motile sperm showed AlexaFluor 555-CTB fluorescence, primarily on the borders of the APM and in the PAPM (Figure 4.4B). Another sub-population of sperm showed only FITC-CTB signal. These sperm were probably not viable during the initial incubation and served as an efficient internal control, showing that the initial surface saturation with the FITC-conjugate was thorough.

Figure 4.4. Identification of intracellular G_{M1} in the sperm head. We saturated all surface-accessible G_{M1} using 250 □g/ml FITC-conjugated CTB (green), and then added 5 □g/ml AlexaFluor 555-conjugated CTB (red) to see if there was exposure of additional G_{M1} during CTB-induced redistribution to the PAPM. (A) Live sperm were incubated with FITC-CTB, fixed using 0.004% PF to induce redistribution, and then AlexaFluor 555-CTB was added. All sperm had an intense FITC-CTB fluorescence and no detectable AlexaFluor 555-CTB fluorescence, showing that FITC-CTB completely saturated G_{M1} in murine sperm. (B) Sperm were incubated with FITC-CTB, then simultaneously treated with AlexaFluor 555-CTB and fixed using 0.004% PF to induce redistribution. Some sperm had intense FITC-CTB fluorescence and no detectable AlexaFluor 555-CTB fluorescence [similar to (A); not shown] and others showed AlexaFluor 555-CTB labeling over the APM and PAPM (shown). This finding suggested that additional molecules of G_{M1} appeared in the plasma membrane during redistribution to the PAPM. (C) Fluorescence intensity measurement over the region of the APM with and without saponin permeabilization in fixed cells. Box-whisker plots show mean pixel intensities measured in the region of the APM (inset; region of quantification outlined) in saponin permeabilized and control cells. The lower and upper ends of the box mark the 25th and 75th quantiles; the median is represented as a horizontal line within the box, and the mean as a horizontal line through the box. Vertical whiskers extend from the ends of the box to the 10th and 90th quantiles. A students t test showed significant differences between the permeabilized and control cells ($P<0.0001$). (D) Sequential labeling before and after saponin permeabilizaton in fixed sperm. After fixation sperm were labeled using AlexaFluor 488-CTB; cells were then washed and subjected to saponin permeabilization. Labeling for newly exposed CTB binding sites after permeabilization was carried out using AlexaFluor 647-CTB, and revealed signal over the acrosome. In the absence of saponin permeabilization, incubation with AlexaFluor 647-CTB yielded no new labeling. These findings provide evidence for an intracellular pool of G_{M1}, accessible to CTB after saponin permeabilization.

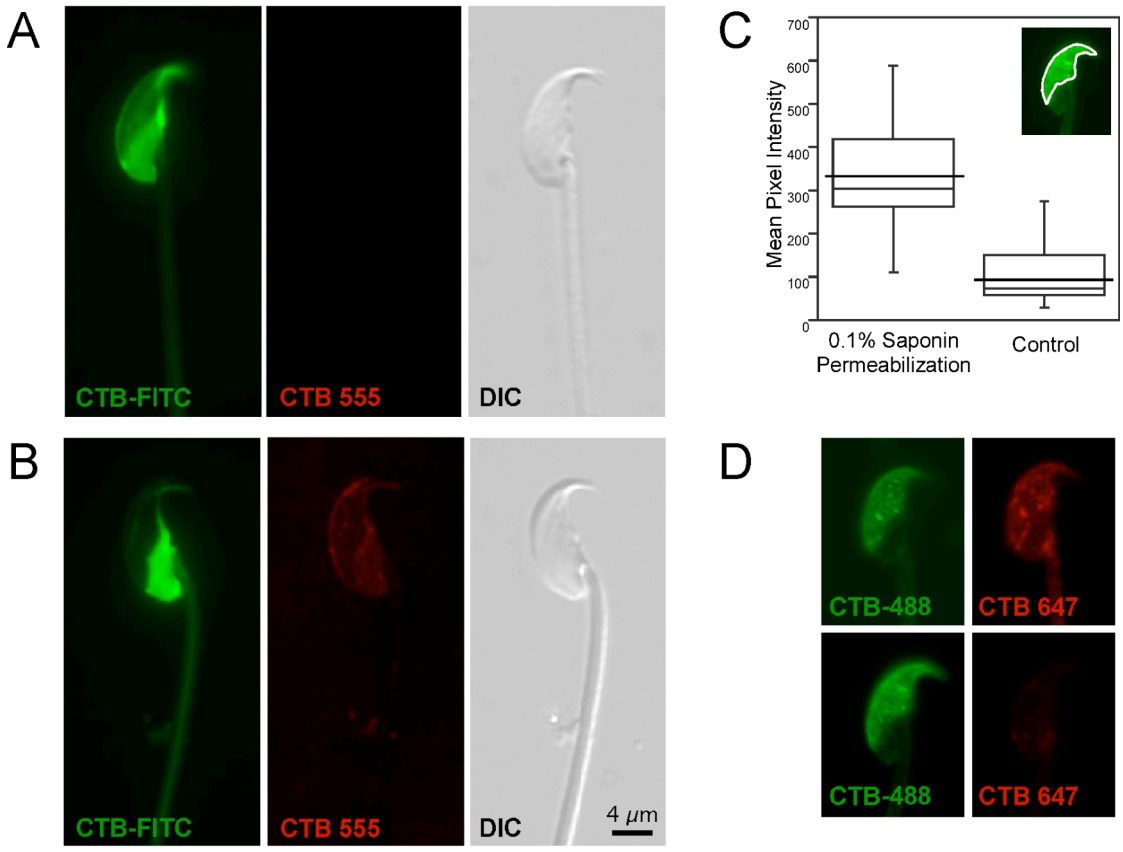
A
CTB-FITC
CTB 555
DIC
B
CTB-FITC
CTB 555
DIC
4 μm
C
Mean Pixel Intensity
700
600
500
400
300
200
100
0
0.1% Saponin Permeabilization
Control
D
CTB-488
CTB 647
CTB-488
CTB 647

In light of the above findings that suggested that redistribution of CTB also involved an increase in G_{M1} on the sperm surface, we investigated whether an internal membranous compartment might represent a source of additional G_{M1}. We addressed this possibility using two different approaches. First, we labeled sperm after strong fixation with or without saponin permeabilization and compared mean fluorescence intensity in the APM. Our results showed that there was significantly higher mean fluorescence intensity over the APM in permeabilized compared to nonpermeabilized sperm (Figure 4.4C; $p<0.0001$). In the second approach, we used CTB conjugated to two different fluorophores to examine whether there was exposure of additional G_{M1} after saponin permeabilization. We found that cells initially labeled with AlexaFluor 488-conjugated CTB showed additional binding sites after saponin permeabilization compared to unpermeabilized controls (Figure 4.4D). These observations suggested that an intracellular pool of G_{M1} existed in mature sperm and was in position to contribute to the increase in fluorescence intensity seen during CTB redistribution.

G_{M1} enrichment in the acrosomal membrane in spermatids and sperm

Because of its location immediately underneath the APM, and because it is the only intracellular vesicle in the sperm head, we hypothesized that the acrosome was the likely intracellular pool of G_{M1}. In mature sperm the APM and OAM are in extremely close apposition, and differential localization to one membrane or the other cannot be distinguished at the level of light microscopy. Therefore, we examined round spermatids for the presence of G_{M1} in the developing acrosome. In these cells one can more easily distinguish between the acrosomal and plasma membranes because they are separated

Figure 4.5. Localization of G_{M1} and sp56 in murine male germ cells. (A) Panels show confocal images of CTB (green) and sp56 (red) localization in round spermatids connected by intercellular bridges. Merged image (yellow) from the two channels and the corresponding Nomarski DIC image are also shown. CTB approximately co-localized with the acrosomal matrix protein sp56 during development of the acrosome. (B) 3D-rendered image compilation of G_{M1} and sp56 localization in a murine round spermatid. Serial z stacks were deconvoluted and reconstructed in 3 dimensions as described. Each row represents frames from rotation along the vertical axis. CTB (green) and sp56 (red) localized to the developing acrosomal vesicle. The nucleus was stained using Hoechst (blue). These frames show that G_{M1} largely enveloped the sp56 fluorescence of the acrosomal matrix. This suggested that G_{M1} was associated with the acrosomal membranes and was not localized within the acrosomal matrix. (C) Correlated secondary electron and backscatter SEMs of an acrosome disrupted murine sperm head labeled with CTB-gold. (I) Shows the entire sperm head. The boxed area indicates the region of plasma membrane and acrosomal disruption. (II) Shows a higher magnification image of the disrupted region. Black arrowheads indicate the SAR and white arrowheads point to the fringes of the plasma membrane. (III) Backscatter image showing the localization of CTB using 10 nm gold particles. Gold labeling was seen within the region of the disrupted acrosome visible between the ragged edges of the broken plasma membrane. These observations were consistent with CTB localization in the acrosomal membranes in mature sperm as well as during male germ cell development.

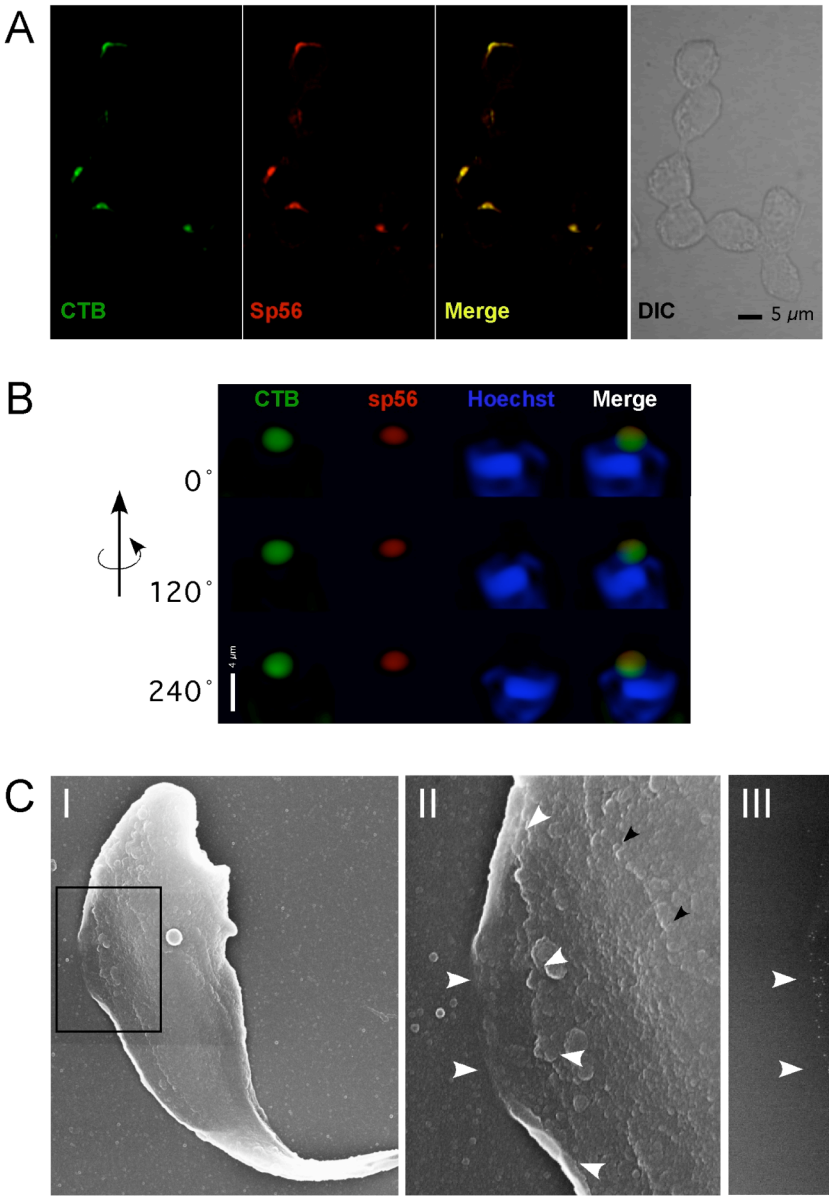
A
CTB
Sp56
Merge
DIC
5 μm
B
CTB
sp56
Hoechst
Merge
0°
120°
240°
C
I
II
III

by cytoplasm. From this experiment, we found that G_{M1} was strongly enriched in the developing acrosome in round spermatids. In cap phase round spermatids, the G_{M1} approximately co-localized with the acrosomal matrix component sp56 in the developing acrosome (Figure 4.5A). Deconvolution and reconstruction of serial sections taken at higher magnification revealed that the G_{M1} appeared to surround the acrosomal matrix (Figure 4.5B). These findings showed that G_{M1} was enriched in the acrosomal membranes of round spermatids and strongly suggested that G_{M1} could be present in the acrosomal membrane of mature sperm.

Although strongly suggestive, these results did not ensure that lipid trafficking did not change the localization of G_{M1} during spermatid remodeling or during epididymal maturation. Therefore, we designed a strategy to first gently disrupt the plasma membrane and the acrosomal vesicle of the sperm head, label them using CTB and perform backscatter SEM imaging for associated gold particles. After gentle disruption of membranes, we found that CTB labeling was seen in regions corresponding to acrosomal membranes in mature sperm (Figure 4.5C). These findings suggested that redistribution involved interactions between the APM and the G_{M1}-rich acrosomal membranes, which resulted in the observed increase in fluorescence intensity.

Redistribution did not result in, nor was caused by, the loss of acrosomal integrity

Experimental evidence clearly suggested that the acrosome could be acting as an intracellular pool of G_{M1}, some of which moved to the plasma membrane at cell death. In sperm, any communication that might occur between the plasma membrane and the acrosomal membranes could mimic or

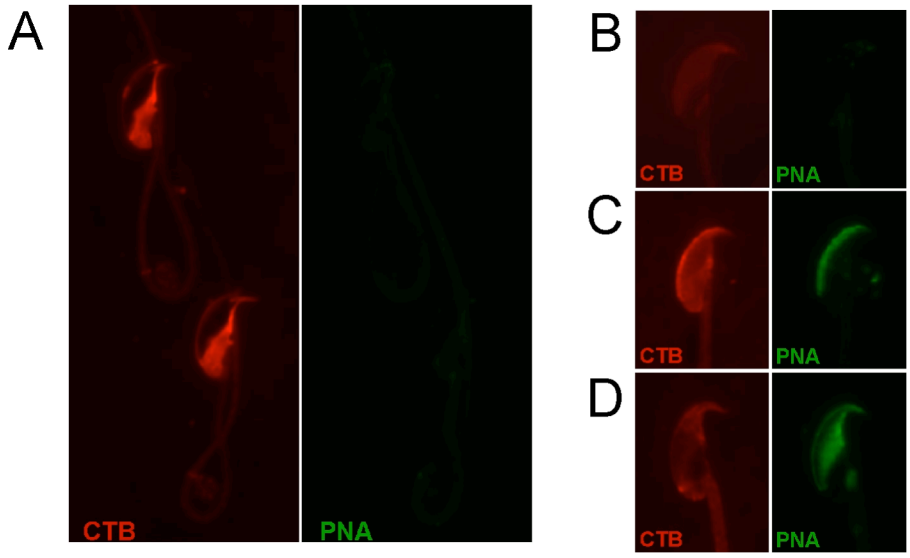

Figure 4.6. Redistribution of CTB-bound G_{M1} was not correlated with full acrosomal exocytosis. Dual labeling experiments using CTB (red) and PNA (green) were performed in unfixed cells. (A) Two dead cells showing CTB redistributed to the PAPM region and no PNA labeling indicating intact acrosomal vesicles. (B) A control live cell with an intact acrosomal vesicle. CTB is in the APM and there is no PNA labeling. (C) A dead sperm cell with acrosomal membranes exposed in the region of the AA had a diffuse CTB labeling with increased intensity in the AA and SAR/PAPM. PNA labeled the AA, revealing a partial acrosomal exocytosis. (D). A damaged cell in which parts of the APM and the OAM were lost, had a loss of CTB labeling and exposure of the acrosomal membranes in the ES.

induce the process of acrosomal exocytosis, resulting in the vesiculation and loss of the fused plasma membrane and OAM as hybrid vesicles. This would ultimately result in release of acrosomal matrix components and exposure of the inner acrosomal membrane (IAM) (Yanagimachi, 1994). To examine whether there was exposure of acrosomal membranes after the redistribution of CTB we labeled sperm with peanut agglutinin (PNA), which binds to the glycoconjugates in the acrosomal membranes of murine sperm (Tao et al., 1993). We found that similar to live intact sperm (Figure 4.6B), PNA did not label sperm after CTB redistribution (Figure 4.6A). PNA patterns seen in rare cells after partial spontaneous acrosomal exocytosis (Figure 4.6C) and in rare acrosome-damaged cells (Figure 4.6D) are shown from the same experiment, and served as internal positive controls. These findings suggest that despite the communication between the acrosomal membranes and the plasma membrane, there was not a full exocytosis.

G_{M1} was mobile in live cells but not after redistribution in dead cells

To understand the nature of the APM, and to test our hypothesis that redistribution of G_{M1} to the PAPM in dead cells was associated with crosslinking by the pentameric CTB molecule, we performed photobleaching experiments to examine the lateral mobility of CTB. Fluorescence loss in photobleaching (FLIP) experiments on the APM in live cells showed that CTB-bound G_{M1} was mobile except for a small region over the perforatorium (Figure 4.7A). A control area of the same dimension was bleached in the PAPM and showed that G_{M1} in the APM was completely segregated from the PAPM in live cells (Figure 4.7B). After CTB redistribution in dead cells, fluorescence recovery after photobleaching (FRAP) experiments showed that there was no

recovery of fluorescence in the photobleached selection within the PAPM (Figure 4.7C). Together, these data suggested that G_{M1} was mobile in the APM, but that cross-linking during redistribution could have rendered it immobile in the PAPM.

Exogenous lipid probes did not share the characteristics of endogenous lipids

To examine sperm membrane properties both ante- and post-mortem, we tested the localization of a variety of exogenous lipid probes in live and dead sperm. One common observation was that irrespective of the nature of the probe used [saturated 1,1'-dioctadecyl-3,3,3',3'-tetramethyl indocarbocyanine (DiI) probes: DiIC12, DiIC16 and DiIC22; unsaturated probes: DiIC18Δ9, DiIC18Δ9,12; fluorescent lipids: BODIPY-G_{M1}, NBD-SM], all of them showed a diffuse labeling pattern across the APM, PAPM and flagellum alike in live cells (Figure 4.8A). In dead cells, the same probes segregated to the APM (Figure 4.8A). All probes except for DiIC18Δ9 showed labeling of the mid-piece of the flagellum in dead cells. NBD-Chol had relatively weak labeling in both live and dead cells and the labeling in both was over the APM. However, sperm motility slowed dramatically immediately after the addition of NBD-Chol, suggestion a deleterious effect on these cells. Co-localization experiments using DiIC16 and CTB showed that the redistribution of CTB to the PAPM in dead cells did not influence the localization of DiIC16 (Figure 4.8B). In fact, there was a clear separation of DiIC16 and CTB fluorescence in these cells. Therefore exogenous probes in sperm did not reflect properties of endogenous lipids.

Figure 4.7. Lateral diffusion of CTB-bound G_{M1} in live and dead cells. (A) Fluorescence loss in photobleaching (FLIP) on the APM in CTB-labeled live sperm. Multiple cells were examined in 4 independent experiments and representative data are shown. (I) Shows the CTB-labeled APM of a live sperm; the red circle on the APM and SAR indicates the region of bleach in this experiment and the red arrow shows the location and direction used for generating the line intensity profile. (II) Panels 1, 2 and 3 represent frames captured after each bleach series of the same sperm. Note that there was still residual signal over the perforatorium (white arrowhead) suggesting that CTB in this region had reduced mobility compared to the AA and ES. (III) Line intensity traces from frames 1, 2 and 3 showing loss of fluorescence intensity over the entire APM (AA and ES) as a result of repeated bleaching of the region indicated (5 bleach iterations before each frame). These data were consistent with CTB-G_{M1} being mobile in the APM. (B) FLIP on the PAPM in CTB-labeled live cells. Multiple cells were examined in 4 independent experiments and representative data are shown. (I) Shows the CTB-labeled APM of a live sperm; the red circle on the PAPM indicates the region of bleach in this experiment and the red arrow shows the location and direction used for generating the line intensity profile. (II) Panels 1, 2 and 3 represent frames captured after each bleach series of the same sperm. (III) Line intensity traces from frames 1, 2 and 3 showed no loss of fluorescence intensity over the entire APM domain (AA and ES) as a result of repeated bleaching of the region indicated on the PAPM. These data demonstrated that G_{M1} in the APM was stably segregated from the PAPM in live cells, and that capturing frames did not produce a bleaching effect in these experiments. (C) Fluorescence recovery after photobleaching (FRAP) in CTB-labeled dead cells. Multiple cells were examined in 5 independent experiments and representative data are shown. (I) Shows the CTB-labeled PAPM of a dead sperm; the red circle on the PAPM indicates the region of bleach and the black circle indicates the location of a control region used for parallel fluorescence intensity values. (II) Panels 1, 2 and 3 represent frames captured before bleaching, 2 seconds after bleaching and 20 seconds after bleaching respectively. Note that there was no visible fluorescence recovery in the bleached region. (III) A representative graph obtained from a FRAP trial. Red trace indicates fluorescence intensity within the bleached region and the black trace represents the fluorescence intensity within the control region of the same sperm. These results showed that there was very limited to no mobility of CTB-bound G_{M1} after redistribution to the PAPM in dead cells.

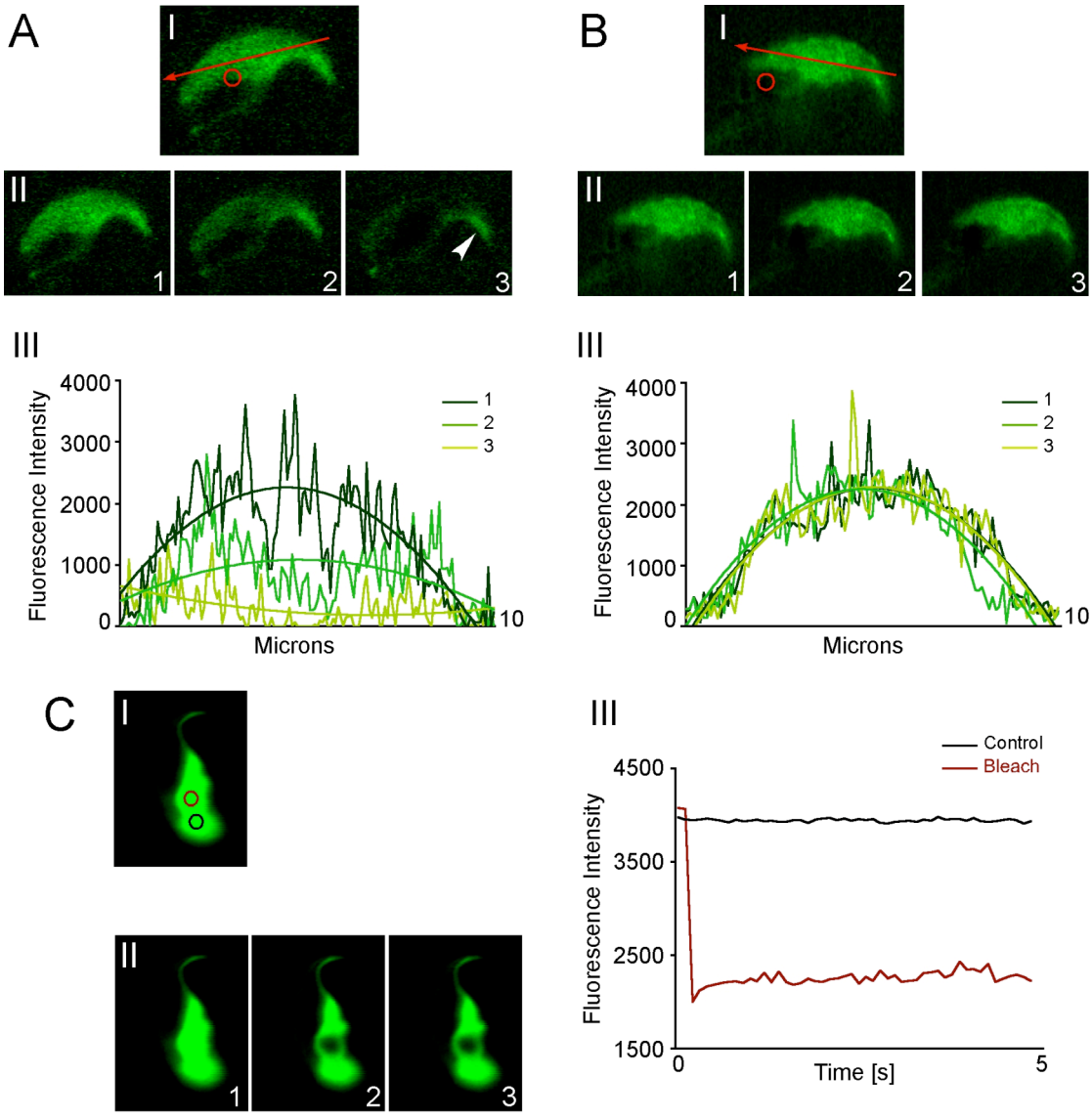
A
I
II
1
2
3
III
Fluorescence Intensity
4000
3000
2000
1000
0
Microns
10
B
C
Control
Bleach
4500
3500
2500
1500
Time [s]
5

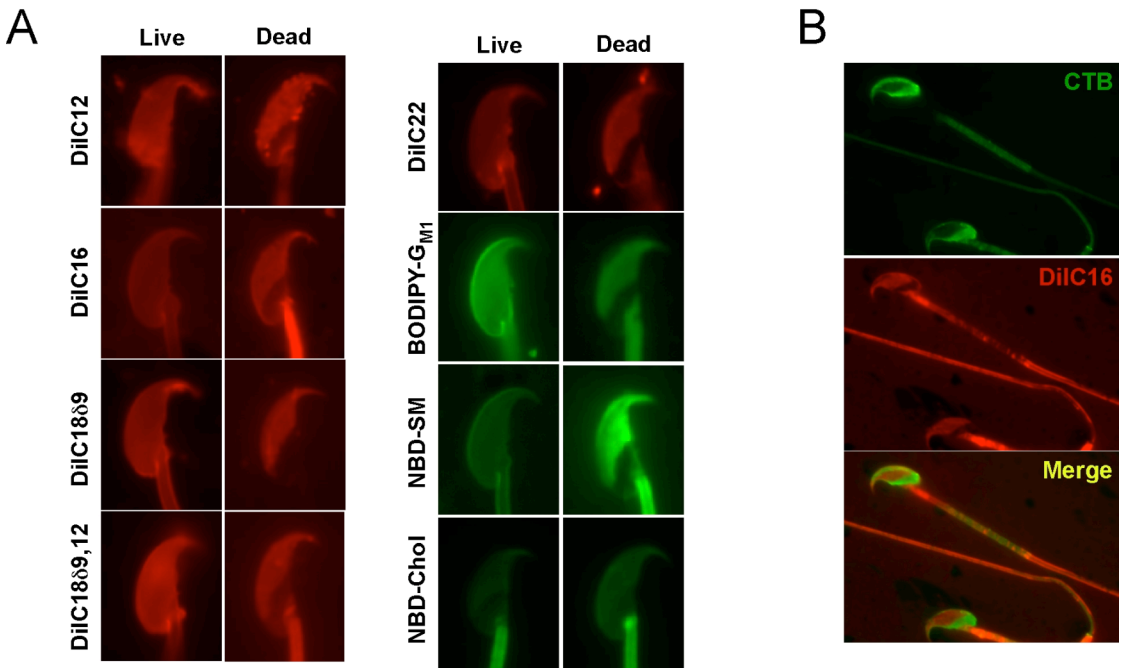

Figure 4.8. Localization of exogenous lipid probes in live and dead murine sperm. (A) Labeling using various lipid probes (saturated probes: DiIC12, DiIC16 and DiIC22; unsaturated probes: DiIC18Δ9, DiIC18Δ9,12; fluorescent lipids: BODIPY-GM1, NBD-SM, NBD-Chol) on live and dead sperm heads are shown. The predominant finding was that irrespective of their nature, all probes except NBD-Chol showed diffuse labeling patterns in live cells. Dead cells had labeling over the APM domain irrespective of the nature of the probe. NBD-Chol had relatively very weak labeling in both live and dead cells and the labeling appeared to be over the APM. All probes except for DiIC18Δ9 and DiIC12 showed intense labeling of the mid-piece of the flagellum. (B) Co-labeling using DiIC16 and CTB in dead cells. Images show two dead unfixed sperm labeled using CTB (green) and DiIC16 (red). The potential crosslinking effect of CTB and redistribution to the PAPM in the sperm head plasma membrane did not affect the preferential localization of DiIC16 in the same cells.

Annexin V localization in live and dead cells

To understand further the nature of the sperm membranes and their changes upon cell death, we investigated potential loss of membrane asymmetry and exposure of phosphatidyl serine (PS) by using annexin V to label PS on the outer leaflet. Annexin V did not label live sperm (Figure 4.9A). In dead cells, there was a regional loss of membrane asymmetry primarily in the PAPM indicated by annexin V labeling in this region (Figure 4.9B). This regional loss of membrane asymmetry could explain some of the membrane property changes seen during sperm death.

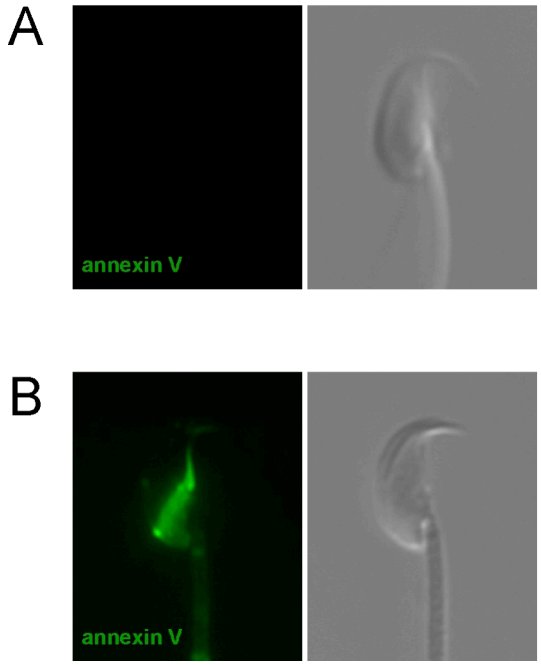

Figure 4.9. Annexin V labeling in live and dead sperm. Panels show an epifluorescence and corresponding DIC image. (A) Images of a live swimming sperm (note the movement of the tail). Annexin V labeling was not seen in live cells. (B) Images of a dead cell from the same experiment. Annexin V labeling was seen in the PAPM. This finding suggested a regional loss of membrane asymmetry in the PAPM of the sperm head. Greater than 100 cells were examined in 5 independent experiments and representative data are shown.

Discussion

Existence of a micron-scale membrane domain enriched in sterols in live sperm

Several laboratories including ours have previously demonstrated that in fixed sperm there is an enrichment of sterols in the APM. This property appears to be conserved among mammals (Friend, 1982; Pelletier and Friend, 1983; Suzuki, 1988; Lin and Kan, 1996; Selvaraj et al., 2006). However, the justified controversy regarding raft-like domains being induced by chemical fixation, and our observation that CTB-bound G_{M1} redistributed dramatically at cell death, called the localization of sterols in live sperm into question. Using PFO-D4, we showed in both live murine and human sperm that the APM was enriched in sterols. PFO-D4 was first introduced as a tool to study membrane sterols by Fujimoto et al., (Fujimoto et al., 1997; Ohno-Iwashita et al., 2004). Since then, several studies have utilized this toxin to detect cholesterol-rich membrane micro-domains (Hayashi et al., 2006; Koseki et al., 2007). However, one significant feature of this reagent's binding property is that it requires high (>20-25 mol%) local cholesterol content (Ohno-Iwashita et al., 1992). Therefore, in addition to segregation to a particular membrane area, this reagent also confers some information regarding the abundance of sterols in a local lipid microenvironment.

Several models have been put forth to explain how membrane domains might be segregated. One property easily demonstrated in synthetic model membranes is lipid-lipid interactions, which result in a range of domain sizes based on the lipid mixture used (Dietrich et al., 2001; de Almeida et al., 2005). The existence of thermodynamic phases has also been recently demonstrated in plasma membrane-derived vesicles (Baumgart et al., 2007). However, in

live cells, the nature of membrane phases is complicated by the interactions of lipids with a variety of proteins; these interactions are dynamic to maintain leaflet asymmetry and facilitate or inhibit signaling or trafficking. Some of these proteins can associate with different membrane lipids and exist as multiple lipid-protein composites (Jacobson et al., 2007). The lipid shell model suggests that specific membrane-associated proteins might induce membrane micro-domains to form due to their preferential binding to certain lipid species or pre-assembled lipid complexes (Anderson and Jacobson, 2002). Although this model allows for dynamic lipid exchange with other bilayer lipids, protein concentrations of the specific lipid-associating proteins could govern the scale and stability of this lateral organization. As a sterol-binding protein known to localize to this area (Travis et al., 2001b), caveolin-1 is a compelling candidate to function in the lipid shell model. However, when we examined sperm from caveolin-1 knockout mice, we found that sterol segregation to the APM remained unchanged (Selvaraj et al., 2006). In addition to providing foci for shells, some of the membrane-associated proteins are cytoskeletal elements themselves (e.g. spectrin) (Maksymiw et al., 1987), or are proteins anchored to cytoskeletal structures (e.g. cadherins) (Causeret et al., 2005). Therefore, the membrane-associated cytoskeleton has been implicated in organizing membrane domains by providing certain lipid and protein tethers within the membrane. By observing single molecule trajectories moving within the membrane, stable regions (200 to 300 nm) called “transient confinement zones” were identified in which a traveling molecule can be trapped for several seconds (Simson et al., 1995; Dietrich et al., 2002). This has been suggested to involve the membrane cytoskeleton, and possibly the existence of transmembrane proteins as a “picket fence” thereby restricting diffusion

(Sheets et al., 1997). Also relating to membrane-cytoskeletal interactions, studies have shown that the plasma membrane of some cells is fabricated as distinct compartments and the diffusion rate of lipids is determined by the size of the compartment and the frequency of jumps between compartments (Sako and Kusumi, 1994, 1995).

Given the dynamic time scale and relatively small size predicted for most rafts, our data might seem incongruous. Based on our FLIP data and the localization of sterols using PFO-D4 in live sperm, we found that the segregation to the APM was stable with no movement of these lipids to the PAPM throughout the lifetime of the cell. However, CTB-G_{M1} was mobile within the APM in live sperm, suggesting the existence of some sort of diffusion barrier. The physical component of the SAR (Selvaraj et al., 2006) lies at the line of demarcation segregating sterols and CTB-bound G_{M1} in the APM from the PAPM. Our SEM studies showed that CTB was enriched at the SAR after redistribution, suggesting that it might offer resistance to G_{M1} movement and either support or itself comprise a diffusion barrier. It is possible that the SAR only traps cross-linked G_{M1} molecules during redistribution, and does not provide a barrier against the diffusion of single molecules. In support of this possibility, photo-bleaching studies using an exogenous lipid probe (DiIC16), showed that there is no restriction of movement across the SAR (Wolf and Voglmayr, 1984; James et al., 2004). Therefore it is possible that the SAR does not act as a complete barrier to diffusion of all molecules but could be a more specialized barrier selective for only specific classes of endogenous lipids or for specific lipid-protein composites. Preliminary attempts to perturb this stable segregation by using cytoskeletal disruptors have not been successful (Selvaraj et al., 2006).

An operational model to explain this micron-scale segregation of enriched sterols in the APM might include a combination of factors: a fence at the region of the SAR, a diversity of lipid shell proteins, and existence of membrane compartments all acting synergistically to provide stability and to maintain this large domain. A working definition of membrane rafts does support the notion that nanometer-scale microdomains can be stabilized or clustered. Sperm appear to provide an extreme example in terms of domain size and duration of stability, although, as discussed below, the APM is clearly not uniform in composition.

Membrane interactions between plasma and acrosomal membranes at the time of cell death

Based on experiments in which surface G_{M1} was saturated, as well as backscatter SEM to detect CTB, we showed an increase in plasma membrane G_{M1} at the time of cell death suggesting movement from an internal membrane compartment. Saponin permeabilization experiments suggested that the acrosome was an intracellular pool of G_{M1}. This finding was confirmed by localization of G_{M1} to the acrosomal membrane both in spermatids and mature sperm. This localization might have functional significance because the acrosome has been postulated to be a calcium store, and G_{M1} has been shown to regulate calcium channels in a number of different cell systems (Carlson et al., 1994; Buckley et al., 1995). Our results suggest interactions between the APM and OAM at the time of cell death. These are consistent with early morphological observations of changes during sperm death (Hancock, 1952; Austin and Bishop, 1958; Bedford, 1963). These interactions do not lead to a complete exocytosis, but rather might represent a loss of regulation of point-

fusion events now believed to occur over time during capacitation (Kim and Gerton, 2003).

Although extensive crosslinking of surface G_{M1} in live sperm is not expected with CTB at the working concentration used for these experiments, it is possible that monomeric or dimeric association with G_{M1} keeps CTB molecules on the plasma membrane poised to bind more G_{M1} that might appear as a result of these interactions with the G_{M1}-enriched acrosome. Cross-linking might then occur during the process of G_{M1} redistribution, resulting in the absence of recovery of fluorescence we observed upon bleaching the PAPM in FRAP experiments.

Membrane properties of sperm

There are fundamental differences between the plasma membrane of sperm compared to that of most somatic cells: (a) sperm largely shut down protein and lipid synthesis when they leave the testis, yet they undergo dramatic plasma membrane modifications by external influences both during transit through the epididymis (Evans and Setchell, 1979) and capacitation in the female reproductive tract (Davis, 1981); (b) they have an abundance of ether-linked lipids (Evans et al., 1980) and very long chain fatty acids (Poulos et al., 1986); (c) they have desmosterol as a mature sterol in the membrane (Bleau and VandenHeuvel, 1974); (d) a large fraction of their lipid chains are poly-unsaturated (e.g. 22:6 and 22:5) (Selivonchick et al., 1980; Wolf et al., 1990).

Several studies have been performed using exogenous lipid probes [DiIC16 and 5-(N-octa-decanoyl) aminofluorescein (ODAF)] to measure lipid diffusion in the different membrane regions of sperm, and showed that the

diffusion coefficients vary for different regions (Wolf and Voglmayr, 1984; Wolf, 1995; Ladha et al., 1997; Wolfe et al., 1998). One of these studies showed that lateral diffusion of ODAF in membranes of bull sperm is abolished after cell death (Ladha et al., 1997). Mouse, boar, ram and guinea pig sperm did not have this property (Wolfe et al., 1998). DiIC16 has also been used to examine vesicles derived from sperm membranes and certain non-diffusing fractions in these membrane blebs have been reported (Wolf et al., 1988). However, all this work was done using ejaculated sperm, which are exposed to lipids and lipid-binding proteins in the seminal plasma. These can bind to sperm membranes and dramatically alter their properties (Greube et al., 2001; Kawano and Yoshida, 2007; Tannert et al., 2007). We have also observed that seminal plasma exposure can inhibit CTB binding to live murine and bovine sperm (Buttke et al., 2006). A more recent report on murine epididymal sperm has claimed that the APM in live cells is liquid ordered based on DiIC16 segregation to this domain (Sleight et al., 2005). However, this conflicts with our observations that this probe segregates to the APM only in dead cells. In live cells all the DiI probes (both saturated and unsaturated) showed a diffuse labeling pattern over the entire sperm and did not segregate to any specific region. These observations suggested that although there were clear segregations of endogenous lipids between distinct regions of sperm membranes, in live cells these membranes permitted incorporation of saturated and unsaturated probes in more or less a homogenous fashion. These data would be consistent with ordered or disordered domains existing on a nanometer scale below the resolution of light microscopy, but would be inconsistent with the large scale segregation of lipids we observed in live sperm.

Exogenous BODIPY-G_{M1} also showed diffuse labeling unlike the endogenous G_{M1} localized using CTB, or when localized indirectly using an antibody against G_{M1} (Selvaraj et al., 2006). Addition of CTB after labeling sperm using BODIPY G_{M1} did not show any change in BODIPY G_{M1} localization in live or dead cells (data not shown). These findings strongly suggested that exogenous G_{M1} did not behave like its endogenous counterpart. NBD-SM was also seen to incorporate diffusely throughout the sperm in live cells. However, upon cell death all the above lipid probes redistributed to the APM, suggesting a large-scale change in membrane property associated with cell death, a phenomenon similar to that seen with CTB-bound-G_{M1}, but opposite in direction of movement. This large-scale change in membrane property associated with cell death could be due to the regional loss of membrane asymmetry as suggested by PS exteriorization only in the PAPM in non-capacitated sperm. This endogenous property could be partially responsible for the behavior of either the lipid probes and/or CTB during cell death. Labeling using exogenous NBD-Chol was very weak in live and dead cells. However, the weak but preferential incorporation in the APM suggested that NBD-Chol behaved similarly to endogenous cholesterol in sperm. Our diffusion studies in live cells showed that CTB-bound G_{M1} was mobile in the APM and was stably segregated from the PAPM, similar to sterols. The properties of CTB-bound G_{M1} support our model that the SAR could be a potential fence restricting specific lipid and protein composites to the APM, whereas molecules not associated with these composites might be freely diffusing. This possibility underscores the importance of examining endogenous rather than exogenous lipids to evaluate membrane properties.

Membrane rafts and sperm

In contrast to many cells in which sterol efflux is induced as a tool to evaluate whether cellular events are mediated by rafts, sperm absolutely require sterol efflux as a stimulus for them to be able to fertilize an egg. In some somatic cells, physiologically-relevant crosslinking is required for activation (such as in the immunological synapse) (Holowka et al., 2005). However, sperm appear to have the opposite organization in that sterols and CTB-bound G_{M1} are stably segregated in quiescent sperm, and then sterol efflux is required for activation. In the oviduct, sterols are removed by albumin and high-density lipoproteins present in the oviductal fluid (Ehrenwald et al., 1990). Along with bicarbonate and calcium influx, these stimuli activate signaling pathways that result in a series of protein tyrosine phosphorylation events. Functionally, these stimuli allow acrosomal exocytosis to occur and induce a hyperactivated pattern of motility (Suarez and Ho, 2003). The existence of marked sterol segregation to the APM and the presence of signaling pathways that are regulated by the modulation of membrane sterol content provide compelling evidence for membrane rafts to have important functions in sperm, either in regulation of capacitation, and/or earlier in germ cell development for targeting proteins to the APM, which is that part of the sperm that first interacts physically with the egg.

Based on data presented here, we hypothesize that in non-capacitated cells, the APM is heavily enriched with sterols to prevent fusion of the APM with the underlying OAM. This could be either due to a biophysical membrane property precluding fusion, or an inhibition of required signaling events. Our model would allow for heterogeneities to exist within the APM, which would contain both raft micro-domains and non-raft regions. This is supported by our

observations using PFO-D4 in which labeling was not uniform, but rather had punctate spots of fluorescence within the APM. The apparent abundance of membrane raft-associated lipids such as sterols and G_{M1} throughout the APM is consistent with the notion that larger-scale enrichments of sterols might represent a stabilized platform of smaller raft micro-domains. Supporting this model is a study in goat sperm using fluorescence anisotropy of 1,6-diphenyl-1,3,5-hexatriene suggesting that there is an increase in membrane "fluidity" with the efflux of sterols before the onset of acrosomal exocytosis (Companyo et al., 2007). However, further studies need to be carried out observing the spatial and temporal kinetics of sterol efflux from the APM.

Acknowledgements

This work was supported by National Institutes of Health grant R01-HD-045664 (A.J.T). We also thank Colin Parrish, John Parker and Claudia Fischbach at the Baker Institute, Cornell University, for sharing laboratory resources used in this study, Darius Paduch and Peter Schlegel at the Weill-Cornell Medical College for help obtaining human sperm, Rodney Tweten, University of Oklahoma for help obtaining PFO, Markus Grebe for providing us with a plasmid containing domain 4 of PFO, Rebecca Williams at the Cornell Molecular Imaging Facility for technical advice during the photo-bleaching experiments, and Malcolm Thomas with the Keck Integrated Microscopy Facility (NSF-MRSEC program; DMR 0520404) at Cornell University for technical help with the FE-SEM imaging.

REFERENCES

Anderson, R.G., and Jacobson, K. (2002). A Role for Lipid Shells in Targeting Proteins to Caveolae, Rafts, and Other Lipid Domains. Science 296, 1821-1825.

Austin, C.R. (1952). The Capacitation of the Mammalian Sperm. Nature 170, 326.

Austin, C.R., and Bishop, M.W.H. (1958). Some Features of the Acrosome and Perforatorium in Mammalian Spermatozoa. Proc Roy Soc B 149, 234-242.

Baumgart, T., Hammond, A.T., Sengupta, P., Hess, S.T., Holowka, D.A., Baird, B.A., and Webb, W.W. (2007). Large-Scale Fluid/Fluid Phase Separation of Proteins and Lipids in Giant Plasma Membrane Vesicles. Proc Natl Acad Sci U S A 104, 3165-3170.

Bedford, J.M. (1963). Morphological Reaction of Spermatozoa in the Female Reproductive Tract of the Rabbit. J Reprod Fertil 6, 245-255.

Bellve, A.R., Cavicchia, J.C., Millette, C.F., O'Brien, D.A., Bhatnagar, Y.M., and Dym, M. (1977a). Spermatogenic Cells of the Prepuberal Mouse. Isolation and Morphological Characterization. J Cell Biol 74, 68-85.

Bellve, A.R., Millette, C.F., Bhatnagar, Y.M., and O'Brien, D.A. (1977b). Dissociation of the Mouse Testis and Characterization of Isolated Spermatogenic Cells. J Histochem Cytochem 25, 480-494.

Bleau, G., and VandenHeuvel, W.J. (1974). Desmosteryl Sulfate and Desmosterol in Hamster Epididymal Spermatozoa. Steroids 24, 549-556.

Buckley, N.E., Su, Y., Milstien, S., and Spiegel, S. (1995). The Role of Calcium Influx in Cellular Proliferation Induced by Interaction of Endogenous Ganglioside Gm1 with the B Subunit of Cholera Toxin. Biochim Biophys Acta 1256, 275-283.

Buttke, D.E., Nelson, J.L., Schlegel, P.N., Hunnicutt, G.R., and Travis, A.J. (2006). Visualization of Gm1 with Cholera Toxin B in Live Epididymal Versus Ejaculated Bull, Mouse, and Human Spermatozoa. Biol Reprod 74, 889-895.

Carlson, R.O., Masco, D., Brooker, G., and Spiegel, S. (1994). Endogenous Ganglioside Gm1 Modulates L-Type Calcium Channel Activity in N18 Neuroblastoma Cells. J Neurosci 14, 2272-2281.

Causeret, M., Taulet, N., Comunale, F., Favard, C., and Gauthier-Rouviere, C. (2005). N-Cadherin Association with Lipid Rafts Regulates Its

Dynamic Assembly at Cell-Cell Junctions in C2c12 Myoblasts. Mol Biol Cell 16, 2168-2180.

Chang, M.C. (1951). Fertilizing Capacity of Spermatozoa Deposited into the Fallopian Tubes. Nature 168, 697-698.

Companyo, M., Iborra, A., Villaverde, J., Martinez, P., and Morros, A. (2007). Membrane Fluidity Changes in Goat Sperm Induced by Cholesterol Depletion Using Beta-Cyclodextrin. Biochim Biophys Acta.

Davis, B.K. (1976). Inhibitory Effect of Synthetic Phospholipid Vesicles Containing Cholesterol on the Fertilizing Ability of Rabbit Spermatozoa. Proc Soc Exp Biol Med 152, 257-261.

Davis, B.K. (1981). Timing of Fertilization in Mammals: Sperm Cholesterol/Phospholipid Ratio as a Determinant of the Capacitation Interval. Proc Natl Acad Sci U S A 78, 7560-7564.

de Almeida, R.F., Loura, L.M., Fedorov, A., and Prieto, M. (2005). Lipid Rafts Have Different Sizes Depending on Membrane Composition: A Time-Resolved Fluorescence Resonance Energy Transfer Study. J Mol Biol 346, 1109-1120.

Dietrich, C., Bagatolli, L.A., Volovyk, Z.N., Thompson, N.L., Levi, M., Jacobson, K., and Gratton, E. (2001). Lipid Rafts Reconstituted in Model Membranes. Biophys J 80, 1417-1428.

Dietrich, C., Yang, B., Fujiwara, T., Kusumi, A., and Jacobson, K. (2002). Relationship of Lipid Rafts to Transient Confinement Zones Detected by Single Particle Tracking. Biophys J 82, 274-284.

Ehrenwald, E., Foote, R.H., and Parks, J.E. (1990). Bovine Oviductal Fluid Components and Their Potential Role in Sperm Cholesterol Efflux. Mol Reprod Dev 25, 195-204.

Evans, R.W., and Setchell, B.P. (1979). Lipid Changes in Boar Spermatozoa During Epididymal Maturation with Some Observations on the Flow and Composition of Boar Rete Testis Fluid. J Reprod Fertil 57, 189-196.

Evans, R.W., Weaver, D.E., and Clegg, E.D. (1980). Diacyl, Alkenyl, and Alkyl Ether Phospholipids in Ejaculated, in Utero-, and in Vitro-Incubated Porcine Spermatozoa. J Lipid Res 21, 223-228.

Friend, D.S. (1982). Plasma-Membrane Diversity in a Highly Polarized Cell. J Cell Biol 93, 243-249.

Fujimoto, T., Hayashi, M., Iwamoto, M., and Ohno-Iwashita, Y. (1997). Crosslinked Plasmalemmal Cholesterol Is Sequestered to Caveolae:

Analysis with a New Cytochemical Probe. J Histochem Cytochem 45, 1197-1205.

Gaus, K., Gratton, E., Kable, E.P., Jones, A.S., Gelissen, I., Kritharides, L., and Jessup, W. (2003). Visualizing Lipid Structure and Raft Domains in Living Cells with Two-Photon Microscopy. Proc Natl Acad Sci U S A 100, 15554-15559.

Greube, A., Muller, K., Topfer-Petersen, E., Herrmann, A., and Muller, P. (2001). Influence of the Bovine Seminal Plasma Protein Pdc-109 on the Physical State of Membranes. Biochemistry 40, 8326-8334.

Hancock, J.L. (1952). The Morphology of Bull Spermatozoa. J Exp Biol 29, 445-450.

Hayashi, M., Shimada, Y., Inomata, M., and Ohno-Iwashita, Y. (2006). Detection of Cholesterol-Rich Microdomains in the Inner Leaflet of the Plasma Membrane. Biochem Biophys Res Commun 351, 713-718.

Holowka, D., Gosse, J.A., Hammond, A.T., Han, X., Sengupta, P., Smith, N.L., Wagenknecht-Wiesner, A., Wu, M., Young, R.M., and Baird, B. (2005). Lipid Segregation and Ige Receptor Signaling: A Decade of Progress. Biochim Biophys Acta 1746, 252-259.

Jacobson, K., Mouritsen, O.G., and Anderson, R.G. (2007). Lipid Rafts: At a Crossroad between Cell Biology and Physics. Nat Cell Biol 9, 7-14.

James, P.S., Hennessy, C., Berge, T., and Jones, R. (2004). Compartmentalisation of the Sperm Plasma Membrane: A Frap, Flip and Spfi Analysis of Putative Diffusion Barriers on the Sperm Head. J Cell Sci 117, 6485-6495.

Kawano, N., and Yoshida, M. (2007). Semen-Coagulating Protein, Svs2, in Mouse Seminal Plasma Controls Sperm Fertility. Biol Reprod 76, 353-361.

Kim, K.S., and Gerton, G.L. (2003). Differential Release of Soluble and Matrix Components: Evidence for Intermediate States of Secretion During Spontaneous Acrosomal Exocytosis in Mouse Sperm. Dev Biol 264, 141-152.

Koseki, M., Hirano, K., Masuda, D., Ikegami, C., Tanaka, M., Ota, A., Sandoval, J.C., Nakagawa-Toyama, Y., Sato, S.B., Kobayashi, T., Shimada, Y., Ohno-Iwashita, Y., Matsuura, F., Shimomura, I., and Yamashita, S. (2007). Increased Lipid Rafts and Accelerated Lipopolysaccharide-Induced Tumor Necrosis Factor-Alpha Secretion in Abca1-Deficient Macrophages. J Lipid Res 48, 299-306.

Kusumi, A., and Suzuki, K. (2005). Toward Understanding the Dynamics of Membrane-Raft-Based Molecular Interactions. Biochim Biophys Acta 1746, 234-251.

Ladha, S., James, P.S., Clark, D.C., Howes, E.A., and Jones, R. (1997). Lateral Mobility of Plasma Membrane Lipids in Bull Spermatozoa: Heterogeneity between Surface Domains and Rigidification Following Cell Death. J Cell Sci 110 (Pt 9), 1041-1050.

Lin, Y., and Kan, F.W. (1996). Regionalization and Redistribution of Membrane Phospholipids and Cholesterol in Mouse Spermatozoa During in Vitro Capacitation. Biol Reprod 55, 1133-1146.

London, E. (2005). How Principles of Domain Formation in Model Membranes May Explain Ambiguities Concerning Lipid Raft Formation in Cells. Biochim Biophys Acta 1746, 203-220.

Maksymiw, R., Sui, S.F., Gaub, H., and Sackmann, E. (1987). Electrostatic Coupling of Spectrin Dimers to Phosphatidylserine Containing Lipid Lamellae. Biochemistry 26, 2983-2990.

Mayor, S., and Rao, M. (2004). Rafts: Scale-Dependent, Active Lipid Organization at the Cell Surface. Traffic 5, 231-240.

Munro, S. (2003). Lipid Rafts: Elusive or Illusive? Cell 115, 377-388.

Ohno-Iwashita, Y., Iwamoto, M., Ando, S., and Iwashita, S. (1992). Effect of Lipidic Factors on Membrane Cholesterol Topology--Mode of Binding of Theta-Toxin to Cholesterol in Liposomes. Biochim Biophys Acta 1109, 81-90.

Ohno-Iwashita, Y., Shimada, Y., Waheed, A.A., Hayashi, M., Inomata, M., Nakamura, M., Maruya, M., and Iwashita, S. (2004). Perfringolysin O, a Cholesterol-Binding Cytolysin, as a Probe for Lipid Rafts. Anaerobe 10, 125-134.

Pelletier, R.M., and Friend, D.S. (1983). Development of Membrane Differentiations in the Guinea Pig Spermatid During Spermiogenesis. Am J Anat 167, 119-141.

Pike, L.J. (2006). Rafts Defined: A Report on the Keystone Symposium on Lipid Rafts and Cell Function. J Lipid Res 47, 1597-1598.

Poulos, A., Sharp, P., Johnson, D., White, I., and Fellenberg, A. (1986). The Occurrence of Polyenoic Fatty Acids with Greater Than 22 Carbon Atoms in Mammalian Spermatozoa. Biochem J 240, 891-895.

Quinn, P., Kerin, J.F., and Warnes, G.M. (1985). Improved Pregnancy Rate in Human in Vitro Fertilization with the Use of a Medium Based on the Composition of Human Tubal Fluid. Fertil Steril 44, 493-498.

Sako, Y., and Kusumi, A. (1994). Compartmentalized Structure of the Plasma Membrane for Receptor Movements as Revealed by a Nanometer-Level Motion Analysis. J Cell Biol 125, 1251-1264.

Sako, Y., and Kusumi, A. (1995). Barriers for Lateral Diffusion of Transferrin Receptor in the Plasma Membrane as Characterized by Receptor Dragging by Laser Tweezers: Fence Versus Tether. J Cell Biol 129, 1559-1574.

Selivonchick, D.P., Schmid, P.C., Natarajan, V., and Schmid, H.H. (1980). Structure and Metabolism of Phospholipids in Bovine Epididymal Spermatozoa. Biochim Biophys Acta 618, 242-254.

Selvaraj, V., Asano, A., Buttke, D.E., McElwee, J.L., Nelson, J.L., Wolff, C.A., Merdiushev, T., Fornes, M.W., Cohen, A.W., Lisanti, M.P., Rothblat, G.H., Kopf, G.S., and Travis, A.J. (2006). Segregation of Micron-Scale Membrane Sub-Domains in Live Murine Sperm. J Cell Physiol 206, 636-646.

Selvaraj, V., Buttke, D.E., Asano, A., McElwee, J.L., Wolff, C.A., Nelson, J.L., Klaus, A.V., Hunnicutt, G.R., and Travis, A.J. (2007). Gm1 Dynamics as a Marker for Membrane Changes Associated with the Process of Capacitation in Murine and Bovine Spermatozoa. J Androl 28, 588-599.

Sharma, P., Varma, R., Sarasij, R.C., Ira, Gousset, K., Krishnamoorthy, G., Rao, M., and Mayor, S. (2004). Nanoscale Organization of Multiple Gpi-Anchored Proteins in Living Cell Membranes. Cell 116, 577-589.

Sheets, E.D., Lee, G.M., Simson, R., and Jacobson, K. (1997). Transient Confinement of a Glycosylphosphatidylinositol-Anchored Protein in the Plasma Membrane. Biochemistry 36, 12449-12458.

Simons, K., and Ikonen, E. (1997). Functional Rafts in Cell Membranes. Nature 387, 569-572.

Simson, R., Sheets, E.D., and Jacobson, K. (1995). Detection of Temporary Lateral Confinement of Membrane Proteins Using Single-Particle Tracking Analysis. Biophys J 69, 989-993.

Sleight, S.B., Miranda, P.V., Plaskett, N.W., Maier, B., Lysiak, J., Scrable, H., Herr, J.C., and Visconti, P.E. (2005). Isolation and Proteomic Analysis of Mouse Sperm Detergent-Resistant Membrane Fractions. Evidence for Dissociation of Lipid Rafts During Capacitation. Biol Reprod 73, 721-729.

Suarez, S.S., and Ho, H.C. (2003). Hyperactivated Motility in Sperm. Reprod Domest Anim 38, 119-124.

Suzuki, F. (1988). Changes in the Distribution of Intramembranous Particles and Filipin-Sterol Complexes During Epididymal Maturation of Golden Hamster Spermatozoa. J Ultrastruct Mol Struct Res 100, 39-54.

Tannert, A., Kurz, A., Erlemann, K.R., Muller, K., Herrmann, A., Schiller, J., Topfer-Petersen, E., Manjunath, P., and Muller, P. (2007). The Bovine Seminal Plasma Protein Pdc-109 Extracts Phosphorylcholine-Containing Lipids from the Outer Membrane Leaflet. Eur Biophys J 36, 461-475.

Tao, J., Critser, E.S., and Critser, J.K. (1993). Evaluation of Mouse Sperm Acrosomal Status and Viability by Flow Cytometry. Mol Reprod Dev 36, 183-194.

Travis, A.J., Jorgez, C.J., Merdiushev, T., Jones, B.H., Dess, D.M., Diaz-Cueto, L., Storey, B.T., Kopf, G.S., and Moss, S.B. (2001a). Functional Relationships between Capacitation-Dependent Cell Signaling and Compartmentalized Metabolic Pathways in Murine Spermatozoa. J Biol Chem 276, 7630-7636.

Travis, A.J., Merdiushev, T., Vargas, L.A., Jones, B.H., Purdon, M.A., Nipper, R.W., Galatioto, J., Moss, S.B., Hunnicutt, G.R., and Kopf, G.S. (2001b). Expression and Localization of Caveolin-1, and the Presence of Membrane Rafts, in Mouse and Guinea Pig Spermatozoa. Dev Biol 240, 599-610.

van Drogen, F., and Peter, M. (2004). Revealing Protein Dynamics by Photobleaching Techniques. Methods Mol Biol 284, 287-306.

Visconti, P.E., Galantino-Homer, H., Ning, X., Moore, G.D., Valenzuela, J.P., Jorgez, C.J., Alvarez, J.G., and Kopf, G.S. (1999). Cholesterol Efflux-Mediated Signal Transduction in Mammalian Sperm. Beta-Cyclodextrins Initiate Transmembrane Signaling Leading to an Increase in Protein Tyrosine Phosphorylation and Capacitation. J Biol Chem 274, 3235-3242.

Waheed, A.A., Shimada, Y., Heijnen, H.F., Nakamura, M., Inomata, M., Hayashi, M., Iwashita, S., Slot, J.W., and Ohno-Iwashita, Y. (2001). Selective Binding of Perfringolysin O Derivative to Cholesterol-Rich Membrane Microdomains (Rafts). Proc Natl Acad Sci U S A 98, 4926-4931.

Wolf, D.E. (1995). Lipid Domains in Sperm Plasma Membranes. Mol Membr Biol 12, 101-104.

Wolf, D.E., Lipscomb, A.C., and Maynard, V.M. (1988). Causes of Nondiffusing Lipid in the Plasma Membrane of Mammalian Spermatozoa. Biochemistry 27, 860-865.

Wolf, D.E., Maynard, V.M., McKinnon, C.A., and Melchior, D.L. (1990). Lipid Domains in the Ram Sperm Plasma Membrane Demonstrated by Differential Scanning Calorimetry. Proc Natl Acad Sci U S A 87, 6893-6896.

Wolf, D.E., and Voglmayr, J.K. (1984). Diffusion and Regionalization in Membranes of Maturing Ram Spermatozoa. J Cell Biol 98, 1678-1684.

Wolfe, C.A., James, P.S., Mackie, A.R., Ladha, S., and Jones, R. (1998). Regionalized Lipid Diffusion in the Plasma Membrane of Mammalian Spermatozoa. Biol Reprod 59, 1506-1514.

Yanagimachi, R. (1994). Mammalian Fertilization (New York: Raven Press, Ltd.).

CHAPTER 5

The role of FABP9 in sperm membrane organization

Vimal Selvaraj, Atsushi Asano, Jacquelyn L. Nelson, Robert S. Weiss and Alexander J. Travis. (In preparation). Mouse sperm lacking FABP9 (Perf15) are fertile and do not show defects in membrane organization or gross structure of the perforatorium.

Abstract

Fatty acid binding protein 9 (FABP9/Perf15) forms the major component of the sperm perforatorium and perinuclear theca. Based on its cytoskeletal association and the membrane binding properties of its closest relative (FABP8/myelin P2), it has been suggested that FABP9 functions to tether membrane components of sperm to the cytoskeletal matrix. Another functional role for FABP9 in the apoptotic regulation of male germ cell numbers has also been suggested. In this study, we investigated structural features of murine FABP9 in relation to its function. We characterized the developmental expression and biochemical properties of FABP9. We also explored FABP9 function by generating mice carrying a targeted mutation in the FABP9 alleles. We found that in these mice lacking FABP9 ($FABP9^{-/-}$) both sexes were fertile and males did not exhibit any of the predicted structural or functional defects in sperm. Moreover, spermatogenesis and sperm numbers in $FABP9^{-/-}$ mice were unaffected in comparison with $FABP9^{+/+}$ cohorts, suggesting that pathways regulating germ cell numbers by apoptosis were also not affected in $FABP9^{-/-}$ mice. We also cloned and sequenced the human homolog of FABP9. Comparing sequence homologies between mouse, rat and human FABP9, we notice evidence for potential functional divergence in the human homolog. We conclude that FABP9 is non-essential or that germ cells possess other protein(s) that could compensate for its loss.

Introduction

Mammalian sperm are highly polarized cells with specialized functions restricted to specific regions (Travis and Kopf, 2002). We have previously shown based on lipid composition that the plasma membrane overlying the acrosome exists as a sterol- and sphingolipid-enriched domain (APM) compared to the post-acrosomal plasma membrane (PAPM) (Selvaraj et al., 2006). The physiological significance of sterol segregation to the APM domain is suggested by the functional requirement for sterol efflux in order for sperm to become fertilization competent by a process called “capacitation” (Chang, 1951; Austin, 1952; Davis, 1976; Visconti et al., 1999). Our investigations of the mechanism behind the maintenance of this unique micron-scale membrane segregation pointed to membrane interactions with the underlying cytoskeletal elements (Selvaraj et al., 2006). On examination of the structural components of the mature sperm head, it has been shown that the perinuclear theca substructure (PT; a dense cytoskeletal network) closely apposes the different membranes of the sperm head (Fawcett, 1970; Lalli and Clermont, 1981; Oko and Clermont, 1988). It has been hypothesized that a component of the PT binds and tethers the different membranes of the sperm head (Fouquet et al., 1992; Oko and Maravei, 1994). The sub-acrosomal layer of the PT appears to anchor the acrosomal vesicle to the nuclear membrane; the post-acrosomal sheath of the PT is between the PAPM and the nuclear membrane; the outer peri-acrosomal layer of the PT links the APM to the outer acrosomal membrane (Oko et al., 1990; Oko and Maravei, 1994). An unusual cytoskeletal assembly of novel basic proteins called calcins has been identified to form the supporting structures of the PT (Longo et al., 1987; Olson and Winfrey, 1988; Paranko et al., 1988; Lecuyer et al., 2000). However, the major protein present

in the perforatorium and associated PT, initially named Perf15 (Oko and Clermont, 1988) was identified as the fatty acid binding protein 9 (FABP9) (Oko and Morales, 1994). The presence of FABP9 in the PT has so far been reported for rat, mouse and bull sperm (Oko and Maravei, 1994; Oko and Morales, 1994; Korley et al., 1997).

Fatty acid-binding proteins (FABPs) belong to the conserved multigene family of intracellular lipid-binding proteins (Chmurzynska, 2006). Nine different FABPs (Figure 5.1A) showing tissue-specific expressions have been characterized in several species: FABP1 (liver; L-FABP), FABP2 (intestine; I-FABP), FABP3 (heart; H-FABP), FABP4 (adipocyte; A-FABP), FABP5 (epidermal; E-FABP), FABP6 (ileum; IL-FABP), FABP7 (brain; B-FABP), FABP8 (peripheral nervous system; M-FABP/myelin P2) and FABP9 (testis/germ cell; T-FABP) (Zimmerman and Veerkamp, 2002). Human homologs for all the FABPs have been sequenced except for FABP9. The different FABPs have a 22-73% sequence similarity with highly conserved three-dimensional structures (Zimmerman and Veerkamp, 2002; Chmurzynska, 2006). Several functions have been demonstrated for FABPs, including the promotion of cellular uptake of fatty acids (Stremmel et al., 1985; Schurer et al., 1994; Trotter et al., 1996), intracellular fatty acid trafficking (Storch and Thumser, 2000; Falomir-Lockhart et al., 2006), fatty acid metabolism (Hotamisligil et al., 1996; Shaughnessy et al., 2000), signal transduction (Graber et al., 1994; Widstrom et al., 2001), cell growth (Burton et al., 1994), differentiation (Yang et al., 1994; Borchers et al., 1997; Aponte, 2002), and regulation of gene expression (Bernlohr et al., 1997; Wolfrum et al., 2001). Because of the significant sequence similarity of FABP9 to the membrane-associated FABP8 (myelin P2) observed on the cytoplasmic face

of the myelin sheath of peripheral neurons (Eylar et al., 1980; Trapp et al., 1984), it has been suggested that FABP9 in the PT could be the component involved in tethering the sperm membranes (Oko and Morales, 1994).

Another functional role for FABP9 in regulating programmed cell death in germ cells has been suggested (Kido and Namiki, 2000). In this study, FABP9 was shown to localize to germ cells undergoing apoptosis. Supporting this observation, transgenic mice overexpressing FABP9 showed an increase in multinucleate symplasts indicative of apoptosis in elongated spermatids, and a reduction in the number of sperm carrying the transgene (Kido et al., 2005). However, fertility remained unaffected in these mice. These studies indicate that FABP9 could be involved in several regulatory processes during germ cell development in addition to its putative function in mature sperm.

Therefore, we examined the functional phenotype resulting from the loss of FABP9 by the targeted disruption of the FABP9 gene in mice. We also sequenced the human homolog of FABP9.

Experimental Methods

Reagents and animals

All reagents were purchased from Sigma (St. Louis, MO), unless otherwise noted. Commercial antibodies used were against α–tubulin (Oncogene Calbiochem, San Diego, CA) and phosphorylated tyrosine (clone 4G10, Millipore, Lake Placid, NY). Fluorophore conjugated cholera toxin subunit B (CTB; Molecular Probes, Eugene, OR) was used to localize the glycosphingolipid G_{M1}. The EGFP-conjugated D4 domain of perfringolysin O used for sterol localization was synthesized as described in the previous chapter. Primers were from Integrated DNA Technologies (Coralville, IA).

Sytox® green (Invitrogen, Carlsbad, CA) was used for nuclear counterstaining of tissue sections. Lipid standards Polar lipid mix, Sphingolipid mix, GLC-10 and PUFA-1 (all from Matreya, LLC, Pleasant Gap, PA) were used for TLC. Pregnant mare serum gonadotropin (PMSG; Calbiochem) and human chorionic gonadotropin (hCG; Calbiochem) were used for superovulation. Mice of the following strains, C57BL/6, 129Sv and B6D2F1 were purchased from the Jackson laboratories (Bar Harbor, ME).

Protein modeling

Three dimensional homology models for FABP9 were constructed by means of comparative protein structure modeling by satisfying spatial restraints (Sali and Blundell, 1993; Fiser et al., 2000). Bovine FABP8 [PDB ID: 1pmp; (Cowan et al., 1993)] and equine FABP8 [PDB ID: 1yiv; (Hunter et al., 2005)] that had the highest sequence homologies (63.4% and 61.8% respectively) and whose crystal structures were known were used. Structural modeling was carried out using the automated alignment algorithms of Modeller 9v2 (http://www.salilab.org/modeller/) (Marti-Renom et al., 2000; Eswar et al., 2003) to derive a homology-based model. The output was visualized using the graphical interface of PyMOL v1.0 (DeLano Scientific, Palo Alto, CA).

FABP9 antibody

Polyclonal antisera against murine FABP9 were raised in two rabbits at Quality Controlled Biochemicals (Hopkinton, MA). The antigenic epitope [Ser_{40}-Cys_{58}] was conjugated with Keyhole Limpet Hemocyanin and emulsified in Freund's complete adjuvant before injections. Pre-immune serum was

collected before antigenic challenges. After initial immunization, boosters were administered at days 14, 28 and 42. Serum was separated from bleeds on days 52 and 56 and was tested for the required experimental applications.

Human FABP9

A human testis large-insert cDNA library (BD biosciences, Palo Alto, CA) was used to clone and sequence the human FABP9 (hFABP9). Based on results from the NCBI-Gnomon gene prediction method, Primers (5'ATGGT TGAGCCCTTCTTGGGAAC and 5'TCACACCTTTTCGTAGATTCTGGTG) were designed to amplify the putative hFABP9. The resulting product was then cloned and sequenced.

Testicular expression of FABP9

Both developmental and spermatogenic stage specific evaluations were carried out for FABP9 expression. For examining developmental expression of FABP9 in the postnatal testis, samples were collected every two days starting from postnatal day-2 to postnatal day-36 and stored in liquid nitrogen after snap freezing. At the end of sample collection, testis lysates were prepared for the different ages. 150 μg of proteins from each lysate was separated by SDS-PAGE, transferred to PVDF membrane and immunoblotted for the presence of FABP9. For examining spermatogenic stage-specific expression of FABP9, murine testes were first decapsulated and incubated in PBS supplemented with 0.75 mg/ml collagenase in a shaking water bath at 33˚C for 30 minutes. The resultant preparation of seminiferous tubules was then washed to remove collagenase and interstitial cells. The separated tubules were visualized and regions containing different stages of seminiferous development (stages I-III, IV-VI, VII-IX and X-XII) were dissected and collected. Lysates were made by

homogenization and 75 μg of proteins from these lysates were separated by SDS-PAGE, transferred to PVDF membrane and immunoblotted for the presence of FABP9.

Sperm biochemical fractionation

Association of FABP9 with sperm membranes was tested. Membranes from sperm were collected with or without the use of detergents by methods previously described (Travis et al., 2001b) with minor modifications as described below. Sperm (10×10^6 cells) were subjected to 20 bursts of sonication for 10 seconds each at output 6 using a Branson Sonifier 450 (Branson Ultrasonics Corporation, Danbury, CT) in the presence of 5x protease inhibitors (Complete protease inhibitor cocktail, Roche Applied Science, Indianapolis, IN). Care was taken to avoid frothing and to keep the sample cool. The cell lysate was then centrifuged at 10,000 ×g for 10 minutes and the supernatant containing soluble proteins and membrane vesicles was carefully collected; the remaining coarse pellet of cellular debris formed the P10 fraction. The supernatant was again centrifuged at 100, 000 ×g for 1 hour. The supernatant (S100 fraction) was carefully separated and the resulting pellet (P100 fraction) contained the disrupted sperm membrane vesicles. Soluble proteins in the S100 fraction were precipitated using 4% trichloro-acetic acid (v/v) followed by neutralization with Tris-buffer. Proteins from the different fractions were separated by SDS-PAGE, transferred to a PVDF membrane and immunoblotted for the presence of FABP9.

Histology and indirect immunofluorescence

Testes fixed in Bouin's solution were processed, embedded in paraffin and sectioned at 4 μm slices. For routine histological examination, sections were stained with hematoxylin and eosin.

For localization of FABP9 in testis sections, slides were de-paraffinized, hydrated and then subjected to antigen retrieval by immersing in 0.01 M citrate buffer and microwaving for 20 min. Nonspecific binding of antibodies was blocked using 5% normal goat serum (NGS), and then samples were incubated with anti-FABP9 antibody (1:100) in 5% NGS in a humidity chamber overnight. After incubation, slides were washed in PBS and incubated with a fluorescent secondary antibody (1:500) in 5% NGS for 1 hour. Fluorescent nuclear counterstaining was carried out using Sytox® Green (1 μM final concentration; Invitrogen) for 10 minutes. Slides were then washed in PBS and mounted using a GVA-based mountant (Invitrogen).

For localization of FABP9 in epididymal sperm, cells were allowed to attach to coverslips and fixed/permeabilized using either 1:1 acetone:methanol mixture for 60 seconds at -20˚C, or 4% formaldehyde (30 minutes) and 0.1% TX-100 (2 minutes). Coverslips were then air-dried, rehydrated in PBS and blocked for 30 minutes with 5% normal goat serum in PBS. Samples were then incubated with anti-FABP9 antibody (1:100 dilution) in 5% NGS for 6 hours at room temperature. They were then washed with PBS and incubated with a fluorescent secondary antibody (1:500 dilution) for 1 hour. Coverslips were then rinsed and mounted on slides with a GVA-based mountant.

FABP9 targeting construct

Murine bacterial artificial chromosome clone bMQ75a12 (Genome Research Ltd., Wellcome Trust Sanger Institute, Cambridge, UK) containing the 129S7 strain genomic locus of FABP9 was transformed into a recombineering competent strain of bacteria [EL350; (Liu et al., 2003)]. A 15 Kb genomic sequence (~6 Kb upstream and downstream of the FABP9 locus) including the FABP9 locus was retrieved into plasmid PL253. PL253 carried a mc1-driven thymidine kinase cassette for negative selection of ES cells. Plasmid PL452 with a neo cassette flanked by loxP sites (loxP-Pgk-em7-Neo-loxP) was used to recombineer and replace exons 1 and 2 of the FABP9 gene in PL253. Bacteria EL350 and plasmids PL253 and PL452 were generous gifts from Neal Copeland, National Cancer Institute, Bethesda, MD.

Targeting, selection and microinjection of ES cells

TC-1 embryonic stem cells (Deng et al., 1996) were electroporated with SalI-linearized construct and selected in media containing G418 and FIAU as described previously (Weiss et al., 2000). Genomic DNA from 85 drug-resistant colonies was screened for homologous recombination at the FABP9 locus by southern blot hybridization after restriction digestion (BamHI) with an external probe (Primers: 5' CCAGGTCTCAACATTGAGGC 3'; 5' CATGTC TAGCTCCAAATCCC 3'), and one correctly targeted clone was identified. This correct targeting of the heterozygous clone was confirmed by performing additional southern blots using an alternative restriction enzyme digest (PsyI), as well as an internal neo probe. ES cells from this targeted clone were microinjected into C57BL/6 blastocysts and transferred into pseudopregnant C57BL/6 recipients. Three chimeric male mice were identified by their

characteristic agouti coat color. They were mated to C57BL/6 females and the germline trasmission of the targeted FABP9 allele was determined by coat color of the pups and southern blot analyses. Crossing heterozygous pairs generated mice homozygous for the targeted FABP9 allele for phenotypic analysis.

Genotyping PCR

Primers were designed flanking the recombination site to detect deletion of exons 1 and 2 of the FABP9 gene [F9: 5'AGGTGGGAAA GCCTCTGATT; F9 WT: 5' AGGCATTCACAACCGAAAAC; F-9 KO: 5' GCCAGAGGCCACTTGTGTAG]. Expected PCR products were 370 bp for the wild-type (WT) genomic FABP9 locus and 252 bp for the targeted FABP9 allele (knockout; KO). Heterozygous mice would show both bands.

Phenotypic analysis

For making functional and morphological comparisons between $FABP9^{-/-}$ and WT mice, 12-week-old mice were used. Parameters including body weight, testis weights and seminal vesicle weights were measured. Cauda epididymal sperm counts were estimated using a hemocytometer. Breeding trials were conducted to quantify litter sizes from $FABP9^{-/-} \times FABP9^{-/-}$ vs WT × WT matings. Sperm abnormalities were estimated and scored as (a) apparently normal, when sperm morphology appeared unaffected under 400x magnification under a dark-field, (b) bent tail, when the flagellum was bent in a hair-pin fashion in the mid-piece or at the annulus, (c) cytoplasmic droplet, when the sperm carried the residual cytoplasm as a proximal or distal droplet in the mid-piece, and (d) abnormal/coiled head, when

there was an obvious defect in sperm head morphology sometimes associated with a bent head and coiled mid-piece around the sperm head. A Kruskal-Wallis rank sum comparison was performed between percentages of abnormalities comparing FABP9$^{-/-}$ and WT sperm.

Assessment of membrane organization

This was performed by assessment of the localization of sterols and the glycosphingolipid G_{M1} in live cells. For visualizing membrane sterols in live sperm, cells were incubated with PFO-D4 (4 μg/ml) in MW medium for 20 minutes at 37˚C. Similarly, for visualizing G_{M1}, cells were incubated with CTB (conjugated with Alexa Fluor 488; 5 μg/ml) for 10 minutes. A stage-mounted incubation chamber (LiveCell, Neue Product Group, Westminister, MD) was used along with an objective heater (Bioptechs, Butler, PA) to maintain sperm at 37˚C during imaging. Visualization was performed using a Nikon Eclipse TE 2000-U microscope (Nikon, Melville, NY) equipped with a Photometrics Coolsnap HQ CCD camera (Roper Scientific, Ottobrunn, Germany). Images were captured using Openlab 3.1 software (Improvision, Lexington, MA).

Capacitation-associated protein tyrosine phosphorylation

A modified Whitten's medium [MW; 22 mM HEPES, 1.2 mM $MgCl_2$, 100 mM NaCl, 4.7 mM KCl, 1 mM pyruvic acid, 4.8 mM lactic acid hemi-calcium salt, 5.5 mM D-glucose, pH 7.35; (Travis et al., 2001a)] was used for all incubations. Incubation with different stimuli for capacitation was carried out with $2x10^6$ sperm in 300 μl of medium with 5.5 mM glucose under one of four conditions: (a) MW base medium, (b) MW supplemented with 10 mM $NaHCO_3$, (c) MW supplemented with 3 mM 2-hydroxypropyl-β-cyclodextrin (2-OHCD)

and (d) MW with both 10 mM $NaHCO_3$ and 3 mM 2-OHCD, for 60 minutes. The pH of medium for all incubation conditions was adjusted to 7.35. The medium in incubation condition "(d)," has been shown to be sufficient to support IVF (Travis et al., 2004) and capacitation-induced tyrosine phosphorylation (Travis et al., 2001a) in murine sperm. After incubation, samples were processed for SDS-PAGE, transferred to a PVDF membrane and immunoblotted for phospho-tyrosine residues.

Scanning electron microscopy

Sperm collected as described above in MW medium were allowed to attach to silicon chips and fixed using using 4% formaldehyde and 0.1% glutaraldehyde in 2.5 mM $CaCl_2$ in PBS (Selvaraj et al., 2006) for 30 minutes. Samples were rinsed 5 times in distilled water for 5 minutes each and then freeze dried. The silicon surface with cells was then sputter coated with gold-palladium. Images were collected using a Zeiss LEO 1550 field emission SEM with a Gemini column (Carl Zeiss Inc., Oberkochen, Germany).

In vitro fertilization

TYH medium [118.8 mM NaCl, 4.78 mM KCl, 1.19 mM KH_2PO_4, 1.19 mM $MgSO_4.7H_2O$, 25 mM $NaHCO_3$, 1.71 mM $CaCl_2.2H_2O$, 5.56 mM D-glucose, 1.01 mM Na-pyruvate, 29.2 mM Na-lactate, 4 mg/ml BSA, 0.05 mg/ml Streptomycin sulfate, 100 IU/ml Penicillin-G potassium, BSA; pH 7.4; (Toyoda et al., 1971)] pre-equilibrated in 5% CO_2 at 37˚C for 12 hours (pH 7.4) was used for the *in vitro* fertilization trials. Nineteen-day-old B6D2F1 female mice were super-ovulated by intra-peritoneal injections of PMSG (5 IU) followed after 48 hours by hCG (5 IU) (Runner and Gates, 1954). The females were

euthanized 13 hours after hCG injection and oocytes were collected from the oviduct into TYH medium as a droplet under mineral oil (Sydney IVF culture oil, Cook Medical, Bloomington, IN) in a Petri dish. One hour before euthanasia of female mice, sperm from the cauda epididymis were collected from the required males by a swim-out procedure as described previously (Travis et al., 2001a) in TYH medium. Sperm were allowed to capacitate at 37˚C in a 5% CO_2 incubator until oocyte collection. Sperm concentration for each sample was then estimated and a final concentration of 1 million sperm/ml was added to the fertilization droplet (final volume 100 μl). The Petri dish was then incubated in a chamber with an atmosphere of 5% O_2, 5% CO_2 and 95% N_2 at 37˚C. After 5 hours of incubation, eggs were rinsed briefly in fresh TYH medium and transferred to KSOM medium [95 mM NaCl, 2.5 mM KCl, 0.35 mM KH_2PO_4, 0.2 mM $MgSO_4$, 1.71 mM $CaCl_2$, 25 mM $NaHCO_3$, 10 mM Na-lactate, 0.2 mM D-glucose, 0.2 mM Na-pyruvate, 1 mM glutamine, 0.01 mM EDTA, 1 mg/ml BSA, 1 ml MEM essential amino acids, 0.5 ml MEM non-essential amino acids, 0.05 mg/ml Streptomycin sulfate, 100 IU/ml Penicillin-G potassium, BSA; pH 7.4; (Erbach et al., 1994)] for embryo development. Embryo development to a 4-cell stage was considered as the endpoint for successful fertilization.

Total lipid extraction and thin layer chromatography

Total lipids were extracted from sperm using the Folch method (Folch et al., 1957). Sperm collected from 3 mice in MW medium were immobilized by adding 10 μM sodium orthovanadate (Gibbons et al., 1978). They were then spun down at 400 ×g for 8 minutes in a swinging bucket-type centrifuge. After centrifugation, the medium was aspirated leaving only the sperm pellet. The

pellet was resuspended in 1 ml of water and transferred to a conical-bottom glass centrifuge tube. Methanol (6.5 ml) and chloroform (13 ml) were added to the sperm suspension and agitated for 30 minutes. The extraction mixture was then subjected to sonication at output 10 for 60 seconds followed by agitation for another 30 minutes. After agitation, samples were centrifuged at 2000 ×g for 8 minutes to pellet the coarse precipitates. The clear supernatant was transferred to another tube and 4.2 ml of water was added to separate the chloroform-methanol phases. Complete phase separation was achieved by centrifugation again at 2000 ×g for 8 minutes. The lower chloroform phase was collected and dried out in a N_2 gas stream (Organomation associates Inc., Berlin, MA).

For thin layer chromoatography, lipid extracts were reconstituted in 60:25:4 (chloroform:methanol:water) and spotted on a silica gel 60 plate (Merck, Damstadt, Germany) along with lipid standards and developed with the 60:25:4 solvent system (Wedgwood et al., 1974). Fluorescent bands were imaged after spraying with a primuline solution [0.005% (w/v) primuline in 80% (v/v) acetone; (Wright, 1971)] and excitation using UV-wavelength transillumination.

Results

Structural features of FABP9

Members of the FABP family share significant sequence homologies (Figure 5.1A). Comparing nucleotide substitutions, murine FABP9 is closely related to FABP8/Myelin P2. Primers designed for the predicted human FABP9 gave a product at the expected length (~400 bp). On sequencing, this product yielded a sequence homologous to known sequences of mouse and rat FABP9. The sequence mapped to a locus in human chromosome 8. On comparing amino acid sequence, human FABP9 showed 71% homology to mouse and 66% homology to rat FABP9 (Figure 5.1B). The two cysteine residues (Cys_{28} and Cys_{35}) in helix-2 in mouse and rat FABP9 were not conserved in the human FABP9 sequence suggesting that the human FABP9 could not be anchored via disulfide bonds.

Based on its homology model, FABP9 shares the conserved features of all other FABPs. It has two α-helices capping an anti-parallel β-sheet forming a barrel (Figure 5.1C). The lipid-binding site is formed by the hydrophobic concavity within the β-barrel. The N-terminal tail formed by a conserved Phe_5 residue forms a characteristic lid for the hydrophobic core. One unique feature of murine FABP9 compared to other FABPs was the presence of two cysteine residues in helix-2 (Figure 5.1C-inset).

Immunoblots of various murine tissues confirmed a testis specific expression of FABP9 (Figure 5.1D).

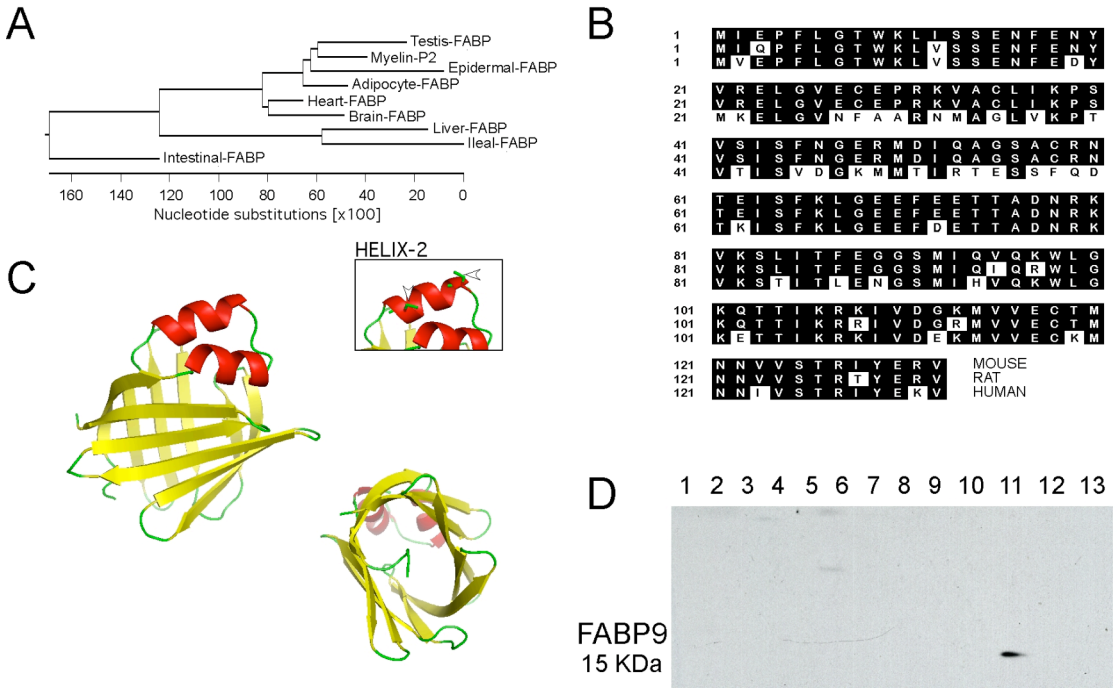

Figure 5.1. Structure, sequence conservation and tissue specific expression of FABP9. (A) A dendrogram showing relative nucleotide substitutions between the different murine FABP genes. Myelin P2 (FABP8) is the closest relative to FABP9, both diverging from Epidermal-FABP (FABP5) (B) Sequence alignments for mouse, rat and human FABP9 proteins showing conserved amino acids (shaded black). (C) Three dimensional structure for murine FABP9 constructed based on homology to bovine FABP8 satisfying spatial restraints. The structure is comprised of two α-helices and one β-barrel (I). The beta barrel forms a hydrophobic pocket for accepting/binding lipids. Note the two cysteine residues in one of the α-helices that might play a role in disulfide bonding of FABP9 protein to structural elements (Arrowheads in inset). (D) Multiple tissue immunoblot showing specific expression of FABP9 in the testis. Lanes: 1. Brain, 2. Heart, 3. Lung, 4. Liver, 5. Kidney, 6. Spleen, 7. Intestine, 8. Muscle, 9. Ovary, 10. Uterus, 11. Testis, 12. Skin, 13. Fat.

Developmental expression and biochemical characterization

Quantitative expression of FABP9 was analyzed using immuno-blots from different stages of testicular development. On dissected seminiferous tubules, FABP9 expression was more abundant in stages containing germ cells in advanced stages of spermiogenesis (Figure 5.2A). During post-natal testicular development, FABP9 expression started from day-16 consistent with the appearance of late pachytene spermatocytes (Figure 5.2B) (Bellve et al., 1977).

Biochemical fractionation of FABP9 showed that unlike other FABPs, FABP9 was not soluble but was strongly associated with structural elements in mature sperm (Figure 5.2C). This association was not disrupted by vigorous sonication, but a small amount of FABP9 could be solubilized using TX-100. The same experiment was also performed using isolated germ cells with similar results (data not shown) suggesting that FABP9 predominantly exists in association with cytoskeletal structures, consistent with its localization to the perinuclear theca and the perforatorium.

Supporting results from the immuno-blots, FABP9 localization was seen in advanced stages of germ cell development. Protein expression appeared to be particularly triggered in elongating spermatids and mature testicular sperm (Figure 5.3A). FABP9 localization appeared cytoplasmic in elongating spermatids and was confined to the perforatorium and the principal piece in testicular sperm. FABP9 was also expressed abundantly in certain spermatocytes (arrowheads: Figure 5.3A). In cauda epididymal sperm, FABP9 localization was similar to testicular sperm. The perforatorium was more intensely labeled than the post-acrosomal region of the perinuclear theca (Figure 5.3B). This was seen only after acetone:methanol fixation and

permeabilization suggesting its deep-seated association with these structures. There was also labeling in the principal piece of the flagellum that was evident with formaldehyde fixation and TX-100 permeabilization (Figure 5.3C).

Generation and phenotypic analysis of FABP9$^{-/-}$ mice

To explore the functional role of FABP9 in sperm membrane organization, we generated mutant mice that do not produce FABP9 by homologous recombination in embryonic stem cells. The targeting construct was designed to replace ~2.7 kb at the FABP9 locus including exons 1 and 2 and part of the promoter region (Figure 5.4A). In addition to preventing transcription of this locus, this would disrupt the synthesis of the entire FABP9 protein (132 amino acids). The genotypes of WT (FABP9$^{+/+}$) and heterozygous (FABP9$^{+/-}$) embryonic stem cell clones were screened by Southern blot analysis of genomic DNA (Figure 5.4B). Genomic DNA from mice generated from transmitting chimeras was also screened using Southern blot analysis and genotyping PCR (Figure 5.4C). Mating between heterozygous F1 siblings was set up to derive homozygous mice (FABP9$^{-/-}$). RT-PCR analysis indicated the absence of FABP9 mRNA in the FABP9$^{-/-}$ testis (Figure 5.4D). In addition, protein extracts of FABP9$^{-/-}$ testis completely lacked the 15-kDa protein corresponding to FABP9 (Figure 5.4E).

Mating of FABP9$^{+/-}$ male and female mice yielded the expected Mendelian frequency of FABP9$^{-/-}$ mice [FABP9$^{-/-}$: FABP9$^{+/-}$: FABP9$^{-/-}$ = 27 (22.0%): 61 (49.6%): 35 (28.5%) for 123 offsprings from 16 litters]. Both male and female FABP$^{-/-}$ mice appeared normal in behavior and body condition. Body weights and testis weights of FABP9$^{-/-}$ mice were not significantly different from age-matched WT cohorts (Figure 5.5 A and B). Morphological

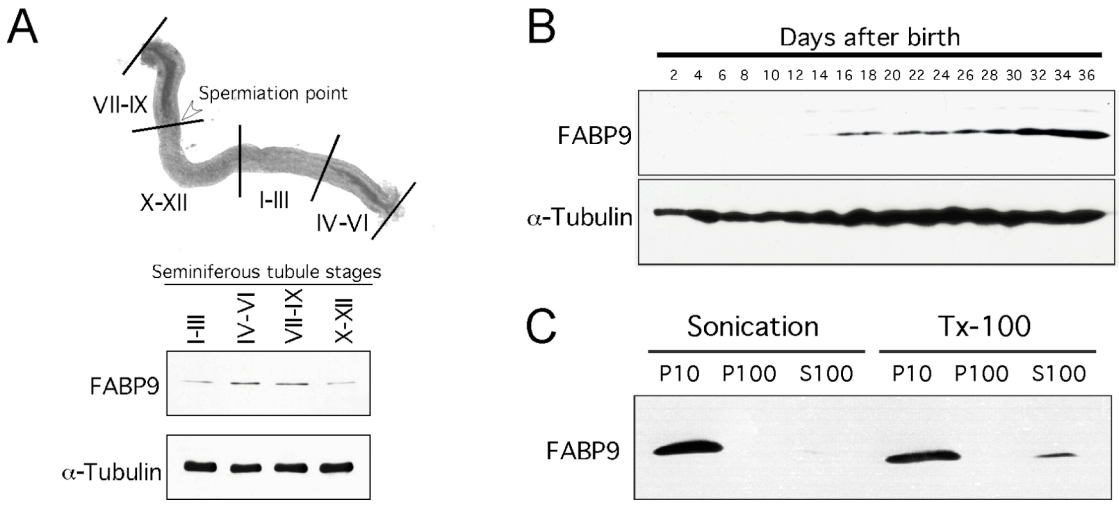

Figure 5.2. Characterization of FABP9. (A) Expression of FABP9 in different stages of germ cells in the seminiferous tubules. Highest expression was seen in tubular stages IV-VI and VII-IX which both contain germ cells in advanced stages of spermiogenesis. (B) FABP9 expression during post-natal testicular development. Immunoblot of testicular proteins collected every 2 days from mice aged day-2 to day-36 shows FABP9 protein expression starting at day-16 consistent with the appearance of pachytene spermatocytes. (C) FABP9 association with different sperm biochemical fractions separated by either physical shear (sonication) or detergent (TX-100). With sonication, FABP9 was found only in the P10 fraction that represents insoluble cytoskeletal structures. With TX-100, FABP9 was also seen predominantly in the P10 fraction with a small percentage completely solubilized and was found in the S100 fraction. FABP9 did not associate with the P100/membrane fraction.

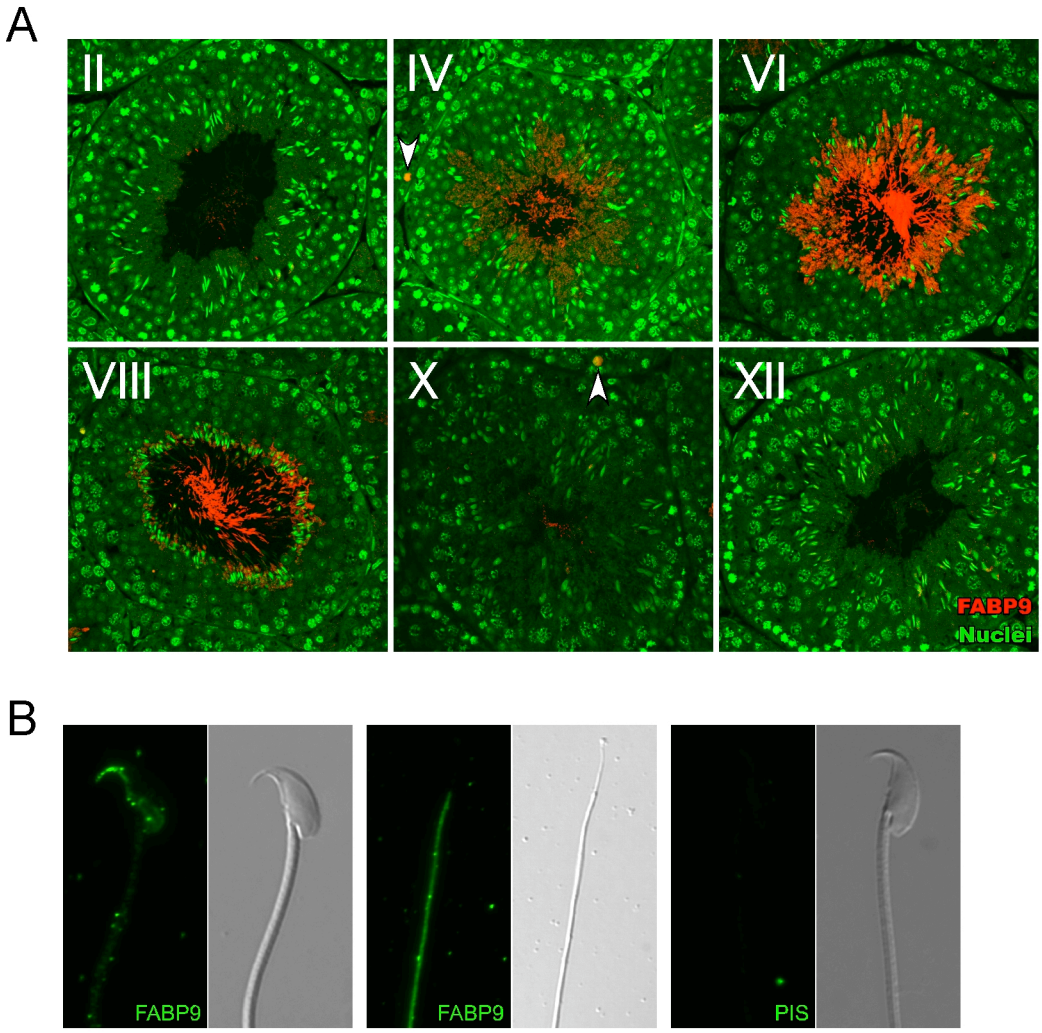

Figure 5.3. Localization of FABP9 in developing male germ cells and sperm. (A) FABP9 localization in testes sections (Green: Nuclei; Red: FABP9). Seminiferous tubule cross sections show FABP9 protein expression significantly turned on in stages IV, VII and VIII of development. FABP9 was localized to regions abundant in late elongating spermatids. In the different stages, FABP9 localization was cytoplasmic in spermatids. Localization was also seen in the principal piece of the flagellum; this is clearly seen in testicular sperm right before spermiation (stage VIII). (B) FABP9 localization in mature sperm. In the permeabilized sperm head, FABP9 was localized to the perforatorium and weakly to the post-acrosomal peri-nuclear theca (Panel 1). FABP9 was also localized to the principal piece of the sperm tail (Panel 2). Control pre-immune serum (PIS) image is also shown (Panel 3).

Figure 5.4. Targeted disruption of the murine FABP9 gene. (A) Schematic showing the FABP9 locus, the targeting construct and homologous recombination. FABP9 gene consists of 4 exons (indicated 1-4). The targeting construct was designed with upstream and downstream regions of homology on either side of a neomycin resistance cassette (neo^r) replacing exons 1 and 2. In this construct, the neo^r served for positive selection and a thymidine kinase cassette (TK) for negative selection. The correctly targeted FABP9 allele shows integration of the neo^r cassette in the genomic locus. The sequence upstream of the recombination site used for screening correctly targeted clones is indicated (Probe). (B) Screening for the targeted FABP9 locus using southern blots. Genomic fragments generated by digestion using BamHI and PsyI were probed for a shift in size of the targeted fragment. The correctly targeted clone was subsequently verified using a neo probe for a single and specific recombination event. (C) Gel showing genotyping PCR for verifying the targeted FABP9 locus. WT allele produces a 370 bp band and the KO allele produces a 252 bp band. (D) Gel showing RT-PCR products for FABP9 mRNA expression in WT, HET and KO testis. FABP9 mRNA was not expressed in KO mice. A germ cell specific glyceraldehyde 3-phosphate dehydrogenase (GAPDHs) was used as a reaction control. (E) FABP9 immunoblot showing expression in WT, HET and KO testis. There was no FABP9 expressed in KO mice. HET mice where one allele of the FABP9 gene was disrupted produced a comparable level of expression to WT mice.

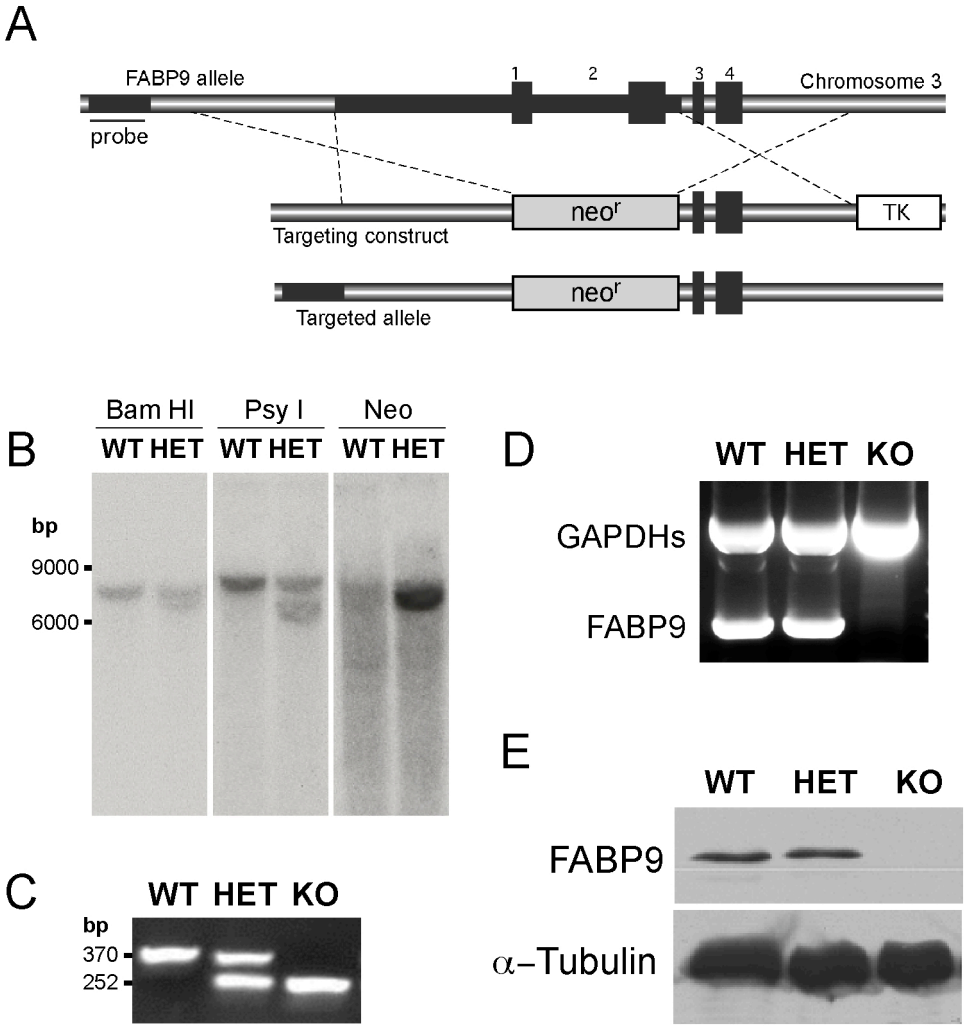
A
FABP9 allele
1
2
3
4
Chromosome 3
probe
neo^r
TK
Targeting construct
neo^r
Targeted allele
B
Bam HI
Psy I
Neo
WT HET WT HET WT HET
bp
9000
6000
C
WT HET KO
bp
370
252
D
WT HET KO
GAPDHs
FABP9
E
WT HET KO
FABP9
α–Tubulin

Figure 5.5. Phenotypic analysis of FABP9$^{-/-}$ mice. Box plots show the spread of values for the different parameters analyzed. The lower and upper ends of the box mark the 25th and 75th quantiles; the median is represented as a horizontal line within the box, and the mean as a horizontal line through the box. Vertical whiskers extend from the ends of the box to the 10th and 90th quantiles. Comparisons for: (A) Body weight, (B) Testis weight, (C) Sperm counts, (D) Litter sizes, and (E) Seminal vesicle weights are shown (n=9 to 11). 12-week-old FABP9$^{-/-}$ and WT mice used for sperm counts and other morphometric parameters; litter sizes were obtained from breeding trials.

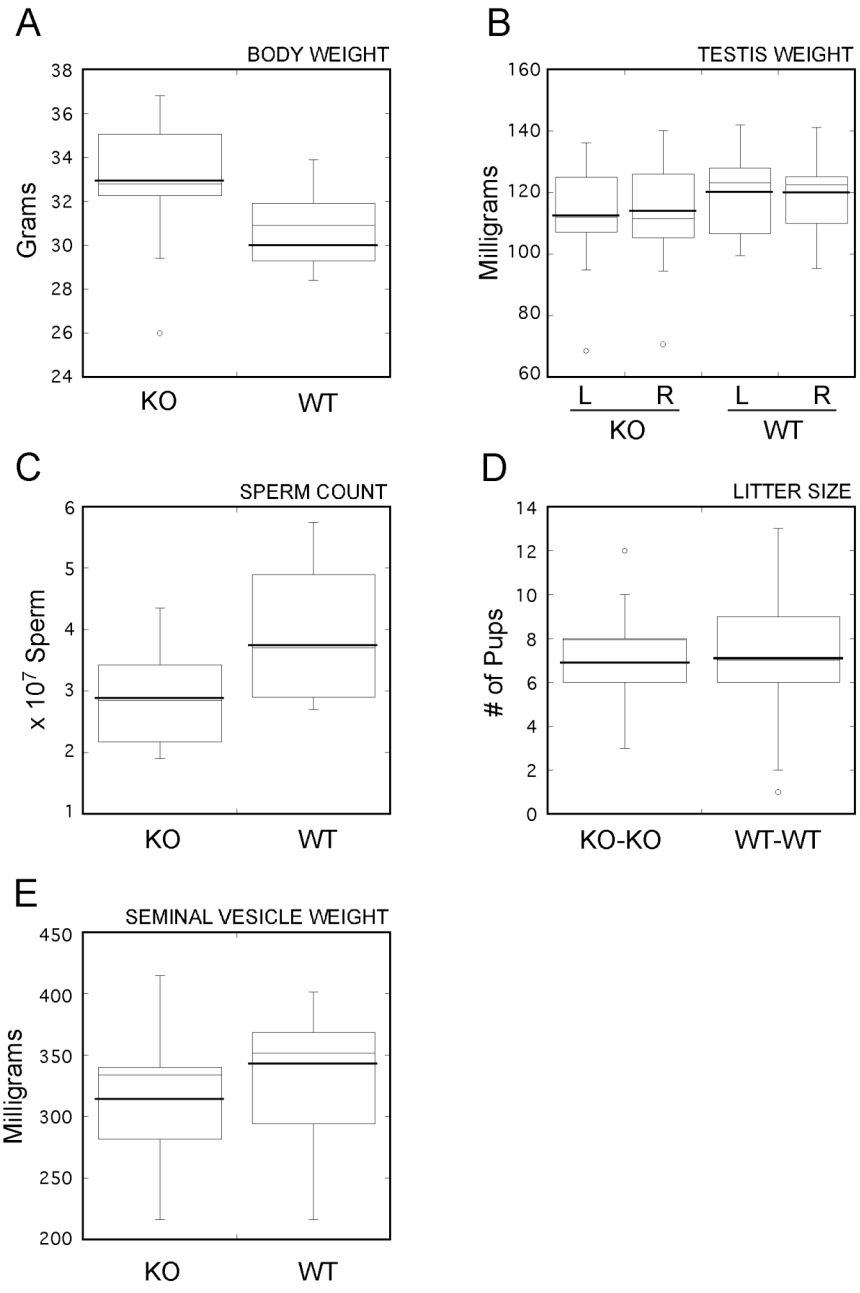
A
BODY WEIGHT
Grams
38
36
34
32
30
28
26
24
KO
WT
B
TESTIS WEIGHT
Milligrams
160
140
120
100
80
60
L
R
L
R
KO
WT
C
SPERM COUNT
x 10^7 Sperm
6
5
4
3
2
1
KO
WT
D
LITTER SIZE
# of Pups
14
12
10
8
6
4
2
0
KO-KO
WT-WT
E
SEMINAL VESICLE WEIGHT
Milligrams
450
400
350
300
250
200
KO
WT

analysis of testis sections did not reveal any differences or pathologies in the FABP9$^{-/-}$ mice (data not shown). Sperm production was not significantly different between FABP9$^{-/-}$ and WT mice (Figure 5.5C). Both male and female FABP9$^{-/-}$ mice were fertile and produced average litter sizes (mean: 7.2 ± 0.3 pups/litter) compared to WT mice (mean: 6.9 ± 0.4 pups/litter; Figure 5.5D). Seminal vesicle weights were not different between FABP9$^{-/-}$ and WT mice (Figure 5.5E).

There were no statistically significant increases in the incidence of structural abnormalities in non-parametric comparisons between FABP9$^{-/-}$ and WT sperm percentages (Figure 5.6; n=9 for each genotype).

Sperm membrane organization in FABP9$^{-/-}$ mice

To investigate whether FABP9 was responsible for tethering membrane components to the perinuclear theca, we localized membrane sterols and G_{M1} to evaluate the functional integrity of the known plasma membrane architecture in sperm. Sperm from FABP9$^{-/-}$ mice did not show any defects in the segregation of sterols and G_{M1} to the plasma membrane overlying the acrosome (Figure 5.7 A and B). We also investigated the capability of FABP9$^{-/-}$ sperm to capacitate by evaluating capacitation-associated protein tyrosine phosphorylation events. Sperm from FABP9$^{-/-}$ mice capacitated normally in response to bicarbonate ions and 2-OHCD in the medium and displayed a normal profile of tyrosine phosphorylated proteins (Figure 5.7C).

In vitro fertilization performance of FABP9$^{-/-}$ sperm

In natural matings, ejaculated sperm are exposed to significant lipid modifications as a result of exposure to seminal plasma and the uterine and

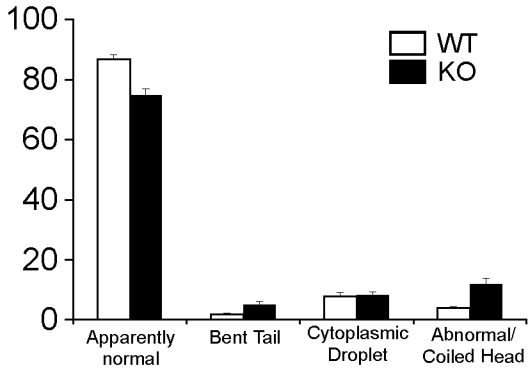

Figure 5.6. Sperm abnormalities in FABP9$^{-/-}$ mice. Percentage of abnormalities in WT and FABP9$^{-/-}$ mice categorized as apparently normal, bent tail, presence of a cytoplasmic droplet and an abnormal/coiled head. Differences between WT and FABP9$^{-/-}$ mice were not statistically significant.

Table 5.1. *In vitro* fertilization performance of FABP9$^{-/-}$ sperm

Trial #	Genotype	Fertilization rate†	% Fertilized†
1	WT	10/11	90.9
	KO	39/46	84.7
2	WT	7/8	87.5
	KO	12/12	100
3	WT	41/49	83.6
	KO	33/40	82.5

†Determined based on the number of 4-cell embryos in culture.

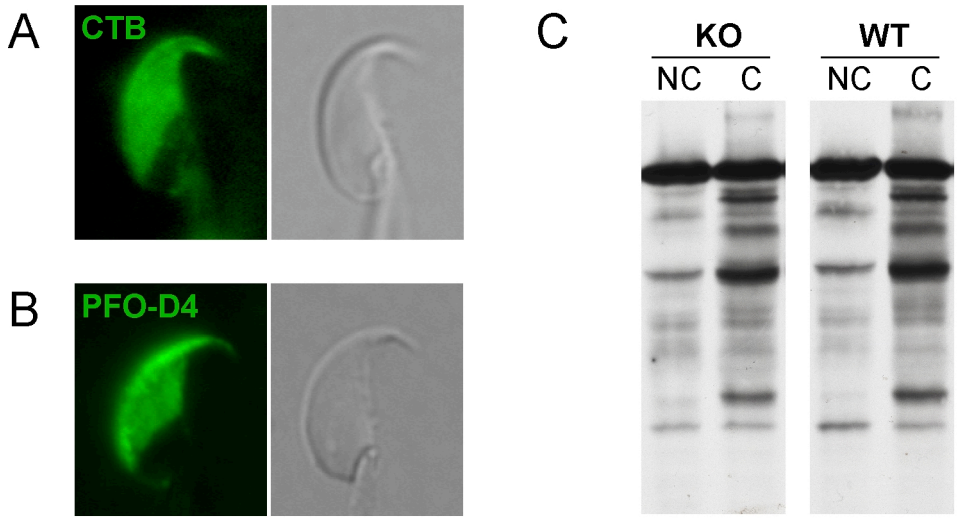

Figure 5.7. Membrane organization and signaling in FABP9$^{-/-}$ mice. (A) Membrane sterol localization. EGFP-conjugated D4 of perfringolysin O (PFO-D4) used to localize sterols in live sperm showed that sterol organization in the membrane was unaffected. There was segregation of sterols to the plasma membrane overlying the acrosome consistent with previous reports (Chapter 4) and WT cohorts (not shown). (B) Glycosphingolipid G_{M1} localization. CTB used to localize G_{M1} in live sperm also showed that membrane organization was unaffected. There was segregation of G_{M1} to the plasma membrane overlying the acrosome consistent with previous reports (Chapter 2) and WT cohorts (not shown). (C) Tyrosine phosphorylation of FABP9$^{-/-}$ and WT sperm proteins on exposure to stimuli inducing capacitation. Capacitation-associated phosphorylation of different sperm proteins was not affected in FABP9$^{-/-}$ sperm compared to WT. [NC- non-capacitated; C- capacitated]

oviductal environments. These modifications might compensate/rescue specific deficits and thereby mask possible functional phenotypes. In order to examine the functional ability of epididymal FABP9$^{-/-}$ sperm to fertilize oocytes, *in vitro* fertilization trials were carried out using FABP9$^{-/-}$ and WT cauda epididymal sperm. Capacitated sperm from FABP9$^{-/-}$ and WT mice were incubated with cumulus intact oocytes for 5 hours and resulting embryos were cultured until the 4-cell stage. Our results showed no significant differences in

fertilization rates between the FABP9$^{-/-}$ and WT sperm (Table 5.1). Thus sperm lacking FABP9$^{-/-}$ did not show any functional deficits compared to WT sperm.

Sperm total lipid profile in FABP9$^{-/-}$ mice

Total lipids extracted from WT and FABP9$^{-/-}$ sperm were eluted on a silica gel TLC plate to compare their relative profiles. In comparison to phospholipid, sphingolipid and fatty acid standards, several classes of lipids were observed in these preparations. However, there were no detectable differences between lipids from WT and FABP9$^{-/-}$ sperm (Figure 5.8).

Discussion

In both mouse and rat sperm, previous studies have shown that FABP9 forms the major constituent of the cytoskeletal networks of the perforatorium and the perinuclear theca (Oko and Morales, 1994; Korley et al., 1997). Functional organization of these cytoskeletal structures during spermiogenesis and in the mature sperm is still an area of active investigation (Lecuyer et al., 2000). Our study shows that FABP9 is not essential for spermatogenesis or function in the mature sperm. FABP9$^{-/-}$ mice did not show any significant reproductive deficits. There are two explanations for the above phenotype, (1) FABP9 is a non-essential gene or, (2) there are other proteins replacing FABP9 function in the FABP9$^{-/-}$ mice.

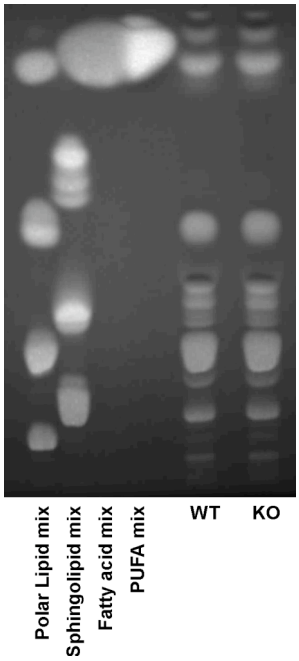

Figure 5.8. Total lipid profile of FABP9$^{-/-}$ and WT sperm. Total lipids were extracted from sperm using the Folch method (Folch et al., 1957), and developed on a silica gel TLC plate using 60:25:4 (chloroform:methanol:water) as the solvent system. Lipid standards indicated are as follows. *Polar lipid mix:* cholesterol, phosphatidyl ethanolamine, lecithin, lyso-lecithin; *Sphingolipid mix:* cerebrosides, sulfatides, sphingomyelin; *Fatty acid mix:* methyl palmitate, methyl stearate, methyl oleate-9, methyl linoleate-9,12, methyl linoleate-9,12,15; *Poly-unsaturated fatty acid (PUFA) mix:* C14, C16, C16:1ω7, C18:1ω7, C18:1ω9, C18:2ω6, C20:1ω9, C18:4ω3, C22:1ω11, C20:5ω3, C22:1ω9, C22:5ω3, C22:6ω3.

Although FABP9 protein was detected as early as day-16 of testicular development, prominent expression was visualized only in late elongating spermatids. This expression pattern of FABP9 late during spermiogenesis strongly suggested its involvement in a terminal differentiation process. Shutdown of nuclear transcription of the haploid genome coincides with nuclear compaction that occurs during mid-spermiogenesis (Kimmins et al.,

2004; Iguchi et al., 2006). Therefore, triggering a compensatory transcript after sensing the deficiency of FABP9 would require a retrospective cue, which is highly improbable. Therefore, the compensatory process for the loss of FABP9, if there were one, would likely be a pre-existing functional redundancy.

Besides FABP9, no other members of the FABP family of proteins have been reported to be present in male germ cells. In a recent study evaluating changes in the testicular proteome, FABP3 was shown to be upregulated progressively during post-natal testicular development (Paz et al., 2006). However, its presence in germ cells has not been examined. Moreover, in the above proteomic study, FABP3 was obtained from the soluble fraction after a simple homogenization of the testis. This shows a clear difference in cellular association of FABP3 compared to FABP9, which was not found in the soluble form but rather tethered to structural elements. Supporting this argument, cysteine residues in helix-2 of the tertiary structure that can potentially form disulfide bonds are present only in FABP9 and not in FABP3.

Human FABP9 also lacks the cysteine residues that are conserved in mouse and rat FABP9. This would suggest that human FABP9 is a soluble protein and not tethered to cytoskeletal elements as in rodents. Speculating upon this evolutionary divergence between rodents and humans, it appears that FABP9 in humans could behave and function in a very different way compared to rodents. It could act as a cytoplasmic fatty acid transport protein similar to several other members of the FABP family (Peeters and Veerkamp, 1989; Storch and Thumser, 2000; Stremmel et al., 2001).

Our studies comparing total lipid profile of FABP9$^{-/-}$ sperm to WT sperm did not show any apparent differences in sperm lipid composition. This suggests that the loss of FABP9 did not affect membrane lipid composition in

the mature sperm or lipid production, transport and metabolism during spermatogenesis.

In addition to membrane lipid composition, membrane tethering, organization and membrane domain segregation of sterols and G_{M1} were also not affected in FABP9$^{-/-}$ sperm. This suggests that FABP9 is either not the primary component of the perinuclear theca and the perforatorium that is responsible for tethering and organizing membranes of the sperm head, or that those underlying structures are not involved with the segregation of the APM domain.

Cauda epididymal sperm counts were also not different between the FABP9$^{-/-}$ and WT mice. This finding showed that the apoptotic regulation of germ cell numbers in the testis was unaffected by the absence of FABP9. Therefore FABP9 might not be directly involved in the germ cell apoptotic pathway under normal physiological conditions unlike the suggestion made after studying its over expression (Kido and Namiki, 2000; Kido et al., 2005).

In summary, expression of the highly conserved male germ cell specific protein FABP9 is triggered during late spermiogenesis. In mature sperm, FABP9 is present in the perforatorium, perinuclear theca and the principal piece of the flagellum. Mice lacking FABP9 are fertile and do not demonstrate any deficits in spermatogenesis or sperm function vis-à-vis fertilization. However, further work needs to be carried out to elucidate whether there are changes in sperm fatty acid profiles in FABP9 null mice, or whether there are functionally redundant proteins/pathways to compensate for the loss of FABP9 in germ cells.

Acknowledgements

This work was supported by National Institutes of Health grant R01-HD-045664 (A.J.T). We thank Ke-Yu Deng, Transgenic Mouse Core Facility at Cornell University and Robert Munroe, Department of Biomedical Sciences at Cornell University for performing the blastocyst microinjections and embryo transfers for generating chimeric mice. We also thank Kathy Mott and Jackie Wright for help with mouse colony management and breeding. Scanning electron microscopy was performed at the Keck Integrated Microscopy Facility (NSF-MRSEC program; DMR 0520404) at Cornell University.

REFERENCES

Aponte, G.W. (2002). Pyy-Mediated Fatty Acid Induced Intestinal Differentiation. Peptides 23, 367-376.

Austin, C.R. (1952). The Capacitation of the Mammalian Sperm. Nature 170, 326.

Bellve, A.R., Cavicchia, J.C., Millette, C.F., O'Brien, D.A., Bhatnagar, Y.M., and Dym, M. (1977). Spermatogenic Cells of the Prepuberal Mouse. Isolation and Morphological Characterization. J Cell Biol 74, 68-85.

Bernlohr, D.A., Coe, N.R., Simpson, M.A., and Hertzel, A.V. (1997). Regulation of Gene Expression in Adipose Cells by Polyunsaturated Fatty Acids. Adv Exp Med Biol 422, 145-156.

Borchers, T., Hohoff, C., Buhlmann, C., and Spener, F. (1997). Heart-Type Fatty Acid Binding Protein - Involvement in Growth Inhibition and Differentiation. Prostaglandins Leukot Essent Fatty Acids 57, 77-84.

Burton, P.B., Hogben, C.E., Joannou, C.L., Clark, A.G., Hsuan, J.J., Totty, N.F., Sorensen, C., Evans, R.W., and Tynan, M.J. (1994). Heart Fatty Acid Binding Protein Is a Novel Regulator of Cardiac Myocyte Hypertrophy. Biochem Biophys Res Commun 205, 1822-1828.

Chang, M.C. (1951). Fertilizing Capacity of Spermatozoa Deposited into the Fallopian Tubes. Nature 168, 697-698.

Chmurzynska, A. (2006). The Multigene Family of Fatty Acid-Binding Proteins (Fabps): Function, Structure and Polymorphism. J Appl Genet 47, 39-48.

Cowan, S.W., Newcomer, M.E., and Jones, T.A. (1993). Crystallographic Studies on a Family of Cellular Lipophilic Transport Proteins. Refinement of P2 Myelin Protein and the Structure Determination and Refinement of Cellular Retinol-Binding Protein in Complex with All-Trans-Retinol. J Mol Biol 230, 1225-1246.

Davis, B.K. (1976). Inhibitory Effect of Synthetic Phospholipid Vesicles Containing Cholesterol on the Fertilizing Ability of Rabbit Spermatozoa. Proc Soc Exp Biol Med 152, 257-261.

Deng, C., Wynshaw-Boris, A., Zhou, F., Kuo, A., and Leder, P. (1996). Fibroblast Growth Factor Receptor 3 Is a Negative Regulator of Bone Growth. Cell 84, 911-921.

Erbach, G.T., Lawitts, J.A., Papaioannou, V.E., and Biggers, J.D. (1994). Differential Growth of the Mouse Preimplantation Embryo in Chemically Defined Media. Biol Reprod 50, 1027-1033.

Eswar, N., John, B., Mirkovic, N., Fiser, A., Ilyin, V.A., Pieper, U., Stuart, A.C., Marti-Renom, M.A., Madhusudhan, M.S., Yerkovich, B., and Sali, A. (2003). Tools for Comparative Protein Structure Modeling and Analysis. Nucleic Acids Res 31, 3375-3380.

Eylar, E.H., Szymanska, I., Ishaque, A., Ramwani, J., and Dubiski, S. (1980). Localization of the P2 Protein in Peripheral Nerve Myelin. J Immunol 124, 1086-1092.

Falomir-Lockhart, L.J., Laborde, L., Kahn, P.C., Storch, J., and Corsico, B. (2006). Protein-Membrane Interaction and Fatty Acid Transfer from Intestinal Fatty Acid-Binding Protein to Membranes. Support for a Multistep Process. J Biol Chem 281, 13979-13989.

Fawcett, D.W. (1970). A Comparative View of Sperm Ultrastructure. Biol Reprod 2, Suppl 2:90-127.

Fiser, A., Do, R.K., and Sali, A. (2000). Modeling of Loops in Protein Structures. Protein Sci 9, 1753-1773.

Folch, J., Lees, M., and Sloane Stanley, G.H. (1957). A Simple Method for the Isolation and Purification of Total Lipides from Animal Tissues. J Biol Chem 226, 497-509.

Fouquet, J.P., Valentin, A., and Kann, M.L. (1992). Perinuclear Cytoskeleton of Acrosome-Less Spermatids in the Blind Sterile Mutant Mouse. Tissue Cell 24, 655-665.

Gibbons, I.R., Cosson, M.P., Evans, J.A., Gibbons, B.H., Houck, B., Martinson, K.H., Sale, W.S., and Tang, W.J. (1978). Potent Inhibition of Dynein Adenosinetriphosphatase and of the Motility of Cilia and Sperm Flagella by Vanadate. Proc Natl Acad Sci U S A 75, 2220-2224.

Graber, R., Sumida, C., and Nunez, E.A. (1994). Fatty Acids and Cell Signal Transduction. J Lipid Mediat Cell Signal 9, 91-116.

Hotamisligil, G.S., Johnson, R.S., Distel, R.J., Ellis, R., Papaioannou, V.E., and Spiegelman, B.M. (1996). Uncoupling of Obesity from Insulin Resistance through a Targeted Mutation in Ap2, the Adipocyte Fatty Acid Binding Protein. Science 274, 1377-1379.

Hunter, D.J., Macmaster, R., Roszak, A.W., Riboldi-Tunnicliffe, A., Griffiths, I.R., and Freer, A.A. (2005). Structure of Myelin P2 Protein from Equine Spinal Cord. Acta Crystallogr D Biol Crystallogr 61, 1067-1071.

Iguchi, N., Tobias, J.W., and Hecht, N.B. (2006). Expression Profiling Reveals Meiotic Male Germ Cell Mrnas That Are Translationally up- and Down-Regulated. Proc Natl Acad Sci U S A 103, 7712-7717.

Kido, T., Arata, S., Suzuki, R., Hosono, T., Nakanishi, Y., Miyazaki, J., Saito, I., Kuroki, T., and Shioda, S. (2005). The Testicular Fatty Acid Binding Protein Perf15 Regulates the Fate of Germ Cells in Perf15 Transgenic Mice. Dev Growth Differ 47, 15-24.

Kido, T., and Namiki, H. (2000). Expression of Testicular Fatty Acid-Binding Protein Perf 15 During Germ Cell Apoptosis. Dev Growth Differ 42, 359-366.

Kimmins, S., Kotaja, N., Davidson, I., and Sassone-Corsi, P. (2004). Testis-Specific Transcription Mechanisms Promoting Male Germ-Cell Differentiation. Reproduction 128, 5-12.

Korley, R., Pouresmaeili, F., and Oko, R. (1997). Analysis of the Protein Composition of the Mouse Sperm Perinuclear Theca and Characterization of Its Major Protein Constituent. Biol Reprod 57, 1426-1432.

Lalli, M., and Clermont, Y. (1981). Structural Changes of the Head Components of the Rat Spermatid During Late Spermiogenesis. Am J Anat 160, 419-434.

Lecuyer, C., Dacheux, J.L., Hermand, E., Mazeman, E., Rousseaux, J., and Rousseaux-Prevost, R. (2000). Actin-Binding Properties and Colocalization with Actin During Spermiogenesis of Mammalian Sperm Calicin. Biol Reprod 63, 1801-1810.

Liu, P., Jenkins, N.A., and Copeland, N.G. (2003). A Highly Efficient Recombineering-Based Method for Generating Conditional Knockout Mutations. Genome Res 13, 476-484.

Longo, F.J., Krohne, G., and Franke, W.W. (1987). Basic Proteins of the Perinuclear Theca of Mammalian Spermatozoa and Spermatids: A Novel Class of Cytoskeletal Elements. J Cell Biol 105, 1105-1120.

Marti-Renom, M.A., Stuart, A.C., Fiser, A., Sanchez, R., Melo, F., and Sali, A. (2000). Comparative Protein Structure Modeling of Genes and Genomes. Annu Rev Biophys Biomol Struct 29, 291-325.

Oko, R., and Clermont, Y. (1988). Isolation, Structure and Protein Composition of the Perforatorium of Rat Spermatozoa. Biol Reprod 39, 673-687.

Oko, R., and Maravei, D. (1994). Protein Composition of the Perinuclear Theca of Bull Spermatozoa. Biol Reprod 50, 1000-1014.

Oko, R., and Morales, C.R. (1994). A Novel Testicular Protein, with Sequence Similarities to a Family of Lipid Binding Proteins, Is a Major Component of the Rat Sperm Perinuclear Theca. Dev Biol 166, 235-245.

Oko, R., Moussakova, L., and Clermont, Y. (1990). Regional Differences in Composition of the Perforatorium and Outer Periacrosomal Layer of the Rat Spermatozoon as Revealed by Immunocytochemistry. Am J Anat 188, 64-73.

Olson, G.E., and Winfrey, V.P. (1988). Characterization of the Postacrosomal Sheath of Bovine Spermatozoa. Gamete Res 20, 329-342.

Paranko, J., Longo, F., Potts, J., Krohne, G., and Franke, W.W. (1988). Widespread Occurrence of Calicin, a Basic Cytoskeletal Protein of Sperm Cells, in Diverse Mammalian Species. Differentiation 38, 21-27.

Paz, M., Morin, M., and del Mazo, J. (2006). Proteome Profile Changes During Mouse Testis Development. Comp Biochem Physiol Part D: Genomics and Proteomics 1, 404-415.

Peeters, R.A., and Veerkamp, J.H. (1989). Does Fatty Acid-Binding Protein Play a Role in Fatty Acid Transport? Mol Cell Biochem 88, 45-49.

Runner, M.N., and Gates, A. (1954). Conception in Prepuberal Mice Following Artificially Induced Ovulation and Mating. Nature 174, 222-223.

Sali, A., and Blundell, T.L. (1993). Comparative Protein Modelling by Satisfaction of Spatial Restraints. J Mol Biol 234, 779-815.

Schurer, N.Y., Stremmel, W., Grundmann, J.U., Schliep, V., Kleinert, H., Bass, N.M., and Williams, M.L. (1994). Evidence for a Novel Keratinocyte Fatty Acid Uptake Mechanism with Preference for Linoleic Acid: Comparison of Oleic and Linoleic Acid Uptake by Cultured Human Keratinocytes, Fibroblasts and a Human Hepatoma Cell Line. Biochim Biophys Acta 1211, 51-60.

Selvaraj, V., Asano, A., Buttke, D.E., McElwee, J.L., Nelson, J.L., Wolff, C.A., Merdiushev, T., Fornes, M.W., Cohen, A.W., Lisanti, M.P., Rothblat, G.H., Kopf, G.S., and Travis, A.J. (2006). Segregation of Micron-Scale Membrane Sub-Domains in Live Murine Sperm. J Cell Physiol 206, 636-646.

Shaughnessy, S., Smith, E.R., Kodukula, S., Storch, J., and Fried, S.K. (2000). Adipocyte Metabolism in Adipocyte Fatty Acid Binding Protein Knockout Mice (Ap2-/-) after Short-Term High-Fat Feeding: Functional Compensation by the Keratinocyte [Correction of Keritinocyte] Fatty Acid Binding Protein. Diabetes 49, 904-911.

Storch, J., and Thumser, A.E. (2000). The Fatty Acid Transport Function of Fatty Acid-Binding Proteins. Biochim Biophys Acta 1486, 28-44.

Stremmel, W., Pohl, L., Ring, A., and Herrmann, T. (2001). A New Concept of Cellular Uptake and Intracellular Trafficking of Long-Chain Fatty Acids. Lipids 36, 981-989.

Stremmel, W., Strohmeyer, G., Borchard, F., Kochwa, S., and Berk, P.D. (1985). Isolation and Partial Characterization of a Fatty Acid Binding Protein in Rat Liver Plasma Membranes. Proc Natl Acad Sci U S A 82, 4-8.

Toyoda, Y., Yokoyama, M., and Hoshi, T. (1971). [Studies on the Fertilization of Mouse Eggs in Vitro. I. In Vitro Fertilization of Eggs by Fresh Epididymal Spermatozoa]. Jpn J Reprod Dev 16, 147-151.

Trapp, B.D., Dubois-Dalcq, M., and Quarles, R.H. (1984). Ultrastructural Localization of P2 Protein in Actively Myelinating Rat Schwann Cells. J Neurochem 43, 944-948.

Travis, A.J., Jorgez, C.J., Merdiushev, T., Jones, B.H., Dess, D.M., Diaz-Cueto, L., Storey, B.T., Kopf, G.S., and Moss, S.B. (2001a). Functional Relationships between Capacitation-Dependent Cell Signaling and Compartmentalized Metabolic Pathways in Murine Spermatozoa. J Biol Chem 276, 7630-7636.

Travis, A.J., and Kopf, G.S. (2002). The Spermatozoon as a Machine: Compartmentalized Pathways Bridge Cellular Structure and Function. In: Assisted reproductive technology: Accomplishments and new horizons. DeJonge CJ, Barratt CL, editors. Cambridge University Press, 26-39.

Travis, A.J., Merdiushev, T., Vargas, L.A., Jones, B.H., Purdon, M.A., Nipper, R.W., Galatioto, J., Moss, S.B., Hunnicutt, G.R., and Kopf, G.S. (2001b). Expression and Localization of Caveolin-1, and the Presence of Membrane Rafts, in Mouse and Guinea Pig Spermatozoa. Dev Biol 240, 599-610.

Travis, A.J., Tutuncu, L., Jorgez, C.J., Ord, T.S., Jones, B.H., Kopf, G.S., and Williams, C.J. (2004). Requirements for Glucose Beyond Sperm Capacitation During in Vitro Fertilization in the Mouse. Biol Reprod 71, 139-145.

Trotter, P.J., Ho, S.Y., and Storch, J. (1996). Fatty Acid Uptake by Caco-2 Human Intestinal Cells. J Lipid Res 37, 336-346.

Visconti, P.E., Galantino-Homer, H., Ning, X., Moore, G.D., Valenzuela, J.P., Jorgez, C.J., Alvarez, J.G., and Kopf, G.S. (1999). Cholesterol Efflux-Mediated Signal Transduction in Mammalian Sperm. Beta-Cyclodextrins

Initiate Transmembrane Signaling Leading to an Increase in Protein Tyrosine Phosphorylation and Capacitation. J Biol Chem 274, 3235-3242.

Wedgwood, J.F., Strominger, J.L., and Warren, C.D. (1974). Transfer of Sugars from Nucleoside Diphosphosugar Compounds to Endogenous and Synthetic Dolichyl Phosphate in Human Lymphocytes. J Biol Chem 249, 6316-6324.

Weiss, R.S., Enoch, T., and Leder, P. (2000). Inactivation of Mouse Hus1 Results in Genomic Instability and Impaired Responses to Genotoxic Stress. Genes Dev 14, 1886-1898.

Widstrom, R.L., Norris, A.W., and Spector, A.A. (2001). Binding of Cytochrome P450 Monooxygenase and Lipoxygenase Pathway Products by Heart Fatty Acid-Binding Protein. Biochemistry 40, 1070-1076.

Wolfrum, C., Borrmann, C.M., Borchers, T., and Spener, F. (2001). Fatty Acids and Hypolipidemic Drugs Regulate Peroxisome Proliferator-Activated Receptors Alpha - and Gamma-Mediated Gene Expression Via Liver Fatty Acid Binding Protein: A Signaling Path to the Nucleus. Proc Natl Acad Sci U S A 98, 2323-2328.

Wright, R.S. (1971). A Reagent for the Non-Destructive Location of Steroids and Some Other Lipophilic Materials on Silica Gel Thin-Layer Chromatograms. J Chromatogr 59, 220-221.

Yang, Y., Spitzer, E., Kenney, N., Zschiesche, W., Li, M., Kromminga, A., Muller, T., Spener, F., Lezius, A., Veerkamp, J.H., Smith, G. H., Salomon, D. S., and Grosse, R. (1994). Members of the Fatty Acid Binding Protein Family Are Differentiation Factors for the Mammary Gland. J Cell Biol 127, 1097-1109.

Zimmerman, A.W., and Veerkamp, J.H. (2002). New Insights into the Structure and Function of Fatty Acid-Binding Proteins. Cell Mol Life Sci 59, 1096-1116.

CHAPTER 6

Final Discussion and Future Directions

Lessons learned from the properties of CTB-bound G_{M1}

The dynamics of the glycosphingolipid G_{M1} in sperm is a topic that has been subject to misinterpretation caused by artifacts (Trevino et al., 2001; Roberts et al., 2003; Shadan et al., 2004). Our studies have reconciled most of these differences which we found to have been caused largely by either temperature and fixation conditions (Selvaraj et al., 2006; Selvaraj et al., 2007), or exposure to seminal plasma (Buttke et al., 2006). Based on initial observations in the lightly fixed sperm head or upon cell death, in which CTB-bound G_{M1} redistributed from the sterol-rich APM to the sterol-poor PAPM, and in the sperm tail, where G_{M1} enrichment was seen in the sterol-poor annulus and flagellar zipper, we proposed a possible explanation that CTB-bound G_{M1} could be migrating to sterol-poor regions of the membrane (Selvaraj et al., 2007). In light of our new findings, the dynamics of redistribution in the sperm head appear to involve intracellular membranous compartments in addition to the plasma membrane.

First, we found that the membrane of the acrosomal vesicle is enriched in G_{M1}. This was unexpected because earlier studies have shown that the membrane of the acrosome is not enriched in sterols (Toshimori et al., 1985; Clark and Koehler, 1990; Seki et al., 1992). This suggests that the pro-acrosomal vesicles released from the Golgi during acrosome biogenesis are selectively enriched in G_{M1} but not sterols. Supporting this theory, recent studies based on membrane fractionation without the use of detergents from others in our lab showed that two G_{M1}-enriched membrane fractions exist in sperm membranes; one was highly enriched in sterols, whereas the other had a much lower relative amount of sterols (Asano et al., under review).

Second, we found that CTB could be driving a membrane event that triggers communication between the APM and the underlying OAM without large-scale exocytotic release of acrosomal contents but with net movement of G_{M1} to the plasma membrane. This explained the disproportionate increase in CTB fluorescence after redistribution. In live sperm, it has been suggested that transitional intermediates of membrane fusion between the APM and the OAM exist, which are analogous to “kiss and run” vesicular exocytotic events in neuronal synapses (Kim and Gerton, 2003). This membrane communication observed in the presence of CTB could be a dysregulation of the exocytotic machinery that is primed for fusion. Moreover, the enrichment of G_{M1} in the acrosomal membrane, coupled with our lab’s biochemical data, suggest the existence of membrane raft sub-types that need to be defined in order to understand and explain the behavior of CTB-bound G_{M1}.

A model encompassing regional diffusion barriers to micro-heterogeneities in sperm membranes

From the studies on the localization of lipid components and associated regional properties of the sperm membranes, we have composed a model describing the different steps of organization of the sperm plasma membrane (Figure 6.1). At the primary step, there are regional separations in the continuous sperm plasma membrane that exist as diffusion barriers at (a) the SAR, (b) the posterior ring and (c) the annulus. This separates the sperm plasma membrane to the APM, PAPM, mid-piece plasma membrane and the principal piece plasma membrane. Compositional differences in the plasma membrane regions separated by these barriers have been reported with respect to sterols, phospholipids, glycosphingolipids and the presence of intra-

Figure 6.1. Different levels in organization of the sperm plasma membrane. (A) *Primary step:* Diffusion barriers are seen at the SAR, posterior ring and the annulus dividing the plasma membrane into the APM, PAPM, mid-piece plasma membrane and principal piece plasma membrane. (B) *Secondary step:* Morphological sub-divisions exist within the primary separations. These include the apical acrosome within the APM domain and the flagellar zipper within the principal piece plasma membrane. (C) *Tertiary step:* Membrane raft microdomains exist under the primary and secondary levels of organization.

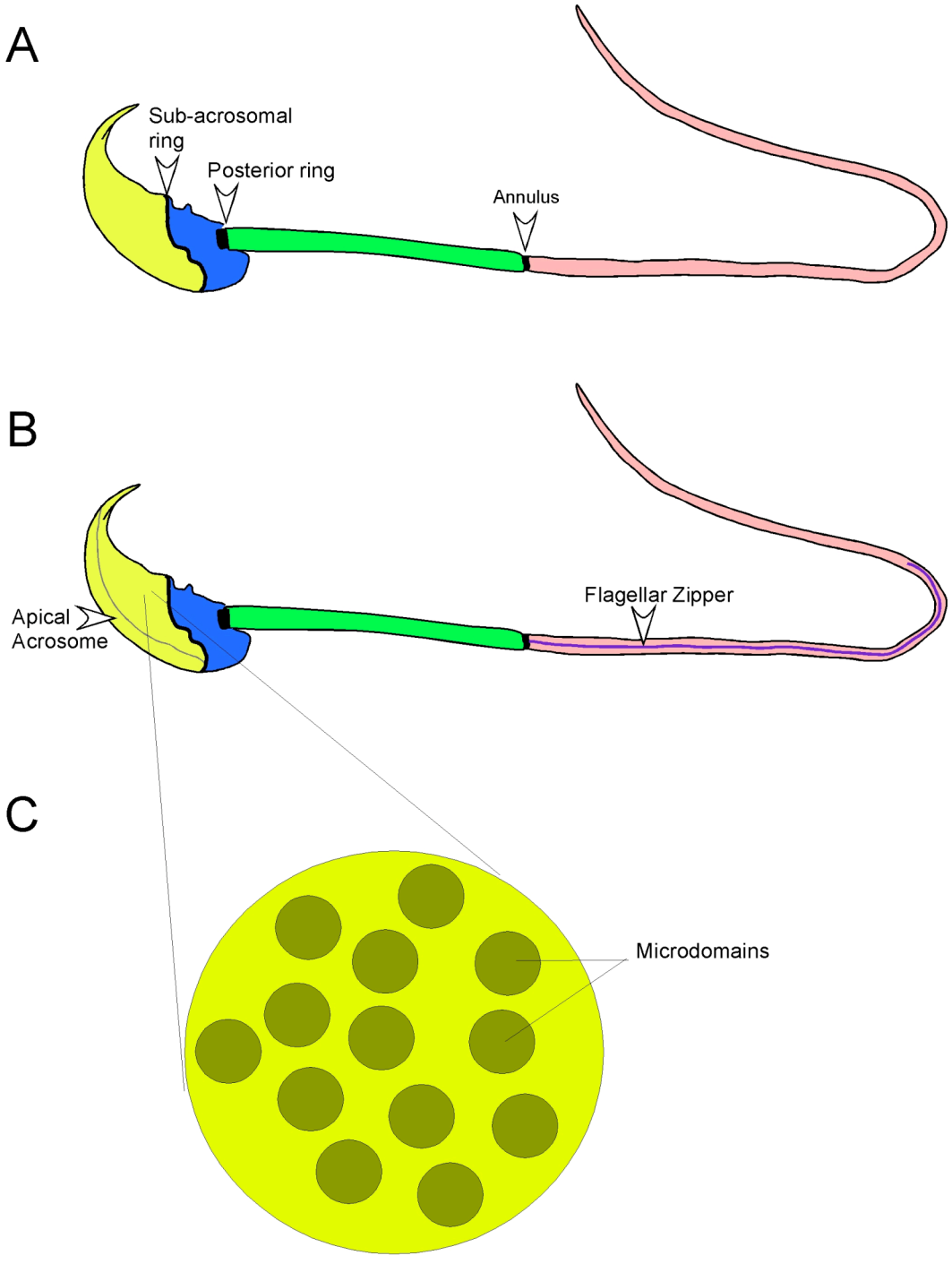
A
Sub-acrosomal ring
Posterior ring
Annulus
B
Apical Acrosome
Flagellar Zipper
C
Microdomains

membranous particles (Friend and Fawcett, 1974; Friend, 1982; Koehler, 1983; Toshimori et al., 1985; Friend, 1989; Lin and Kan, 1996; Selvaraj et al., 2006; Selvaraj et al., 2007). We show that the SAR acts as a diffusion barrier for endogenous G_{M1}. Our SEM studies also show that the SAR, posterior ring and the annulus are morphologically distinct. At the secondary step, there are localized membrane areas within the aforementioned regional separations that show definitive structural sub-divisions. These include (1) the apical acrosome within the APM domain and (2) the flagellar zipper within the principal piece plasma membrane. At the tertiary step, there are membrane raft microdomains that exist within the separated regions, at least within the APM domain. This organizational pattern can be related to functional requirements in the different regions. The functional organization of the plasma membrane of the sperm head is discussed below.

Mechanisms behind maintenance of the APM domain

Based on studies detailed in this dissertation, the mechanism(s) behind the maintenance of the APM domain was not easily explained by any of the known models for membrane raft formation and maintenance in somatic cells. We showed that the APM domain is not a transient confinement zone; although there might be membrane compartmentation within the APM, there was definitely no “hop diffusion” across the SAR; lipid segregation was not maintained just by lipid-lipid interactions; a well characterized sterol-binding protein, caveolin-1, although abundant in this region was not involved in this segregation. Lipids within the APM had lateral mobility showing that the SAR was acting as a boundary for this domain. The existence of a boundary was supported by our SEM studies that showed an enrichment of CTB-bound G_{M1}

Figure 6.2. Model for the mechanism of segregation of the APM domain. The schematic shows a model involving several complementary mechanisms of lipid segregation acting at different levels that can explain the mechanism of segregation of the APM domain. (A) *First level:* there are free uni-molecular membrane lipids and proteins that follow the tenets of the Singer-Nicholson fluid-mosaic model (e.g. most phospholipids). (B) *Second level:* the existence of proteins and lipids in pre-assembled macromolecular composites. These could be heterogeneous in composition but are stable in not allowing sterol or G_{M1} exchange across the SAR. (C) *Third level:* the existence of cytoskeletal-anchored transmembrane proteins as picket fences at the SAR restricts lateral diffusion of the macromolecular composites. This would require that all segregated molecules be components of these composites. Alternatively, cytoskeletal elements underlying the membrane might interact directly with membrane lipids and remove the necessity for transmembrane pickets. (D) *Fourth level:* spatial and temporal restrictions of specific sub-types of the macromolecular composites might lead to localized specializations (seen in the region of the AA within the APM domain; a black arrow beneath the bilayer demarcates this region). Note: the depictions regarding the diversity of molecules are highly simplified in this schematic.

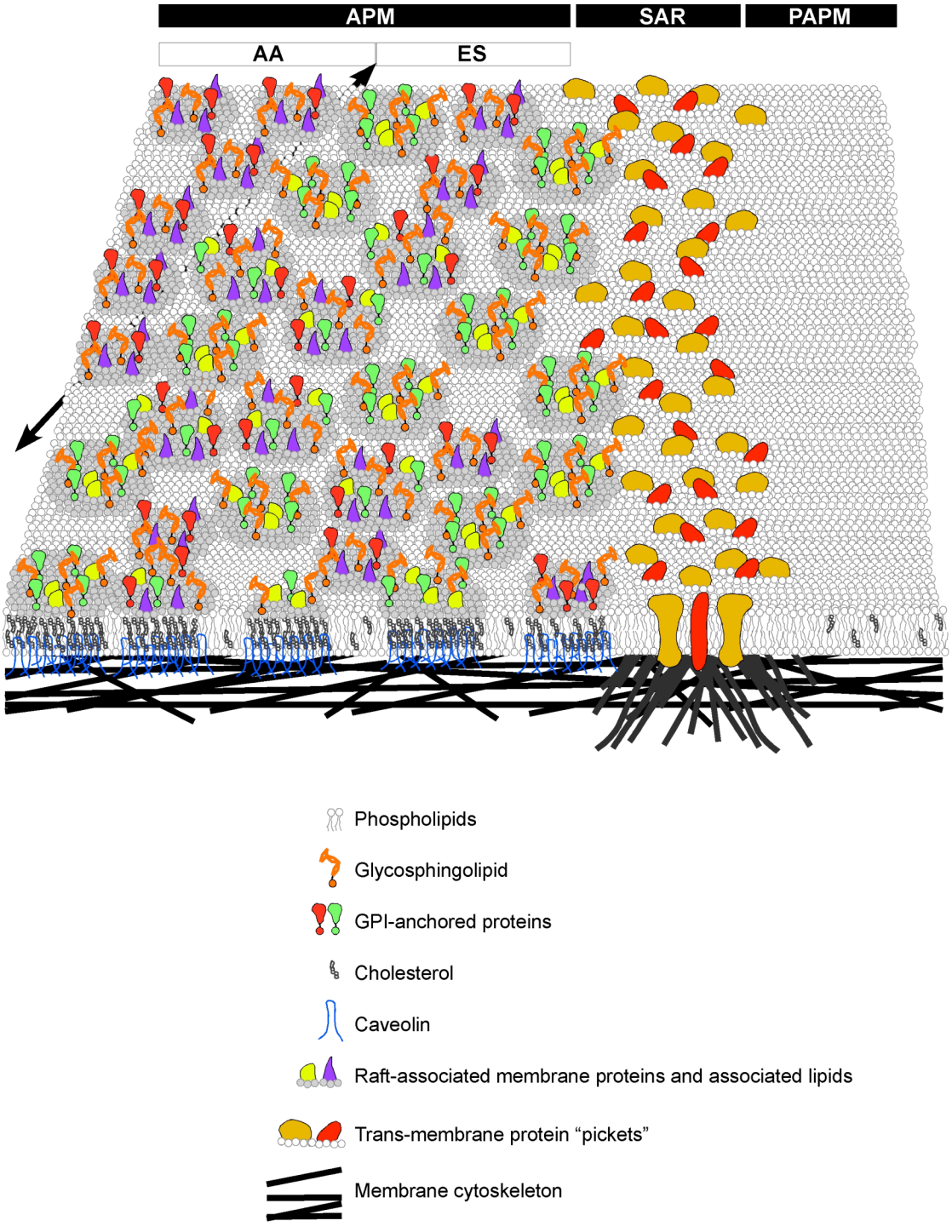
APM
SAR
PAPM
AA
ES
Phospholipids
Glycosphingolipid
GPI-anchored proteins
Cholesterol
Caveolin
Raft-associated membrane proteins and associated lipids
Trans-membrane protein “pickets”
Membrane cytoskeleton

“stuck” at the SAR after redistribution suggesting that it offers some hindrance to lipid movement (albeit we have only definitively identified this for CTB-bound G_{M1} molecules).

Combining all these observations we propose a hierarchical model driven by a combination of mechanisms. According to this model (Figure 6.2), the first level describes free uni-molecular membrane lipids and proteins that follow the tenets of the Singer-Nicholson fluid-mosaic model. The SAR does not restrict movement of these molecules and they can travel freely between the APM and the PAPM. The second level describes the existence of proteins and lipids in pre-assembled macromolecular composites (e.g. stable lipid shells or protein-lipid aggregates). Our model allows for these composites to be either heterogeneous or restricted to specific compositional sub-types but does not allow for dynamic protein or lipid exchange either between composites or with other bilayer molecules (because of the failure for either sterols or G_{M1} to ever move across the SAR). The third level describes the existence of cytoskeletal-anchored transmembrane proteins as picket fences at the SAR completely restricting lateral diffusion of the macromolecular composites. This model would require that all segregated molecules in the APM domain need to be components of stable macromolecular composites. The fourth and final level of organization describes restrictions of specific compositional sub-types of the macromolecular complexes that might lead to localized specializations such as those evident at the region of the apical acrosome within the APM domain.

APM domain and sperm function

In sperm, the APM domain is of great physiological interest because it is the region that first comes in contact with the oocyte. It has been hypothesized that the APM domain targets functional proteins required for sperm-egg interactions (Martinez and Morros, 1996). Besides the oocyte recognition molecules, it also carries the machinery required for driving acrosomal exocytosis, an event critical for fertilization. Based on data presented, we propose that in non-capacitated sperm, the APM domain is saturated with sterols and that at this state the AA cannot fuse with the underlying acrosomal vesicle to release its lytic contents and facilitate egg penetration. This could be either due to a direct biophysical property of the membrane precluding fusion at this physiological state or the obstruction of specific signaling events.

Supporting the former case is the finding that lysophosphatidyl choline (LPC) can induce acrosomal exocytosis in bull sperm (Parrish et al., 1988). LPC can insert into the outer leaflet of the membrane and induce membrane curvature augmenting the activity of mechanosensitive channels (Perozo et al., 2002). The latter case would suggest that the APM domain is heterogenous in which there are different types of raft microdomains and non-raft regions. The enrichment of membrane raft microdomains might be stabilizing them as a platform thereby decreasing fusigenic regions or dampening signaling activity (perhaps by suppressing local ion channel function). Sterol efflux could be decreasing the surface ratio of rafts to non-rafts within this domain. Therefore, in non-capacitated cells, signaling molecules might be lethargic and caught in a congested raft-rich membrane lattice-like structure that then becomes more laterally mobile after sterol efflux facilitating signaling. This is also supported

by our observations using PFO-D4 where labeling appeared to be coarse with punctate spots of fluorescence within the APM domain suggesting heterogeneity within the domain. Therefore, after sterol removal, the sperm might become more responsive to signaling driven by proteins of the egg coat (e.g. ZP3) and/or the hormone progesterone, both of which are capable of inducing acrosomal exocytosis (Leyton and Saling, 1989; Roldan et al., 1994). The increase in membrane fluidity after efflux (Companyo et al., 2007) might also facilitate membrane fusion events required for exocytosis. However, further studies need to be carried out observing the spatial and temporal kinetics of sterol efflux from the APM domain. It will be interesting to see if there is preferential loss of sterols over the AA where the fusion events take place during exocytosis, rather than at the ES.

After penetrating the coat, fusion takes place with the egg plasma membrane at the region of the ES and PAPM (Stefanini et al., 1969; Yanagimachi, 1978). It is currently not known whether the SAR regulates the segregation of components in the inner acrosomal membrane (IAM) after acrosomal exocytosis when the IAM becomes continuous with the PAPM. After exocytosis, there is evidence for the movement of molecules mediating fusion of the sperm and the egg plasma membranes from the IAM to the PAPM region across the SAR (e.g. Izumo-1) (Yamashita et al., 2007) and vice versa (e.g. PH-20) (Cowan et al., 1987). It should be noted that the IAM has been shown to be refractory to fusion and does not fuse with the oocyte plasma membrane (Clark and Koehler, 1990; Szollosi et al., 1990).

Future directions

The understanding provided by these studies on sperm membranes sets the stage for exploring capacitation-related changes in the micro-heterogeneities that exist within the APM domain. Important questions regarding signaling events regulated by the efflux of plasma membrane sterols and the regulation of membrane fusion events during acrosomal exocytosis need to be addressed. Elucidating the mechanism behind the lipid segregation and identifying the component(s) at the proposed different regulatory levels should be of broad interest to cell biologists. Given the existence of a stable, defined and visible membrane domain, sperm are an excellent model for studying membrane organization.

Furthermore, development of the use of CTB-bound G_{M1} dynamics as a diagnostic tool to evaluate sperm response to stimuli for capacitation could be valuable when screening for male fertility and deciding between technologies of assisted reproduction. We have demonstrated the use of G_{M1} localization as a promising assay for evaluating murine and bovine sperm. Exploring the applicability to human sperm, we recently found that human sperm also exhibit different patterns of CTB-bound G_{M1}, indicative of membrane changes that occur during capacitation (Figure 6.3). Moreover, G_{M1} patterns could also reveal sperm with membrane abnormalities that are not otherwise visible (data not shown).

Although FABP9 did not to play a role in sterol or G_{M1} segregation in the sperm plasma membrane and its function was not required for fertilization, investigations to identify a more specialized role for FABP9 in germ cell fatty acid metabolism and/or apoptosis need to be carried out.

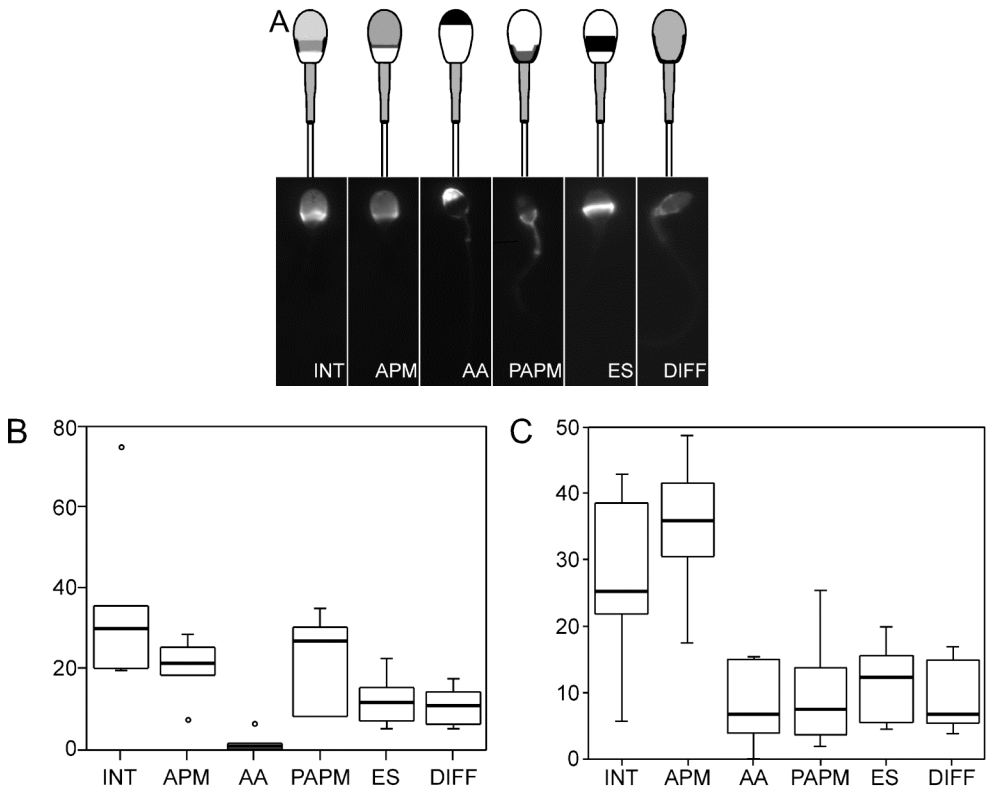

Figure 6.3. Patterns of G_{M1} localization in human sperm. (A) Fluorescence images of CTB labeling and schematic diagrams (drawn as negative images) showing the range of G_{M1} localization patterns in human sperm after fixation using 0.5% formaldehyde (A). Box-whisker plots show the percentages of sperm with each pattern under non-capacitating conditions (B), and capacitating conditions [n=5 for each] (C). Note the increases in the APM and AA patterns under capacitating conditions.

The studies on G_{M1} dynamics have raised questions on the function of G_{M1} in sperm. Why is it enriched in the APM domain and the acrosome? Does it play a role in regulating calcium as reported for neurons? Or does it function via other/additional signaling pathways? Studies from others in the lab suggest that G_{M1} can modulate calcium entry and signaling during the process of capacitation. These are promising areas that require further exploration.

REFERENCES

Buttke, D.E., Nelson, J.L., Schlegel, P.N., Hunnicutt, G.R., and Travis, A.J. (2006). Visualization of Gm1 with Cholera Toxin B in Live Epididymal Versus Ejaculated Bull, Mouse, and Human Spermatozoa. Biol Reprod 74, 889-895.

Clark, J.M., and Koehler, J.K. (1990). Observations of Hamster Sperm-Egg Fusion in Freeze-Fracture Replicas Including the Use of Filipin as a Sterol Marker. Mol Reprod Dev 27, 351-365.

Companyo, M., Iborra, A., Villaverde, J., Martinez, P., and Morros, A. (2007). Membrane Fluidity Changes in Goat Sperm Induced by Cholesterol Depletion Using Beta-Cyclodextrin. Biochim Biophys Acta 1768, 2246-2255.

Cowan, A.E., Myles, D.G., and Koppel, D.E. (1987). Lateral Diffusion of the Ph-20 Protein on Guinea Pig Sperm: Evidence That Barriers to Diffusion Maintain Plasma Membrane Domains in Mammalian Sperm. J Cell Biol 104, 917-923.

Friend, D.S. (1982). Plasma-Membrane Diversity in a Highly Polarized Cell. J Cell Biol 93, 243-249.

Friend, D.S. (1989). Sperm Maturation: Membrane Domain Boundaries. Ann N Y Acad Sci 567, 208-221.

Friend, D.S., and Fawcett, D.W. (1974). Membrane Differentiations in Freeze-Fractured Mammalian Sperm. J Cell Biol 63, 641-664.

Kim, K.S., and Gerton, G.L. (2003). Differential Release of Soluble and Matrix Components: Evidence for Intermediate States of Secretion During Spontaneous Acrosomal Exocytosis in Mouse Sperm. Dev Biol 264, 141-152.

Koehler, J.K. (1983). Structural Heterogeneity of the Mammalian Sperm Flagellar Membrane. J Submicrosc Cytol 15, 247-253.

Leyton, L., and Saling, P. (1989). Evidence That Aggregation of Mouse Sperm Receptors by Zp3 Triggers the Acrosome Reaction. J Cell Biol 108, 2163-2168.

Lin, Y., and Kan, F.W. (1996). Regionalization and Redistribution of Membrane Phospholipids and Cholesterol in Mouse Spermatozoa During in Vitro Capacitation. Biol Reprod 55, 1133-1146.

Martinez, P., and Morros, A. (1996). Membrane Lipid Dynamics During Human Sperm Capacitation. Front Biosci 1, d103-117.

Parrish, J.J., Susko-Parrish, J., Winer, M.A., and First, N.L. (1988). Capacitation of Bovine Sperm by Heparin. Biol Reprod 38, 1171-1180.

Perozo, E., Kloda, A., Cortes, D.M., and Martinac, B. (2002). Physical Principles Underlying the Transduction of Bilayer Deformation Forces During Mechanosensitive Channel Gating. Nat Struct Biol 9, 696-703.

Roberts, K.P., Wamstad, J.A., Ensrud, K.M., and Hamilton, D.W. (2003). Inhibition of Capacitation-Associated Tyrosine Phosphorylation Signaling in Rat Sperm by Epididymal Protein Crisp-1. Biol Reprod 69, 572-581.

Roldan, E.R., Murase, T., and Shi, Q.X. (1994). Exocytosis in Spermatozoa in Response to Progesterone and Zona Pellucida. Science 266, 1578-1581.

Seki, N., Toyama, Y., and Nagano, T. (1992). Changes in the Distribution of Filipin-Sterol Complexes in the Boar Sperm Head Plasma Membrane During Epididymal Maturation and in the Uterus. Anat Rec 232, 221-230.

Selvaraj, V., Asano, A., Buttke, D.E., McElwee, J.L., Nelson, J.L., Wolff, C.A., Merdiushev, T., Fornes, M.W., Cohen, A.W., Lisanti, M.P., Rothblat, G.H., Kopf, G.S., and Travis, A.J. (2006). Segregation of Micron-Scale Membrane Sub-Domains in Live Murine Sperm. J Cell Physiol 206, 636-646.

Selvaraj, V., Buttke, D.E., Asano, A., McElwee, J.L., Wolff, C.A., Nelson, J.L., Klaus, A.V., Hunnicutt, G.R., and Travis, A.J. (2007). Gm1 Dynamics as a Marker for Membrane Changes Associated with the Process of Capacitation in Murine and Bovine Spermatozoa. J Androl 28, 588-599.

Shadan, S., James, P.S., Howes, E.A., and Jones, R. (2004). Cholesterol Efflux Alters Lipid Raft Stability and Distribution During Capacitation of Boar Spermatozoa. Biol Reprod 71, 253-265.

Stefanini, M., Oura, L., and Zamboni, L. (1969). Ultrastructure of Fertilization in the Mouse: Ii. Penetration of Sperm into the Ovum. J Submicrosc Cytol 1, 1-23.

Szollosi, D., Szollosi, M.S., Czolowska, R., and Tarkowski, A.K. (1990). Sperm Penetration into Immature Mouse Oocytes and Nuclear Changes During Maturation: An Em Study. Biol Cell 69, 53-64.

Toshimori, K., Higashi, R., and Oura, C. (1985). Distribution of Intramembranous Particles and Filipin-Sterol Complexes in Mouse Sperm Membranes: Polyene Antibiotic Filipin Treatment. Am J Anat 174, 455-470.

Trevino, C.L., Serrano, C.J., Beltran, C., Felix, R., and Darszon, A. (2001). Identification of Mouse Trp Homologs and Lipid Rafts from Spermatogenic Cells and Sperm. FEBS Lett 509, 119-125.

Yamashita, M., Yamagata, K., Tsumura, K., Nakanishi, T., and Baba, T. (2007). Acrosome Reaction of Mouse Epididymal Sperm on Oocyte Zona Pellucida. J Reprod Dev 53, 255-262.

Yanagimachi, R. (1978). Sperm-Egg Association in Animals. Curr Top Dev Biol 12, 83-105.